

AD-A060 156 SYSTEMS RESEARCH LABS INC, DAYTON OH AEROSYSTEMS RESE--ETC F/G 21/4
HIGH ENERGY MHD FUELS DEVELOPMENT PROGRAM. (U)
APR 78 R E ECKELS F33615-75-C-2043

UNCLASSIFIED

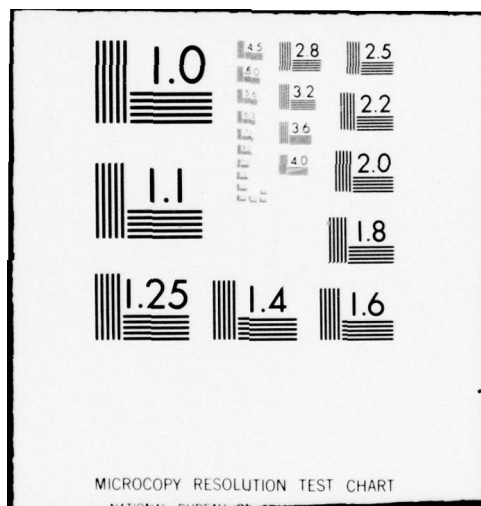
AFAPL-TR-78-10

NL

1 of 4

AD
A060 156





AFAPL-TR-78-10

② LEVEL II

ADA060156

HIGH ENERGY MHD FUELS DEVELOPMENT PROGRAM

SYSTEMS RESEARCH LABORATORIES, INC.
AEROSYSTEMS RESEARCH DIVISION
2800 INDIAN RIPPLE ROAD
DAYTON, OHIO 45440

New
410 898

APRIL 1978

DDC
RECEIVED
OCT 23 1978
B

TECHNICAL REPORT AFAPL-TR-78-10
Final Report for Period March 1975 - December 1977

Approved for public release; distribution unlimited.

AIR FORCE AERO PROPULSION LABORATORY
AIR FORCE WRIGHT AERONAUTICAL LABORATORIES
AIR FORCE SYSTEMS COMMAND
WRIGHT-PATTERSON AIR FORCE BASE, OHIO 45433

78 10 19 065

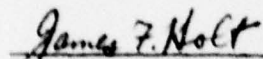
DDC FILE COPY

NOTICE

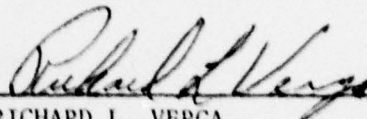
When Government drawings, specifications, or other data are used for any purpose other than in connection with a definitely related Government procurement operation, the United States Government thereby incurs no responsibility nor any obligation whatsoever; and the fact that the government may have formulated, furnished, or in any way supplied the said drawings, specifications, or other data, is not to be regarded by implication or otherwise as in any manner licensing the holder or any other person or corporation, or conveying any rights or permission to manufacture, use, or sell any patented invention that may in any way be related thereto.

This report has been reviewed by the Information Office (OI) and is releasable to the National Technical Information Service (NTIS). At NTIS, it will be available to the general public, including foreign nations.

This technical report has been reviewed and is approved for publication.



JAMES F. HOLT
Physicist
High Power Branch
Aerospace Power Division



RICHARD L. VERGA
Actg Technical Area Manager
High Power Branch
Aerospace Power Division

FOR THE COMMANDER



JAMES D. REAMS
Chief
Aerospace Power Division

"If your address has changed, if you wish to be removed from our mailing list, or if the addressee is no longer employed by your organization please notify AFAPL-POD-1, W-PAFB, OH 45433 to help us maintain a current mailing list".

Copies of this report should not be returned unless return is required by security considerations, contractual obligations, or notice on a specific document.

SECURITY CLASSIFICATION OF THIS PAGE (When Data Entered)

REPORT DOCUMENTATION PAGE		READ INSTRUCTIONS BEFORE COMPLETING FORM	
1. REPORT NUMBER AFAPL TR-78-10	2. GOVT ACCESSION NO.	3. RECIPIENT'S CATALOG NUMBER	
4. TITLE (and Subtitle) HIGH ENERGY MHD FUELS DEVELOPMENT PROGRAM	5. TYPE OF REPORT & PERIOD COVERED Final Rept. March 1975 - December 1977		
6. AUTHOR(s) Richard E. Eckels	7. CONTRACT OR GRANT NUMBER(s) F33615-75-C-2043 Project 3145		
8. PERFORMING ORGANIZATION NAME AND ADDRESS Systems Research Laboratories, Inc. 2800 Indian Ripple Road Dayton OH 45440	9. PROGRAM ELEMENT, PROJECT, TASK AREA & WORK UNIT NUMBERS Program Element: 62203F Project: 3145 Task: 314526 Work Unit: 31452633		
10. CONTROLLING OFFICE NAME AND ADDRESS Air Force Aero Propulsion Laboratory (POD-1) AF Wright Aeronautical Laboratories, AFSC Wright-Patterson Air Force Base, Ohio 45433	11. REPORT DATE April 1978		
12. MONITORING AGENCY NAME & ADDRESS (if different from Controlling Office)	13. SECURITY CLASS. (of this report) UNCLASSIFIED		
14. DISTRIBUTION STATEMENT (of this Report) Approved for public release; distribution unlimited.			
15. NUMBER OF PAGES 347			
16. DISTRIBUTION STATEMENT (of the abstract entered in Block 20, if different from Report)			
17. SUPPLEMENTARY NOTES			
18. KEY WORDS (Continue on reverse side if necessary and identify by block number) MHD Magnetohydrodynamic Power MHD Fuels Combustion High Energy Open Cycle MHD			
19. ABSTRACT (Continue on reverse side if necessary and identify by block number) An analytical study compared the electrical conductivity and velocity squared product for several MHD liquid or liquified fuels. Aluminum additive to liquid hydrocarbon was found to be attractive for high power density MHD. A number of MHD power tests showed that developed emulsified slurry fuels were engineeringly feasible. Various emulsification processes are described.			

DD FORM 1 JAN 73 1473 EDITION OF 1 NOV 65 IS OBSOLETE

SECURITY CLASSIFICATION OF THIS PAGE (When Data Entered)

78 10 19 06

FOREWORD

This report documents the results of the High Energy Fuels Development Program conducted by Systems Research Laboratories, Inc. (SRL), 2800 Indian Ripple Road, Dayton, Ohio 45440. This program was carried out under Contract No. F33615-75-C-2043, Project 3145, Task 314526, with the Air Force Aero Propulsion Laboratory, High Power Branch (AFAPL/POD). As a result of this effort, patent disclosures have been filed with the AF relative to the high energy fuels developed and tested, and MHD seeding techniques, discussed in Section IV3, V4F and J, and XI.

The period of performance is from March 1975 to December 1977, and the report was submitted in December 1977.

SRL's project engineer was Mr. Richard E. Eckels. The AFAPL/POD project engineer was Dr. James F. Holt.

The author would like to express his appreciation to Dr. James F. Holt for his assistance in the preparation of the final report.

ACCESSION for		
NTIS	White Section	<input checked="" type="checkbox"/>
DDC	Buff Section	<input type="checkbox"/>
UNANNOUNCED		<input type="checkbox"/>
JUSTIFICATION _____		
BY _____		
DISTRIBUTION/AVAILABILITY CODES		
Dist.	Avail.	and/or SPECIAL
A		

TABLE OF CONTENTS

SECTION	PAGE
I INTRODUCTION	1
II HIGH ENERGY FUELS DEVELOPMENT	2
1. Introduction	2
2. Combustion Requirements	8
3. High Energy Fuel Potential	14
4. Fuel Properties	59
III EMULSIFIED FUELS	64
1. History and Experience	64
2. Emulsion Characteristics	68
IV FUEL EMULSION MIXING TECHNOLOGY	71
1. Introduction	71
2. Early Fuel Emulsion Mixing	83
3. Emulsion Mixing Techniques	92
V FUEL TESTING	105
1. Fuel Spray Tests	105
2. Calibration Tests	116
3. Combustion Testing	122
A. Introduction	122
B. Combustion Checkout Tests, HEF-1 and HEF-1A	127
C. Emulsified Toluene Combustion Tests, HEF-2 and HEF-3	133
D. Emulsified JP-4/Coal Combustion Test, HEF-4	138
E. Emulsified Toluene/Magnesium Combustion Test, HEF-5	140
F. Emulsified Toluene/Aluminum Combustion Tests, HEF-6 and HEF-6A	144
4. MHD Generator Power Testing	153
A. Introduction	153
B. MHD Channel Checkout Test with Toluene, HEF-7 and HEF-7A	153
C. Granulated Cs_2CO_3 Seeding Rate Optimization Tests, HEF-8, HEF-8A, HEF-8B, HEF-8C, and HEF-8D	160
D. Toluene Baseline, O/F Optimization, and Load Switch Checkout Tests, HEF-9, HEF-9A, and HEF-9B	181
E. Toluene Emulsion Power Tests With Load Switching, HEF-10 and HEF-10A	189

PRECEDING PAGE BLANK

TABLE OF CONTENTS (cont.)

SECTION		PAGE
	F. Emulsified Toluene/ CsNO_3 Seed Power Tests, HEF-11, HEF-11A, HEF-11B, and HEF-11C	197
	G. Emulsified Toluene/Aluminum Power Tests, HEF-12 and HEF-12A	215
	H. Neat Toluene Repeat Test With Variable O/F and Load Switching, HEF-13 and HEF-13A	220
	I. Neat Toluene Repeat Test With Variable O/F, HEF-14 and HEF-14A	225
	J. Emulsified Toluene/ CsNO_3 Seed Repeat With Increased Seed Flow Rate, HEF-15 and HEF-15A	229
	K. Neat JP-4 Fuel Power Baseline Test, HEF-16 and HEF-17	232
	L. Emulsified Toluene/Aluminum Power Test With Increased O/F, HEF-18 and HEF-18A	240
	M. Emulsified Toluene/Magnesium Power Test, HEF-19	246
	5. Discussion and Conclusions of Power Testing	246
VI	FUEL HANDLING	252
	1. General	252
	2. Magnesium Powders	254
	3. Aluminum Powders	259
	4. Miscellaneous Fuel Particulates	264
	5. Toluene	266
	6. Benzene	276
	7. Napthalene	277
	8. Cesium Salts	278
VII	GENERAL OPERATING PRACTICES IN THE KIVA-I MHD FACILITY	281
VIII	DISASSEMBLY AND INSPECTION OF THE KIVA-I 45° CONDUCTING WALL MHD GENERATOR CHANNEL	283
	1. Channel Disassembly and Inspection	283
	2. Diffuser Disassembly and Inspection	291
IX	REFURBISHMENT OF THE KIVA-I HEAT SINK PEG WALL MHD CHANNEL	298
X	TEST DATA	309

TABLE OF CONTENTS (cont.)

SECTION	PAGE
XI FUEL EMULSION MIXTURE FORMULATIONS	334
APPENDIX	345
REFERENCES	346

LIST OF ILLUSTRATIONS

FIGURE		PAGE
1	γ Dependency of KIVA - I Nozzle Flow Parameters	7
2	Typical Droplet Histories for Sprays - Initial Mass-Median Drop Radius of 75μ ; Initial Drop Velocity of 3000 cm/sec; Chamber Pressure, 20 atm; Initial Drop Temperature, 278 K; Chamber Gas Temperature, 278 K; Chamber Gas Temperature 2780 K	10
3	Combustion Temperature of Neat Toluene and Gaseous Oxygen - Cs_2CO_3 Seed (4.22% Cs)	15
4	Combustion Temperature of Neat JP-4 and Gaseous Oxygen - Cs_2CO_3 Seed (3.90% Cs)	16
5	Combustion Temperature of Neat Benzene and Gaseous Oxygen - Cs_2CO_3 Seed (4.28% Cs)	17
6	Combustion Temperature of Toluene/3% H_2O Emulsion and Gaseous Oxygen - Cs_2CO_3 Seed (4.35% Cs)	18
7	Combustion Temperature of JP-4/3% H_2O Emulsion and Gaseous Oxygen - Cs_2CO_3 Seed (4.02% Cs)	19
8	Combustion Temperature of Benzene/3% H_2O Emulsion and Gaseous Oxygen - Cs_2CO_3 Seed (4.41% Cs)	20
9	Combustion Temperature of Toluene/3% H_2O Emulsion and Gaseous Oxygen - CsNO_3 Seed (4.57% Cs)	21
10	Combustion Temperature Comparison (Reference Fuel - Neat Toluene)	23
11	Combustion Temperature Comparison Cs_2CO_3 Seeded Neat Toluene Fuel (Reference Fuel Seeded with Cs_2CO_3 , Cs = 15% of Fuel)	24
12	Combustion Temperature Comparison of Emulsified Fuels Seeded with Cs_2CO_3 , Cs = 15% of Fuel - (Reference Fuel - Neat Toluene + 15% Seed)	25
13	Combustion Temperature Comparison of Emulsified Fuels Seeded with Cs_2CO_3 , Cs = 15% of Fuel - (Reference Fuel - Emulsified Toluene, 15% Seed)	26

LIST OF ILLUSTRATIONS (cont.)

FIGURE		PAGE
14	Combustion Temperature Comparison of Toluene Emulsion Fuel Seeded with CsNO_3 and Cs_2CO_3 , Cs = 15% of Fuel - (Reference Fuel Seed - Cs_2CO_3)	27
15	Combustion Temperature Comparison of Emulsified Toluene Fuel Seeded with CsNO_3 - (Reference Fuel - Seeded with CsNO_3 , Cs = 15% of Fuel)	28
16	Combustion Temperature Comparison of Emulsified Toluene Fuel with Varying H_2O % Seeded with Cs_2CO_3 , Cs = 15% of Fuel - (Reference Fuel Contains 3% H_2O)	29
17	Combustion Temperature Comparison of Waterless Emulsion Seeded with Cs_2CO_3 , Cs = 15% of Fuel - (Reference Fuel - Toluene/3% H_2O Emulsion, 15% Seed)	30
18	Combustion Temperature Comparison of Toluene/Aluminum Emulsion Fuels Seeded with Cs_2CO_3 , Cs = 15% of Fuel - (Reference Fuel - Emulsified Toluene, 15% Seed)	31
19	Combustion Temperature Comparison of Toluene/Boron Emulsion Seeded with Cs_2CO_3 , Cs = 15% of Fuel - (Reference Fuel - Emulsified Toluene 15% Seed)	32
20	Combustion Temperature Comparison of Toluene/Magnesium Emulsion Seeded with Cs_2CO_3 , Cs = 15% of Fuel - (Reference Fuel - Emulsified Toluene, 15% Seed)	33
21	Combustion Temperature Comparison of High C/H Ratio Emulsified Fuels Seeded with Cs_2CO_3 , Cs = 15% of Fuel - (Reference Fuel - Emulsified Toluene, 15% Seed)	34
22	Combustion Temperature Comparison of Emulsified Carbon Fuels Seeded with Cs_2CO_3 , Cs = 15% of Fuel - (Reference Fuel - Emulsified Toluene, 15% Seed)	35
23	Combustion Temperature Comparison of Emulsified Toluene/and Solid Particulate Fuels Seeded with Cs_2CO_3 , Cs = 15% of Fuel - (Reference Fuel - Emulsified Toluene, 15% Seed)	36

LIST OF ILLUSTRATIONS (cont.)

FIGURE		PAGE
24	Combustion Temperature Comparison of Emulsified Benzene/Napthalene/Aluminum Fuels Seeded with Cs_2CO_3 , Cs = 15% of Fuel - (Reference Fuel - Emulsified Toluene, 15% Seed)	37
25	σC^2 Comparison of Neat JP-4, Toluene, and Benzene Fuels with Cs_2CO_3 Seed	41
26	σC^2 Comparison of Neat Toluene Fuel with Various Seed Ratios of Cs_2CO_3	42
27	σC^2 Comparison of Emulsified JP-4, Toluene, and Benzene Fuels Seeded with Cs_2CO_3	43
28	σC^2 Comparison of Neat and Emulsified Fuels with Cs_2CO_3 Seed	44
29	σC^2 Comparison of Cs_2CO_3 and CsNO_3 Seeded Toluene Fuel	45
30	σC^2 Comparison of Emulsified Toluene Fuel with Various Ratios of CsNO_3 Seed	46
31	σC^2 Comparison of Emulsified Toluene with Various Percentages of H_2O External Phase	47
32	σC^2 Comparison of Emulsified Fuels with H_2O and Waterless External Phase Seeded with Cs_2CO_3	48
33	σC^2 Comparison of Emulsified Toluene Fuel with Varying Percentages of Al Additive	49
34	σC^2 Comparison of Emulsified Toluene and Boron Additive Fuel Seeded with Cs_2CO_3	50
35	σC^2 Comparison of Emulsified Toluene with Varying Percentages of Mg Additive and Cs_2CO_3 Seed	51
36	σC^2 Comparison of Hydrocarbon Additive Fuel with Cs_2CO_3 Seed	52
37	σC^2 Comparison of Emulsified Toluene with Varying Carbon Additive Ratio	53
38	σC^2 Comparison of Various Fuel Additives with Cs_2CO_3 Seed	54

LIST OF ILLUSTRATIONS (cont.)

FIGURE		PAGE
39	oC ² Comparison of High Energy Fuel Composition with and without H ₂ O as an Emulsifier External Phase	55
40	Examples of Simple Slurries of Left to Right: Toluene/Aluminum, Toluene/Magnesium, JP-4/Magnesium, JP-4/Aluminum in the As Mixed Condition, Mix + 5 Minutes, and Mix + 10 Minutes	61
41	Particle Size Distribution of Reynolds Aluminum 400 Atomized Aluminum Powder Sample	73
42	Particle Size Distribution of Reade Manufacturing Company RMC 325 Magnesium Powder Sample	75
43	Particle Size Distribution of Kawecki Berylco Amorphous Elemental Boron - Grade 1 Sample	76
44	Particle Size Distribution of Asland Chemical Company - N330 Carbon Block Sample	77
45	Fuel Additive Particle Photo Micrographs	79
46	Fuel Additive Particle Photo Micrographs	79
47	Fuel Additive Particle Photo Micrographs	80
48	Fuel Additive Particle Photo Micrographs	80
49	Fuel Additive Particle Photo Micrographs	81
50	Fuel Additive Particle Photo Micrographs	81
51	Fuel Additive Particle Photo Micrographs	82
52	Fuel Additive Particle Photo Micrographs	82
53	Particle Size Analysis of <10mm Magnesium Powder	84
54	Particle Size Analysis of 10 to 20mm and >20mm Magnesium Powder	85
55	Simulated KIVA - I Propellant Injector Triplet Used for Spray Tests	106

LIST OF ILLUSTRATIONS (cont.)

FIGURE		PAGE
56	Injector Block Construction, Simulated KIVA - I Propellant Injector (Dimensions Are In Inches)	107
57	Fuel Spray Test Apparatus Schematic	108
58	Fuel Spray Test Set Up	109
59	Water Discharged Through the Spray Test Injector Block Without Gas Stream	110
60	Water Discharged Through the Spray Test Injector Block with Impinging Gas Stream	111
61	Neat Water Spray Pattern -1- 0.16 id Injector 1 atm Pressure Drop -2- 0.084 id Injector 15 atm Pressure Drop	112
62	Neat Water Calibration Curve for KIVA - I Injectors	117
63	97/3 H ₂ O Emulsion Calibration Curve for KIVA - I Injectors	118
64	95/5 H ₂ O Emulsion Calibration Curve for KIVA - I Injectors	119
65	H ₂ O/20% Coal Emulsion Calibration Curve for KIVA - I Injectors	120
66	Fuel System Pressure Loss Curve with Emulsified Toluene	121
67	Combustion Test Flame Tube Exhausting into Facility Exhaust Duct	123
68	Extrapolated Al ₂ O ₃ Temperature-Vapor Pressure Curve	126
69	Combustion Check Out Test with Flame Tube, Fuel - Straight Toluene	128
70	Straight Toluene Fuel Flow Calibration Curves	131
71	Combustion Check Out Test Parameters	132
72	Emulsified Toluene Fuel Flow Calibration Curves	134

LIST OF ILLUSTRATIONS (cont.)

FIGURE		PAGE
73	Combustion Test - HEF-2, Fuel - Emulsified Toluene	136
74	Combustion Test - HEF-3, Fuel - Emulsified Toluene Variable O/F	137
75	Fuel Calibration Curves for Coal and CsNO_3 Seed Particle Additives	139
76	Combustion Test Run - HEF-4, Fuel - Emulsified JP-4 62%, Coal 30%	141
77	Calibration Curves for Emulsified Toluene/ Magnesium	142
78	Combustion Test Run - HEF-5, Fuel - Emulsified Toluene 65%, Magnesium 30%	143
79	Combustion Nozzle Inlet	145
80	Combustion Chamber and Injector Plate - Note Magnesium Oxide Deposits on Walls and Injector Plate Face - Deposit Flakes at Bottom Were Broken Loose During Disassembly	145
81	Magnesium Oxide Deposit Removed From Combustor Nozzle Inlet, Nozzle Contact Surface Shown With Nozzle Cross-section Facing Out	146
82	Magnesium Oxide Deposit Removed From Combustor Nozzle Inlet, Gas Flow Surface Facing Out	146
83	Magnesium Oxide Deposit Flakes Removed From Combustion Chamber Walls and Deposit Chip Removed From Nozzle Inlet - Gas Flow Surface on the Chip is Up and Flow Direction is Left to Right as Gas Enters the Nozzle Convergent Section	147
84	Calibration Curves For Emulsified Toluene/ Aluminum	149
85	Combustion Test - HEF-6, Fuel - Emulsified Toluene 65%, Aluminum 30%	150
86	Combustion Test - HEF-6A, Fuel - Emulsified Toluene 65%, Aluminum 30%	152

LIST OF ILLUSTRATIONS (cont.)

FIGURE		PAGE
87	KIVA - I Water Cooled, 45 ⁰ , Diagonally Conducting Wall, MHD Generator	154
88	KIVA - I MHD Generator Control Room	155
89	Neat Toluene Fuel Flow Calibration Curve	156
90	MHD Generator Check Out Test - HEF-7A, Fuel - Neat Toluene, Modified .772cm, Oxidizer Venturi Installed	157
91	0.772 Diameter Oxidizer Venturi (Modified) Total Pressure and Throat Static Pressure	159
92	Calculated Pressure Decay For O ₂ Venturi Throat Pressure Line	161
93	Diagonal Wall Generator Electrical Connections	162
94	Seeder Calibration For Seed Classified >20 But <40 Mesh, Percent of Full Scale Setting Vs. Seed Flow	163
95	Seeder Calibration, Percent of Full Scale Setting Vs. Seed Wheel RPM	164
96	Powermeter Current & Voltage Oscilloscope Trace	167
97	Power Test Run HEF-8A Combustion Parameters, Fuel - Straight Toluene, Load Resistance 10Ω	169
98	Powermeter Current, Voltage and Differential Load Voltage Oscilloscope Trace	171
99	Power Test Run HEF-8B Combustion Parameters, Fuel - Straight Toluene, Load Resistance 10Ω	172
100	Powermeter Current, Voltage and Differential Load Voltage Oscilloscope Trace	173
101	Power Test Run HEF-8C Combustion Parameters, Fuel - Straight Toluene, Load Resistance 10Ω	174
102	Powermeter Current, Voltage and Differential Load Voltage Oscilloscope Trace	176

LIST OF ILLUSTRATIONS (cont.)

FIGURE		PAGE
103	Power Test Run HEF-8D Combustion Parameters, Fuel - Straight Toluene, Load Resistance 10Ω	178
104	Effectiveness of Granulated Cs_2CO_3 Seed in the KIVA - I MHD Generator	179
105	Effectiveness of CsCO_3 Seed in KIVA - I MHD Generator	180
106	KIVA - I Generator Load Resistance Schematic - Early Load Switching Systems Shown Within Dashed Line	182
107	Oxygen Venturi Flow Curve for 0.926cm Throat Venturi	183
108	Fuel System Calibration with Toluene Fuel	184
109	Power Test Run HEF-9 Combustion Parameters, Fuel - Straight Toluene, Variable Load Resistance, Seeder Failed	186
110	Power Test Run HEF-9A Combustion Parameters, Fuel - Straight Toluene, Load Resistance Variable, Seeder Failed	187
111	Power Test Run HEF-9B Combustion Parameters, Fuel - Straight Toluene, Load Resistance Variable, Load Shorted	188
112	Toluene Emulsion Fuel Calibration	191
113	Differential Load Voltage Oscilloscope Trace	192
114	Power Test Run HEF-10 Combustion Parameters, Fuel - Emulsified Toluene, Load Resistance 10Ω	193
115	Power Test Run HEF-10F Combustion Parameters, Fuel - Emulsified Toluene, Load Resistance Variable 14Ω to 12Ω	195
116	Differential Load Voltage Oscilloscope Trace	196
117	Power Test Run HEF-10B Combustion Parameters, Fuel - Emulsified Toluene, Load Resistance Variable 10Ω to 8Ω	198
118	Test Series HEF-10 Load Line	199

LIST OF ILLUSTRATIONS (cont.)

FIGURE		PAGE
119	Fuels System Calibration Curve with Emulsified Toluene and CsNO_3 Seed Fuel	201
120	Differential Load Voltage Oscilloscope Trace	203
121	Seeder Feed Schematic	204
122	Power Test HEF-11 Combustion Parameters, Fuel - Emulsified Toluene/ CsNO_3 , Load Resistance Variable 10Ω to 8Ω	205
123	Power Test Run HEF-11A Combustion Parameters, Fuel - Emulsified Toluene/ CsNO_3 , Load Resistance Variable 14Ω to 12Ω	207
124	Test Series HEF-11, 11A Load Line	208
125	Test Series HEF-11, 11A Specific Power	209
126	Differential Load Voltage Oscilloscope Trace	211
127	Power Test Run HEF-11B Combustion Parameters, Fuel - Emulsified Toluene/ CsNO_3 , Load Resistance Variable 10Ω to 8Ω	212
128	Power Test Run HEF-11C Combustion Parameters, Fuel - Emulsified Toluene/ CsNO_3 , Load Resistance Variable 14Ω to 12Ω	213
129	Differential Load Voltage Oscilloscope Trace	216
130	Power Test Run HEF-12 Combustion Parameters, Fuel - Emulsified Toluene/Aluminum, Load Resistance Variable 10Ω to 8Ω	217
131	Power Test Run HEF-12A Combustion Parameters, Fuel - Emulsified Toluene/Aluminum, Load Resistance Variable 14Ω to 12Ω - Fuel Exhaustion at 8.2 Seconds	219
132	Power Test Run HEF-13 Combustion Parameters, Fuel - Straight Toluene, Load Resistance Variable 10Ω to 8Ω	221
133	Differential Load Voltage Oscilloscope Trace	222
134	Power Test Run HEF-13A, Fuel - Straight Toluene, Load Resistance Variable 14Ω to 12Ω - Arcing Destroyed Instrumentation	224

LIST OF ILLUSTRATIONS (cont.)

FIGURE		PAGE
135	Power Test Run HEF-14 Combustion Parameters, Fuel - Straight Toluene, Load Resistance Variable 10 Ω to 8 Ω	226
136	Differential Load Voltage Oscilloscope Trace	227
137	Power Test Run HEF-14A Combustion Parameters, Fuel - Straight Toluene, Load Resistance Variable 14 Ω to 12 Ω	228
138	Power Test Run HEF-15 Combustion Parameters, Fuel - Emulsified Toluene/CsNO ₃ (4% Cs), Load Resistance Variable 10 Ω to 8 Ω	230
139	Differential Load Voltage Oscilloscope Trace	231
140	Power Test Run HEF-15A Combustion Parameters, Fuel - Emulsified Toluene/CsNO ₃ (4% Cs), O/F Variable from 2.4 to 2.5, Load Resistance Variable 14 Ω to 12 Ω	233
141	Fuel Flow Calibration Curve	235
142	Power Test Run HEF-16 Combustion Parameters, Fuel - Neat JP-4, O/F Variable from 3.45 to 3.55, Load Resistance Variable 10 Ω to 8 Ω	236
143	Differential Load Voltage Oscilloscope Trace	237
144	Power Test Run HEF-17 Combustion Parameters, Fuel - Neat JP-4, O/F Variable from 3.61 to 3.71, Load Resistance Variable 10 Ω to 8 Ω	238
145	Differential Load Voltage Oscilloscope Trace	239
146	Fuel System Calibration Curve for Emulsified Toluene/Aluminum Fuel	241
147	Power Test Run HEF-18 Combustion Parameters, Fuel - Emulsified Toluene/Aluminum, O/F Variable 2.74 to 2.90, Load Resistance Variable 10 Ω to 8 Ω	242
148	Differential Load Voltage Oscilloscope Trace	243
149	Power Test Run HEF-18A Combustion Parameters, Fuel - Emulsified Toluene/Aluminum, O/F at Start 2.82, Load Resistance Variable 14 Ω to 12 Ω	245

LIST OF ILLUSTRATIONS (cont.)

FIGURE		PAGE
150	Fuel System Calibration Curve for Emulsified Toluene/Magnesium Fuel	247
151	Power Test Run HEF-19 Combustion Parameters, Fuel - Emulsified Toluene/Magnesium, O/F at 2.72, Load Resistance 10 Ω	248
152	MgO - Al ₂ O ₃ Phase Diagrams Showing Eutectic Points	251
153	Chemical Safety Data Sheet SD-63	265
154	KIVA - I MHD Generator Inlet Transition Piece with Fiberfrax Insulation	284
155	KIVA - I MHD Generator Exit Transition Piece	286
156	KIVA - I MHD Generator Electrodes with Fiberfrax Insulation	287
157	KIVA - I MHD Generator Electrodes Showing Al ₂ O ₃ Plasma Sprayed Side of Electrodes	288
158	Arc Tracks in Al ₂ O ₃ Plasma Sprayed Electrodes	289
159	Arc Tracks in Interelectrode Fiberfrax Insulation and Al ₂ O ₃ Coated Electrode Gas Surface	290
160	KIVA - I MHD Generator Electrode Coolant Passage End Plug Removed	292
161	Coolant Passage End Plugs Showing Extent of Intergranular Corrosion	293
162	Electrode Coolant Port Having Minimal Corrosion	294
163	KIVA - I MHD Generator Diffuser with One Sidewall Removed	295
164	KIVA - I MHD Generator Diffuser Side Wall	296
165	KIVA - I Pegwall Heat Sink MHD Channel Top Electrode and Right Side	299
166	KIVA - I Pegwall Heat Sink MHD Channel Bottom Electrode and Left Side	300

LIST OF ILLUSTRATIONS (cont.)

FIGURE		PAGE
167	KIVA - I Heat Sink MHD Generator Electrode with Arc Track in Al_2O_3 Grout	301
168	KIVA - I Heat Sink Generator Electrode Showing Al_2O_3 Grout and Fiberglas Insulator Construction with Arc Tracks in Grout	302
169	KIVA - I Heat Sink MHD Generator End Block, Insulator and Matching Electrode with Arc Tracks	303
170	KIVA - I Heat Sink MHD Generator Matching Electrodes and Interelectrode Insulator	304

LIST OF TABLES

TABLE		PAGE
1	Fuel Formulation Table	60
2	Potential Cesium Seed Materials	102
3	Ballast Resistor Values for Diagonal Wall Channel	165
4	Toluene Vapor Responses	273

NOMENCLATURE

A	generator effective cross sectional area
A_c	combustor cylindrical cross sectional area
A_d	detector area
A/A^*	nozzle expansion area ratio
A^*	nozzle throat area
A_0	output voltage
a	spray nozzle constant
a_1, a_2	input scale factors
B	magnetic field strength
B_0	output bias
B_1, B_2	input bias
b	spray nozzle constant
C_D	discharge coefficient
C_D^∞	value of C_D for inviscid flow or value as $R_D \rightarrow \infty$
$(1-C_D)^*$	contribution to $(1-C_D)$ from boundary layer displacement thickness
$(1-C_D)^*_{lam}$	contribution to $(1-C_D)$ from a laminar boundary layer
$(1-C_D)^*_{turb}$	contribution to $(1-C_D)$ from a turbulent boundary layer
c	local plasma sonic velocity
c	speed of light
C_p	constant pressure specific heat
C_g	combustor plasma sonic velocity
d	diameter
d_I	injector nozzle I.D.
E	electric field

NOMENCLATURE (cont.)

E_x	x component of electric field
E_y	y component of electric field
F	Lorentz force
f	frequency
G_c	gravitational constant
h	Planck's constant, 6.626×10^{-27} erg-sec.
j	current density
j_x	x component of current density
j_y	y component of current density
K	MHD loading parameter
k	Boltzman's constant, 1.38×10^{-16} erg/°K
k_0, k_1	constants
L	generator length
ℓ	length of combustion chamber required to achieve 99 percent vaporization
ℓ'	distance from detector to dV
ℓ_c	cylindrical combustor length
ℓ_n	convergent nozzle length
ℓ_0	length of optical energy flow path
M	local Mach number
\dot{M}	mass flow rate
N	number of droplets larger than δ
N	number of seed feeder gear teeth
n_a	number of moles of Al_2O_3 present in combustion products
n_g	number of moles of gaseous combustion products
O/F	oxidizer - fuel mass ratio

NOMENCLATURE (cont.)

P	generator power
\dot{p}	pressure change rate
P_A	partial pressure of Al_2O_3
P_a	Parachor constant
P_c	combustion chamber pressure
P_g	Partial pressure of gaseous combustion products
P_s	Static pressure
P_0	total pressure
P_2	venturi throat static pressure
p	pressure
q	spray nozzle constant
R	universal gas constant
R_d	Reynolds number
R_v	radius of dV
r	nozzle approach radius of curvature
r_m	mass median drop radius
S	nozzle shape factor, A_c/ℓ_n
S_e	Surface energy force (surface tension)
T	static temperature
T_c	critical temperature of propellant
T_I	Initial temperature of propellant
T_s	static temperature
TSFC	thrust specific fuel consumption
T_o	total temperature
t	time
U	velocity

NOMENCLATURE (cont.)

$U(v)$	specific energy density
u	plasma velocity
V	volume
V_C	combustor characteristic velocity
V_{L1}	voltage reference to ground at the grounded end of the load resistance
V_{L2}	voltage referenced to ground at the high end of the load resistance
V_O	output voltage
V_r	relative velocity
V_0	initial droplet velocity
V_1, V_2, V_3	input voltages
W_m	molecular weight
\dot{w}	weight flow rate
\dot{w}_f	fuel mass flow rate
\dot{w}_0	oxidizer mass flow rate
w_1	initial weight
w_2	final weight
α	detector optical acceptance angle
β	pressure exponent = $\frac{\gamma-1}{\gamma}$
γ	ratio of specific heats
δ	droplet diameter
η	latent heat of vaporization
λ	wavelength
ν	frequency

NOMENCLATURE (cont.)

ρ	mass density
σ	plasma electrical conductivity
σ	statistical standard deviation
τ	time period
$d\phi$	energy in dV
ϕ^*/ϕ^*i	ratio of real gas sonic flow function to ideal gas counterpart sonic flow function
χ	power density
ψ	power density incident on the detector
ω	cyclotron frequency
ω_τ	Hall parameter

Section I

INTRODUCTION

This report summarizes the progress and results of the High Energy MHD Fuels Development Program. It presents the development and test of the fuels, a narrative of the dis-assembly of a heat sink and a steady-state MHD power channel.

In the fuel development work an analytical study was performed in which the parameter oc^2 was evaluated wherein liquid fuel (hydrocarbon) type, seed ratio, seed type (cesium carbonate vs cesium nitrate), solid particulate high energy additives, and emulsification combinations were parametrically varied. The emulsification techniques for inclusion of seed and high energy particulates were studied. Fuel spray injection procedures with emulsified fuels were studied and preliminary fuel combustion tests were run. A number of power tests were run using fuels with emulsified seed and/or high energy particulate additives. During the power tests two-point load switching was performed in an attempt to better define the load curve for each fuel.

Facility improvements and modifications were made with the intent to accomplish three objectives:

- 1) To increase data acquisition rate and reliability,
- 2) To more accurately measure and control the flow of propellants, and
- 3) To improve operational safety and test turnaround rate.

All modifications and improvements were fully documented in addition to fully documenting the existing operational systems to reflect the as-modified state of previously altered systems.

Section II

HIGH ENERGY FUELS DEVELOPMENT

1. INTRODUCTION

This discussion describes some considerations which must be applied in the operation of MHD generators at different power levels. Primarily, interest is in the increased power output from MHD generators obtained by varying the fuel combustion characteristics and composition. Subsequently the interest is in fuel physical characteristics required to satisfy the combustion and composition characteristics.

The generalized Ohm's law for conditions encountered in an MHD generator may be written as

$$\mathbf{j} = \sigma \left(\bar{\mathbf{E}} + \bar{\mathbf{u}} \times \bar{\mathbf{B}} \right) - \frac{\omega \tau}{B} \bar{\mathbf{j}} \times \bar{\mathbf{B}} \quad (1)$$

For maximum power density an MHD generator must operate with neutralized Hall current (i.e., $j_x = 0$) [1, 2] so that the component form of Ohm's law becomes

$$j_x = 0 = \sigma (E_x - \omega \tau j_y)$$

$$j_y = \sigma (E_y + uB)$$

Defining the customary loading parameter

$$K = - \frac{E_y}{uB}$$

the term for j_y becomes

$$\mathbf{j} = (1-K) \sigma u \mathbf{B} \quad (2)$$

The output power delivered to the load per unit volume of generator may now be written as

$$\frac{P}{V} = \bar{j} \cdot \bar{E}$$

or

$$\frac{P}{V} = -j_y E_y = K(1-K) \sigma u^2 B^2 \quad (3)$$

Note that for neutralized Hall current $j_x E_x = 0$ so that the above result is the same as that obtained in the absence of Hall effects.

The Lorentz force per unit volume of gas opposes the flow and is given by

$$F = j_y B = (1-K) \sigma u B^2$$

In order for the flow to move against this force it must develop a pressure given approximately by

$$p \sim FL = (1-K) \sigma u B^2 L \quad (4)$$

where L is the generator length.

The relationship of total generator output may be represented by multiplying Eq. (3) by the generator volume AL to get

$$P = K(1-K) \sigma u^2 B^2 AL \quad (5)$$

Equation (4) can be used to eliminate the magnetic field to get the dependence of power upon velocity and pressure

$$P = K u p A \quad (6)$$

From this it is easily seen that to increase the power of an MHD generator it is necessary to increase the operating pressure and/or the flow velocity.

Several comments are in order concerning Eq. (6). First, increasing the flow velocity causes a decrease in the gas static temperature according to $T + u^2/2c_p = \text{const.}$ This decrease in static temperature results in a corresponding decrease in gas conductivity, but in order to maximize power output the product ou^2 should be maximized. This may easily be seen from Eq. (5).

Secondly, the flow velocity must be kept at a high enough level throughout the channel to maintain a high interaction between the gas flow and the magnetic field. This dictates that the flow must be supersonic and that the expansion of the generator channel must be great enough to prevent either shocking to subsonic velocities or choking from the heat addition due to joule dissipation. This second requirement must be compromised with the requirement in the preceding paragraph for scaling purposes: given the generator geometry and B field, the velocity will be assumed constant.

We may now say that the scaling law for a generator, all other things being equal, may be given by

$$P \sim pA \quad (7)$$

which agrees with Rosa [2].

A third comment is pertinent at this point. Under MHD generator conditions the electrical conductivity of the gas is, with reasonable accuracy, inversely proportional to the square root of the gas pressure. The above scaling law assumes that conductivity remains constant. However, there is no reason to assume that the decrease in conductivity due to pressure will be

offset by an increase due to a temperature increase. Consequently, Eq. (7) must be reduced by a factor $(1/p)^{1/2}$ to account for the conductivity decrease due to the higher pressure level. The final scaling law now becomes

$$P \sim (p)^{1/2} A,$$

or with constant geometry

$$P \sim (p)^{1/2}. \quad (8)$$

Noting that for constant cross section and velocity, and that pressure is proportional to the mass flow rate, \dot{M} , then Eq. (8) may be written alternatively

$$P \sim (\dot{M})^{1/2}. \quad (9)$$

Returning to Eq. 5, if the geometry of the generator is fixed along with the magnetic field intensity a variation in power is possible only by maximizing the quantity ou^2 . The plasma velocity, u , is calculated, assuming a fixed inlet nozzle geometry, by $u = Mc$ where M is the local Mach number and c is the local sonic velocity. The parameter c can be easily calculated from

$$\left(\frac{\gamma RT}{W_m} \right)^{1/2} \quad (10)$$

and is related to the combustion sonic velocity by replacing T with

$$\left(1 + \frac{\gamma-1}{2} M^2 \right)^{-1} T_0 \quad (11)$$

The Mach number is dependent upon γ and the nozzle expansion ratio by the equation

$$\frac{A}{A^*} = \frac{1}{M} \left[\left(\frac{2}{\gamma+1} \right) \left(1 + \frac{\gamma-1}{2} M^2 \right) \right]^{\frac{\gamma+1}{2(\gamma-1)}} \quad (12)$$

This relationship is shown graphically for the KIVA-I nozzle exit geometry in Figure 1 with the associated pressure ratio and temperature ratio curves. Now if it is assumed that the effect of γ on Mach number for the various fuels at their respective combustion temperatures is minimal, then, rather than calculating the σu^2 term for each fuel, a comparison can be made based upon σc_0^2 since it is comparable by $\sigma u^2 \sim \sigma c_0^2 M^2$. The Mach number term can be dropped only if comparisons are made and the Mach number is essentially equivalent between fuels at their combustion temperatures. Hence, the fuels studied analytically here have been compared on the basis of σc_0^2 for the sake of simplification of the calculations. It should also be noted that this assumption of minimal γ variation is in error by less than 5% on such radically differing fuels as neat toluene and an emulsion of 30% aluminum at their respective combustion temperatures as will be noted later.

The dependence of the product σu^2 , or as used here, σc_0^2 , on plasma temperature is very strong since both σ and c are favorably affected by increases in temperature. For this reason the first approximation of relative fuel potential lies in its combustion temperature. Comparison of σc^2 will be performed subsequently and will show trends similar to temperature.

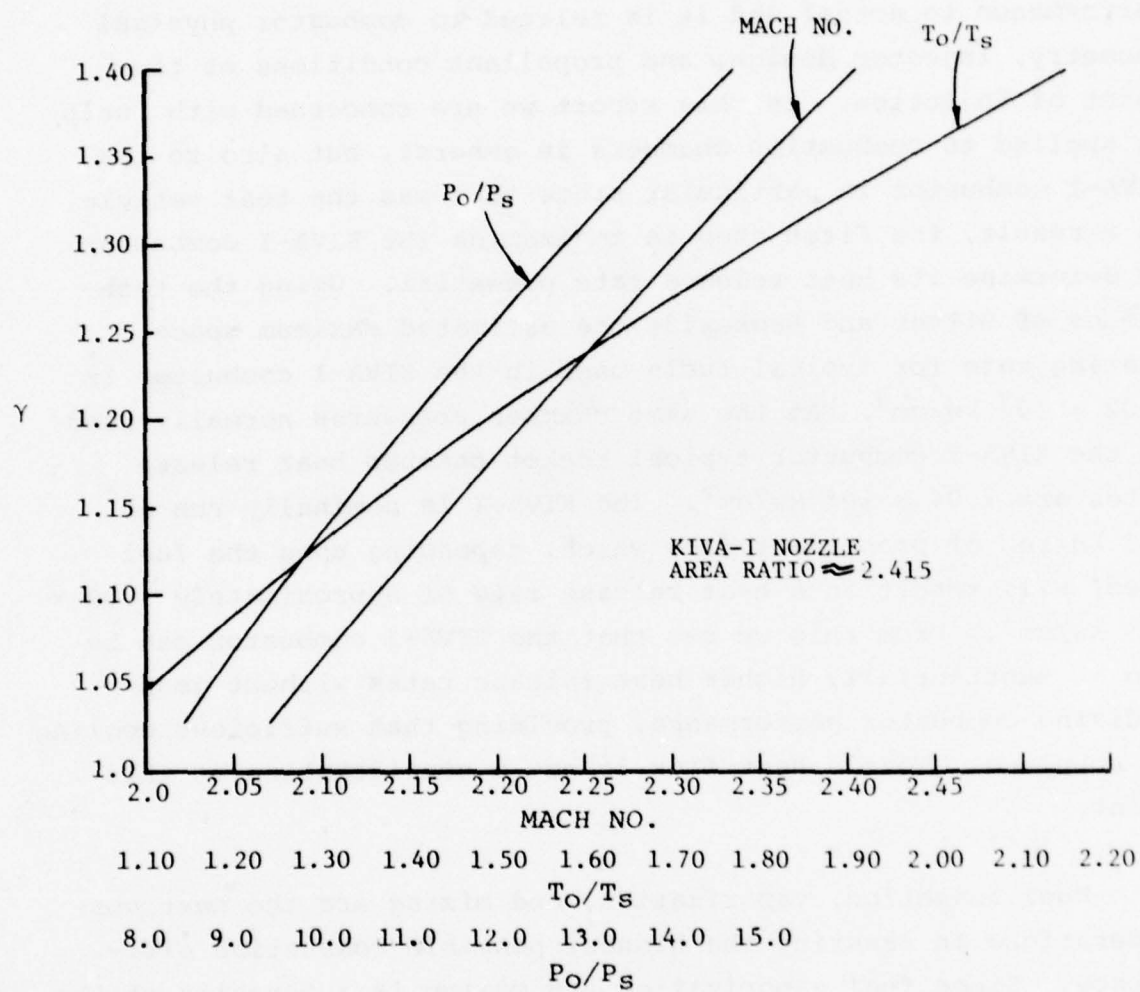


Figure 1. γ Dependency of KIVA - I
 Nozzle Flow Parameters

2. COMBUSTOR REQUIREMENTS

In any combustion chamber the factors determining thermal output are oxidizer and fuel composition, O/F ratio, propellant mass flow rate and combustor efficiency. This last item is an empirically determined parameter which relates the efficiency of a combustor in its ability to convert theoretically potential performance to actual and it is related to combustor physical geometry, injector design, and propellant conditions at the point of injection. In this report we are concerned with fuels as applied to combustion chambers in general, but also to the KIVA-I combustor in particular since that was the test vehicle. As a result, the first step is to examine the KIVA-I combustor to determine its heat release rate potential. Using the techniques of Bitter and Brokaw[3] the estimated maximum space heating rate for typical fuels used in the KIVA-I combustor is 4.02×10^9 kw/cm³. At the same chamber pressures normally used in the KIVA-I combustor typical rocket chamber heat release rates are 7.04×10^3 kw/cm³. The KIVA-I is nominally run at 0.6 kg/sec of propellant flow which, depending upon the fuel used, will result in a heat release rate of approximately 1.02×10^3 kw/cm³. From this we see that the KIVA-I combustor can be run at substantially higher heat release rates without jeopardizing combustor performance, providing that sufficient cooling is supplied. Nozzle heat flux is not a consideration at this point.

Fuel injection, vaporization, and mixing are the next considerations in assuring the highest possible combustion efficiency. Since fuel vaporization and mixing is a function of the fuel injector design, it will be superficially treated along with other aspects of fuel injection.

Injector design is largely empirical since a complete theory for relating design parameters to combustion performance has not been devised; but trends, design rules, and performance

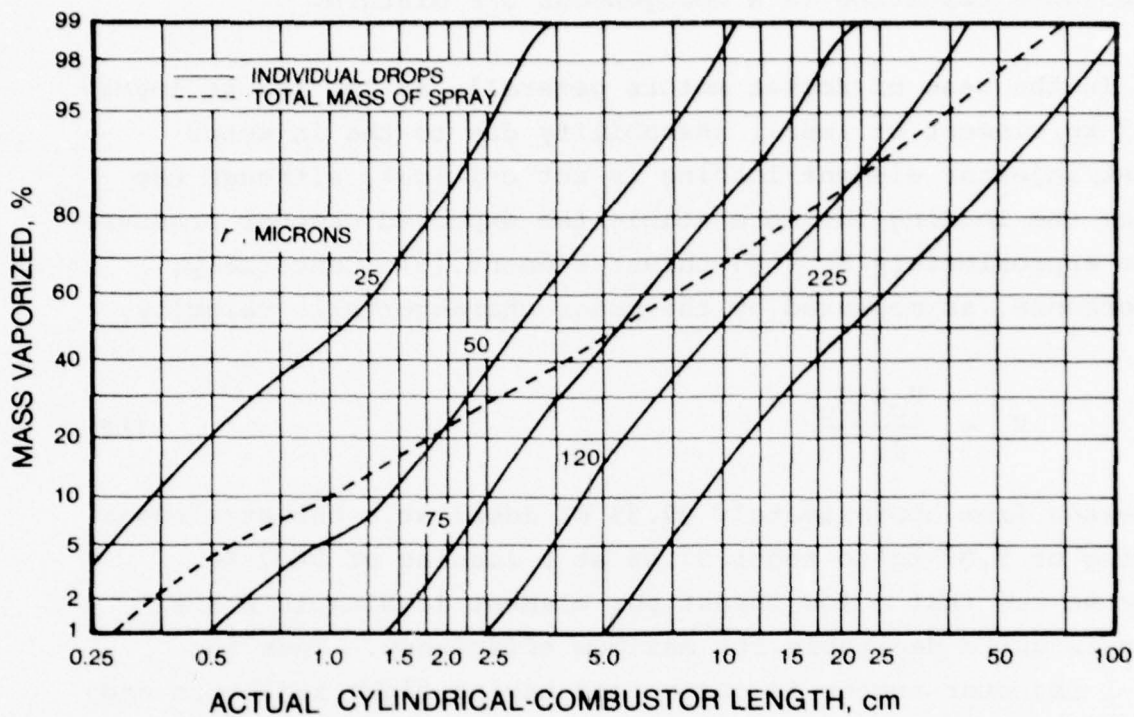
of certain type designs are known and therefore dictate the requirements for various injection systems. The primary function of the injector is to introduce into and meter fuel flow to the combustion chamber in a manner that will atomize and mix the propellants resulting in a homogeneous O/F mixture.

In the case of rocket motors generally at low thrust levels (90.7 kg/element or less), instability due to the injector thrust/injector element loading is not critical, although the higher the loading the more stable the expected chamber pressure up to approximately 90.7 kg thrust/element.[5] Conversely, performance, as measured by the motor characteristic velocity,

$$V_c = \frac{P_c A^* G_c}{\dot{M}} \quad (13)$$

decreases from approximately 99.5% of ideal at a thrust/element loading of 9.07 kg to about 97.5% at a loading of 90.7 kg. Hence we see that a low thrust per element loading in a small motor is quite desirable for maximum efficiency. Thus the KIVA-I injector number is quite good having eight injectors and a theoretical thrust at 10 atm chamber pressure of 106.1 kg for a F/E loading of 13.3 kg.

It has been calculated[6] that a fuel spray consisting of 150 μ m diameter droplets initially moving at 30.5 m/sec requires typically 20.3 cm of travel before 99% of the mass is vaporized. If the spray consists of 50 μ m diameter droplets the combustor length required to achieve 99% vaporization is only 3.81 cm (see Figure 2). In [6] the generalized equation for chamber length to achieve 99% vaporization is:



Mass vaporized of individual drops and total mass of spray

Figure 2. Typical droplet histories for sprays. Initial mass-median drop radius of 75μ ; initial drop velocity of 3000 cm/sec; chamber pressure, 20 atm; initial drop temperature, 278 K; chamber gas temperature, 2780 K.

$$\ell = \left(\frac{\ell_c}{A^{.44}} + \frac{0.83\ell_n}{A^{.22}S^{.33}} \right) \times \frac{(P_0/300)^{.66}}{(1-T_I/T_c)^{.4} \left(\frac{r_m}{.003} \right)^{1.45} \times \left(\frac{V_0}{1200} \right)^{.75}} \\ \times \frac{1}{\left(\frac{\lambda}{140} \right)^{.8} \times \left(\frac{M}{100} \right)^{.35}} \quad (14)$$

Obviously the resultant spray from an injector has a distribution of droplet sizes and has been described by equations of the form[13]

$$\frac{dN}{d\delta} = a\delta^{q-4} e^{-b\delta q}$$

and

$$\frac{dN}{d\delta} = a\delta^2 e^{-b\delta q}$$

both of which predict particle sizes from zero to infinity, and both sizes being unrealistic since there are upper and lower bounds to the possible droplet sizes. However, both equations do accurately predict real sprays and indicate that the probability of occurrence of particles approaches zero as the particle size is increased beyond the size of greatest probability. For triplet injection the spray droplet prediction equation defining mass median drop radius is

$$r_m = 10^{(.62134 \log d_I + 1.906)} \quad (17)$$

assuming an injection jet velocity of approximately 19.81 m/sec achieved with an injector pressure drop of at least

7.03 kg/cm². Although the initial droplet velocity in the KIVA-I combustor is approximately 45.72 m/sec rather than 19.81 m/sec, the use of this equation will result in a conservative estimate of the mean droplet radius, that is, larger than actual. This is a result of an increasing Weber number ($\rho V_r^2 d / S_e$) with increasing liquid jet velocity. Note that the Weber number is the dimensionless ratio of inertia and surface tension forces where numbers above approximately 10 result in droplets shattering into smaller droplets until the forces are balanced. Hence, higher liquid jet velocity will result in smaller droplets. Where S_e , the surface tension, at any temperature up to a reduced temperature of 0.8 can be calculated from the equation,

$$S_e = \left(\frac{P_a}{W_m} \right)^4 \rho \quad (18)$$

where the reduced temperature is the ratio of actual temperature to the critical temperature,

- S_e = surface tension in dynes/cm
- P_a = Parachor, a constant based on molecular structure
- W_m = molecular weight
- ρ = liquid density

When the constant can be calculated from an experimental data point, the error is typically 2-5%.

The most important consideration to be remembered is that vaporization of the fuel is controlled by its heat of vaporization and that the smaller the droplet the less time required to transfer necessary heat to accomplish vaporization.

In the case of the two-phase fuels, considered here to be composed of a solid and a liquid phase, an additional problem occurs in analyzing the combustion characteristics. First, the

liquid fuel shell around the solid particle must be vaporized and subsequently the solid particle surface must be vaporized before combustion can proceed. Secondly, the solid particle temperature can at no time exceed the boiling temperature of the liquid fuel phase until all liquid is vaporized. Although combustion rates of relatively large magnesium and aluminum stationary spheres have been evaluated in the exhaust of rocket motors, no similar evaluation has been made experimentally with particles of the size normally included in a fuel. A Russian reference[7] addressing the problem of two-component fuel combustion stated that it was assumed that temperature gradients within the particle were negligibly small which appears obvious until combustion of the particulates starts, at which time temperature gradients will be extreme. Based on the previous comment concerning vaporization of liquid fuels and considering the vaporization of solid particulates to be controlled by heat of vaporization and heat of solidification, it appears that particles of 40 μ m diameter will vaporize within a combustor length of approximately 20.3 cm in addition to that required to vaporize the liquid phase. The same approach can be applied to the seed particles injected into the combustion chamber to ionize the combustion gases. One major difference is the heat flux, since the vaporized gases of seed particles tend to insulate the particle until washed away from the particle by turbulence, whereas combustion takes place at the interface of the vaporized material and oxidizer in the case of combustible solid particles. This results in a longer period to vaporize completely and to reach equilibrium with the surroundings, for seed particles. An estimate of the residence time is approximately 11-12 msec, or approximately 25.4 cm of combustor length to completely vaporize a 40 μ m particle. At this point it is apparent that a fuel composed of 40 μ m or smaller particles and liquid droplets of no greater than this size or a combination droplet no greater than 70 μ m diameter will be 99% vaporized within the 30.30 cm combustion length of the KIVA-I combustor. From this preliminary and

superficial analysis the fuel injectors of the KIVA-I combustor should, for complete combustion, produce droplets of $<70\mu\text{m}$. It is also apparent that solid fuel and seed particulates should be $<40\mu\text{m}$. To accomplish this the particles should pass a 325 mesh standard sieve. Referring to equation (15), the fuel injector inside diameter required to produce this size particles is .061 cm. Hypodermic tubing of .090 O.D. and .016 wall (.058 I.D.) is in fact available which meets the required minimum I.D., although the smallest injectors existing for the KIVA-I combustor are .084 cm I.D.

3. HIGH ENERGY FUEL POTENTIAL

To evaluate the combustion temperature of a series of possible fuels and baseline fuels of long-standing use, the NASA combustion computer code developed by Gordon and McBride[14] was utilized and combustion temperatures were calculated for a series of pressures. Figures 3 through 9 present the flame temperature of the following seeded fuel mixtures for a number of combustion chamber pressures. Note that all fuel component percentages presented here and subsequently are weight percentages unless otherwise specified.

Toluene and	Cs_2CO_3 (4.22% Cs)
JP-4 and	Cs_2CO_3 (3.90% Cs)
Benzene and	Cs_2CO_3 (4.28% Cs)
Toluene/3% H_2O emulsion and Cs_2CO_3 (4.35% Cs)	
JP-4/3% H_2O emulsion and Cs_2CO_3 (4.02% Cs)	
Benzene/3% H_2O emulsion and Cs_2CO_3 (4.41% Cs)	
Toluene/3% H_2O emulsion and CsNO_3 (4.57% Cs)	

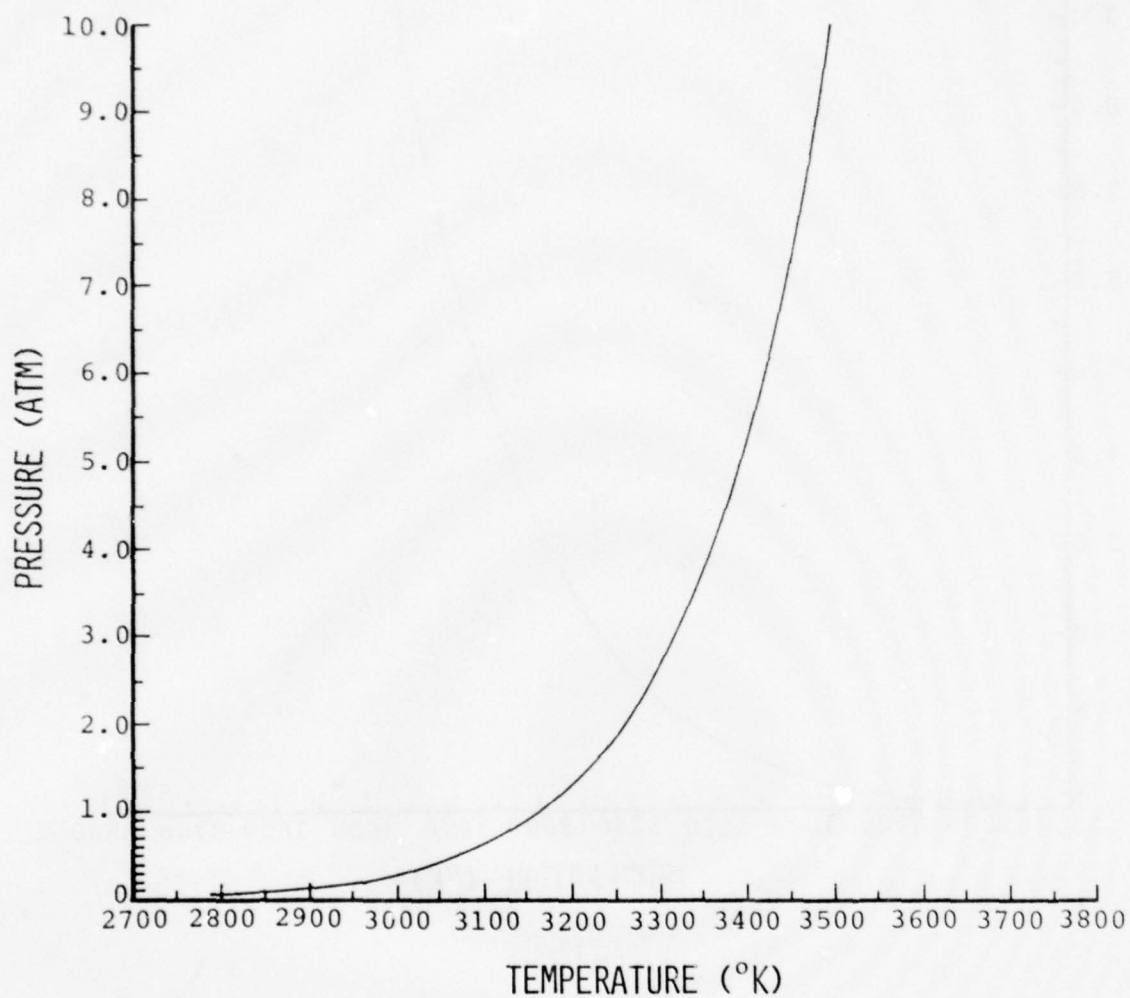


Figure 3. Combustion Temperature of Neat Toluene and Gaseous Oxygen - Cs_2CO_3 Seed (4.22% Cs)

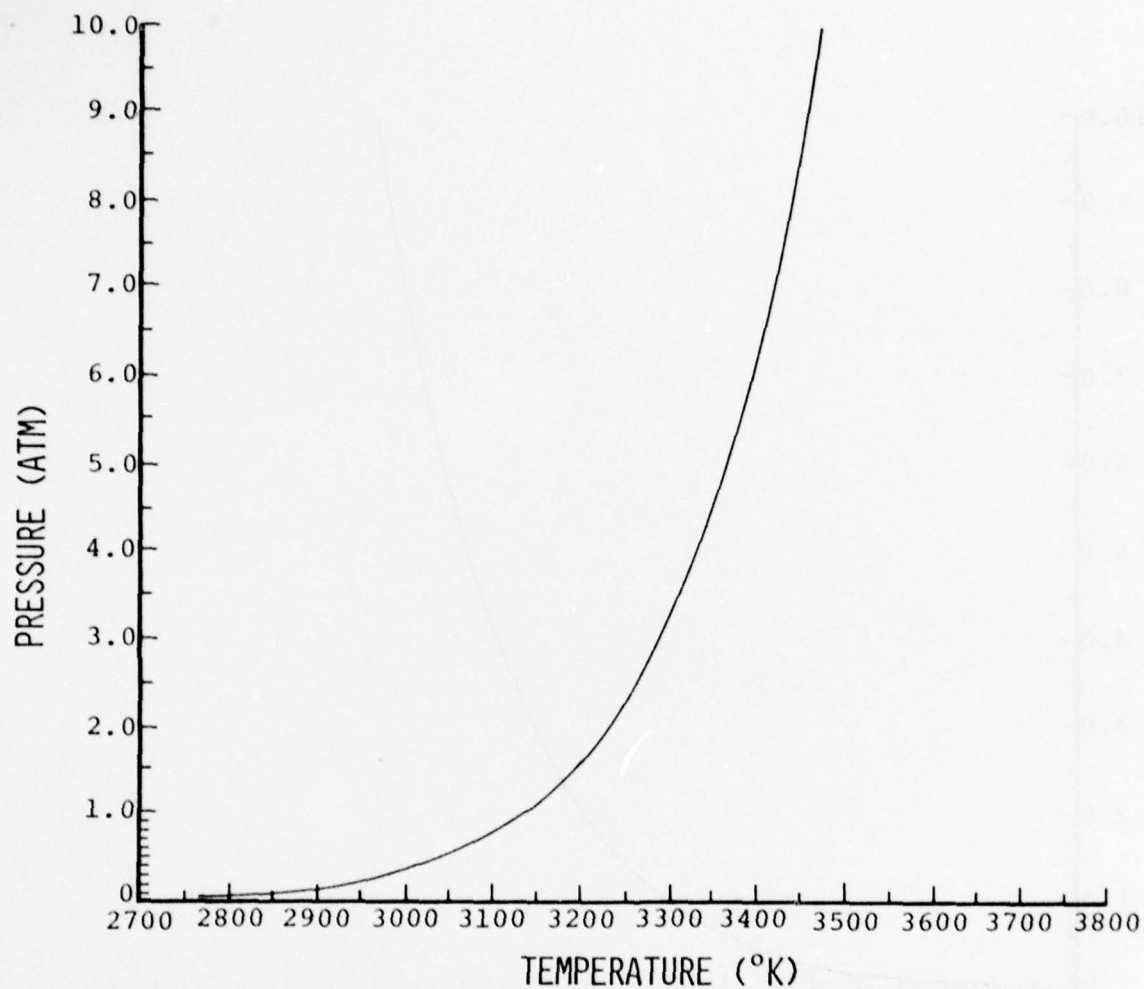


Figure 4. Combustion Temperature of Neat JP-4 and Gaseous Oxygen - Cs_2CO_3 Seed (3.90% Cs)

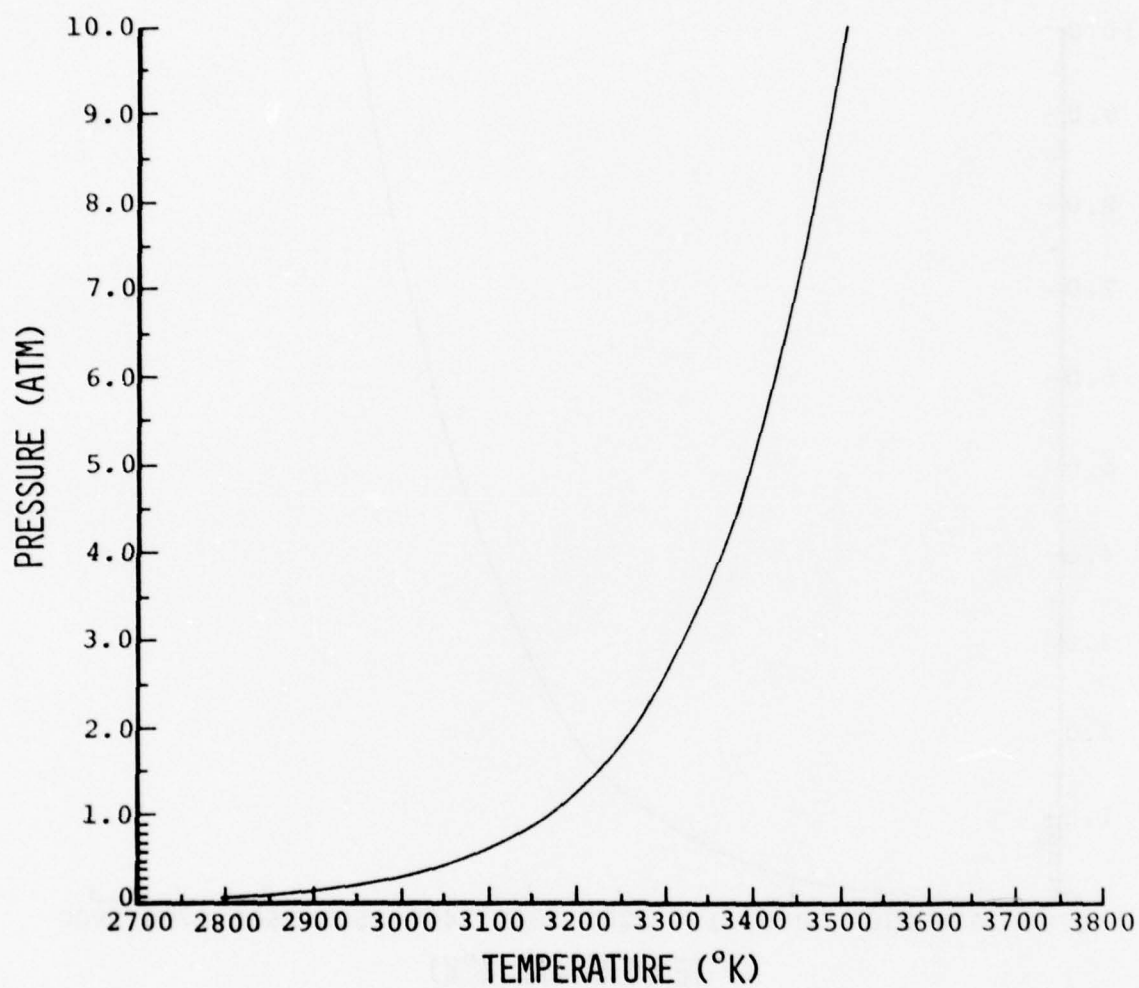


Figure 5. Combustion Temperature of Neat Benzene and Gaseous Oxygen - Cs_2CO_3 Seed (4.28% Cs)

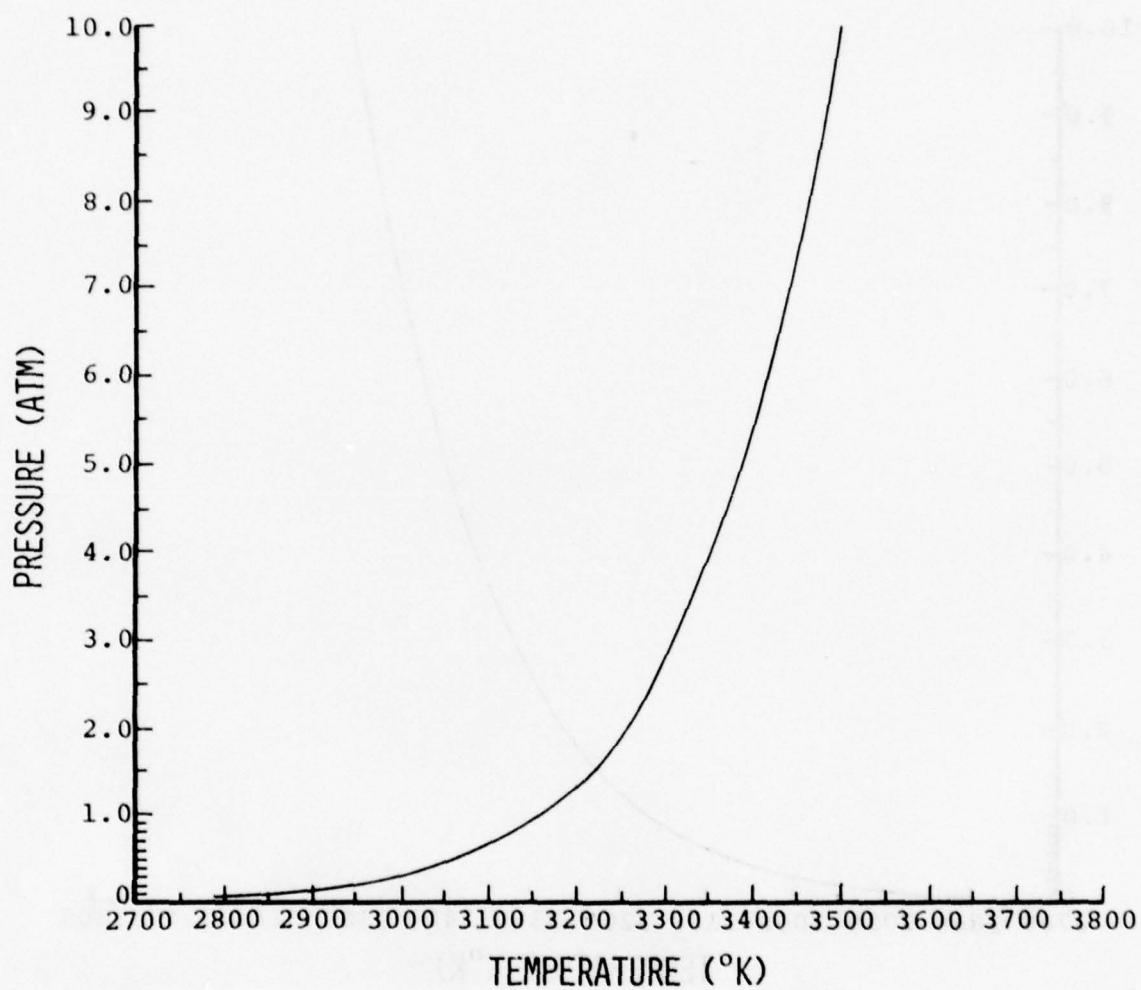


Figure 6. Combustion Temperature of Toluene/3% H₂O Emulsion and Gaseous Oxygen - Cs₂CO₃ Seed (4.35% Cs)

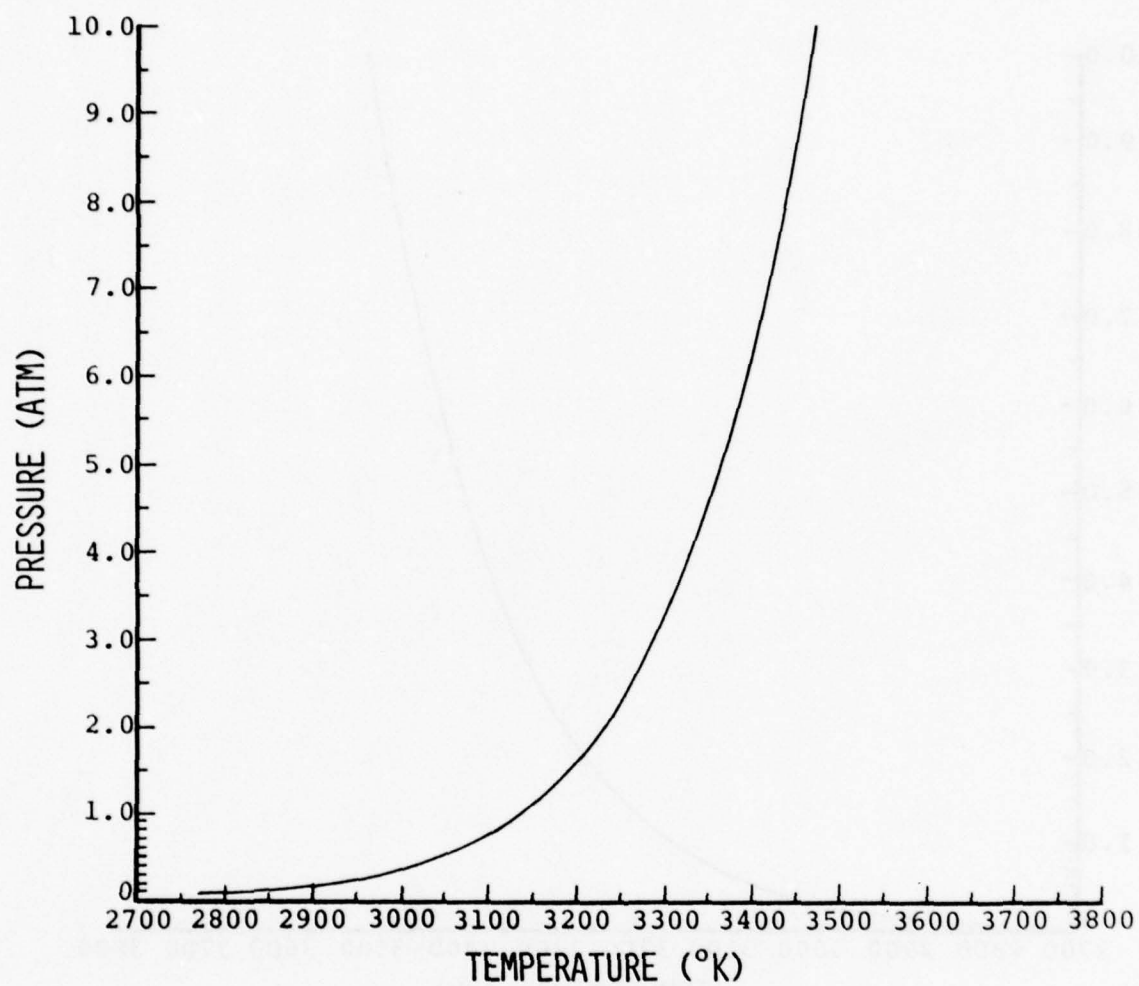


Figure 7. Combustion Temperature of JP-4/3% H₂O Emulsion and Gaseous Oxygen - Cs₂CO₃ Seed (4.02% Cs)

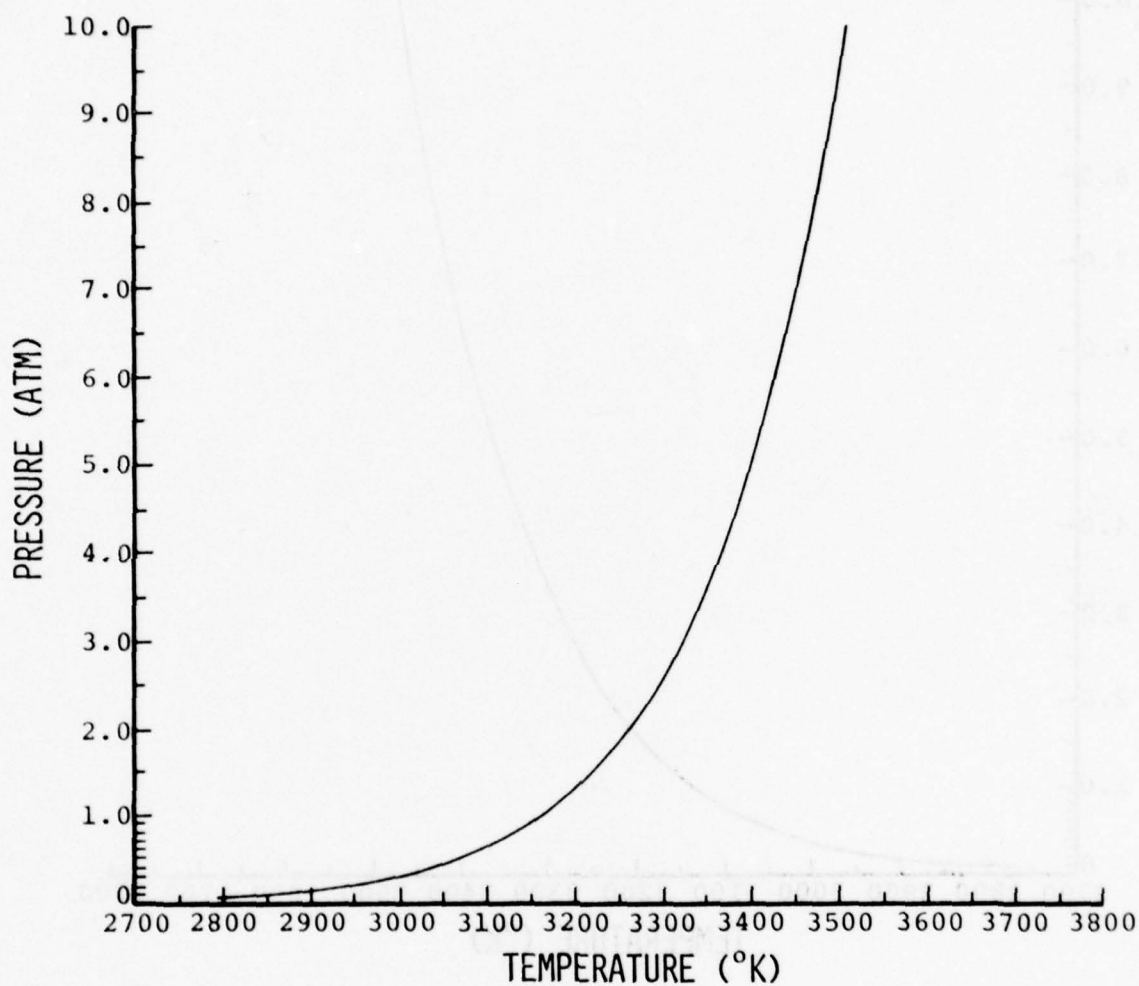


Figure 8. Combustion Temperature of Benzene/3% H₂O Emulsion and Gaseous Oxygen - Cs₂CO₃ Seed (4.41% Cs)

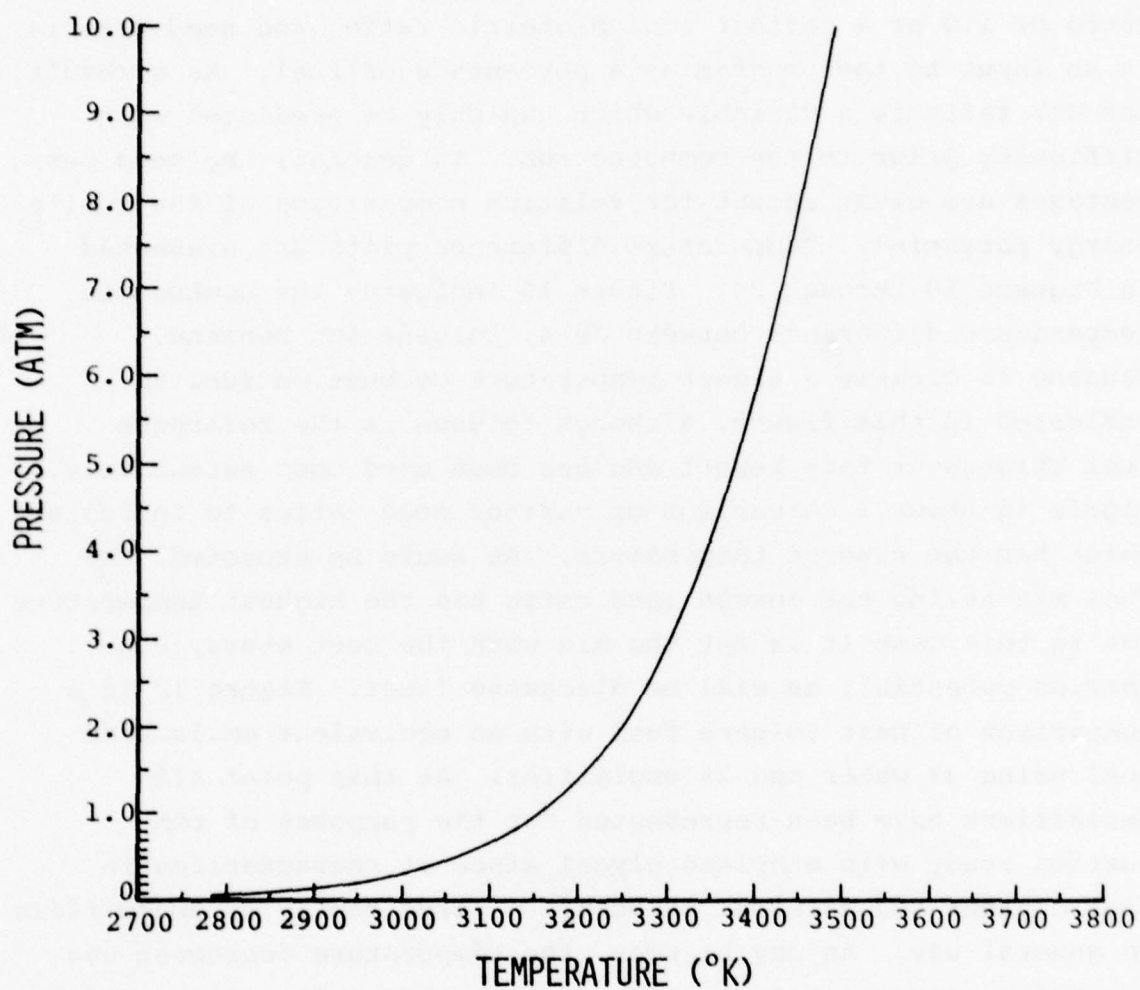


Figure 9. Combustion Temperature of
Toluene/3% H₂O Emulsion and
Gaseous Oxygen - CsNO₃ Seed
(4.57% Cs)

As may be noted, although the cesium percentage of total propellant is variable, the cesium percentage of fuel or propellant exclusive of oxidizer is a fixed 15%. Obviously, it would be desirable to compare the fuels with a constant seed percentage of total propellant but this would have taken more time than was available since the computer was run with a fixed equivalence ratio of 1.0 or a perfect stoichiometric ratio, and seed material is an input to the program as a percentage of fuel. As a result, the O/F ratio is a variable which can only be predicted with difficulty prior to the computer run. In general, the seed percentages are close enough for relative comparisons of the fuel's energy potential. Temperature difference plots are presented in Figures 10 through 24. Figure 10 indicates the combustion temperature difference between JP-4, toluene and benzene. Benzene is clearly a higher temperature combustion fuel as indicated in this figure, although toluene is the reference fuel throughout this report and has been used most extensively. Figure 11 shows a comparison of various seed ratios to indicate which has the highest temperature. As would be expected, the fuel mix having the lowest seed ratio has the highest temperature but in this case it is not the mix with the best energy conversion potential, as will be discussed later. Figure 12 is a comparison of neat toluene fuel with an equivalent emulsified fuel using 3% water and 2% emulsifier. At this point all emulsifiers have been represented for the purposes of combustion study with ethylene glycol since it characterizes in heat content and chemical structure a large family of emulsifiers in general use. As may be seen, the temperature decrement was generally approximately 1-2° K, or less than 0.1%. Figure 13 is a comparison of emulsified JP-4, toluene, and benzene and, as expected, shows the same results as the equivalent Figure 10 which compares the neat fuels. Figure 14 is an interesting plot from the standpoint of seed handling vs performance. This comparison is between an emulsified toluene fuel seeded with both Cs_2CO_3 and CsNO_3 at the rate of 15% Cs in the fuel. The

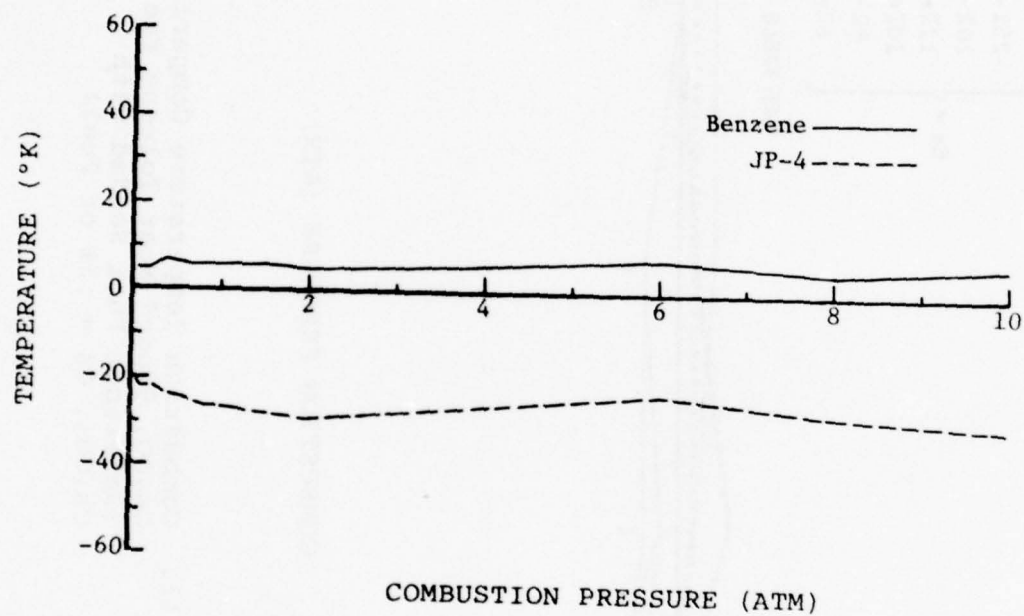


Figure 10. Combustion Temperature Comparison (Reference Fuel - Neat Toluene)

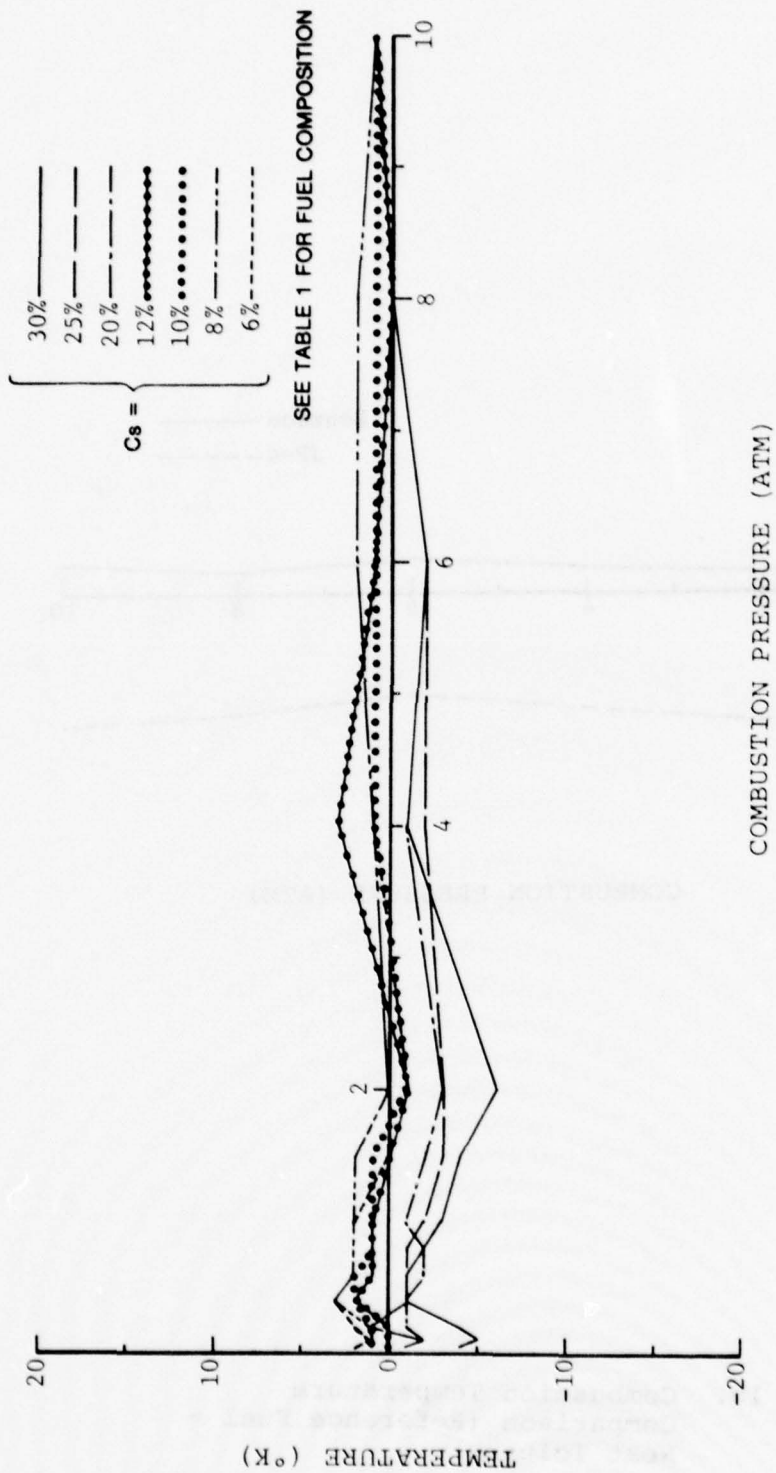


Figure 11. Combustion Temperature Comparison
 Cs_2CO_3 Seeded Neat Toluene Fuel
 (Reference Fuel Seeded with
 Cs_2CO_3 , Cs = 15% of Fuel)

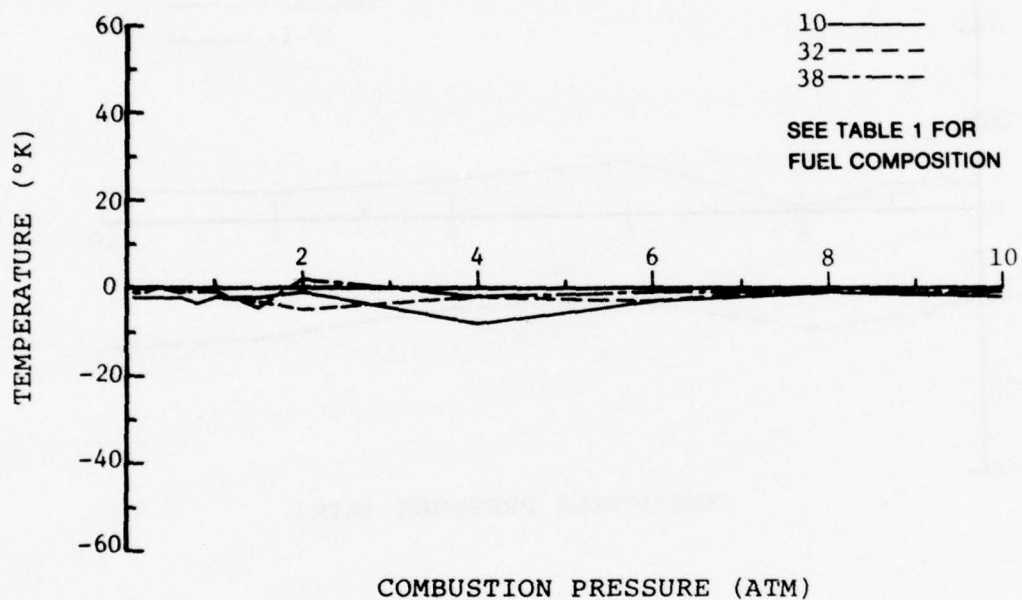


Figure 12. Combustion Temperature Comparison of Emulsified Fuels Seeded with Cs_2CO_3 , Cs = 15% of Fuel - (Reference Fuel - Neat Toluene + 15% Seed)

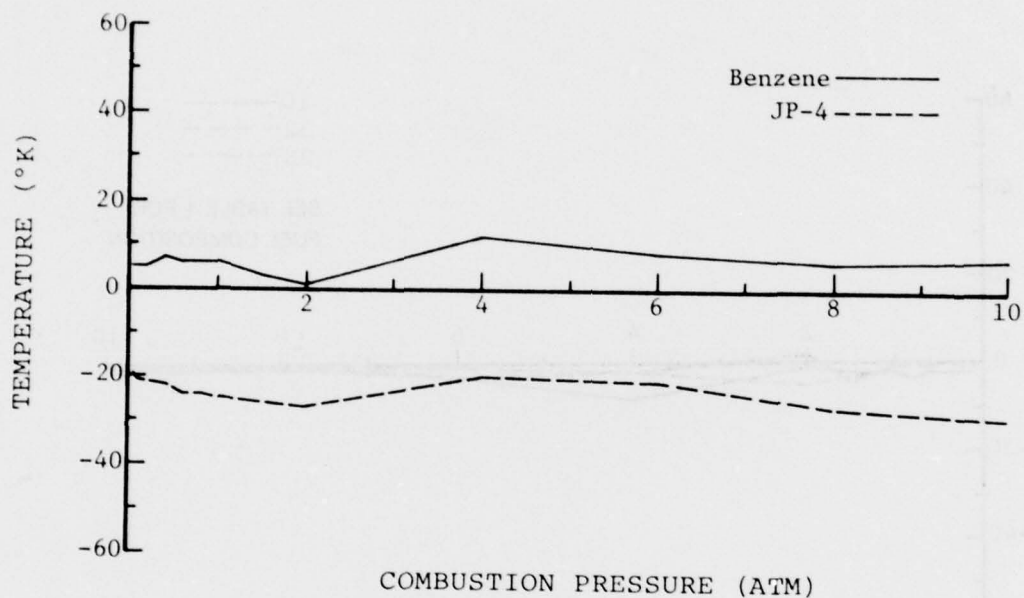


Figure 13. Combustion Temperature Comparison of Emulsified Fuels Seeded with Cs_2CO_3 , Cs = 15% of Fuel - (Reference Fuel - Emulsified Toluene, 15% Seed)

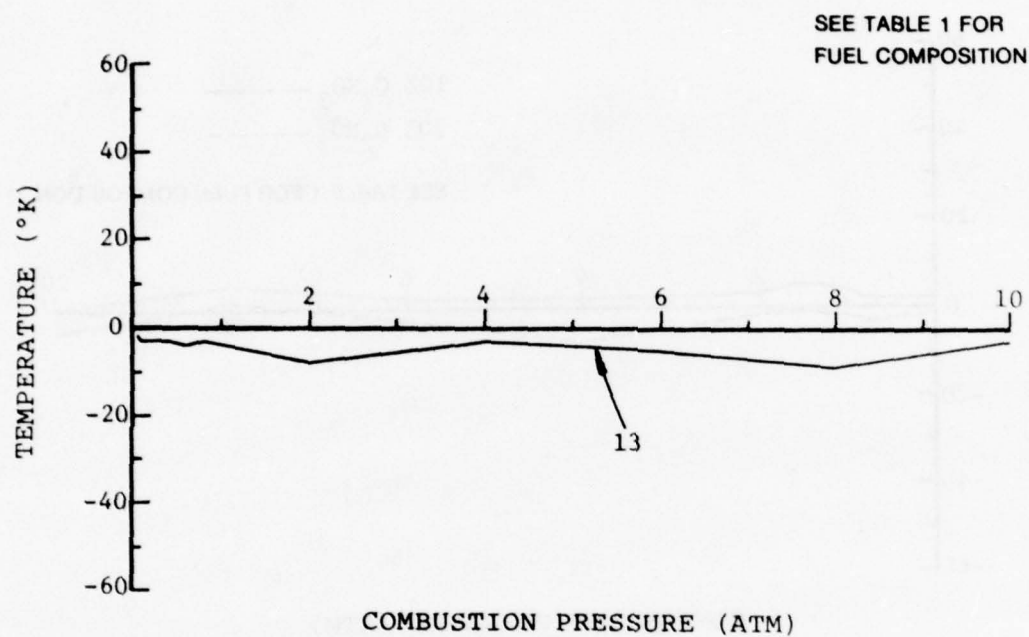


Figure 14. Combustion Temperature Comparison of Toluene Emulsion Fuel Seeded with CsNO_3 and Cs_2CO_3 , Cs = 15% of Fuel - (Reference Fuel Seed - Cs_2CO_3)

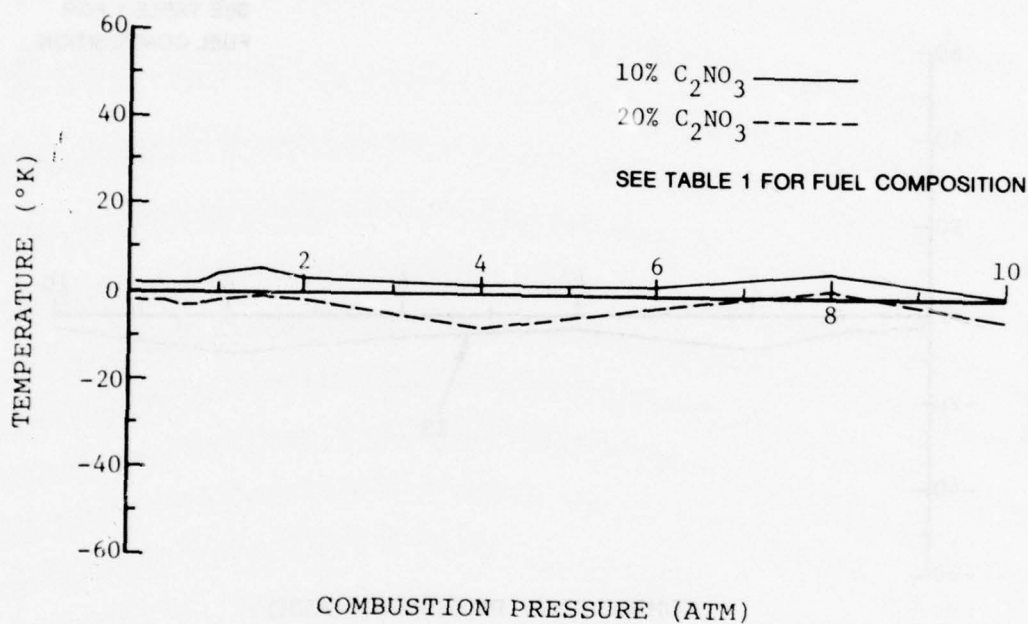


Figure 15. Combustion Temperature Comparison of Emulsified Toluene Fuel Seeded with $CsNO_3$ - (Reference Fuel - Seeded with $CsNO_3$, Cs = 15% of Fuel)

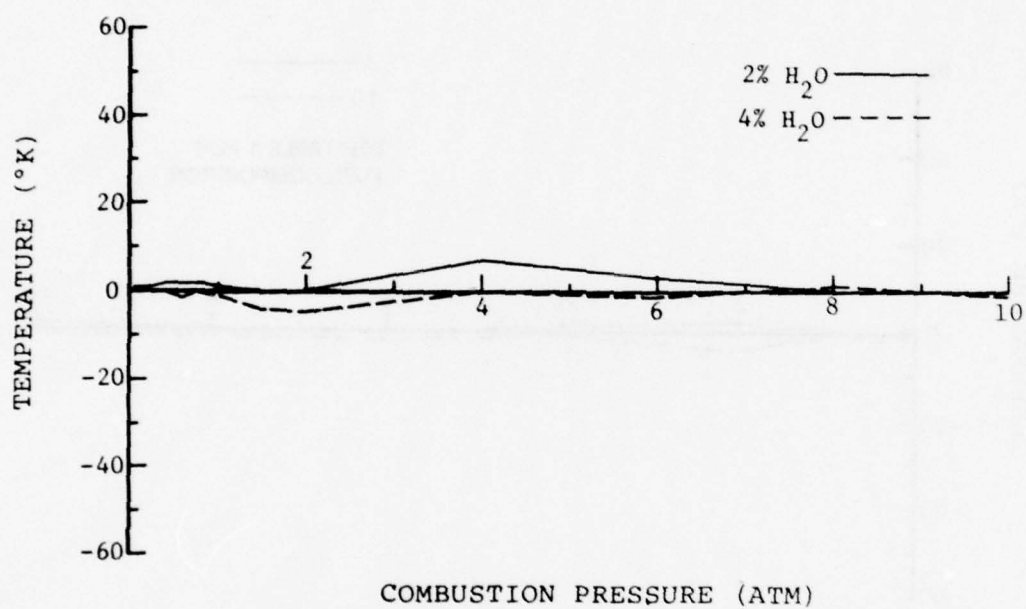


Figure 16. Combustion Temperature Comparison of Emulsified Toluene Fuel with Varying H₂O% Seeded with Cs₂CO₃, Cs = 15% of Fuel - (Reference Fuel Contains 3% H₂O)

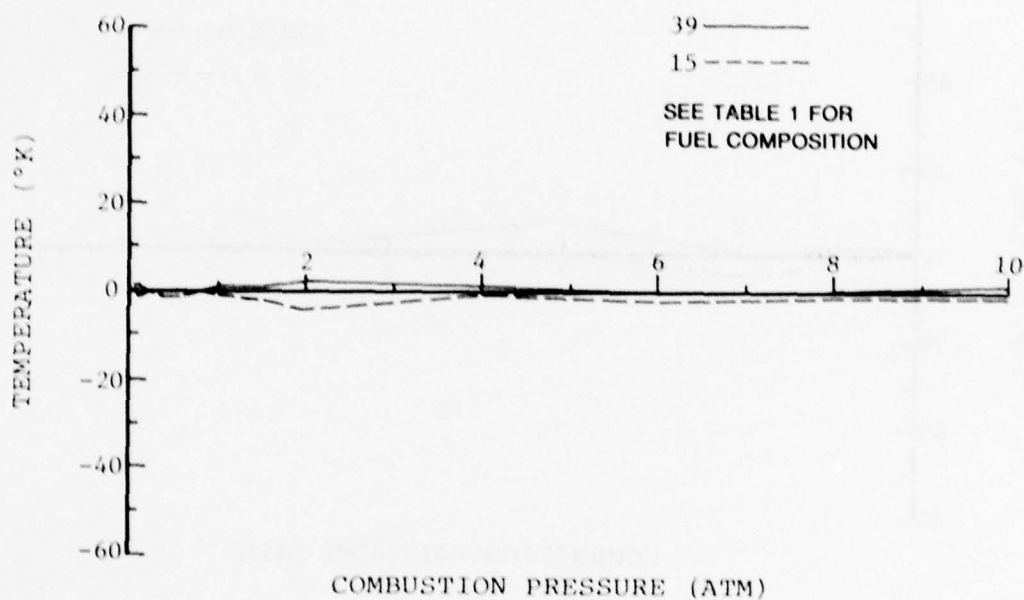


Figure 17. Combustion Temperature Comparison of Waterless Emulsion Seeded with Cs_2CO_3 , Cs = 15% of Fuel - (Reference Fuel - Toluene/3% H_2O Emulsion, 15% Seed)

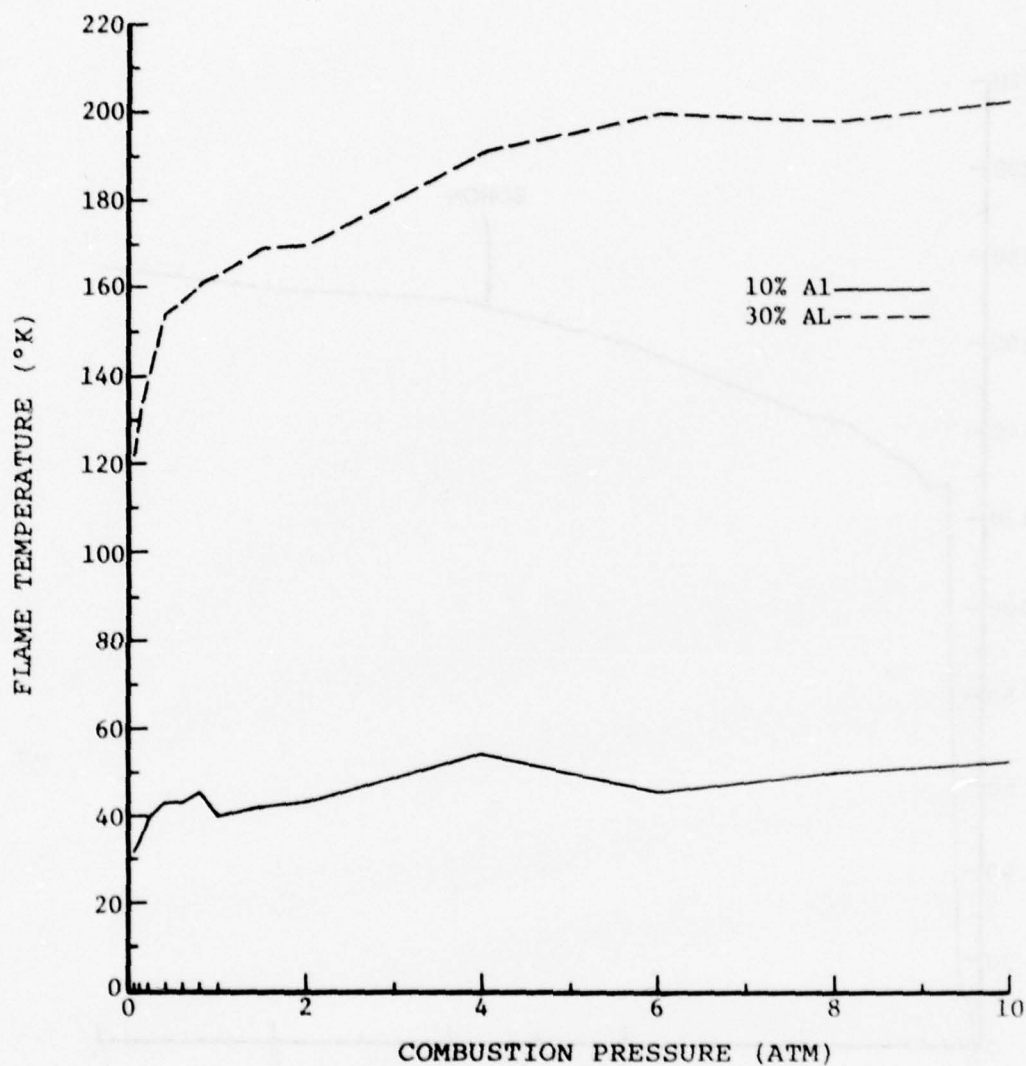


Figure 18. Combustion Temperature Comparison of Toluene/Aluminum Emulsion Fuels Seeded with Cs_2CO_3 , Cs = 15% of Fuel - (Reference Fuel - Emulsified Toluene, 15% Seed)

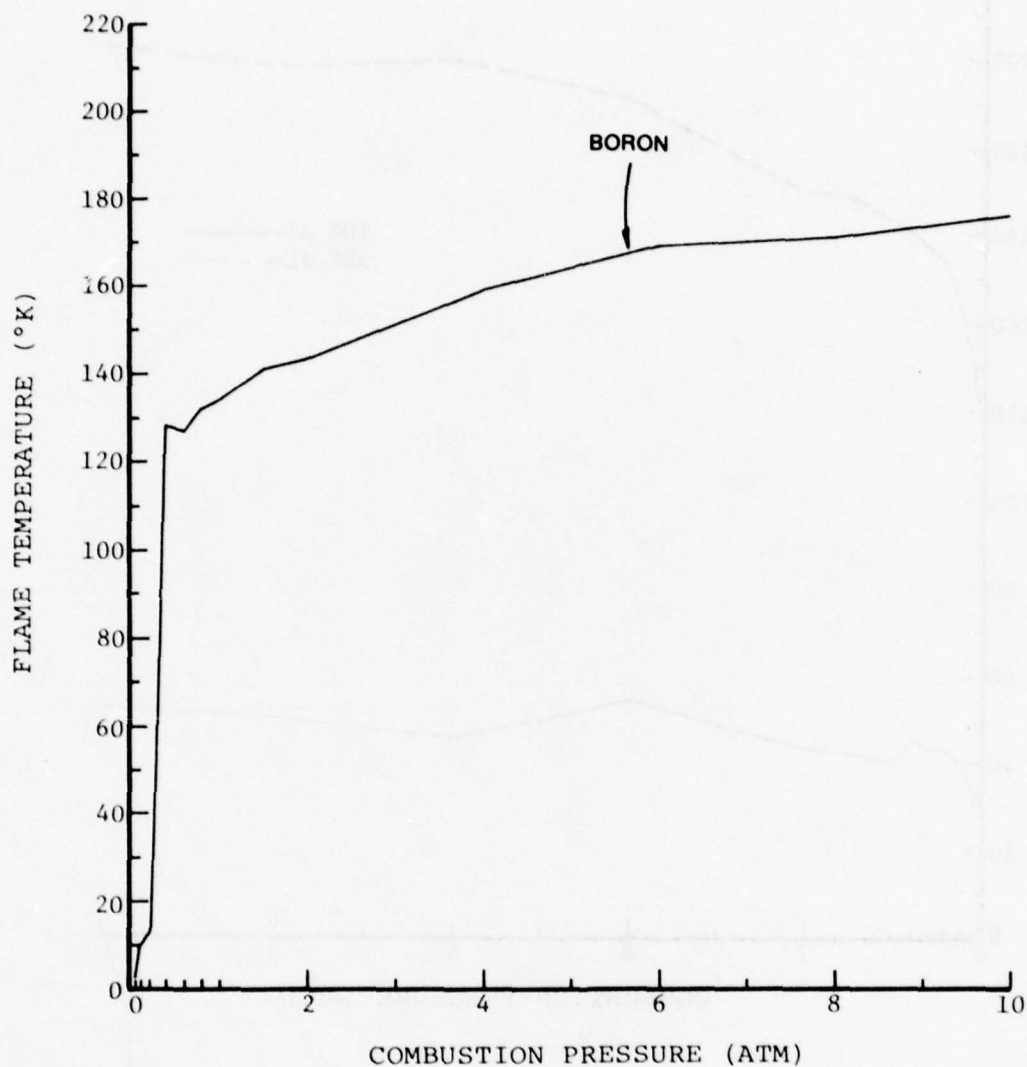


Figure 19. Combustion Temperature Comparison of Toluene/Boron Emulsion Seeded with Cs_2CO_3 , Cs = 15% of Fuel - (Reference Fuel - Emulsified Toluene 15% Seed)

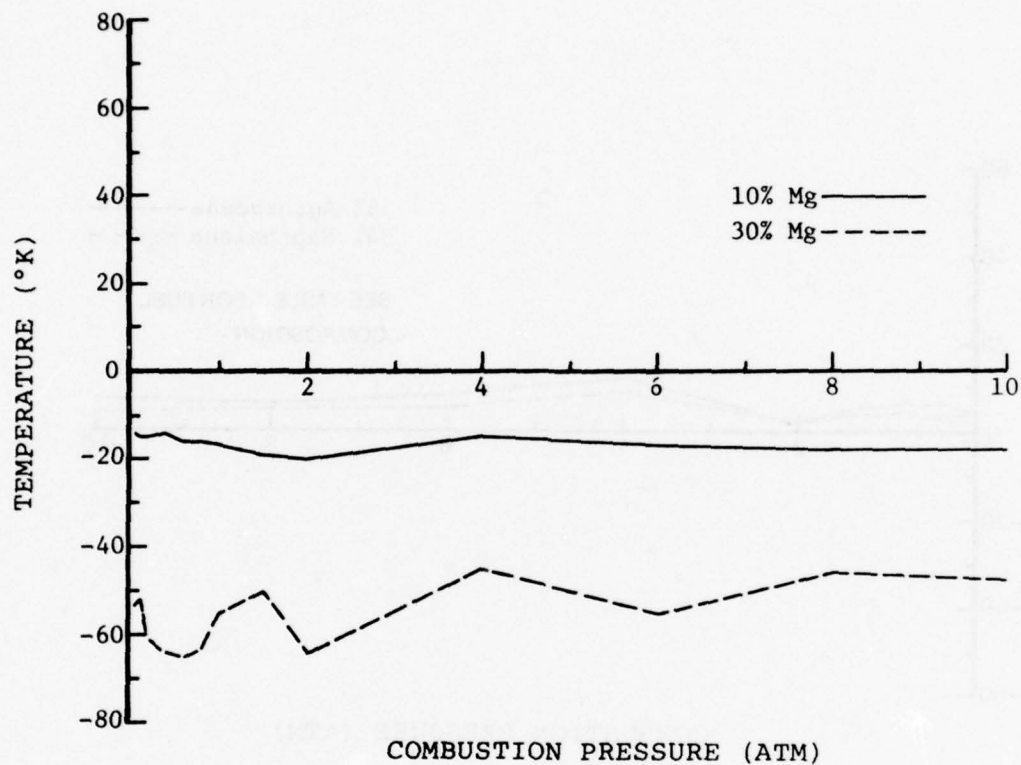


Figure 20. Combustion Temperature Comparison of Toluene/Magnesium Emulsion Seeded with Cs_2CO_3 , Cs = 15% of Fuel - (Reference Fuel - Emulsified Toluene, 15% Seed)

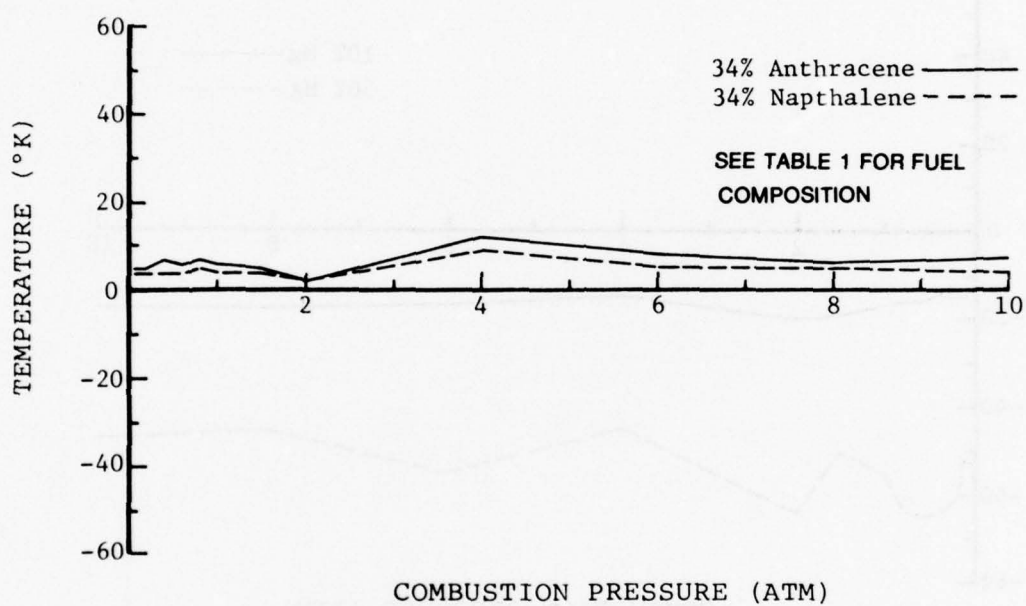


Figure 21. Combustion Temperature Comparison of High C/H Ratio Emulsified Fuels Seeded with Cs_2CO_3 , Cs = 15% of Fuel - (Reference Fuel - Emulsified Toluene, 15% Seed)

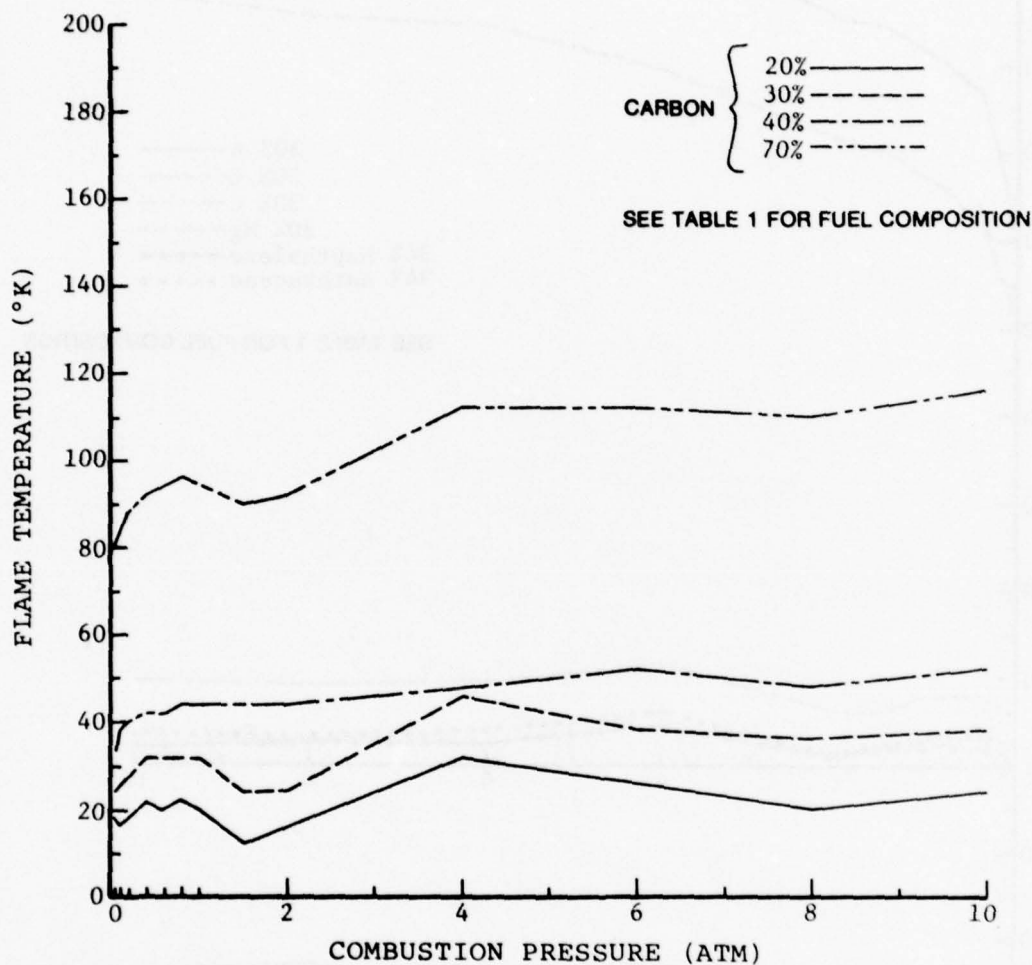


Figure 22. Combustion Temperature Comparison of Emulsified Carbon Fuels Seeded with Cs_2CO_3 , Cs = 15% of Fuel - (Reference Fuel - Emulsified Toluene, 15% Seed)

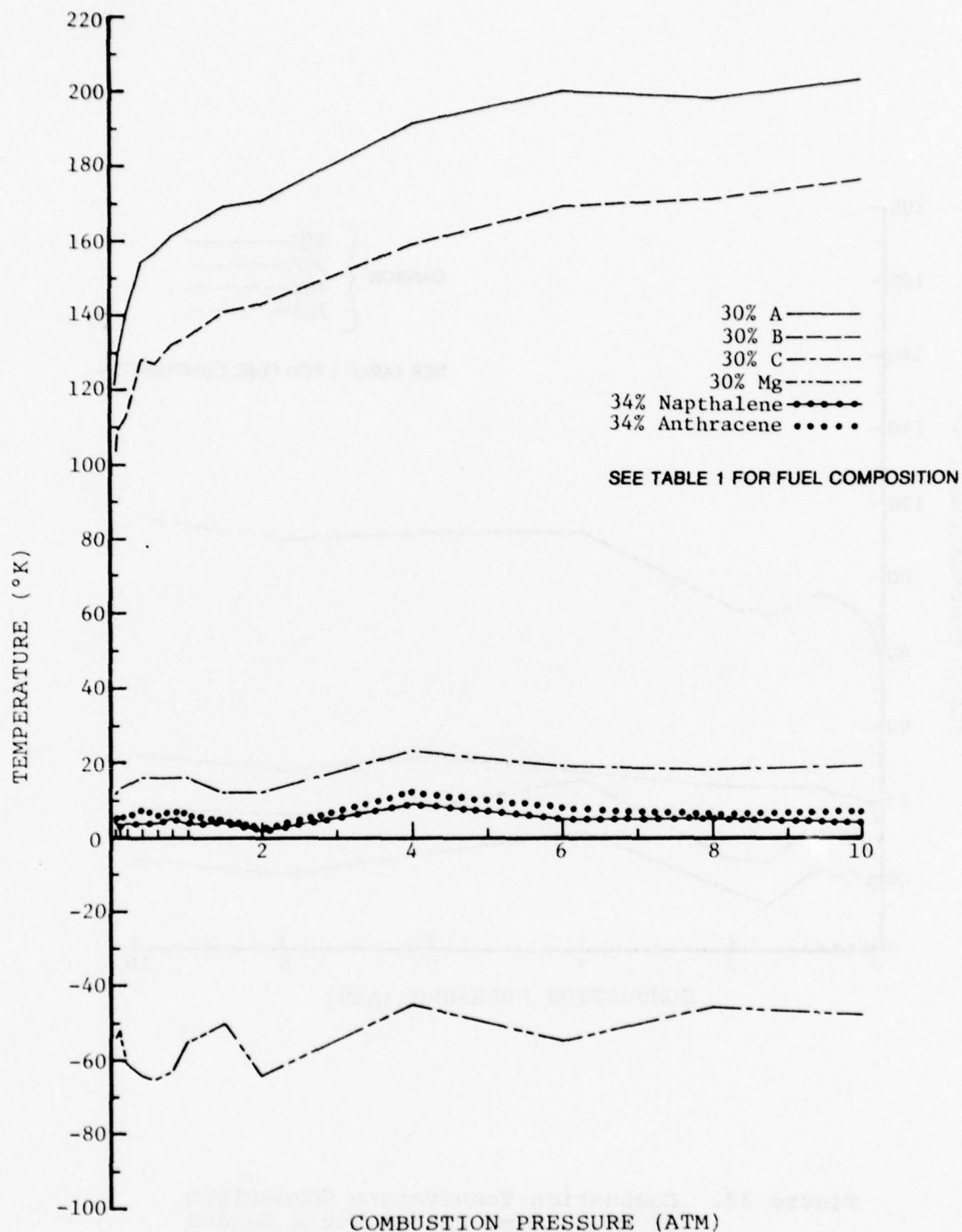


Figure 23. Combustion Temperature Comparison of Emulsified Toluene/and Solid Particulate Fuels Seeded with Cs_2CO_3 , Cs = 15% of Fuel - (Reference Fuel - Emulsified Toluene, 15% Seed)

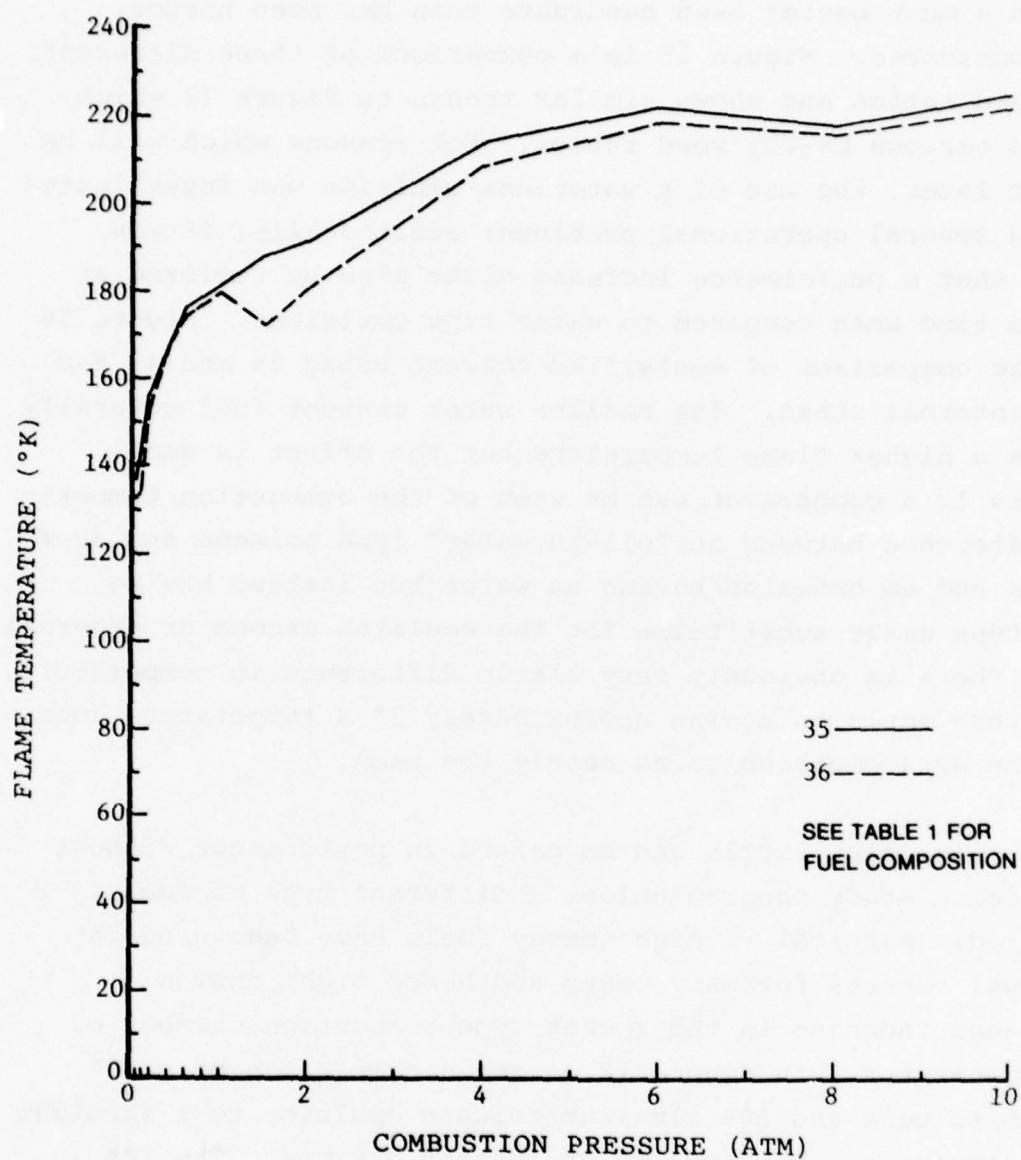


Figure 24. Combustion Temperature Comparison of Emulsified Benzene/Napthalene/Aluminum Fuels Seeded with Cs_2CO_3 , Cs = 15% of Fuel - (Reference Fuel - Emulsified Toluene, 15% Seed)

figure shows an average temperature loss of 4.3° K and a median of 3° K which is less than might be normally expected. As will be seen later, the σc^2 curve is even closer, indicating that CsNO_3 is a much better seed candidate than has been historically considered. Figure 15 is a comparison of three different CsNO_3 seed ratios and shows similar trends to Figure 11 which compared various Cs_2CO_3 seed ratios. For reasons which will be apparent later, the use of a waterless emulsion was investigated to solve several operational problems; additionally, it was thought that a performance increase might also be realized at the same time when compared to water type emulsions. Figure 16 shows the comparison of emulsified toluene using 2% and 4% H_2O as the internal phase. The smaller water content fuel naturally produces a higher flame temperature but the effect is small. In Figure 17 a comparison can be seen of the combustion temperature difference between an "oil-in-water" type toluene and JP-4 emulsion and an emulsion having no water but instead having glycol type water substitutes for the emulsion second or external phase. There is obviously very little difference in temperature, the toluene emulsion having approximately 1° K temperature loss while the JP-4 emulsion gains nearly the same.

At this point little can be gained in performance without an extensive study program unless a different type of fuel is considered. Particulate high energy fuels have been used in solid fuel rockets for many years and hence might show a performance increase in the rocket type combustion chamber of an MHD generator. In Figure 18 we see a comparison of a 10% aluminum/toluene and 30% aluminum/toluene emulsion to a straight toluene emulsion. The results are rather obvious. The 10% aluminum emulsion improves the temperature between 30° and 50° K while 30% aluminum increases combustion temperature from 120° to 200° K. The next particulate fuel examined was boron in Figure 19. Results here are nearly as dramatic but show an interestingly low temperature increase at low pressures. At

the combustion pressures of greatest interest, 6 to 10 atm, the temperature increase is approximately 170° K. Magnesium has long been a constituent of flares and other pyrotechnic devices and was therefore a logical candidate additive. Figure 20 shows the results of 10% magnesium/toluene and 30% magnesium/toluene emulsions compared to a straight toluene emulsion. Here the results are curiously negative, with increasing loss of temperature with increasing percentages of magnesium. We see that 10% magnesium decreases the combustion temperature from 15° to 20° K while a 30% magnesium emulsion decreases temperature between 40° and 60° K. Since the results of changing from toluene (methyl benzene) with a chemical formula of C_7H_8 to benzene (C_6H_6) yielded an increase in temperature it was reasoned that perhaps the use of other increased carbon content fuels too might yield the same gains. Again the results were an increase in temperature, but increases were the same, 5° - 8° K, when using a saturated solution emulsion of 34% naphthalene or 34% anthracene as when comparing toluene to benzene. Figure 21 shows only a 4.5° K average increase for naphthalene and 6.2° K increase for anthracene. Although not shown here, emulsions of naphthalene and anthracene with benzene yield temperature increases of 3° and 4° K respectively over straight benzene emulsions. Extending the previous logic it was decided that there might be profit in burning solid carbon particulates. The use of 20%, 30%, 40% and 70% carbon fuels was examined next. In Figure 22 we see the anticipated temperature increases with 20% yielding an average increase of 10° K. For carbon percentages of 30%, 40% and 70% we find temperature increases of 15° K, 22° K, and 48° K respectively. Figure 23 shows the comparative improvement to be expected by 30% mixtures of Al, Mg, B, C, naphthalene and anthracene. The final temperature difference curve, Figure 24, shows a comparison of a 30% aluminum/benzene/naphthalene "oil-in-water" emulsion and an equivalent waterless emulsion to a straight toluene emulsion. The result is that, based on combustion temperature only, the

"oil-in-water" emulsion of 30% aluminum/benzene/naphthalene has the highest combustion temperature increase of the fuel combinations considered, 225° K.

As mentioned previously, combustion temperature gives a strong indication of the potential for MHD energy conversion, but the controlling parameter is in reality σc^2 . For purposes of convenience already discussed, σc^2 has been used which is an equivalent parameter for comparison purposes. Figures 25 through 39 show logarithmic displays of σc^2 at the combustion temperatures of each particular fuel mixture vs combustion pressure. The plots are arranged with the same comparison already discussed. The only major surprise is in Figure 34 where the combustion temperature of boron emulsion was not quite as high as that of an equivalent aluminum emulsion. When compared on the basis of σc^2 , boron is a better additive by an average of 1.4% and by nearly 4% in the 6 to 10 atm pressure range. In Figure 29, as previously noted, the effect of σc^2 for Cs_2CO_3 vs CsNO_3 is not as favorable to Cs_2CO_3 as previously thought. In this figure we see only 1.2% average loss in the use of CsNO_3 .

Figure 25, as in Figure 10, shows a small but significant increase in σc^2 for a benzene fuel over the use of toluene. Although JP-4 is a readily available and easy fuel to work with, this figure shows a very significant loss of potential power conversion as compared to benzene or even toluene. From this figure it would appear that the use of JP-4, except as a test fuel to work out other non-fuel associated MHD development problems, would be ruled out and toluene, or preferably benzene since it shows ~ 5% improvement in output power (σc^2), become the fuel of preference. This is true even recognizing the problems and health hazard associated with benzene operations. Problems of this type can be eliminated through adaptive design and operating procedures.

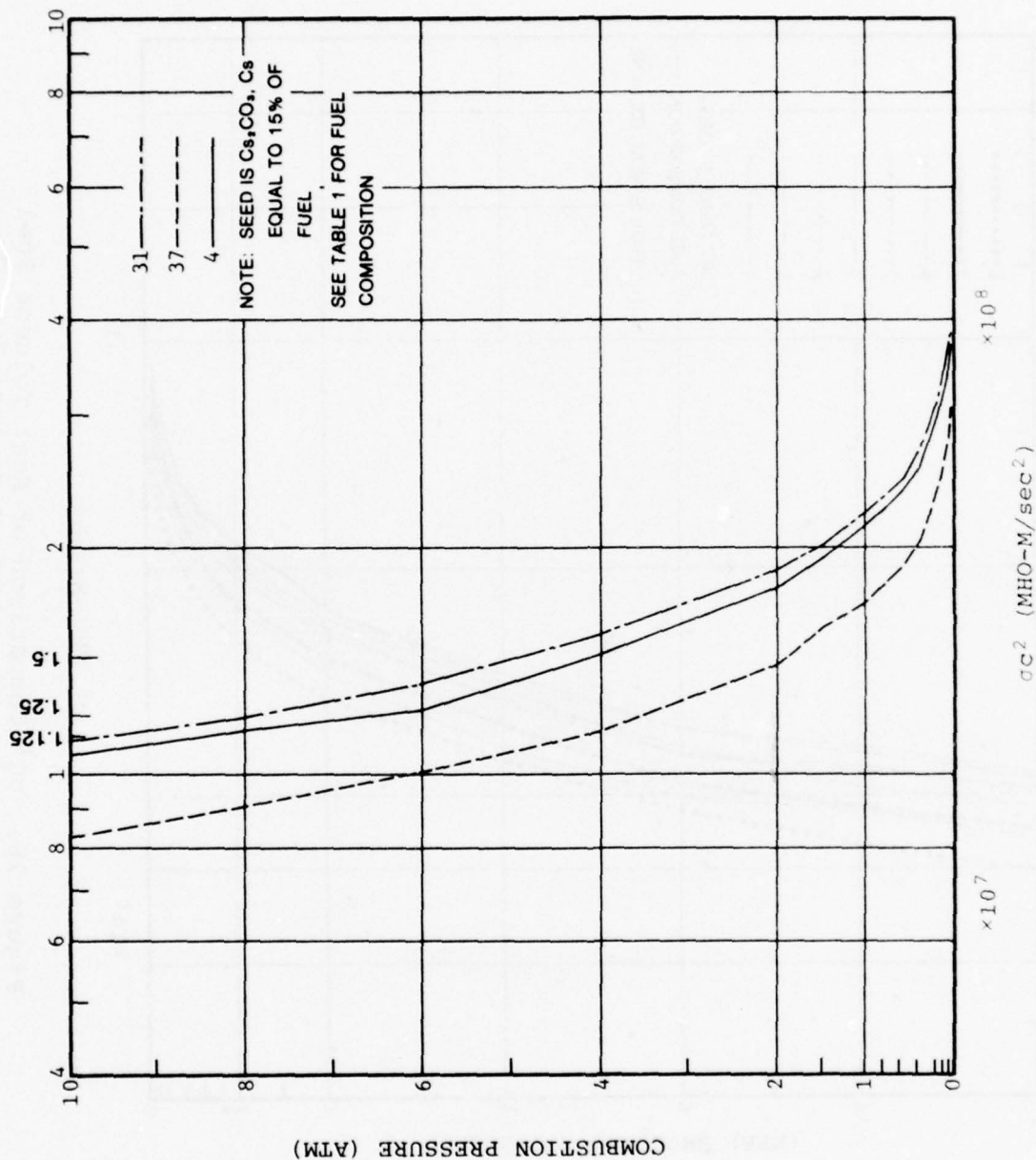


Figure 25. σ_{C^2} Comparison of Neat JP-4, Toluene, and Benzene Fuels with Cs_2CO_3 Seed

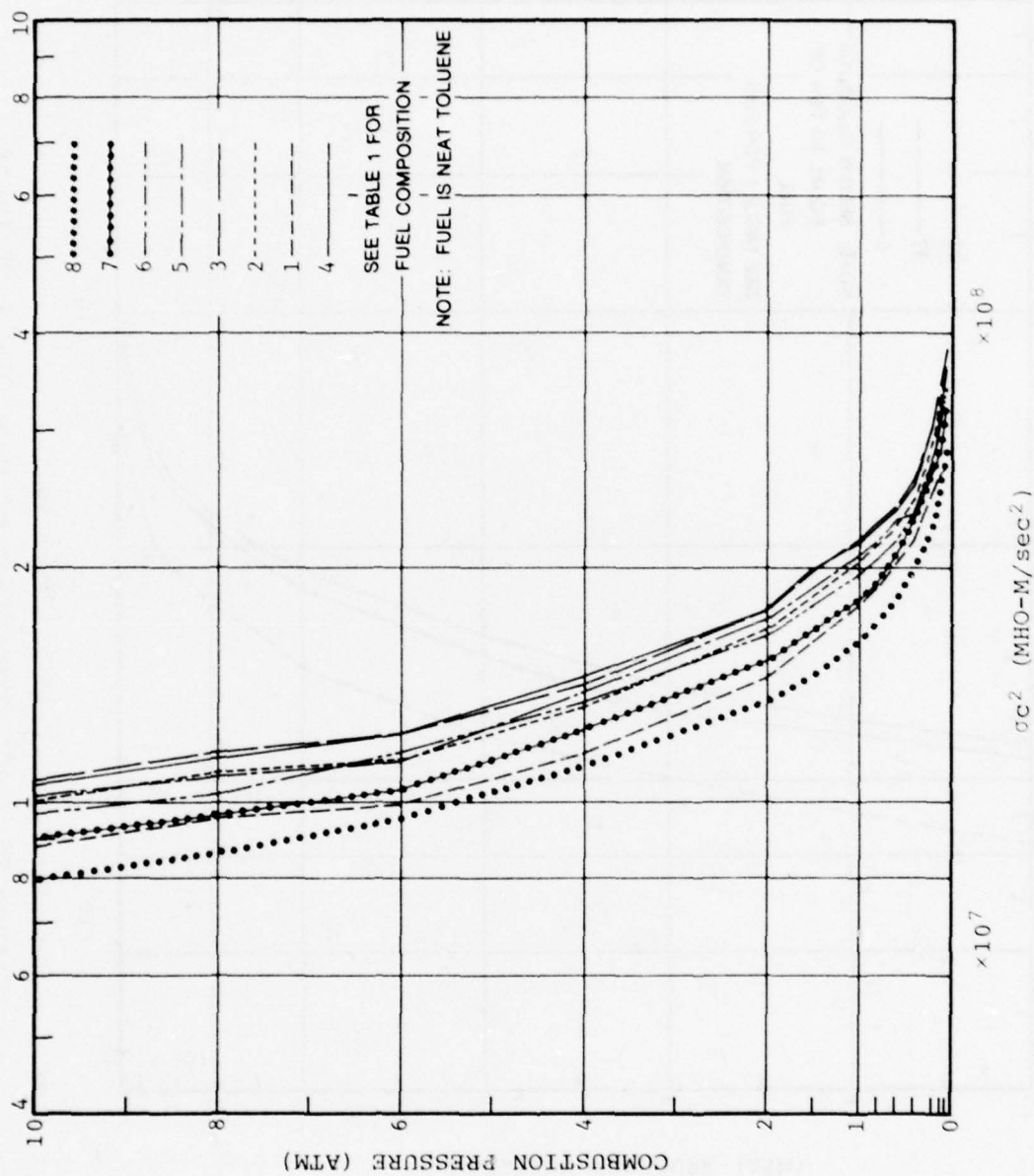


Figure 26. σC^2 Comparison of Neat Toluene Fuel with Various Seed Ratios of Cs_2CO_3

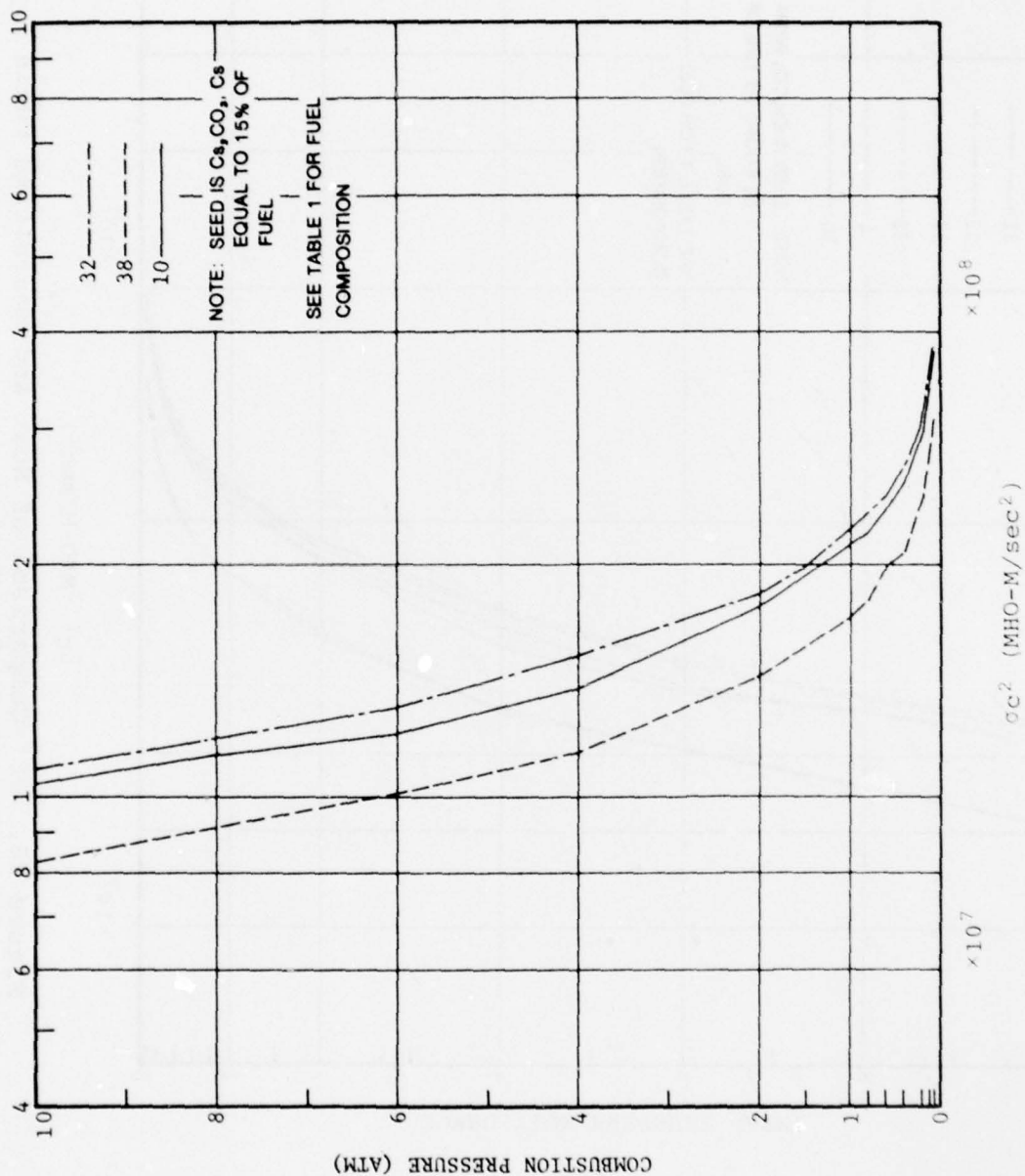


Figure 27. σC^2 Comparison of Emulsified JP-4, Toluene, and Benzene Fuels Seeded with Cs_2CO_3

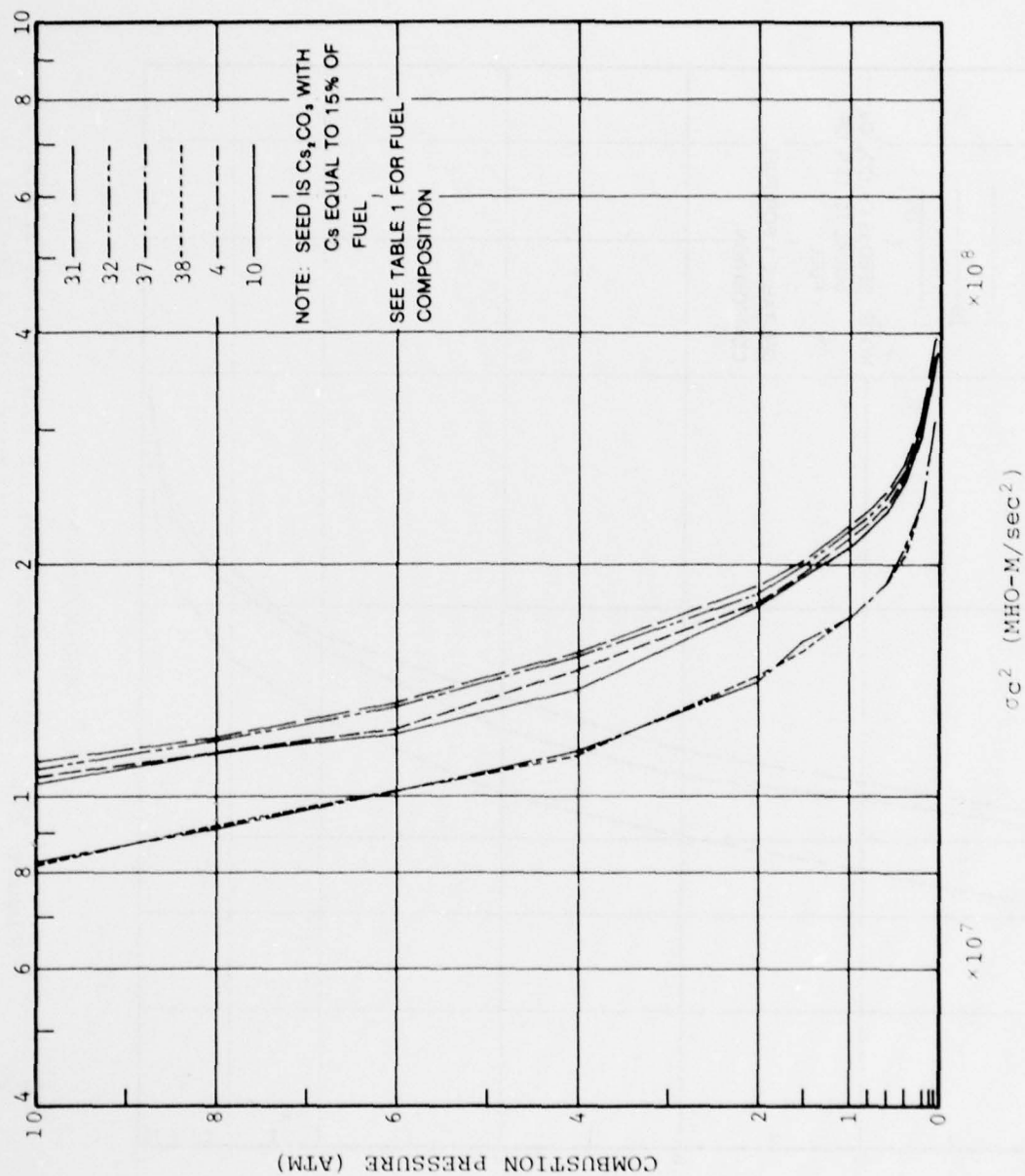


Figure 28. σC^2 Comparison of Neat and Emulsified Fuels with $C_2H_5CO_2$ Seed

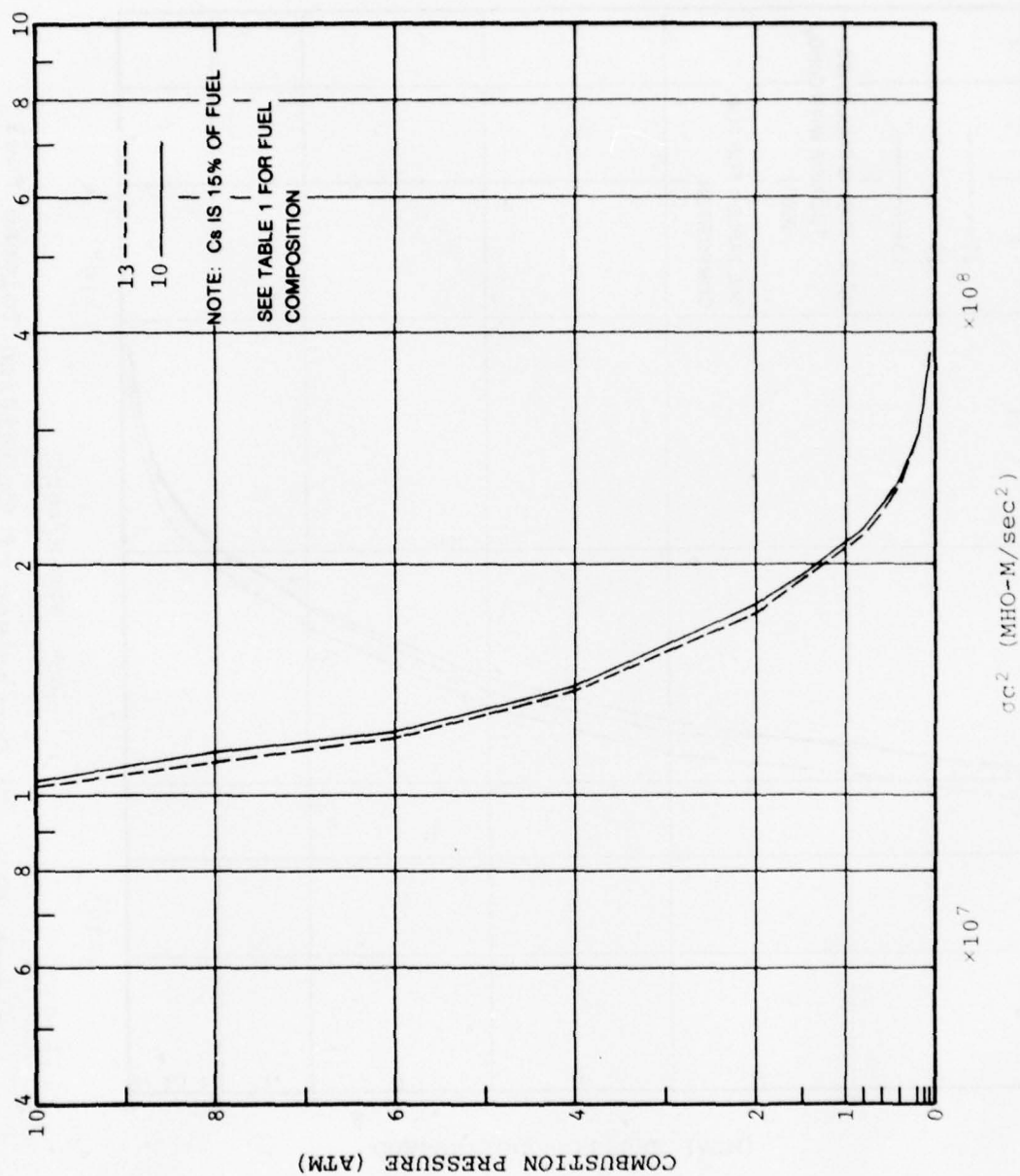


Figure 29. σC^2 Comparison of Cs_2CO_3 and $CsNO_3$ Seeded Toluene Fuel

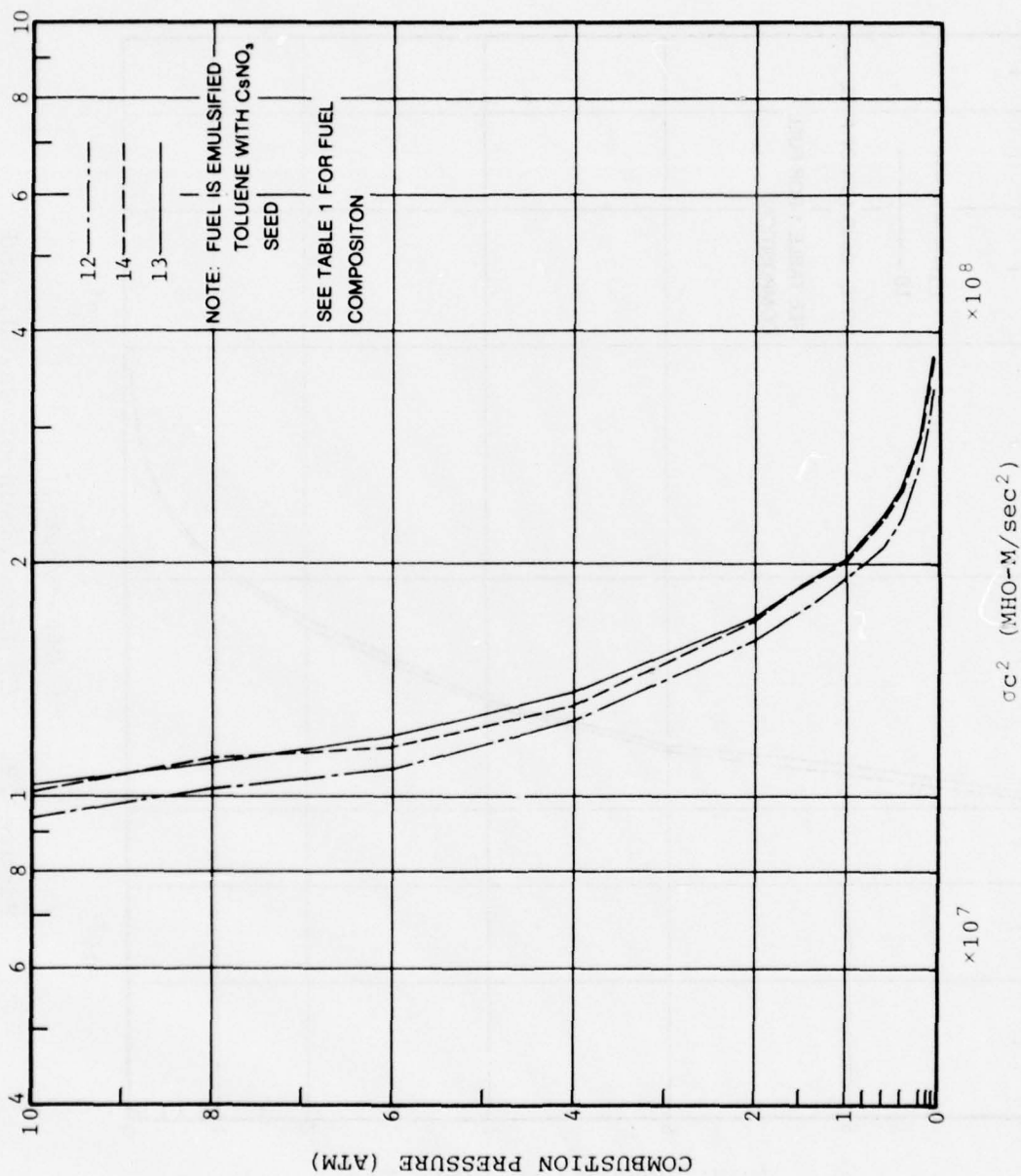


Figure 30. σC^2 Comparison of Emulsified Toluene Fuel with Various Ratios of CsNO_3 Seed

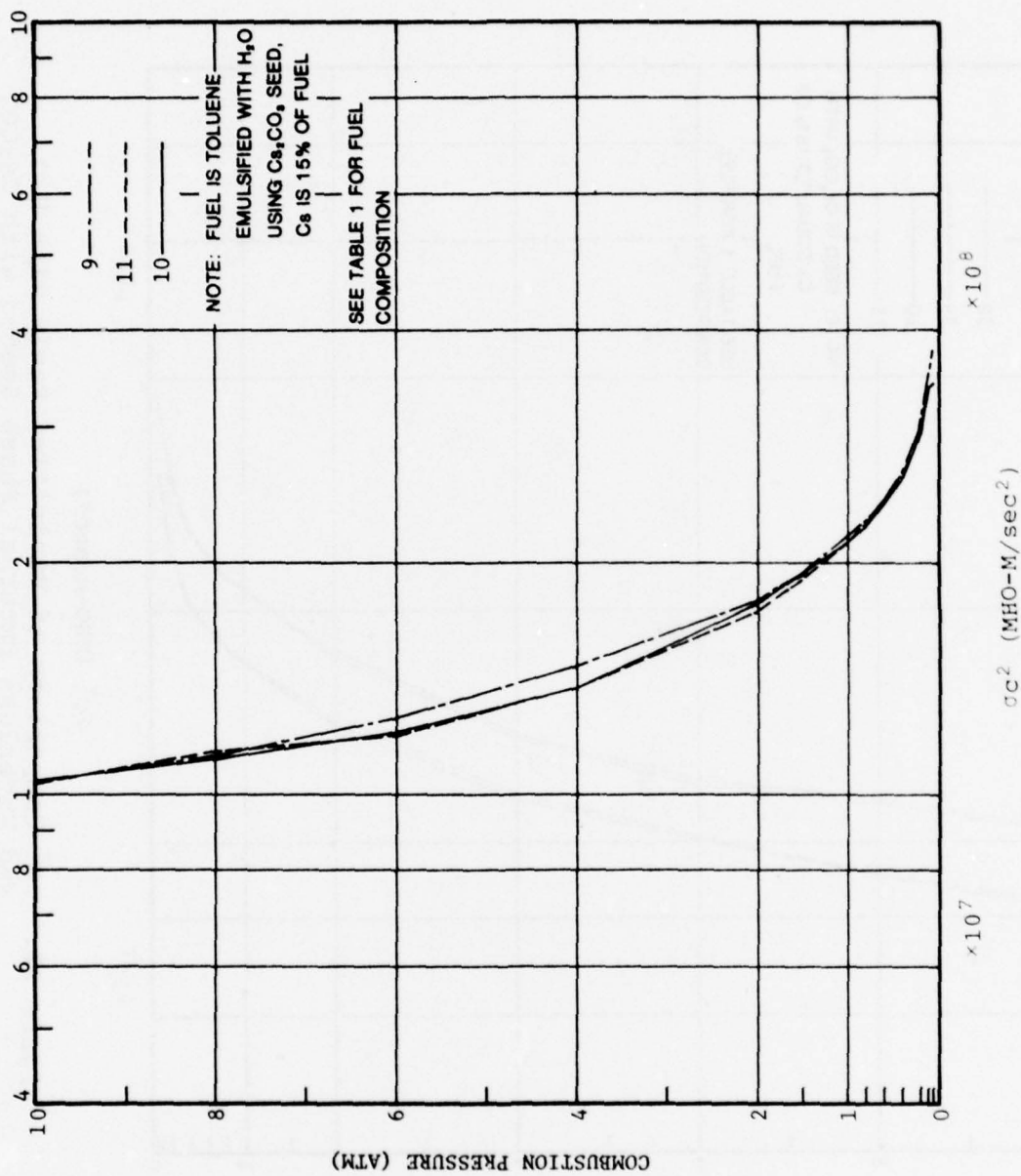
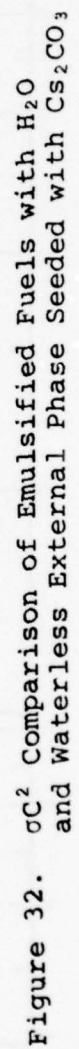


Figure 31. σC^2 Comparison of Emulsified Toluene with Various Percentages of H₂O External Phase



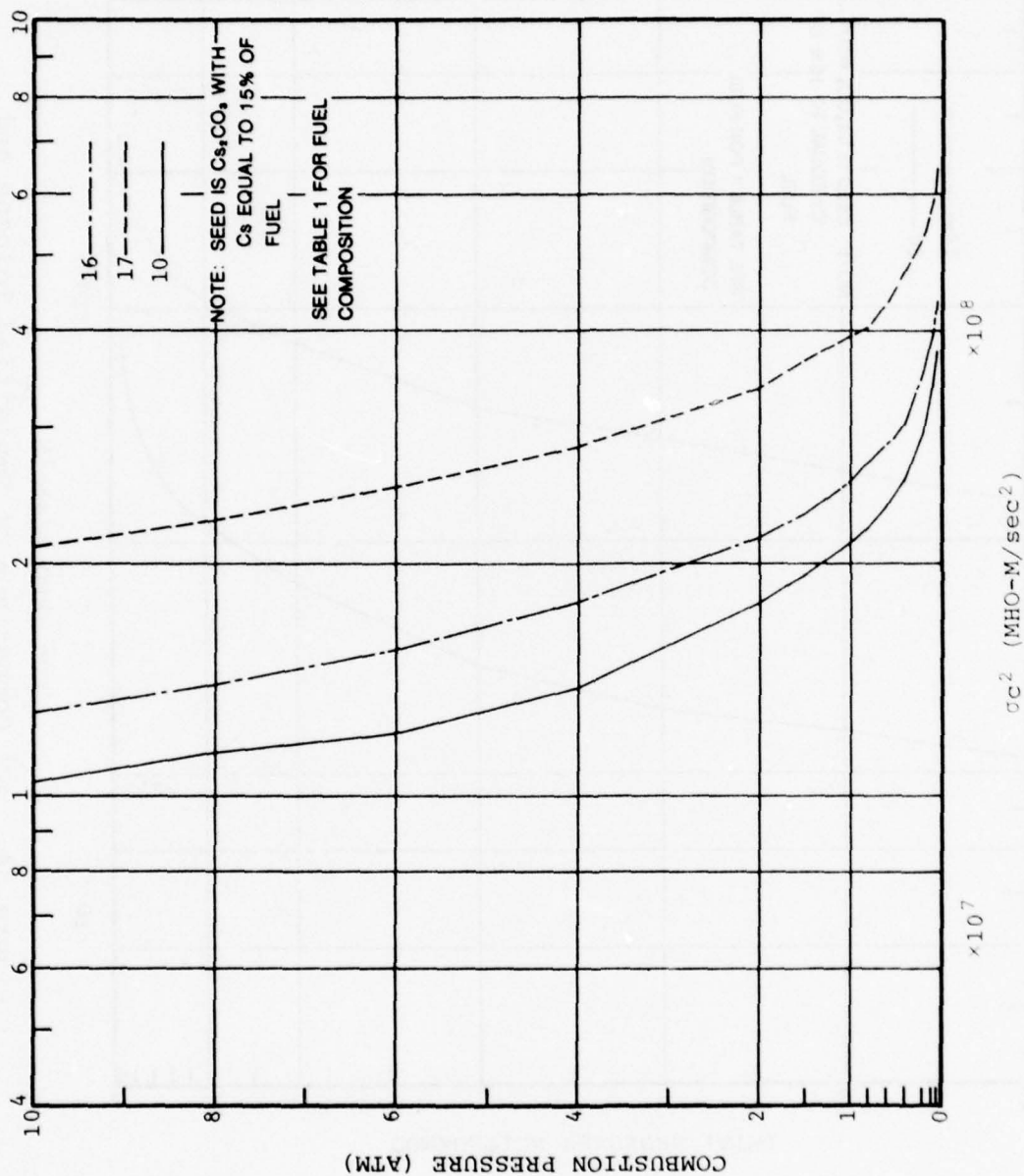


Figure 33. σ_{C^2} Comparison of Emulsified Toluene Fuel with Varying Percentages of Al Additive

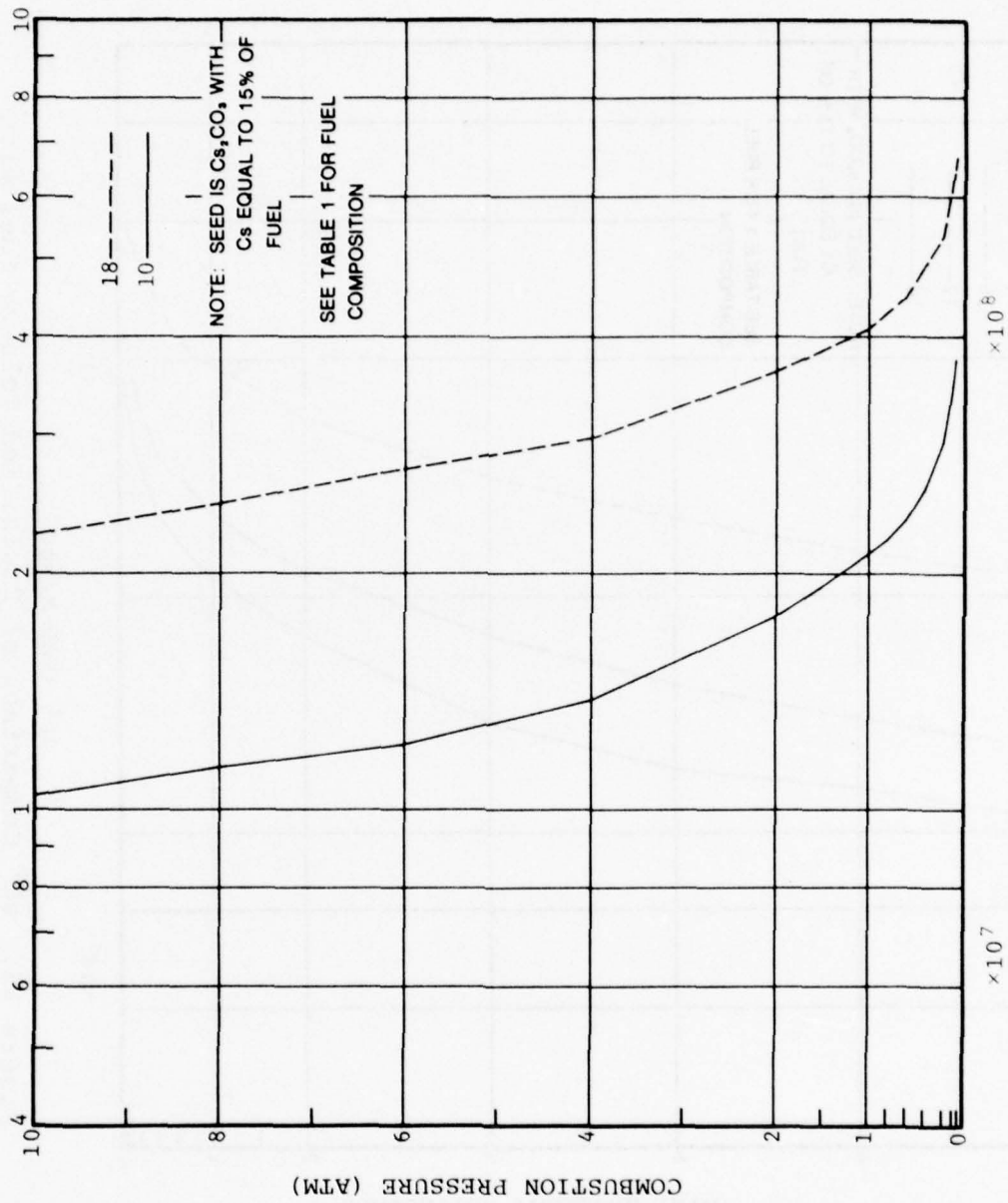


Figure 34. σC^2 Comparison of Emulsified Toluene and Boron Additive Fuel Seeded with Cs_2CO_3

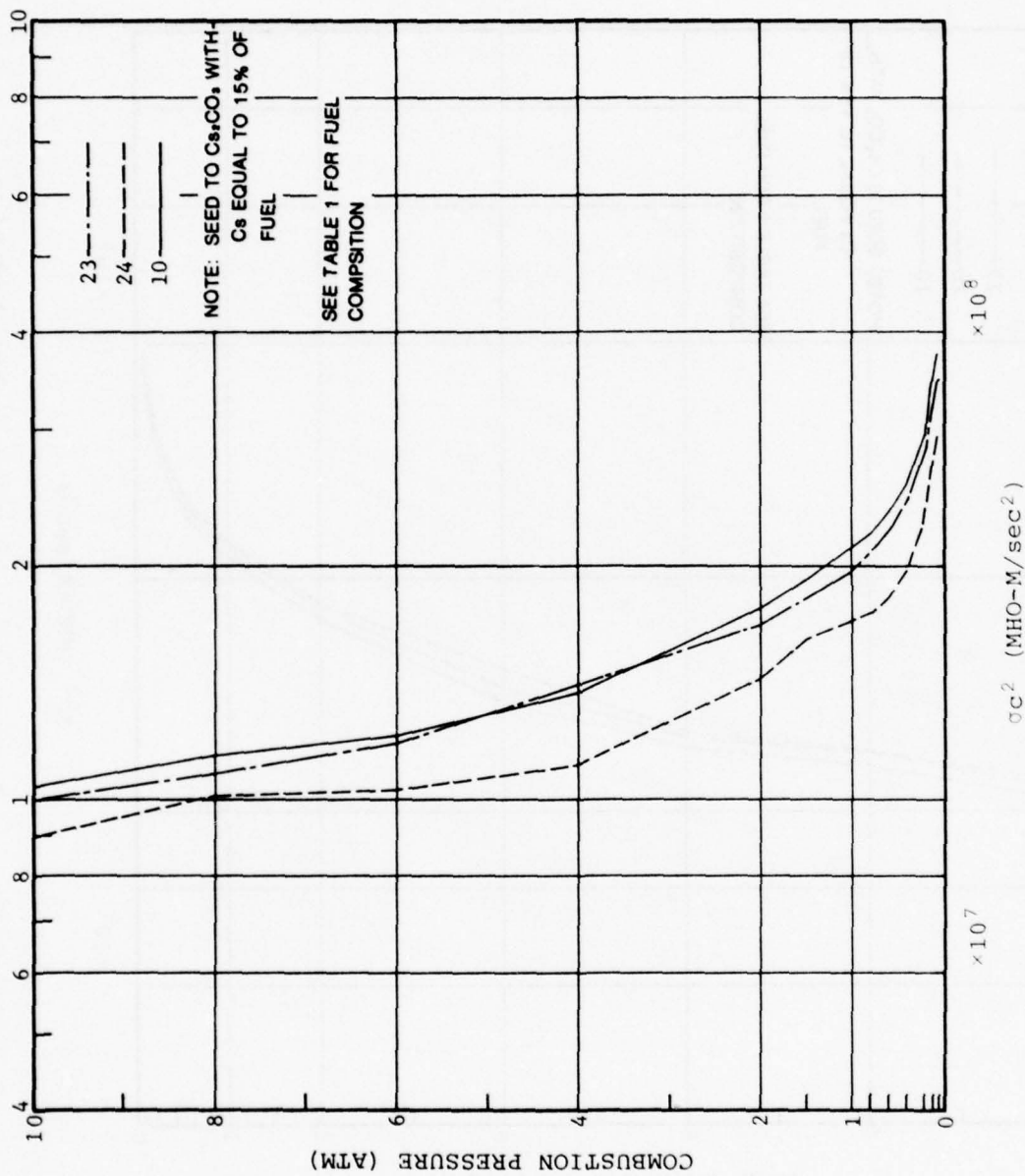


Figure 35. σ_{C^2} Comparison of Emulsified Toluene with Varying Percentages of Mg Additive and Cs_2CO_3 Seed

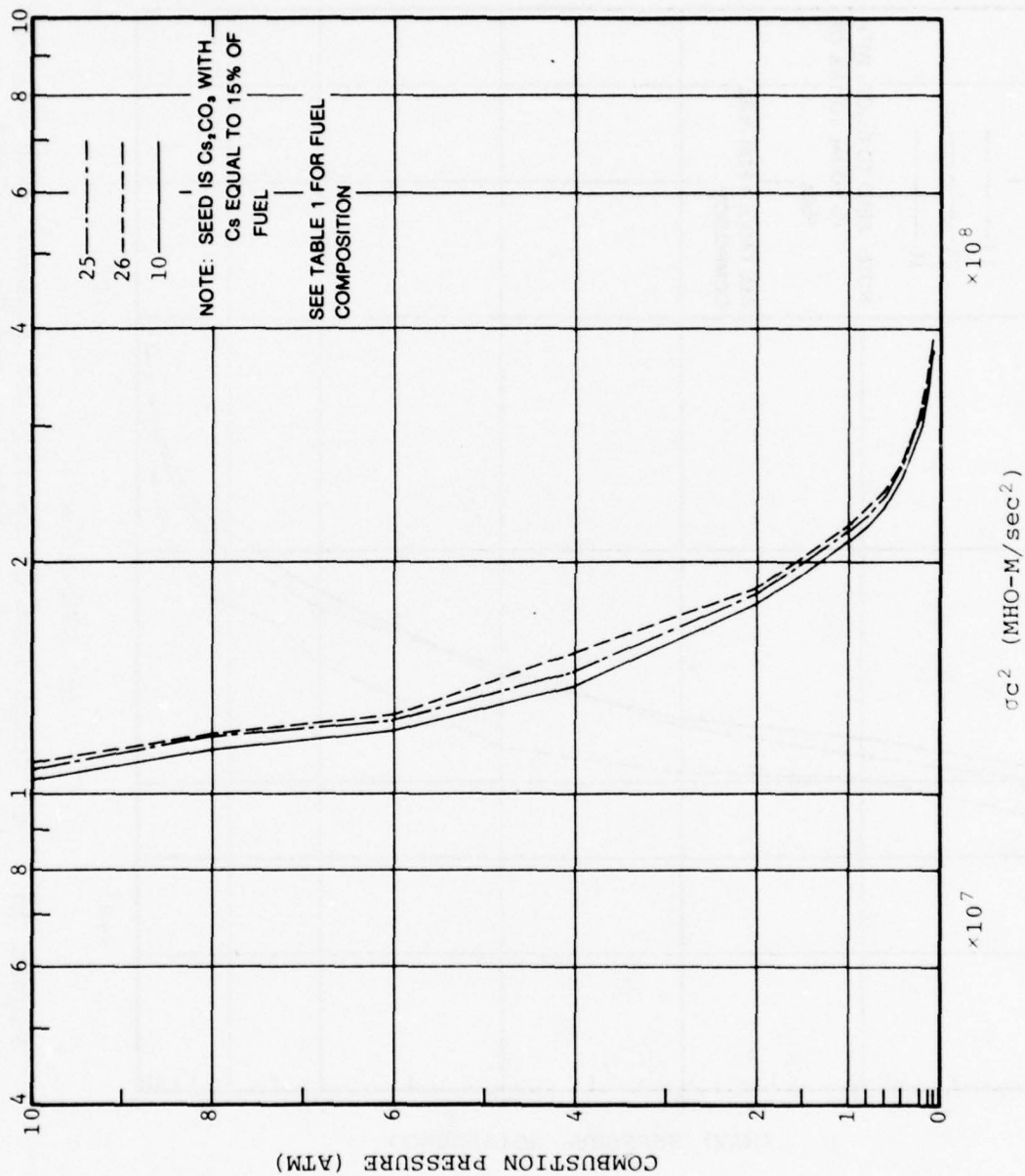


Figure 36. σC^2 Comparison of Hydrocarbon Additive
Fuel with Cs_2CO_3 Seed

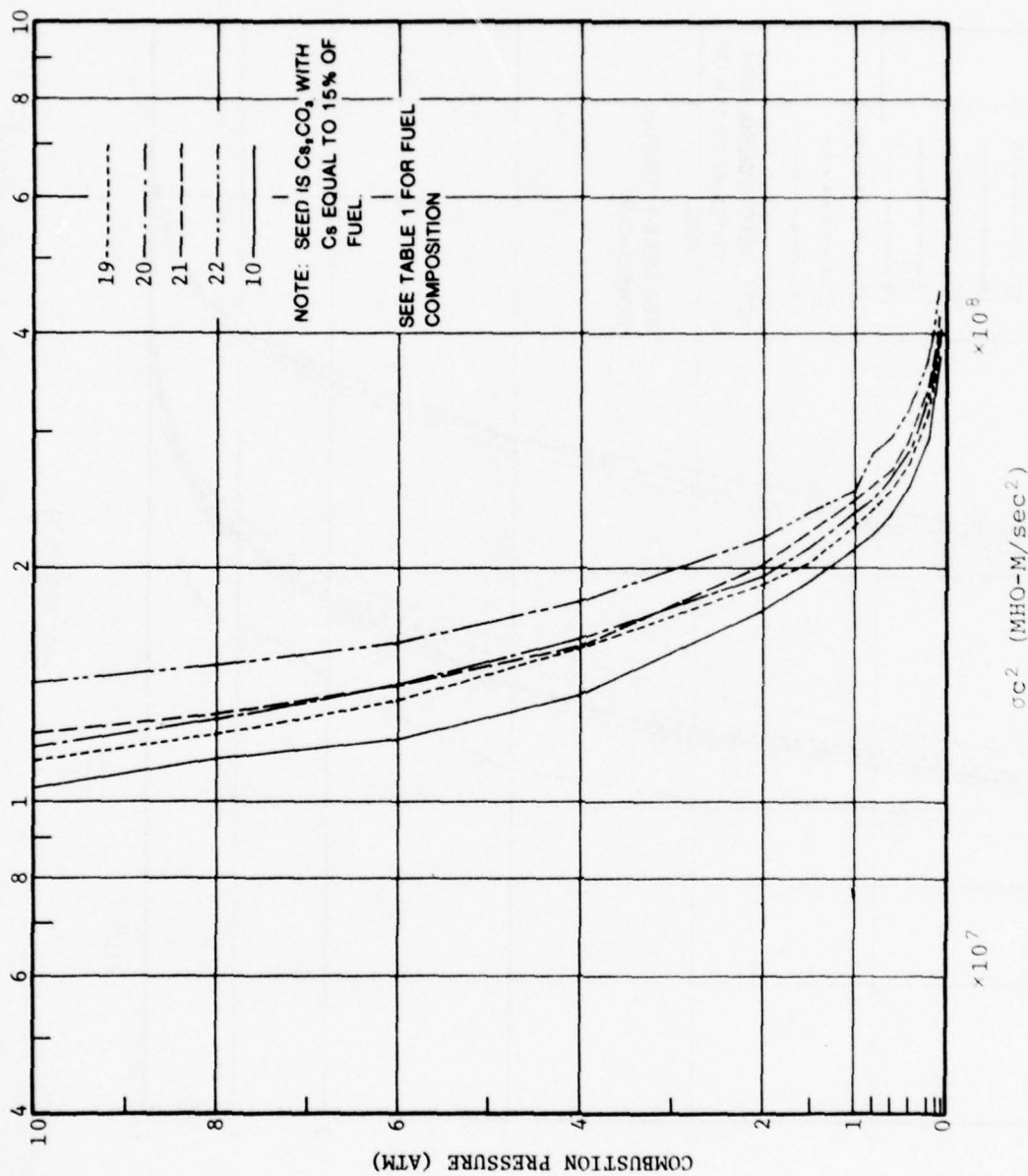


Figure 37. σC^2 Comparison of Emulsified Toluene with Varying Carbon Additive Ratio

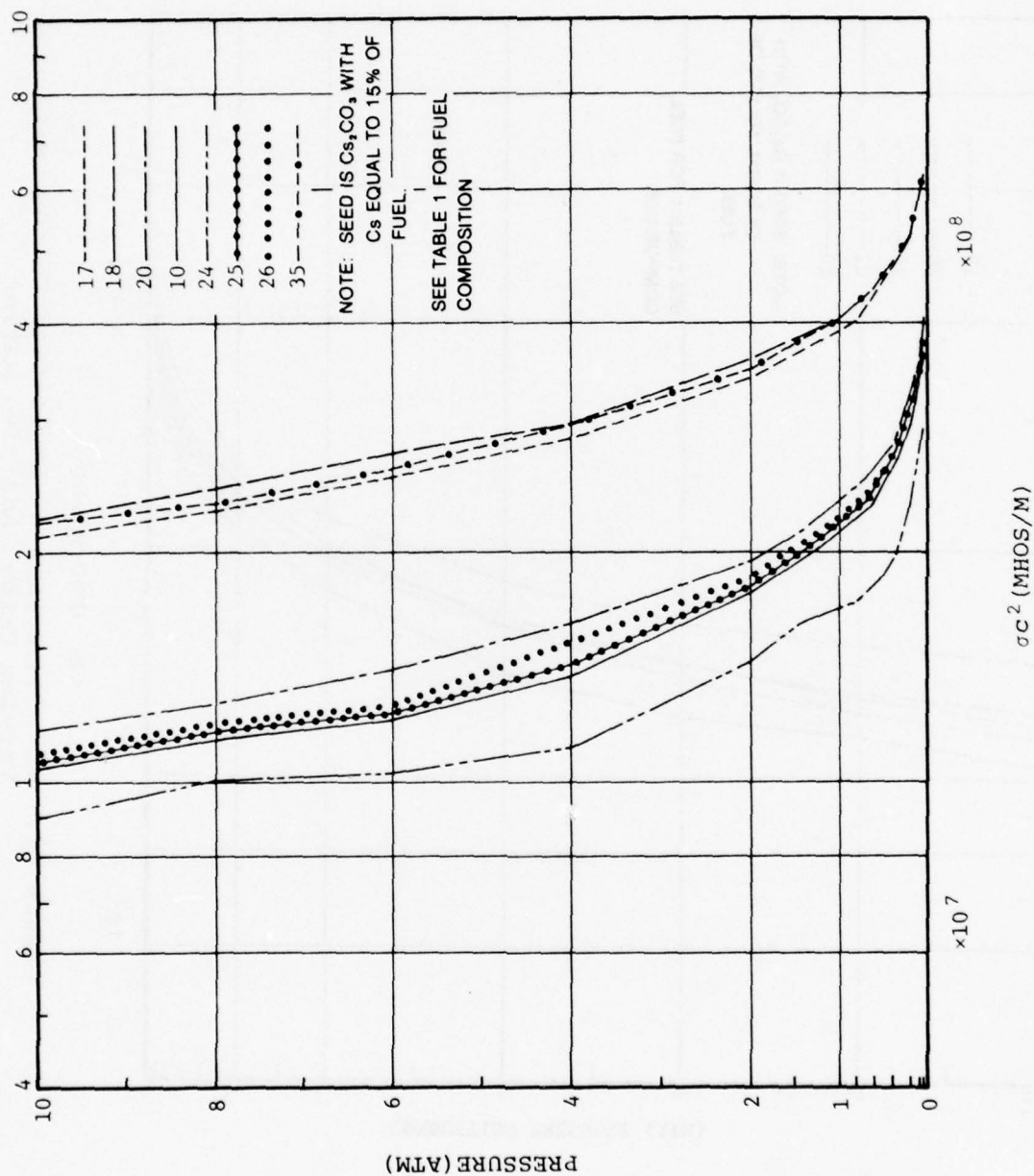


Figure 38. σC^2 Comparison of Various Fuel Additives with Cs_2CO_3 Seed

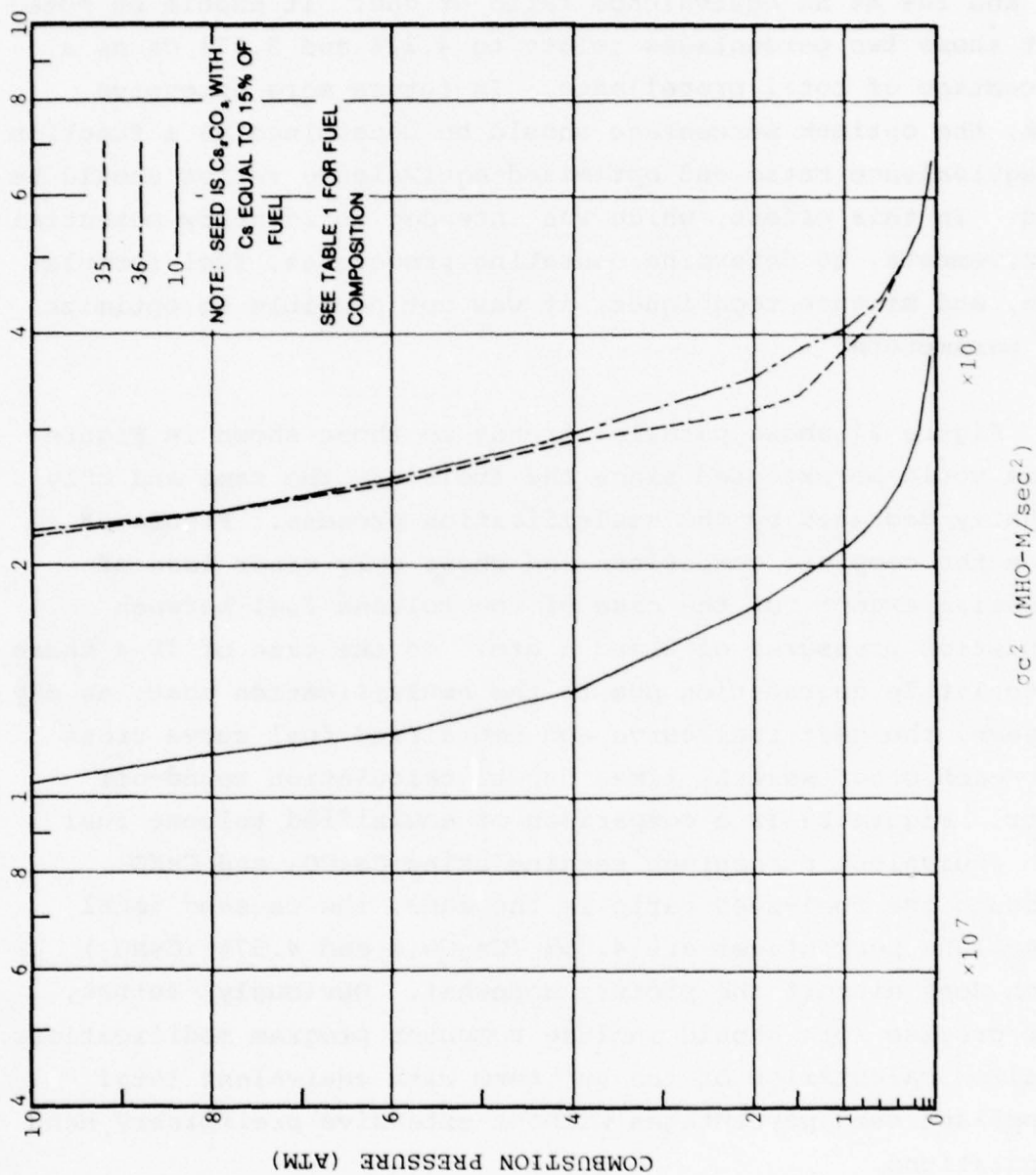


Figure 39. σC^2 Comparison of High Energy Fuel Composition with and without H_2O as an Emulsifier External Phase

In Figure 26 we see a comparison of fuels using various percentage seed ratios. It is evident that a seed percentage based on percent of fuel reaches an optimum for toluene between 15% and 20% at an equivalence ratio of one. It should be noted that these two percentages relate to 4.22% and 5.97% Cs as a percentage of total propellants. In future more extensive work, the optimum percentage should be determined as a function of equivalence ratio and optimized equivalence ratios should be used. In this effort, which was intended to identify potential improvements, to determine operating procedures, fuel formulation, and mixture techniques, it was not possible to optimize all parameters.

Figure 27 shows parallel trends to those shown in Figure 25 as would be expected since the fuels are the same and only slightly degraded by the emulsification process. Figure 28 makes the complete comparison and shows only minor loss of potential except for the case of the toluene fuel between combustion pressures of 2 and 6 atm. In the case of JP-4 there is so little degradation due to the emulsification that, as may be seen, the neat fuel curve and emulsified fuel curve cross over each other several times due to calculation round-off error. Figure 29 is a comparison of emulsified toluene fuel with equivalent percentage seeding using Cs_2CO_3 and CsNO_3 . Although the fuel-seed ratio is the same, the Cs seed total propellant percentages are 4.35% (Cs_2CO_3) and 4.57% (CsNO_3) which does distort the picture somewhat. Obviously, future, more precise work should include computer program modifications to allow calculation of the ϕu^2 term with equivalent total propellant seed percentages without extensive preliminary hand calculations.

Figure 30 is intended to show information similar to that depicted in Figure 26, but for CsNO_3 seed rather than Cs_2CO_3 . Similar trends are obvious and again the 15% seed percentage

yields the highest power conversion potential. Figure 31, too, is a parametric variation plot. In this figure the variation of water as a part of the emulsion external phase is shown. As would be anticipated, the lowest water percentage yields the highest potential power conversion but, with the exception of the 2% H₂O curve from 4 atm to 6 atm, the curves are extremely close and do not reflect degradation proportional to H₂O percentage in the external phase. In Figure 32 we see a continuation of the theory that reduction of water as the external phase of the emulsions will improve power conversion potential. Two waterless emulsions are shown in this figure compared to their equivalent 3% water external phase toluene and benzene emulsions. Although small, there is a consistent decrease at all pressures in the σc^2 value. It should be noted that this is but one possible fuel emulsion formulation; others may not result in such a trend although improvements will be small.

Figure 33 shows the comparison of a toluene emulsion, a 10% Al/toluene emulsion and a 30% Al/toluene emulsion. The results indicate that this is a high potential fuel. Similar results are revealed for a 30% boron emulsion in Figure 34. Figure 35 is the picture of an idea gone awry. Magnesium as a potential high energy candidate is decidedly not effective. Increasingly higher percentages of magnesium result in increasingly poorer energy conversion potential. It would appear that the use of magnesium or any further pursuit of magnesium as an additive is fruitless. One possible contradiction to this is found in a recent AFOSR study of fuel-rich propellants for solid rocket motors by Atlantic Research Corp. [15] It was found that although boron and, to a far smaller extent, aluminum are difficult to burn, the addition of magnesium as a "combustion improver" was quite effective, the rationale being that Mg rapidly combined with O₂ to form MgO and at the same time created intensely reactive nascent oxygen.

In Figure 36 we see the results of increasing both energy content and carbon content of the fuel. The addition of naphthalene to the point of creating a saturated solution (34% of the weight of toluene) and emulsifying it is shown, as is an equivalent amount of anthracene. As will be noted later, anthracene is not nearly as soluble in toluene or benzene as is naphthalene and would therefore require suspension in the emulsion. It would appear then that naphthalene, since it does not alter the physical characteristics of the basic toluene or benzene liquid fuel appreciably, would be an ideal "secondary" additive.

In Figure 37 we see a comparison of four different percentages of carbon as emulsified and a toluene emulsion. The 70% carbon emulsion does improve performance, as do the lesser amounts. Considering effectiveness, the 20% carbon emulsion yields a far greater improvement than the 30% or 40% carbon emulsions.

Figure 38 is a comparison of all of the additives at the 30% level when emulsified with toluene plus a "super" fuel which consists of benzene, 34% naphthalene and 30% aluminum. The benzene/naphthalene/aluminum fuel oc^2 value is not quite as high as that of the toluene/boron fuel. The conclusion to be drawn is not necessarily that the benzene/naphthalene liquid fuel combination is not as good as toluene, but rather that boron is a better additive to the extent that it masks the higher potential of the benzene/naphthalene combination. As a result, additional work should be directed toward improvements which could be gained from a benzene/naphthalene/boron emulsion and the trade-offs in emulsion rheology vs energy potential gains of even higher boron content fuels. Figure 39 is presented as a comparison of a normal 3% water benzene/naphthalene/aluminum emulsion and an equivalent waterless emulsion. As previously noted, the waterless emulsion formulation used does not generally produce as high a oc^2 value as does the 3% water external phase

emulsion. It is assumed that this effect is the result of combustion of the high (6%) glycol portion of the external phase. Combustion of the glycol produces effectively 9% of the original glycol weight as water vapor. Hence, if 6% glycol fuel emulsion were combusted, this would be equivalent to combustion of a fuel originally containing 5.7% water.

Table 1 is a listing of the constituents and percentages of the fuels studied analytically. Unfortunately, a JP-4/coal emulsion and a toluene/coal emulsion, which were physically manufactured and tested, could not be examined analytically. Although a computer study was attempted, no data was generated due to singularities in the computer specie matrix being formed. It is presumed that equivalence ratio modifications might have prevented this.

4. FUEL PROPERTIES

Fuels can exist in several physical forms and each exhibits different characteristics. The usual classifications are liquid and solid each with its own well known physical properties. Additionally there are simple slurries, sols, gels and emulsions. Simple slurries consist of two phases, a liquid and a solid, composed of small particles held in suspension by agitation of the liquid. Figure 40 shows an example of toluene/aluminum, toluene/magnesium, JP-4/magnesium and JP-4/aluminum simple slurries in as-mixed condition and after being allowed to settle for 5 and 10 minutes. Specific characteristics of simple slurries are: ability to form high solid percentage mixtures and rapid settling of particulates in the absence of agitation of the liquid phase.

Sols are characteristically formed of low percentages by weight of very small particles, molecular to several molecule size, and are stable insofar as precipitation is concerned. The

Table 1. Fuel Formulation Table

JP-4	Internal Phase			External Phase				Additive			Seed			Cs % of Total Propellants
	C ₇ H ₈	C ₈ H ₈	C ₁₀ H ₈	H ₂ O	C ₂ H ₄ O ₂	C ₃ H ₆ O ₂	Al	B	C	Mg	C ₁₂ H ₁₀	Cs ₂ CO ₃	CsNO ₃	
1	63	-	-	-	-	-	-	-	-	-	-	37	-	10.09
2	75.1	-	-	-	-	-	-	-	-	-	-	30.9	-	7.92
3	75.3	-	-	-	-	-	-	-	-	-	-	24.7	-	5.97
4	81.5	-	-	-	-	-	-	-	-	-	-	18.5	-	4.22
5	83.2	-	-	-	-	-	-	-	-	-	-	12.3	-	3.27
6	87.7	-	-	-	-	-	-	-	-	-	-	9.9	-	2.66
7	90.1	-	-	-	-	-	-	-	-	-	-	7.4	-	2.10
8	92.6	-	-	-	-	-	-	-	-	-	-	18.5	-	1.54
9	73.3	-	-	1.6	-	-	-	-	-	-	-	18.5	-	4.32
10	76.6	-	-	2.4	-	-	-	-	-	-	-	18.5	-	4.35
11	31.0	-	-	2.6	-	-	-	-	-	-	-	18.5	-	4.39
12	77.4	-	-	2.3	-	-	-	-	-	-	-	-	-	2.84
13	77.0	-	-	2.1	-	-	-	-	-	-	-	-	-	4.57
14	67.1	-	-	2.4	-	-	-	-	-	-	-	-	-	6.54
15	73.4	-	-	2.4	6.5	-	-	-	-	-	-	-	-	4.36
16	59.3	-	-	2.4	-	-	8.2	-	-	-	-	-	-	4.60
17	51.1	-	-	2.4	-	-	24.4	-	-	-	-	-	-	5.17
18	51.1	-	-	2.4	-	-	24.4	-	-	-	-	-	-	4.55
19	61.2	-	-	2.4	-	-	-	-	16.3	-	-	-	-	4.45
20	53.1	-	-	2.4	-	-	-	-	24.4	-	-	-	-	4.50
21	44.9	-	-	2.4	-	-	-	-	32.6	-	-	-	-	4.55
22	20.5	-	-	2.4	-	-	-	-	57.0	-	-	-	-	4.71
23	53.3	-	-	2.4	-	-	-	-	-	8.2	-	-	-	4.62
24	32.1	-	-	2.4	-	-	-	-	-	24.4	-	-	-	5.27
25	43.8	-	-	2.4	-	-	-	-	-	-	-	-	-	4.40
26	81.5	-	-	2.4	-	-	-	-	-	-	27.7	-	-	4.41
27	77.5	-	-	2.4	-	-	-	-	-	-	-	-	-	4.28
28	49.8	-	-	2.4	-	-	-	-	-	-	-	-	-	4.41
29	49.8	-	-	2.4	-	-	-	-	-	-	-	-	-	4.43
30	25.1	-	-	2.4	-	-	-	-	-	-	27.7	-	-	4.45
31	21.3	-	-	2.4	-	-	24.4	-	-	-	-	-	-	5.26
32	-	-	-	-	6.5	-	24.4	-	-	-	-	-	-	5.27
33	-	-	-	-	-	-	-	-	-	-	-	-	-	3.90
34	-	-	-	-	-	-	-	-	-	-	-	-	-	4.02
35	-	-	-	-	-	-	-	-	-	-	-	-	-	4.04
36	-	-	-	-	-	-	-	-	-	-	-	-	-	4.90
37	-	-	-	-	-	-	-	-	-	-	-	-	-	4.90
38	-	-	-	-	-	-	-	-	-	-	-	-	-	4.90
39	-	-	-	-	-	-	-	-	-	-	-	-	-	4.90
40	-	-	-	-	-	-	-	-	-	-	-	-	-	4.90

* Note: Runs 27, 28, 29, 30 were coal runs

C₇H₈ = Toluene
 C₈H₈ = Benzene
 C₁₀H₈ = Naphthalene
 C₂H₄O₂ = Ethylene Glycol
 C₃H₆O₂ = Propylene Glycol
 C₁₂H₁₀ = Anthracene

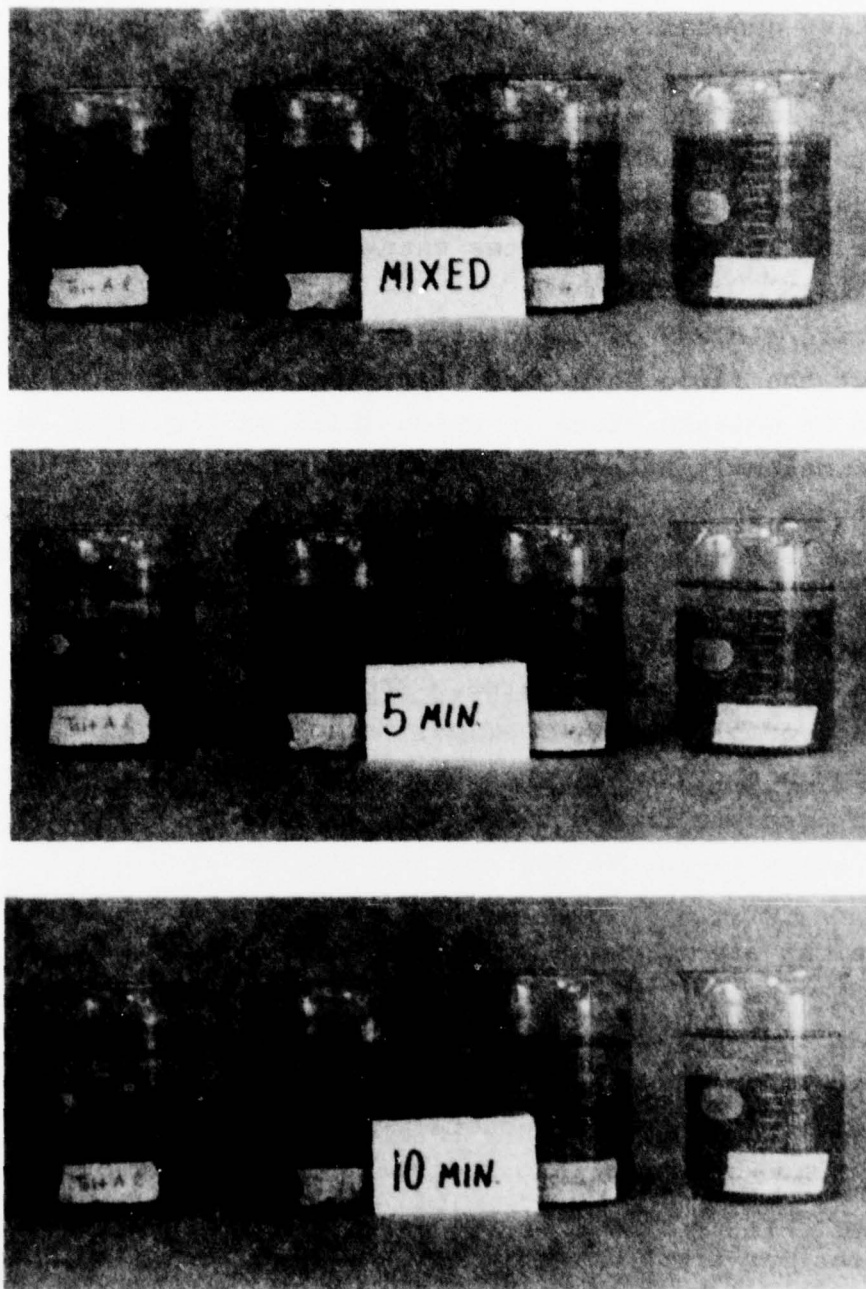


Figure 40. Examples of Simple Slurries of
 Left to Right: Toluene/Aluminum,
 Toluene/Magnesium, JP-4/Magnesium,
 JP-4/Aluminum in the As Mixed
 Condition, Mix + 5 Minutes, and
 Mix + 10 Minutes

particles are generally in constant motion (Brownian motion) of a random nature similar to molecular movement of gaseous molecules. Both sols and simple slurries maintain Newtonian fluid characteristics although a highly loaded simple slurry will exhibit greatly increased viscous shear dependent upon the percentage of solid particulates entrained in the liquid.

Gels are a class of colloids similar to sols and slurries except that the fluid phase has been chemically modified to a semi-solid or gelatin state in which solid particulates are more or less permanently suspended. Gels can be caused to flow in pipes or tubes retaining their ability to suspend particulates. At all times the gel liquid phase will revert to its semi-solid state as soon as the pumping shear force is removed. Like simple slurries and unlike sols, a gel can suspend a high percentage of solid particulates. Breakdown of a gel must usually be accomplished by chemical means in order to effect a spray although spraying of gels has been performed in some cases using high pressure drop nozzles.[16, 17] After chemical breakdown, the gel will assume the characteristics of a simple slurry.

Emulsions are mixtures of two immiscible liquids, one of which has been altered chemically to change its surface tension. By chemical and physical means the two immiscible liquids form a stable mixture in which solid particulates can be suspended indefinitely. Emulsions in general which contain a high ratio of oil in water or water in oil display thixotropic or non-Newtonian viscosity characteristics. Additionally, excessive shear forces can break an emulsion resulting in a simple slurry of the two liquid phases and the solid phase if one is present.

We have already seen the possible gains available from the use of high energy solid fuel particulates. As a result, attention must be directed to the means of placing such particulates into suspension, storing, transporting, pumping and finally

injecting and burning such fuels. Liquid fuels display no undesirable or insurmountable characteristics as related to the previously mentioned requirements of a fuel. Totally solid fuels meet all of the desirable characteristics except the ability to be turned off and on at will any variable number of times. Simple slurries, although not difficult to mix, require agitation to prevent settling in tankages and will precipitate particulates in stagnation areas of piping. Pumps display inordinate amounts of wear when subjected to pumping of solid particulates. Sols meet the desired fuel requirements but the particulate sizes needed are difficult to produce and only low solid loading ratios can be accomplished. Gels, too, are easy to mix, store, and transport although, as with simple slurries, pumps show excessive wear rates when used with high solids ratios. Additionally, a gel does not form a satisfactory spray for combustion without pretreatment to chemically break the gel. Emulsions can be easily manufactured, stored and pumped. It is a characteristic of emulsions that, as pumping shear is increased, viscosity decreases reducing the needed pump work. Pumps also are not prone to excessive wear in the presence of 30 to 40% solid emulsions, a characteristic resulting from the means whereby the solids are suspended. Injection of fuel into a combustion chamber as an emulsion would present the same spray problems inherent in a gel if the emulsion is not first broken. Again it is a characteristic of emulsions that the excessively high shear forces found in an injector spray nozzle will break an emulsion into its original constituents and form a simple slurry which will spray equally as well as a neat liquid. It would appear at this point that a high phase ratio emulsion satisfies all the fuel requirements and should be examined further.

Section III

EMULSIFIED FUELS

1. HISTORY AND EXPERIENCE

The use of emulsified fuels is not totally new, although, as applied to MHD power generation, it is believed to be. A patent was issued June 1960 to the Monsanto Company entitled, "Emulsified Motor Fuel," which described the emulsification of JP-4 jet fuel, the technique and emulsifiers.[18] In 1956 Standard Oil and Gas Company received a patent for emulsified oil containing metallic salts to be used in fracturing underground rock formations.[19] The Ethyl Corporation obtained a patent in 1960 for dispersions of finely divided metals in jet fuels, although, the technique used was technically a gel, rather than an emulsion.[20] Skolnik and Margolin received a patent in 1965 for a thixotropic propellant for rockets.[21] Their technique included mono-propellants, bipropellants, and the use of carbon, coal, aluminum, magnesium, and boron as finely divided particulate additives. Again the suspension technique was a gel rather than an emulsion. Patents 3,352,109; 3,539,406; 3,613,372; and 3,617,095 were issued to Dr. K. J. Lissant of Petrolite Corporation and pertain to the formation of O/W emulsions of jet and rocket fuels, transportation of bulk solids, "Essentially Nonaqueous Emulsions," and "Method of Providing Power with Essentially Nonaqueous Emulsions." [22-25] Based upon the experience of the Petrolite Corporation with emulsified fuels, it was decided that their procedures, techniques and surfactants would be utilized to develop fuel emulsions of carbon 10% - 70%, magnesium 30%, aluminum 30% and boron 30%, and that a study of past experience with emulsified fuels would be made.

It was found that extensive experience with emulsified fuels has been developed by the various military services,

airframe manufacturers and aircraft engine manufacturers. Pratt & Whitney Aircraft[26] found while testing a JT-12 engine with emulsified JP-4 that there was a 2.5% increase in TSFC (specific fuel consumption) which corresponded to the noncombustibles contained in the emulsion. They also found severe dirt contamination and clogging of fuel pump and fuel control filters. This was not anticipated during their test and was found by other users of this type fuel to be a recurrent problem. The reason for the fuel filter clogging is found in one inherent characteristic of an emulsion: its ability to suspend particulates in the emulsion. The surfactants also have a cleaning quality and will, therefore, pick up any foreign material in a fuel line, tank or pump. Few additional problems of this type were encountered after thorough cleaning of the fuel system. Upon disassembly, Pratt & Whitney Aircraft found that at the engine pump inlet the fuel line contained fuel which was 80% emulsified, whereas beyond the pump only 10% of the fuel was found to be emulsified. Slight rust deposits were also found on cams and levers of the fuel control, multiplying lever assembly and acceleration limit cam. Otherwise, there were no other problems and engine operation was normal in all other respects.

Another study of emulsified fuel usage performed by Pratt & Whitney Aircraft[27], using engine components in a laboratory environment, produced similar results. Spray and combustion studies produced no problems and nozzle spray characteristics were found to be identical to neat JP-4. As expected, the net heat of combustion of the emulsified fuel was lower than JP-4 minimum specification of 18,400 Btu. Considerable emulsion breakdown was found to occur as the emulsified JP-4 passed through the gear type fuel pump, although it was found that this too could be altered by emulsion formulation and pressure rise across the pump.

Esso Research and Engineering Company in studying JP-4 emulsions for the U. S. Army Aviation Material Labs[28] found reduced rate of combustible vapor release made them excellent safety fuels from the standpoint of weapons hazards and post-crash fire hazards. The emulsions were stable over a range of temperatures from -65°F to 160°F, and they were compatible with most metals and elastomers used in construction. The fuels were evaluated in a Lycoming T-55 engine with no difficulty and system response equivalent to the neat JP-4 reference fuel. No rust, sticking of moving parts, fungal or bacterial growth was found during the tests. Bench tests with 1,000 gallon batch sizes created some problems due to breakdown of some batches during transit. These difficulties were traced to inadequate plant mixing and too rapid addition of JP-4 to the emulsion. Nozzle studies showed emulsion breakdown in the spray nozzles, but with as much as 20% emulsion passing through the nozzles without breakdown. Particle sizes of the atomized fuel were equivalent to that of referee fuel. Plugging of nozzles with contaminants was a problem solved by filtering the fuel prior to its entering the nozzles. This is the same type of problem encountered by Pratt & Whitney. Preliminary pumping studies showed that the emulsions could be pumped using conventional low-speed, high-output pumps without difficulty. High-speed, low-output pumps were found to break the emulsion prematurely. It was noted that additional effort was needed to better define the relation between emulsion yield stress and breakdown within the nozzles.

Thiokol Chemical Corporation[29] also found emulsified JP-4 to be an excellent safety fuel during its Rheological Evaluation of Emulsified JP-4 Fuel for the U. S. Army Aviation Material Labs. It was found that extra mixing temporarily increased the yield point of the emulsified fuels but that the increased yield point had very little effect on droplet size. It was also found that the emulsified fuel "formed a spray which ranged from good

atomization to almost no atomization." It is probable that this was a result of emulsion composition and mixing procedure, since it was concluded that the emulsion must be broken before efficient atomization can take place.

Douglas Aircraft performed a study[16] for the FAA using a DC-8-62 aircraft to investigate the use of emulsified JP-4 as safety fuels. In their study they found some tendency to corrosion enhancement and that solid particle contaminants entrained by the emulsified fuel will not settle out. It was determined that centrifugal pumps were not compatible with emulsified fuels due to emulsion breakdown. Published data on non-Newtonian fluids is insufficient to permit performance predictions. Aircraft venting, fill, jettison and fuel transfer systems are not presently compatible with emulsified fuels.

Continental Aviation[30] in a test of emulsified JP-4 fuel in a T-67 engine found substantial sulfidation of turbine blades which was traced to sodium in quantities of 30 parts per million of fuel. This was found to be a result of the catalyst used in manufacture of the emulsifier. No other adverse problems were noted.

In a study[31] of vulnerability of emulsified fuels it was reported that while it took 15 - 20 minutes for both a broken emulsion and referee JP-4 to reach an equilibrium vapor pressure of 2.55 to 2.80 psi, it required 36 - 48 hours to reach similar levels for the emulsified fuel.

Considering the information in these references, it should be obvious that emulsified fuels are not new but do pose some unusual problems. Most of the problems which occur are a result of not understanding the emulsion characteristics, but it should be pointed out that formulation and mixing technique are extremely important to the resulting emulsion characteristics.

2. EMULSION CHARACTERISTICS

Having previously established that emulsions might provide an ideal MHD generator fuel, a closer examination of emulsions, their characteristics and formation is in order. As previously mentioned, high ratio emulsions exhibit non-Newtonian characteristics. This means that under conditions of low or no shear stress the emulsion exhibits a very high apparent viscosity, approximately 50,000 - 200,000 centipoise, while appearing to have the approximate viscosity of the neat liquid once sufficient shear energy has been applied to the emulsion to start flow. At rest, the emulsion will suspend for extended periods of time a high percentage of solid particulates, up to approximately 60%, and still flow easily when pumped by conventional methods. At solids ratios above 65% the emulsion becomes extremely thick and pasty, losing most of the characteristics of an emulsion.

From classical physical chemistry an emulsion is defined as a continuous liquid phase having a second discontinuous liquid phase dispersed in the first. It is a well-known fact, when two immiscible liquids are placed in a container and agitated, one of the liquids is dispersed in the other. Modern terminology differentiates between dispersion and emulsion. In the absence of a stabilizing agent such a dispersion rapidly coalesces. When an appropriate agent or emulsifier is used, it will dissolve into the external liquid phase so that the minute droplets of internal phase remain discrete droplets. The reason for this ability is an enhanced surface energy of the external phase. If the surface energy strength of the external phase is sufficient, solid particulates can be dispersed throughout the emulsion in a three-phase structure. In this structure a solid particle is surrounded by a variable thickness film of the internal discontinuous phase. These minute droplets are suspended and isolated in the continuous external phase.

This description of emulsion internal structure does not explain its macroscopic physical characteristics or its unusual behavior; i.e., decreasing apparent viscosity with increasing flow velocity. The explanation is found in understanding the emulsion microscopic geometry. The formation of an emulsion takes place by progressive subdivision of the internal phase droplets within the external phase. As the droplets become smaller, eventually the droplets must impinge upon each other separated only by an external phase film whose thickness may be measured in molecules. The droplets are now controlled by packing factor geometry and will assume one of several shapes none of which are spherical, although this is the initial droplet shape. At internal phase ratios of 60 - 74% by volume the droplet shape can still be spherical with optimum packing. Above 68% by volume internal phase ratio the droplets assume a polyhedral shape, which is a modified rhomboidal dodecahedron (MRDH) at slightly above 74% by volume, the modification being in the form of rounded edges and points of the polyhedron. As the internal phase ratio is increased to approximately 94% by volume, the rhomboidal dodecahedral shape is less and less modified. An increase above 94% by volume internal phase ratio causes a rearrangement in droplet shape to that of a modified tetrakaidecahedron (MTKDH) or truncated octahedron which has six square faces and eight hexagonal faces. Once packed into such a three-dimensional honeycomb, either MRDH or MTKDH, the droplets have great difficulty in moving past one another and do so only by breaking down the emulsion. Effectively, the formation of an emulsion results in a relatively stiff or viscous material capable of supporting solid particles. Introduction of sufficient shear to cause flow partially breaks down the emulsion along the walls of a fuel line, for instance, and results in what is essentially plug flow. The film of broken emulsion will, due to boundary layer turbulent mixing, reform an emulsion as flow is slowed to a stop.

Fuel injector nozzles are designed to produce, for existing combustor conditions, the most complete mixing of fuel and oxidizer possible. Techniques which have been used with neat liquid fuels to obtain fuel atomization include simplex and dual orifice nozzles, parallel and impinging jets, parallel and impinging sheets, cone and triplet nozzles. All of these approaches have utilized the low surface tension of the neat liquids to obtain fuel atomization. Emulsions, by design, employ surface active agents for stability. This counteracts the spray dispersing effect of the nozzle types normally used. At this point, a characteristic of high internal phase ratio emulsions can be used to promote satisfactory spray dispersal. If an emulsion is properly formulated, excessively high shear rates will break an emulsion down into its original constituents and allow normal spraying of the liquid and entrained solid particulate fuels. The technique which has proved effective is to employ low average shear through the fuel system (wall shear only) obtaining essentially plug flow up to the fuel injectors. At this point, the emulsion enters a hypodermic tube where the boundary layer shear region becomes a major portion of the overall flow area and essentially complete emulsion breakdown occurs. The high flow velocity and lack of stagnation areas in this tube now prevents the settling of any entrained particulates and the broken emulsion behaves as a simple slurry. The very small diameter injector tube precludes the use of most injector techniques except for direct injection with impinging oxidizer streams. Fortunately, this is an effective and efficient injection technique.

Section IV

FUEL EMULSION MIXING TECHNOLOGY

1. INTRODUCTION

This program was started with the plan that fuel emulsions would be manufactured if possible and that, if not, simple slurries would be tested along with the equipment needed to maintain simple slurry suspensions. It was required that stable slurries (emulsions) containing aluminum, magnesium, and boron powders in ratios of 10% to 35% of the total fuel mix exclusive of seed fraction and 10% to 70% carbon be prepared. Although the reference fuel was to be toluene, the emulsified fuels could include or be composed of any hydrocarbon compound.

Initially, discussions with the Illinois Institute of Technology Research Institute were held to determine the present state of research in particulate fuels. Primarily, their work had been performed using submicron magnesium, JP-4, and surfactants to maintain low viscosity as particulates are added. Such slurries, although stable for periods of up to three weeks, i.e., with only minor separation, are not true emulsions. Additionally, it was stated that solvent type hydrocarbon fuels such as toluene and benzene would break down their surfactants. Subsequently, it was learned that the Petrolite Corporation had been able to form fuel emulsions for some time, as indicated by the patents on this subject held by them since 1967. The Tretolite Division of the Petrolite Corporation was then sub-contracted to develop emulsifiers to meet contract requirements based upon their patents and experience.

Based upon IITRI recommendations and calculations indicated previously, aluminum, magnesium, boron and carbon particulate fuels having 100% $<10\mu\text{m}$ particulate sizes were solicited from the various vendors of metal powders. Samples were received

AD-A060 156

SYSTEMS RESEARCH LABS INC, DAYTON OH AEROSYSTEMS RESE--ETC F/G 21/4
HIGH ENERGY MHD FUELS DEVELOPMENT PROGRAM. (U)

APR 78 R E ECKELS

F33615-75-C-2043

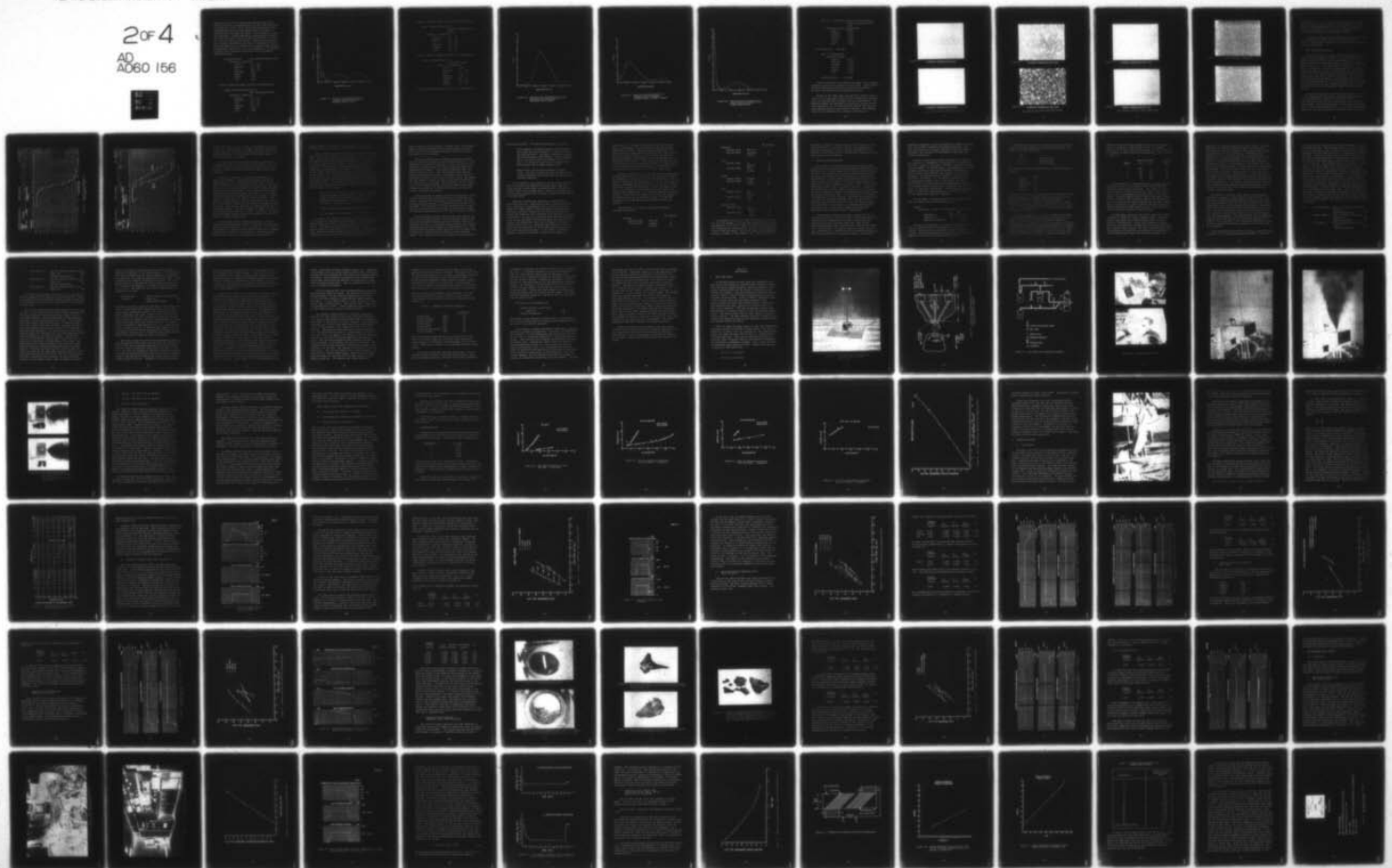
UNCLASSIFIED

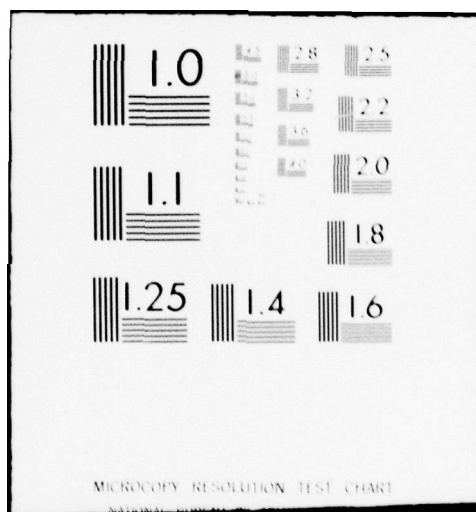
AFAPL-TR-78-10

NL

2 of 4

AD
A060 156





categorized as -325 mesh, meaning all particles are $<44\mu\text{m}$, rather than $<10\mu\text{m}$ as requested except for the carbon which was all submicron in size. It was found that the particle sizes requested were only available through special sieving or classification processing and carbon is not available in larger size particles. Further examination confirmed that as much as 25% of the total was $<10\mu\text{m}$ and could be classified into $<10\mu\text{m}$ and $>10\mu\text{m}$ but $<44\mu\text{m}$ particle groups. Materials were ordered in the -325 mesh category with the intent of subsequently classifying the material since grinding of the ductile materials must be performed cryogenically in an inert atmosphere. The following materials were ordered and had particle sizes and chemical analyses as shown.

Aluminum-Reynolds 400 atomized aluminum powder

Analysis of impurities

Silicon	.01 - .05%
Magnesium	.01 - .05%
Iron	.10 - .25%
Manganese	$<.005$
Copper	$<.005$
Nickel	$<.005$
Zinc	$<.005$

Figure 41 shows the sample particle size distribution.

Magnesium-Reade Manufacturing Co.

RMC 325 magnesium powder

Analysis of impurities

Silicon	.01 - .05
Manganese	.10 - .25
Iron	.05 - .10
Aluminum	.01 - .05
Copper	$<.005$
Zinc	$<.005$

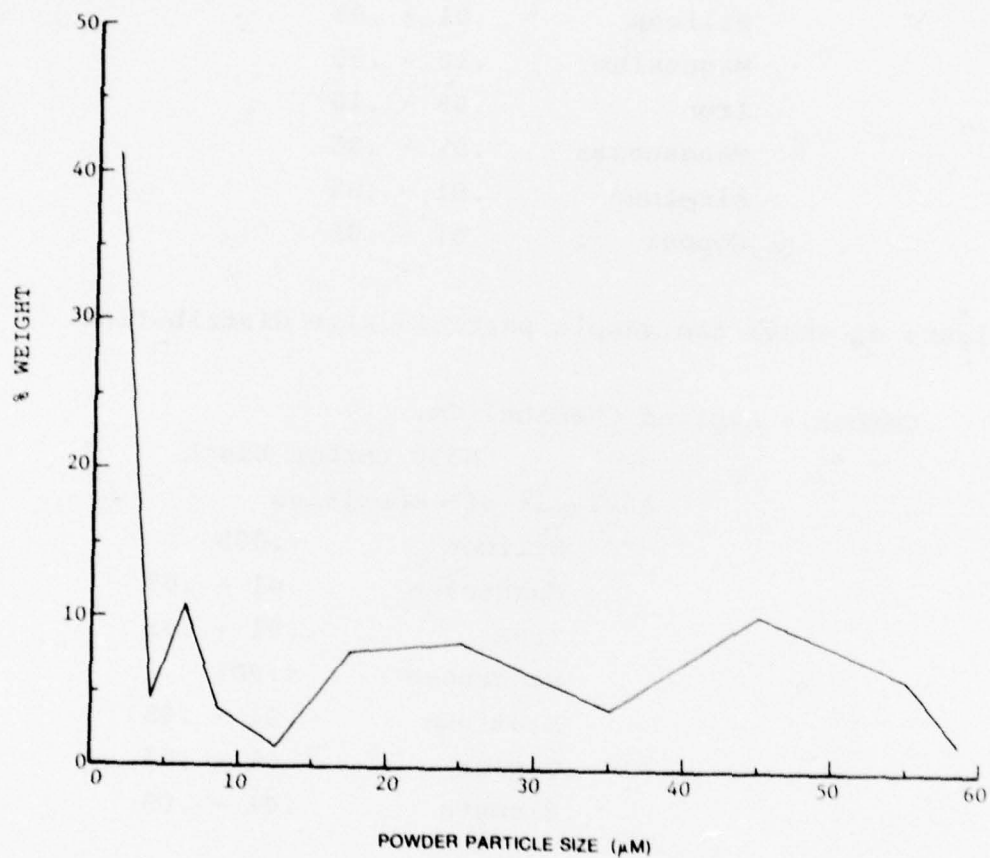


Figure 41. Particle Size Distribution of Reynolds Aluminum 400 Atomized Aluminum Powder Sample

Figure 42 shows the sample particle size distribution.

Boron - Kawecki Berylco, Inc.

amorphous elemental boron

Grade 1

Analysis of impurities

Silicon	.01 - .05
Magnesium	.10 - .50
Iron	.05 - .10
Manganese	.01 - .05
Aluminum	.01 - .05
Copper	.01 - .05

Figure 43 shows the sample particle size distribution.

Carbon - Ashland Chemical Co.

N330 carbon black

Analysis of impurities

Silicon	<.005
Magnesium	.01 - .05
Iron	.01 - .05
Manganese	<.005
Aluminum	.01 - .05
Copper	.01 - .05
Bismuth	.01 - .05

Figure 44 shows the sample particle size distribution.

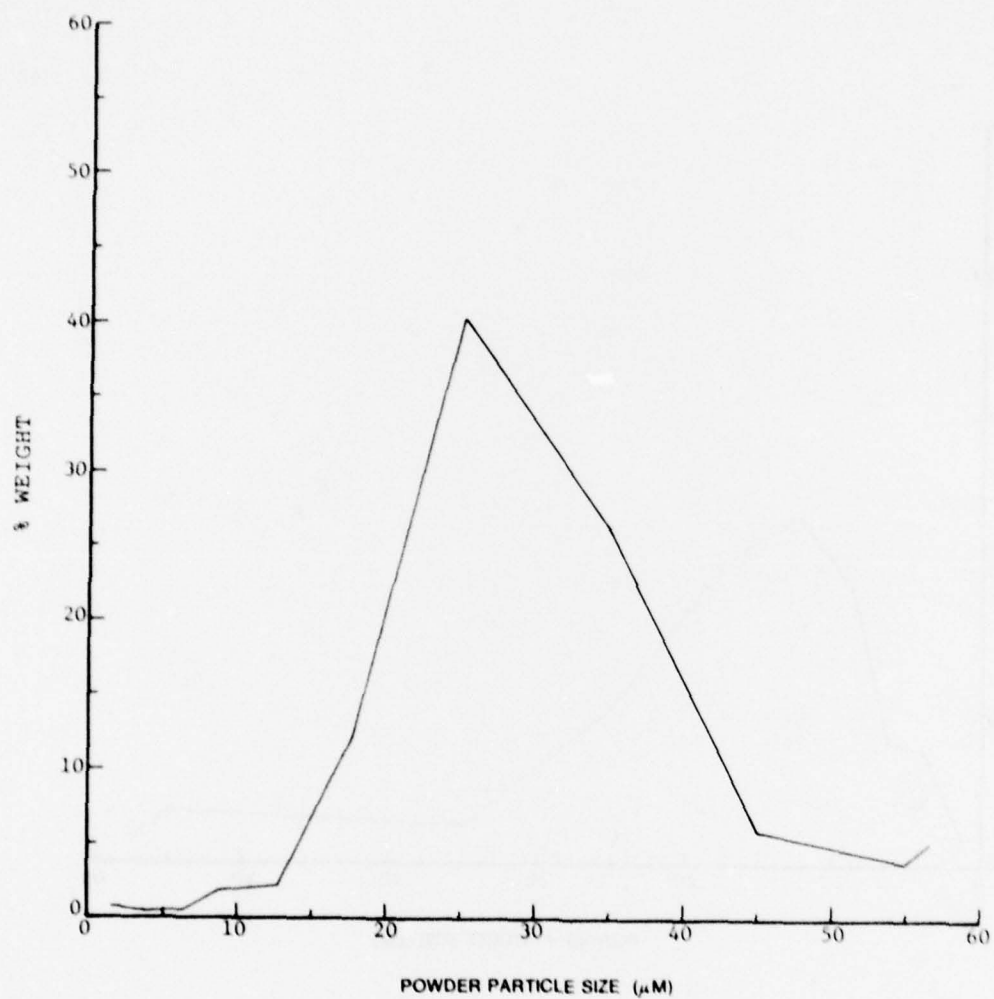


Figure 42. Particle Size Distribution of Reade Manufacturing Company RMC 325 Magnesium Powder Sample

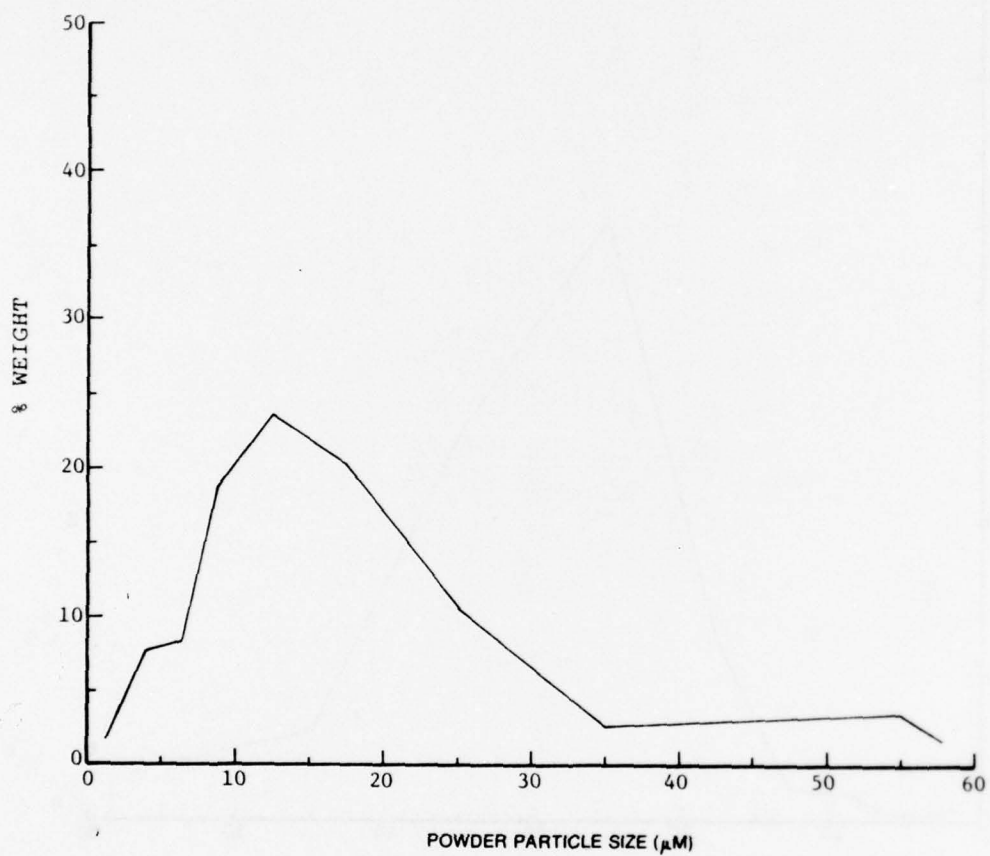


Figure 43. Particle Size Distribution of
Kawecky Berylco Amorphous
Elemental Boron - Grade 1 Sample

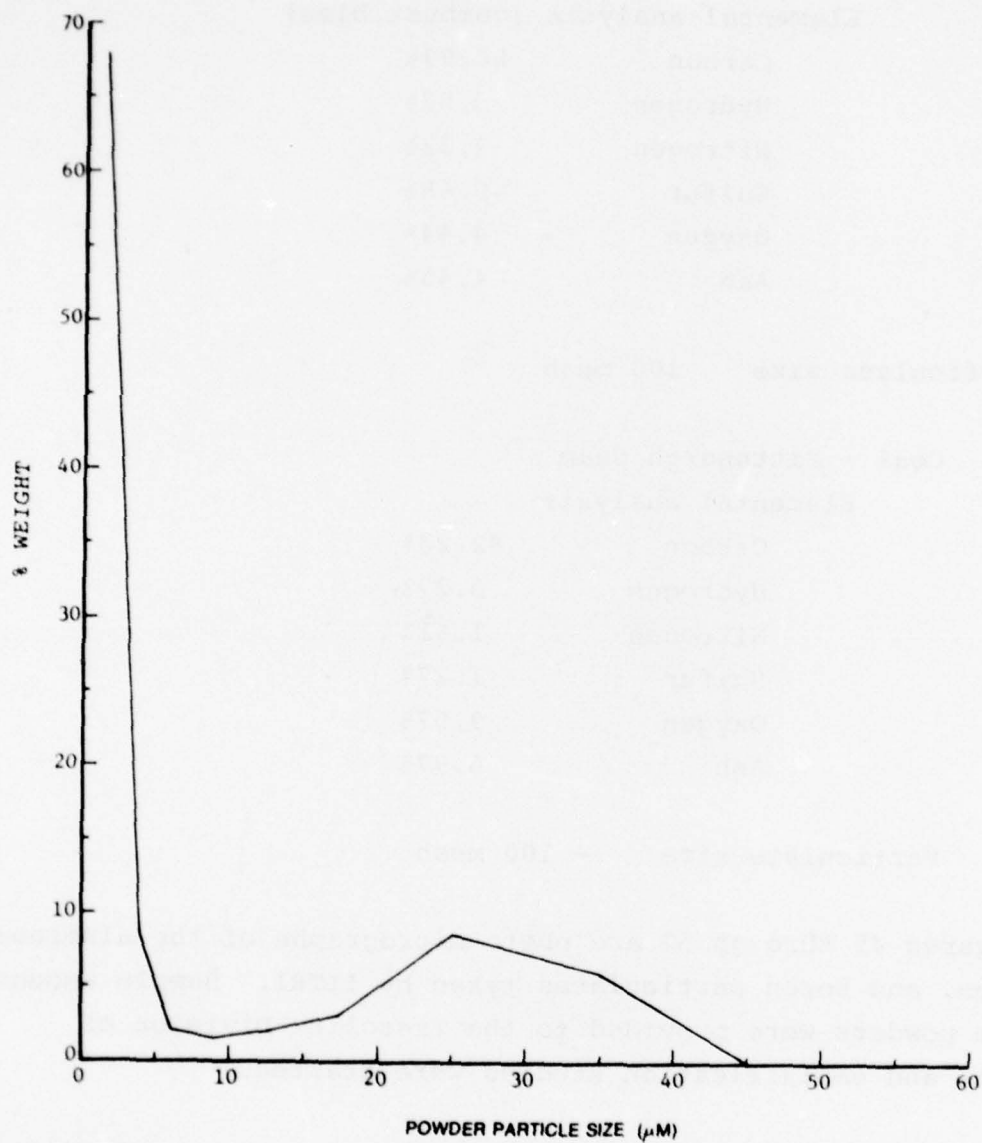


Figure 44. Particle Size Distribution of
Asland Chemical Company - N330
Carbon Block Sample

SRC Coal - Pittsburgh & Midway Coal Mining Company
Solvent Refined Coal Pilot
Plant.

Elemental analysis (combustibles)

Carbon	86.99%
Hydrogen	5.57%
Nitrogen	2.32%
Sulfur	0.68%
Oxygen	4.44%
Ash	4.45%

Particulate size 100 mesh

Coal - Pittsburgh Seam

Elemental analysis

Carbon	82.23%
Hydrogen	5.27%
Nitrogen	1.61%
Sulfur	1.27%
Oxygen	9.57%
Ash	6.97%

Particulate size - 100 mesh

Figures 45 through 52 are photo micrographs of the aluminum, magnesium, and boron particulates taken by IITRI. Sample amounts of these powders were provided to the Tretolite Division of Petrolite and emulsification studies were started.

Results of the IITRI study indicated that further classification of the boron would require liquid sedimentation techniques since the particles were too small for air classification. The magnesium powders are adaptable to sieving for limited particle range separation, but air classification would be the only procedure whereby specific sizes could be obtained. The aluminum could not be processed by any technique other than air

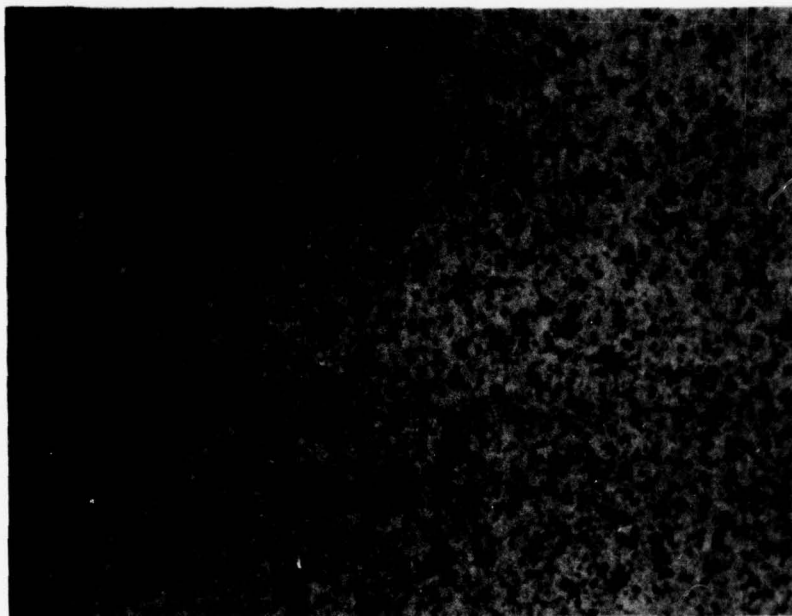


Figure 45.

ALUMINUM TRANSMITTED LIGHT 65X

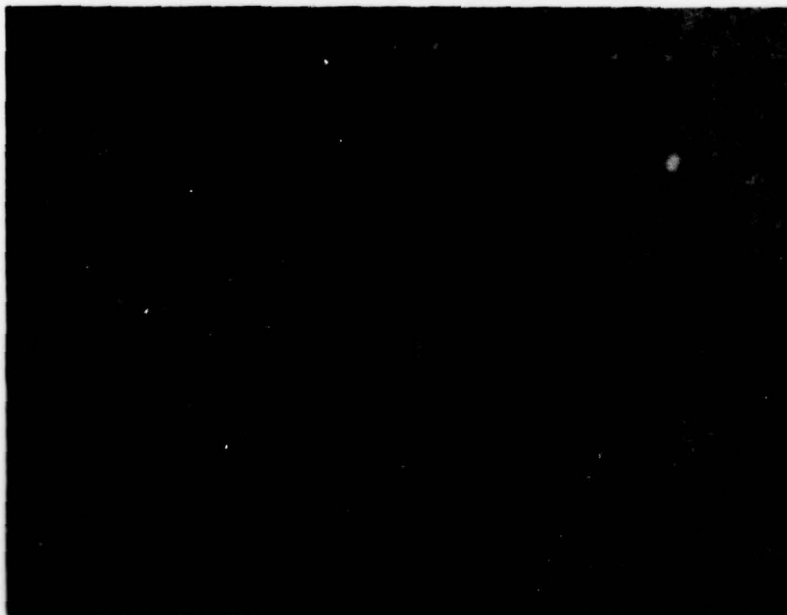


Figure 46.

MAGNESIUM TRANSMITTED LIGHT 65X

Fuel Additive Particle Photo Micrographs

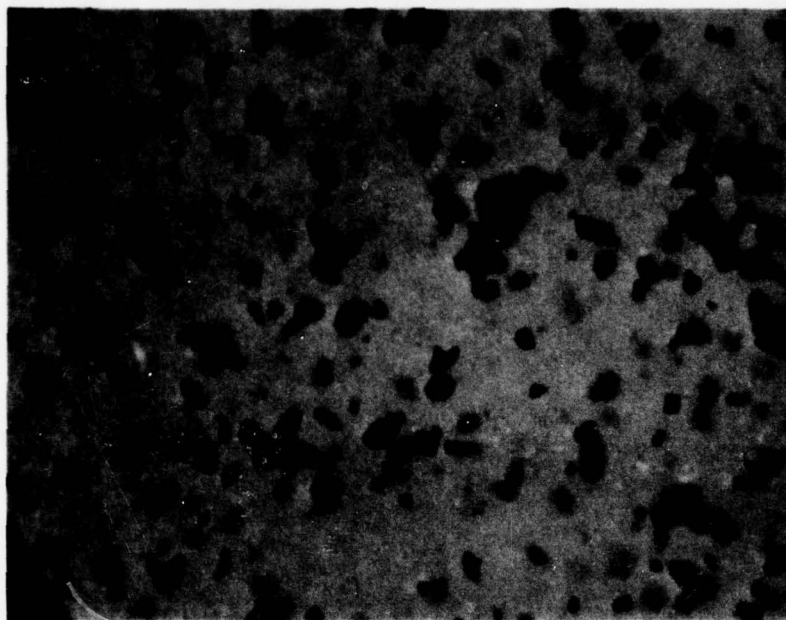


Figure 47.

ALUMINUM TRANSMITTED LIGHT 420X

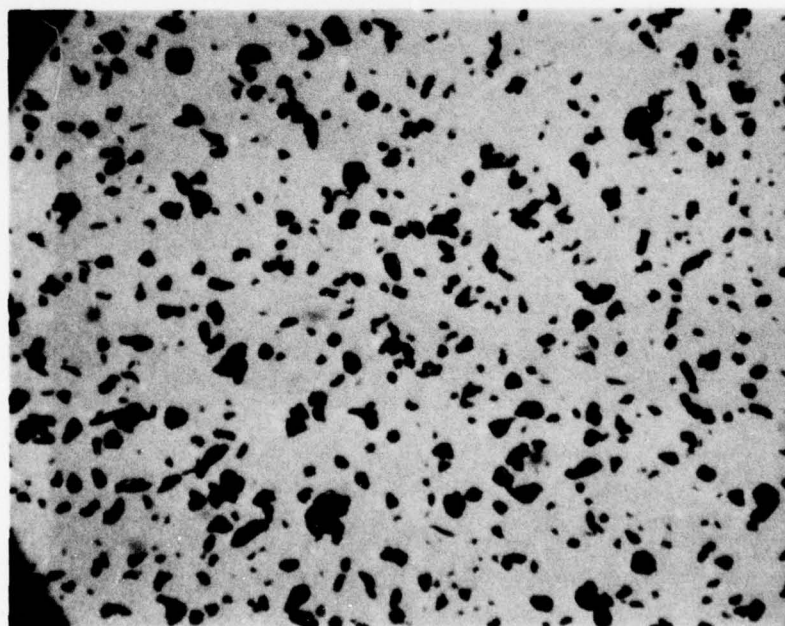


Figure 48.

MAGNESIUM TRANSMITTED LIGHT 163X

Fuel Additive Particle Photo Micrographs



Figure 49. ALUMINUM TRANSMITTED LIGHT 163X

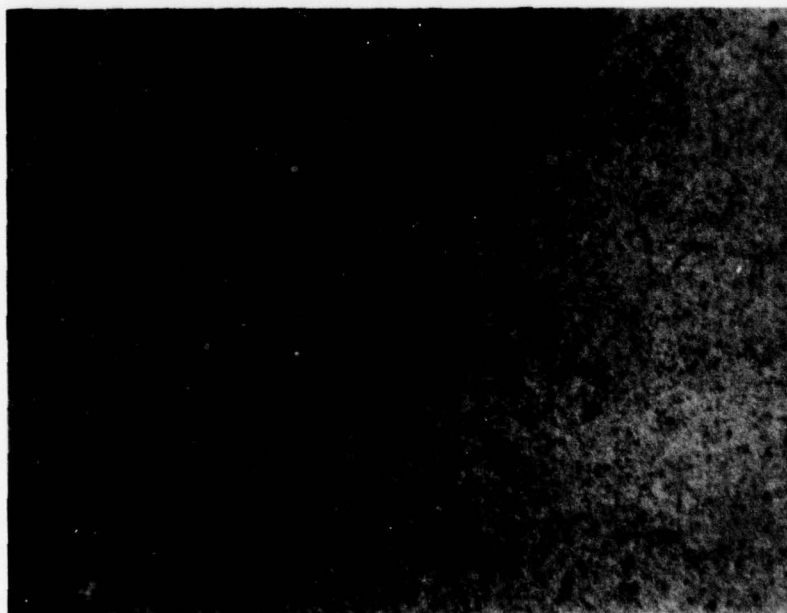


Figure 50. BORON TRANSMITTED LIGHT 163X
Fuel Additive Particle Photo Micrographs

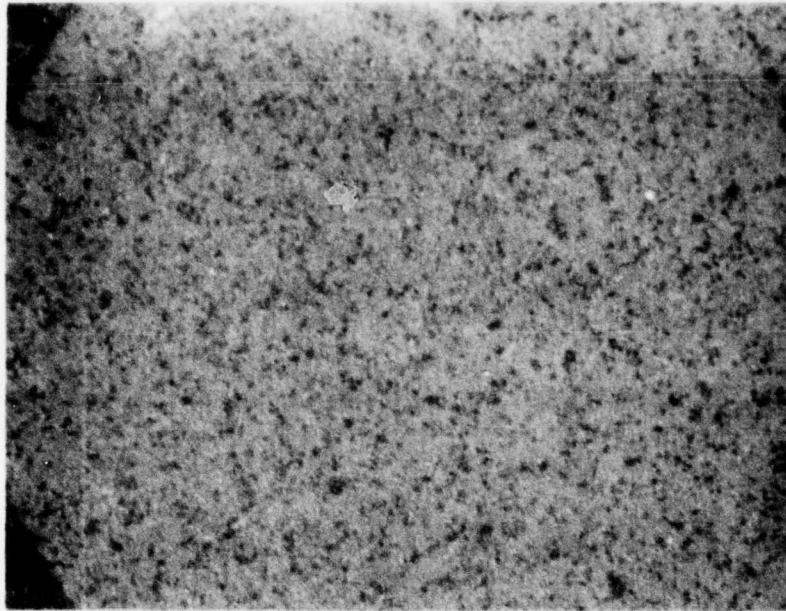


Figure 51. BORON TRANSMITTED LIGHT 420X

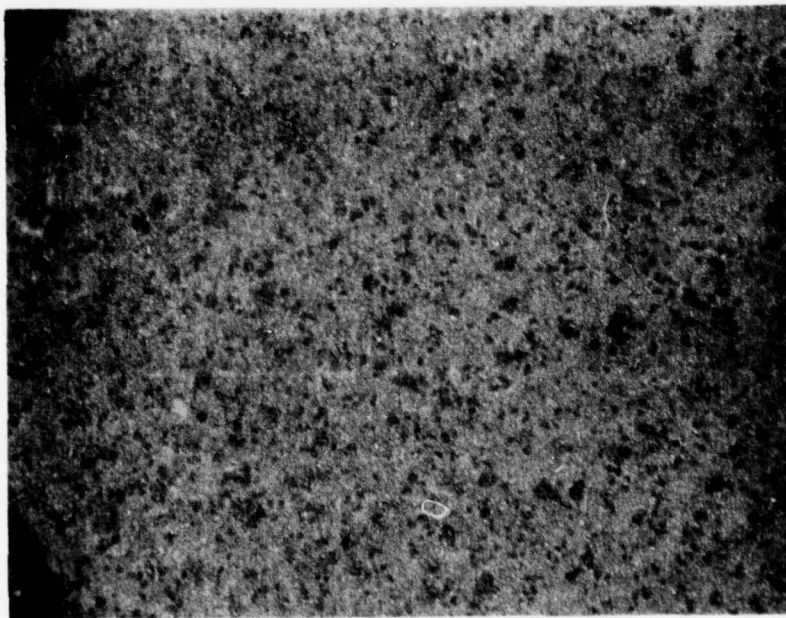


Figure 52. BORON TRANSMITTED LIGHT 663X

Fuel Additive Particle Photo Micrographs

classification. As can be seen in the Figures 45, 47, and 49, the particles are highly irregular in shape and many are flattened into flake configurations. This is not an undesirable situation and should result in more rapid combustion than the major particle dimensions would otherwise indicate.

Following the IITRI study the magnesium was classified into three particle size groups, $<10\mu\text{m}$, 10 to $20\mu\text{m}$, and $>20\mu\text{m}$. Figures 53 and 54 show a particle size analysis of the resultant classified magnesium.

2. EARLY FUEL EMULSION MIXING

Tretolite was able to quickly provide emulsifiers and procedures for the formation of water in oil (W/O) emulsions for injector nozzle testing to be described subsequently. The emulsion was made by thoroughly mixing an amount of emulsifier EM-120 equal to 1 to 2% of the final mix weight with 2 to 3% of JP-4 or a light oil. Water was slowly added until final mix weight was attained. Mixing of small samples was done using a Kitchen Aid mixer, Model 4C, while larger batches for injector testing were mixed using a Hobart A-200 mixer. All mixing was performed at very slow speeds to avoid breaking the emulsion. Results indicated that the 97/3 (W/O) emulsion was not as stable as the 95/5 mix as shown by complete breakdown within 24 hours while the 95/5 ratio was completely stable over the same time period.

Proprietary emulsifiers were developed by Tretolite for oil in water emulsions of JP-4 using a mixing procedure similar to that described above except that 2% emulsifier EM-23D was mixed with 6% H_2O and the internal phase, JP-4, was then slowly added. Mixing continued until a thick mass was obtained with no free internal phase liquid. A very similar emulsion was made using the same percentages of Tretolite emulsifier EM-23D

COULTER COUNTER Model T & TA		PARTICLE SIZE ANALYSIS	
DATE	10/23/75	FOR MODEL, TA	FOR MODEL, TA
OPERATOR	DB	FOR MODEL, TA	FOR MODEL, TA
EQUIPMENT	4947-4F	FOR MODEL, TA	FOR MODEL, TA
REAGENT	2% NaCl	FOR MODEL, TA	FOR MODEL, TA
SAMPLE	ethylene glycol 100μ	FOR MODEL, TA	FOR MODEL, TA
ANALYST	SPP/US	FOR MODEL, TA	FOR MODEL, TA
LABORATORY	Magnesium	FOR MODEL, TA	FOR MODEL, TA

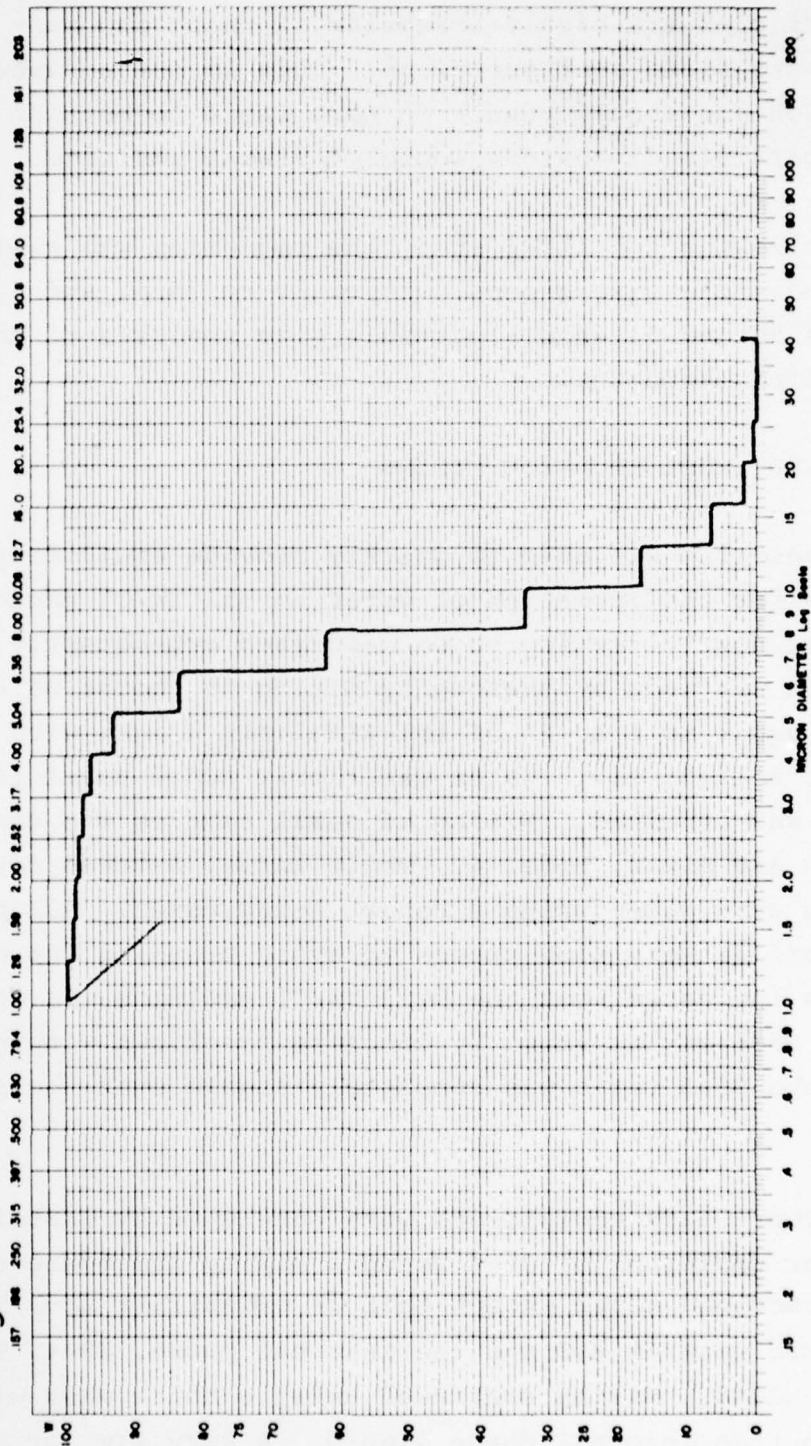


Figure 53. Particle Size Analysis of
<10mm Magnesium Powder

COULTER COUNTER Model T A T A		PARTICLE SIZE ANALYSIS		CONQUEST ELECTRONICS INC. 11-288- PO BOX 57 MALLARD FLA 32049	
OPERATOR	MAJAC				
DATE	KM				
TEST	TA				
4947-SF		20% NAC ethylene glycol		SAMPLE METHOD	
TSP		TSP			
Ultrasonic					
Magnesium					

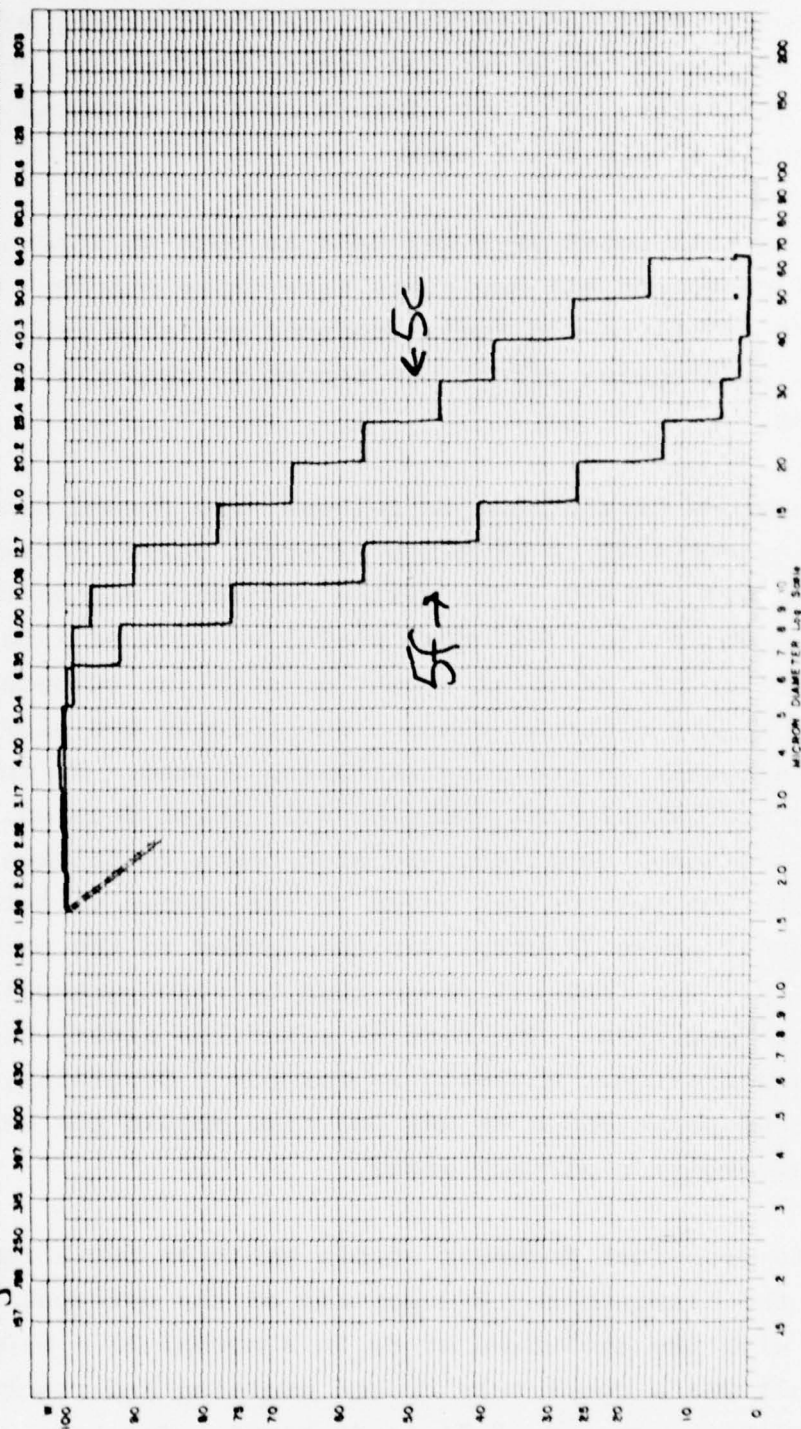


Figure 54. Particle Size Analysis of 10 to 20mm and >20mm Magnesium Powder

and H_2O and then using this mixture to thoroughly wet a weight of 30% coal. This results in a crumbly and caking mass which neither sticks to the mixer and mixing bowl walls, nor has any dusting qualities. To this mixture JP-4 is added slowly to obtain again a very thick mass.

Up to this point JP-4 was used as both an internal and external phase and all emulsions were quite stable. Work with the other additives and fuels produced variable results and, initially, extensive effort was needed to obtain satisfactory emulsions.

Emulsions of aluminum in toluene were formed using 5% emulsifier LMF-4229, a premixed external phase, containing approximately 75% H_2O . The mixing procedure was as follows. An amount of emulsifier (external phase) was placed into the mixer and a portion of the total amount of straight toluene was added directly to the external phase. The toluene was slowly added, making sure that an emulsion was being formed. If the toluene is added too quickly the emulsion will never develop. Straight toluene was added until the emulsion began to thicken. The balance of the toluene was added to the powder to form a slurry. The internal phase (slurry) was then added to the emulsion mixed previously. The internal phase must be added gradually while mixing the emulsion. The rate at which the slurry is added can be increased as more emulsion is formed. Generally, the amount of internal phase added at any one time should not exceed the amount of emulsion already mixed.

This procedure formed a stable emulsion but a reaction between the aluminum and H_2O portion of the external phase soon started with the evolution of H_2 in a normal $Al + H_2O$ reaction. The result was a completely broken emulsion and reacted aluminum powder within a period of 24 to 48 hours. The same procedure and emulsifier was used to form magnesium emulsions which

appeared stable upon formation, but started to react within minutes and the reaction was completed within several hours.

Unless a means of preventing reaction of the Mg and Al with water of the external phase could be developed, efforts to form stable particulate emulsions would be fruitless. The answer to the problem finally used, but which should not be considered to be a final solution, was to produce a surface oxide film on the Al and Mg. The emulsion is a three-phase matrix where solid particles are surrounded by the internal liquid fuel (hydrocarbon) phase, which will not react with the Al or Mg, and H₂O external phase. It is possible to prevent reaction of the Al or Mg particles at the points where they contact the H₂O portion of the external phase by protecting the particles from contact with the external phase. This was done by pretreating the Al and Mg powders with a chromic acid solution to form an oxide film on the Al or Mg particles as follows:

- o Mix a slurry of 50 weights of magnesium or 80 weights of aluminum powder, with 1 weight of chromic acid, 25 weights of water and sufficient toluene to form a slurry and mix thoroughly for approximately 15 to 20 minutes. Drain the liquid.
- o Filter, wash with acetone and refilter the powder.
- o Dry the powder in a vacuum oven or vacuum chamber.

The powder was mixed into an aqueous solution of chromic acid; toluene was then added to form a slurry. This composition was thoroughly mixed then filtered to separate the liquid and powder. The powder was then washed with acetone to remove excess chromic acid and placed in an oven to dry at approximately 325K. The powder becomes granular after this process due to coagulation of particles during the reaction; therefore, the

material must be sifted through a 325 mesh sieve. The treated powder contains approximately 0.6% percent by weight chromic acid in the form of a magnesium chromate (Mg_2CrO_4) coating on the surface of the particles.

Initially, emulsions were formed as previously indicated with the pretreated powder and the LMF 4229 emulsifier. It was found that the emulsions would start to react in much the same manner as noted previously, but after having been stable for approximately 48 hours. It was found accidentally after the emulsion had been left in fuel lines between tests that the aluminum would partially react, precipitate from the emulsion and become "plated" on fuel lines, fittings, valves, and tankage. The only method of removal was then to soak the affected parts in a strong solution of NaOH. The same result was also found as a result of incomplete purging of the fuel system after tests. Changing the emulsifier to LMF 4234 and mixing, as noted previously, eliminated the problem.

Initial attempts to emulsify boron with toluene were unsuccessful, but emulsifier modifications were developed that produced an emulsion which was stable for many months. The boron emulsion produced requires a 3/1 maximum ratio of boron to external phase. This means that for boron concentrations of higher than 15% the external phase percentage is greater than 5% which is considered unacceptable due to the high H_2O content required.

The toluene-boron emulsion was mixed by first wetting the boron with the external phase. This is different from the emulsions with aluminum and magnesium since the boron tends to be wetted by the water in the external phase, whereas, the aluminum and magnesium tend to be wetted by the hydrocarbon fuel. This presents problems with the boron emulsions since the powder must be wetted by a relatively small amount of liquid (external phase). As a result the 3/1 ratio of boron to external phase is

presently maintained. The mixing procedure was as follows:

First, measure the desired quantity of boron powder, then slowly mix into the boron a 3/2 ratio of water/LMF 4235 emulsifier. The water + emulsifier comprise the external phase of the emulsion. As was mentioned above, the ratio of boron to external phase is 3/1; that is, an emulsion containing 30% by weight boron would require 10% by weight external phase.

While mixing, add the desired amount of toluene slowly. The same care must be exercised when mixing the boron emulsion as was noted with the magnesium and aluminum emulsions.

In all attempts to mix emulsions, if the internal phase is added too rapidly, the emulsion will break down. When this occurs as much internal phase as possible must be drained off without removing the external phase. Mixing is continued until the mix surface appears "dry," and then restart the slow addition of internal phase.

Emulsions of carbon were formed in a manner similar to those used with coal. Emulsifier LD 4240, a premixed external phase consisting of approximately 60% to 80% H₂O, was used to prewet the carbon powder as with the previous coal emulsions. Emulsifier and water contents are not specified exactly here, because the emulsifiers are considered to be proprietary materials by Petrolite. As with all of the previously described emulsions, after wetting the powder with external phase the internal phase, toluene, was added slowly until the full amount of internal phase had been mixed in. The carbon emulsions had an unusual characteristic attributed to the extremely small particle size. This was a very high viscosity. At 30% carbon the emulsion became so extremely thick that it could not be pumped in a

normal manner. An attempt to emulsify SRC (Solvent Refined Coal), as a substitute for carbon with toluene was notably unsuccessful although a different approach might work. Upon contact with the toluene SRC coal dissolves into a very viscous tar which resisted attempts at emulsification by Petrolite. Future work might be successful by using the tar-like mass and emulsifying that directly. Emulsification of the SRC coal with JP-4 was quite successful and was performed in a manner similar to the technique used with unrefined coal. Emulsification of unrefined coal and toluene by Petrolite was unsuccessful.

Seed/fuel emulsions of Cs_2CO_3 by Petrolite were unsuccessful although emulsions of up to 10% CsNO_3 and toluene were formed. The procedure is similar to that used with Al and Mg. First an amount of emulsifier LMF 4229 equal to 1% of the final weight of emulsion was added and mixed with 4% H_2O . An amount of toluene sufficient to slurry the 10% weight of CsNO_3 was added to the CsNO_3 . The remainder of the toluene was slowly added to the external phase (emulsifier + H_2O) until the emulsion started to thicken. At this point the slurried CsNO_3 was slowly added to the emulsion until it was thoroughly mixed. The remaining toluene was then added and mixed until emulsification was complete.

The following is a listing of emulsion formulations developed by Petrolite:

		<u>Wt. Percent</u>
Aluminum		
External Phase	LMF-4234	5
Internal Phase	aluminum	30
	toluene	65

			<u>Wt. Percent</u>
Magnesium			
External Phase	LMF-4234		5
Internal Phase	magnesium		30
	toluene		65
Boron			
External Phase	H ₂ O		6
	LMF-4235		4
Internal Phase	boron		30
	toluene		60
Carbon			
External Phase	LD-4240		8
Internal Phase	carbon		30
	toluene		62
Coal			
External Phase	H ₂ O		6
	EM-23D		2
Internal Phase	coal		30
	JP-4		62
Cesium Nitrate			
External Phase	H ₂ O		4
	LMF-4229		1
Internal Phase	WC ₂		10
	toluene		85

No attempts by Petrolite to emulsify benzene were successful, nor were attempts to include seed material with Al or Mg. Seed material in the form of CsNO₃ was successfully emulsified with toluene/boron, toluene/carbon, and JP-4/coal in amounts up to 10% of the fuel weight. As may be noted from the foregoing sections, an amount of seed equal to 15% - 20% of the fuel is

desirable. Attempts to combine CsNO_3 with Al or Mg in an emulsion failed due to a reaction of the NO_3^- ion attacking the aluminum and magnesium. Until a means of preventing NO_3^- ion mobility or protecting the Al or Mg particles is developed, such emulsions will not be possible.

3. EMULSION MIXING TECHNIQUES

As a result of similar but unassociated work being done during the same time period by Systems Research Laboratories the possibilities of several commercially available emulsifiers were revealed. At the same time, an expired patent[19] was found where chloride salts were used to enhance the effectiveness of the emulsifier. Several quick tests proved the validity of the patent claims and the theory of emulsifier enhancement by the chloride salts was extrapolated to nitrate salts. Similar tests proved the nitrate salts to be equally effective in improving the performance of several types of emulsifiers. As a result, the first attempts to emulsify JP-4 and then toluene with nitrate salts were successfully made. In consideration of the expense of cesium salts and their chemical similarity to potassium salts the tests were performed using KNO_3 until the emulsification technique was perfected and then the KNO_3 was replaced successfully with CsNO_3 . Little specific information was available concerning high internal-external phase ratio emulsions, especially those containing volatile hydrocarbons.

Atlas Chemical Industries produces an extensive list of primary emulsifiers as do numerous other chemical manufacturers indicated by the McCutcheon's Directory of Detergents and Emulsifiers[32] which provides trade name, index of HLB, emulsifier/detergent class, manufacturer, classification index, type, form available, and remarks concerning general types of use or application. A publication of Atlas Chemical Industries, "The Atlas HLB System"[33] describes a means of classifying

emulsifiers according to type and Hydrophilic-Lipophilic Balance (HLB) and provides a system for developing emulsions. The Atlas HLB system was originally developed in the late 1940s to systematize the procedure for development of emulsions and selecting emulsifiers.

Briefly, the HLB system enables assignment of a number to the ingredient or combination of ingredients to be emulsified, and then to choose an emulsifier or blend of emulsifiers having this same number. In the HLB system, each emulsifier is assigned a number representing the relative balance of hydrophilic (water-loving) polar molecules and lipophilic (oil-loving) molecules. Emulsifiers having a lipophilic composition are assigned a low number 0 - 9. Hydrophilic emulsifiers are assigned numbers greater than 11, the general limit being approximately 20 although some strongly hydrophilic emulsifiers are assigned numbers as high as 80. Surfactants in the 9 to 11 range are considered intermediate. The McCutcheon's Directory which contains some 6,000 surfactants lists the HLB number of all the commercially available compounds.

The HLB number of blended emulsifiers is calculated based upon the weight ratio of the emulsifiers used.

Example:

Emulsifier A - HLB = 16, Emulsifier B - HLB = 4

	Wt. %	HLB
Emulsifier A	80%	$80 \times 16 = 12.8$
Emulsifier B	20%	$20 \times 4 = .8$
Emulsifier blend HLB		$= 13.6$

The HLB of an emulsifier is related to its solubility. Thus, an emulsifier having a low HLB will tend to be oil-soluble, and one having a high HLB will tend to be water-soluble, although two emulsifiers may have the same HLB and yet exhibit quite different solubility characteristics.

Therefore the formation of O/W emulsions requires a water soluble or high HLB emulsifier, and W/O emulsions require oil soluble or low HLB emulsifiers.

HLB	
4 - 6	W/O emulsifiers
7 - 9	Wetting agents
8 - 10	O/W emulsifiers

Some materials and their required HLB are listed below for O/W emulsions.

	HLB
Benzene	15
Kerosene	14
Nitrobenzene	13
Toluene	15
Xylene	14

This does not mean that any emulsifier having an HLB of 15 will emulsify benzene. It does mean that with the proper class or family of emulsifiers a blend of emulsifiers having a blended HLB of 15 will work best. From experience, it seems that to make emulsions having high phase ratios an HLB approximately .5 - 1.0 higher than listed in the references is needed to assure long stability.

The HLB requirement for the likely candidate hydrocarbon fuels has been mentioned, but the specific requirement of an emulsion containing seed salts and energetic additives in suspension are not listed and in most cases completely unknown. The technique of determining the necessary HLB can be considered a systematic approach to experimentally zeroing in on a number. First a family pair of emulsifiers is chosen, one with a high HLB and the other with a low HLB. A series of emulsion test

samples are made with varying amounts of the two surfactants to produce a resultant variable series of HLB. For example, knowing that the basic fuel HLB requirement is ~ 14 a series of test samples are made with the two surfactants A, (HLB = 16) and B, (HLB = 4).

<u>SAMPLE</u>	<u>EMULSIFIER BLEND</u>		<u>RESULTANT</u>
	<u>A</u>	<u>B</u>	<u>HLB</u>
1	100%	-	16
2	92%	8%	15
3	83%	17%	14
4	75%	25%	13
5	67%	33%	12

In the formation of these emulsions an excessive amount of emulsifier, 10% to 15%, is used to cover the fact that the emulsifier family may not be correct. The result will be an emulsion which is better than the rest, that is, more stable, longer lived, and suspends particulates longer or in larger amount. A second stepwise series of tests using smaller steps is then in order to more accurately identify the HLB requirement. In the event that several samples are the same, a smaller amount of emulsifier is used to make the test more sensitive. Having identified the HLB, further testing is now required to identify the ideal emulsifier family and type.

The HLB number identified will remain relatively constant regardless of emulsifier type or chemical family. The surfactant types which can be used include anionic, cationic, nonionic, and amphoteric. During this program the nonionic types were used primarily although several cationic types were used without notable success. The basic classifications include the glycerides, sorbitan fatty acid esters, POE sorbitan acid esters, POE sorbital esters, POE acids, POE alcohols, POE

adducts N.O.C., chelates, and glycerol fatty esters. The first approach to selecting an emulsifier class is to examine the "oil" phase, in the case of fuels in this program they are the internal phase "oil" of O/W emulsions. The question to be examined is, is it a saturated or unsaturated hydrocarbon. By definition a saturated hydrocarbon is one in which there are no double or triple carbon bonds and cannot add other molecules. Benzene and toluene are both members of the aromatic series and have classically been thought to contain both single- and double-carbon bonds. More recent theory finds that all of the bonds are the same and "extra" electrons cannot be localized in the ring, but rather belong to the molecule as a whole and therefore the aromatic series hydrocarbons resemble saturated hydrocarbons and react similarly. The result of this discourse indicates the choice of emulsifiers. For example, unsaturated fuels would be most "attracted" to POE sorbitan oleate esters whereas saturated fuels will be "attracted" to POE sorbitan stearate esters, laurate or palmitate esters.

The results of the fuel mixing studies include numerous emulsions in addition to those required by the contract. As a result of very early work performed by Petrolite, it was known that carbon emulsions with the very small particle sizes become unmanageable due to their extremely high viscosity. Boron emulsions, too, were considered to be less than ideal fuels to work with, at least at this early stage, due to the possibility of poor combustion and resultant ejection of unburned boron particles into the atmosphere. This presented too great a possibility of health hazard and further work with carbon and boron were stopped. As a substitute, it was planned that emulsions of coal with JP-4 and seed with toluene, benzene and other fuels would be investigated.

The first emulsions developed by SRL were, as has been noted, emulsions of JP-4, toluene and benzene with CsNO_3 . Initially

JP-4 emulsions were made and the technique developed to include toluene and benzene. The technique used was to mix the emulsifier (1%) with the H₂O (2%) to form the external phase, continue mixing the external phase and add 0.5% of the seed to the external phase. A portion of this seed will dissolve depending upon the external phase temperature. The remaining seed should be slurried with sufficient internal phase (liquid fuel) to cover the seed material. Approximately half of the remaining internal phase is then slowly added to the external phase to form an emulsion. As the internal phase was added, the consistency changed from that of a translucent cream to an opaque white thin mayonnaise. At this point, the major portion (slurried) of seed material was slowly added to the emulsion. This continued to increase the viscosity as seed and fuel were added. When all seed material was added, the remaining internal phase was slowly added until the emulsion contained all that was required by the mix proportions. Variable seed ratios have been manufactured by this procedure up to 30% CsNO₃ seed. This is naturally far more than is needed, but was done to demonstrate the ability of the emulsion to suspend seed for long periods of time (6 months). The JP-4, toluene, and benzene emulsions are all produced using the same basic procedure. The emulsifier in this case is formed as follows:

For:	toluene emulsion -- POE (20)	Sorbitan lauryl ester	
		(Tween 20)	92%
		Sorbitan Monolaurate	8%
	benzene emulsion -- POE (20)	Sorbitan Laurylester	
		(Tween 20)	94%
		Sorbitan Monlaurate	6%
	JP-4 emulsion -- POE (20)	Sorbitan lauryl ester	
		(Tween 20)	79%
		Sorbitan Monolaurate	21%

JP-4 emulsion	--	POE (20) Sorbitan palmitate ester (Tween 40)	85%
		Sorbitan Monopalmitate	15%
JP-4 emulsion	--	POE (20) Sorbitan Stearate ester (Tween 60)	98%
		Sorbitan Monostearate	2%
JP-4 emulsion	--	POE (20) Sorbitan Oleate ester (Tween 80)	100%

Note that these emulsions require only 2% H₂O by weight of water as opposed to 4% or more for the early emulsions. Experience suggests that the emulsifier content could be reduced from 1% to as low as 0.5%, but specific tests have not been conducted to verify this.

The next test series involved emulsification of JP-4, coal and seed. In the emulsification of coal several techniques were tried with some giving better results than others; that is, a more stable emulsion. The best compromise technique appears to be similar to that mentioned earlier for coal. The procedure began with mixing of the external phase, 1% emulsifier and 3% water (here again, experience indicates a possible decrease to 2% without degrading the emulsion stability); 0.5% seed was added and mixed thoroughly. At this point all of the coal was added and mixed until dusting of the coal had ceased and most of the coal lumping was very small or crumbly. The seed was slurried with sufficient internal phase (liquid fuel JP-4) to just cover it and mixed to assure wetting of the seed. The remaining internal phase was added to the wetted coal slowly while mixing until an emulsion formed and started to become viscous. Initially the wetted coal will start to "ball up" around the mixer and the large lumps require breaking to facilitate rapid assimilation of the JP-4. The next stage of mixing involved a decreasing slurry viscosity and then increasing viscosity as the emulsion forms. When the emulsion viscosity

started to increase, the slurried seed was slowly added, followed by the remainder of the internal phase. It is recognized that these techniques are not readily adaptable to production line operation, but technique modifications can be made to allow procedures more conducive to production operation. The first change would be to add seed and internal phase simultaneously. In a laboratory environment it is simpler to add constituents one at a time. The emulsifier for coal/JP-4/seed emulsions is formulated as follows:

Coal/JP-4/seed	-	POE (20) Sorbitan Laurate ester	
emulsion		(Tween 20)	96%
		Sorbitan Monolaurate	4%

As might be noticed by calculating the HLB of this mixture, the result is much higher than normally expected for JP-4. The cause of this requirement appears to be a much higher surface energy requirement than usual, created by the coal particles. The coal particles are quite irregular in shape and extremely sharp, similar to needles, since the layered material is sheared along layer planes during the grinding process. The result is an HLB requirement of approximately 16.4 - 16.5 rather than 14 which is normal for JP-4. At the same time, toluene/coal emulsions were tried with varying techniques and although one very good emulsion was obtained, it could not be duplicated with the result that further toluene/coal study was stopped.

When several emulsions with treated aluminum and seed had been attempted with the result that the CsNO_3 and aluminum had reacted, the idea of waterless emulsions was first developed with the intent of preventing ionization of the CsNO_3 in solution. The idea also appeared to have merit from the standpoint of preventing the same occurrence with Cs_2CO_3 with the resultant attack on the emulsifier esters by the strong alkali solution formed by water and Cs_2CO_3 . Although it is now quite obvious

why early attempts to emulsify Cs_2CO_3 did not succeed, it was not so obvious during those attempts. Since Cs_2CO_3 ionizes in the presence of H_2O , forming a strongly basic solution, the ester linkages of the emulsifiers used were broken by the alkali solution, resulting in destruction of the emulsifier and an inability to form emulsions. In general, the nitrate salts have a relatively neutral pH and therefore have no effect on the ester linked emulsifiers.

Emulsions are formed from two immiscible liquids dispersed and stabilized through the use of an emulsifying agent. In general, most emulsions have been formed using water and a second liquid (generally a hydrocarbon) generically termed an oil. The emulsions thus formed, as has been pointed out, are considered oil in water (O/W) or water in oil (W/O) emulsions depending upon which is the internal phase. As mentioned previously, we are interested here only in the O/W emulsions and specifically in the minimal possible use of water since it depresses the combustion flame temperature, and OH-ions produced from dissociated H_2O poison the plasma. The question was posed: could a glycol be used as a polar liquid to replace water and also to prevent the ionization of Cs_2CO_3 in solution. As has been noted, the use of glycols does not improve either flame temperature or conductivity due primarily to the larger amount of glycol needed to form an emulsion when compared to the water needed to accomplish the same task. The second hoped-for advantage was realized in that the CsNO_3 did not react with the aluminum or magnesium. JP-4/aluminum/ CsNO_3 and JP-4/magnesium/ CsNO_3 waterless emulsions were successfully formed as will be described. The third anticipated advantage was not realized either. All attempts to utilize alkali carbonate salts in waterless emulsions using glycols were unsuccessful. For some time the reason was unknown and created quite a puzzle. Finally a beaker of glycol was tested for pH with the expected neutral result. When only a small amount of Cs_2CO_3 was dropped into the

beaker, the pH meter quickly recorded a value of 13+. Obviously the carbonate salt was reacting with the glycol and, although an analysis was not performed for verification, was probably forming glycolates. This conclusion was drawn from the reddish-brown precipitate formed during an emulsion test using Cs_2CO_3 rather than the normally used Na_2CO_3 . This is indicative of the reaction of cesium with ethylene.

The JP-4/aluminum/ CsNO_3 and JP-4/magnesium/ CsNO_3 waterless emulsions were formed as follows. The emulsifier, POE(20) sorbitan monolaurate, 0.7% was mixed thoroughly with 5.6% $\text{C}_3\text{H}_8\text{O}_2$ and the untreated aluminum or magnesium were added and mixed thoroughly. JP-4 was added slowly as mixing continued to form a thick highly viscous emulsion. This emulsion had a stable life of approximately 72 hours. Similar emulsions without the seed or metal additives were stable for several months.

The problem of emulsification of carbonate seed material had still not been solved at this point and further investigation finally revealed that the POE alcohol family of emulsifiers were stable in the presence of alkali solutions. Only preliminary tests were run to verify that these emulsifiers would emulsify the JP-4 and be stable in the presence of Cs_2CO_3 in a JP-4 emulsion. The emulsifier used was POE(23) lauryl alcohol (Brij 35). The emulsifier was heated in a double boiler to liquify the solid and H_2O was added in the amount to ratio the emulsifier and water at the rate of two parts emulsifier to three parts water. When the external phase had been prepared, external phase equivalent to five percent was placed in the mixer. The carbonate seed had been previously slurried with enough JP-4 to completely wet the seed. The remaining JP-4 was split into two equal parts. The first was used to form a normal emulsion. At this point the seed was added slowly. When the slurried seed had been added, the remaining JP-4 was added forming a stable appearing emulsion. This emulsion was stable during the

remainder of the day in which it was prepared, but had completely broken by the following morning. The conclusion is that the emulsion was stable for 6 - 12 hours, a phenomenal increase in stability when compared to the fact that previously, carbonate seed had immediately broken emulsions already formed or prevented the formation of any emulsions. Further effort in this direction should yield satisfactory stability of carbonate seed emulsions with proper emulsifier blending or modification.

With the success of the carbonate seed emulsions, an ensuing theoretical possibility is use of CsOH as a seed material. Other possible cesium seed materials might include those shown in Table 2.

TABLE 2. POTENTIAL CESIUM SEED MATERIALS

		Cs% of Molecular Wt
Cesium amide	CsNH ₂	89
Cesium borohydride	CsBH ₄	90
Cesium carbonate	Cs ₂ CO ₃	81
Cesium cyanide	CsCN	84
Cesium hydride	CsH	99
Cesium hydrogen carbide	CsHC ₂	84
Cesium hydroxide	CsOH	88

These cesium salts become potential seed materials with the advent of waterless emulsions and alkali stable emulsifiers since several of the materials listed decompose in the presence of H₂O. Additionally, several of the compounds have high energy content.

In the use of large MHD generators where there is no seed recovery system, the cost of seed material can become a major part of generator operation. The cost of the seed is primarily

in handling, processing and conversion of the ore to the desired salt form. If pollucite (cesium ore) could be emulsified, a high cost item could be removed from the operating costs. Solution of this problem was studied at the request of the USAF APL with positive results. Although not optimized, a stable emulsion of -200 mesh pollucite ore was successfully formed with toluene. The emulsifier (1%) was mixed with H₂O (3%) and the pollucite ore was added in total forming a thick slurry as mixing continued. Toluene was slowly added to the slurry with continuing mixing until all toluene had been added. This emulsion was completely stable for a period of three to four weeks with 20% pollucite ore.

The emulsifier was blended from:

POE(20) sorbitan lauryl esters	
(Tween 20)	81%
Sorbitan monolaurate	19%

Additionally, since pollucite is quite inert in the presence of H₂O, it can be easily used in conjunction with aluminum as with any other of the reactive additives.

In an attempt to produce high energy liquid fuels, saturated mixtures of toluene and naphthalene, and benzene and naphthalene were prepared. At room temperatures this mixture has the ratio of 5:9, that is, five parts naphthalene to nine parts toluene or benzene. Both solutions were prepared and emulsified both with and without seed. Although not tested, since the toluene or benzene/naphthalene mixture is a true solution and does not contain particulates, there is no reason why such solutions cannot be emulsified with high energy particulates as described in the analytical investigation at percentages up to the theoretical maximum. The only problem arises when the mixture is cooled; the naphthalene crystallizes from the solution. This was

experienced on several occasions with resultant partial breakage of the emulsion. Subsequent reheating to room temperature and minimal remixing restored the emulsion to its original form. The toluene and benzene/naphthalene/seed emulsions were formed similarly to previous seed emulsions. The toluene or benzene and naphthalene were mixed in proper proportion to obtain a solution. The emulsifier POE(20) sorbitan monolaurate (Tween 20) -1% and 4% H₂O were mixed. Although not tested, it is believed that the H₂O content can be reduced to at least 3% and probably 2%. To this mixture 0.5% seed was added. The emulsion mixing was started with addition of 50% of the toluene or benzene/naphthalene solution. The remaining seed was slurried with sufficient solution to cover the CsNO₃ and the slurry was added to the started emulsion. When all slurried seed had been added, the remaining solution was added to bring the emulsion to its target proportions. No unusual problems were encountered and in spite of the highly combustible nature of the internal phase, when an attempt to destroy the excess mixture by burning was attempted it was quite slow both to ignite and to burn when placed on an open plate and open to atmosphere. This again demonstrated the safety aspects of the emulsified fuels.

Another interesting fuel developed by SRL under another contract involved emulsification of toluene and pulverized artificial and actual coal slag with both pollucite and KNO₃ as seed additives. This was developed to simulate the combustion of coal while retaining the simplified fuel feed aspects of a liquid.

Section V

FUEL TESTING

1. FUEL SPRAY TESTS

An extensive series of spray tests were conducted using neat liquid, neat emulsions, and particulate emulsions to determine flow rates, pumping pressures, emulsion breakdown, spray pattern characteristics and the effects of emulsions on the injector and plumbing. The spray tests were conducted using an injector triplet, Figures 55 and 56 simulating one triplet of the KIVA-I injector plate. Figure 57 shows a schematic sketch of this injector block and fuel supply apparatus setup. Figure 58 shows the setup from different angles. Spray tests were conducted with water, water-in-oil emulsions and coal/water-in-oil emulsions. The flows through the injectors were kept constant at 18 and 15 gm/sec for the fluid and gas respectively. The nominal KIVA-I flow for each injector is approximately 18 gm/sec. The spray patterns and pressure drops of the slurries and emulsified slurries were compared to those with the neat liquids (Figures 59 and 60).

Figure 61 shows the spray pattern of neat water through two different injectors at different pressure drops. The spray in Figure 61-1 is from a 0.16 i.d. injector at 1 atm pressure drop. Figure 61-2 shows the spray from a 0.084 i.d. injector with a 15 atm pressure drop. Note that all pressures referred to in tests are "gage" pressures since all data pressure transducers are referenced to atmospheric pressure. This is also the case for subsequent power generation tests. Similar tests were run in addition to neat water with:

- o 95% H₂O in 5% emulsion
- o 97% H₂O in 3% emulsion

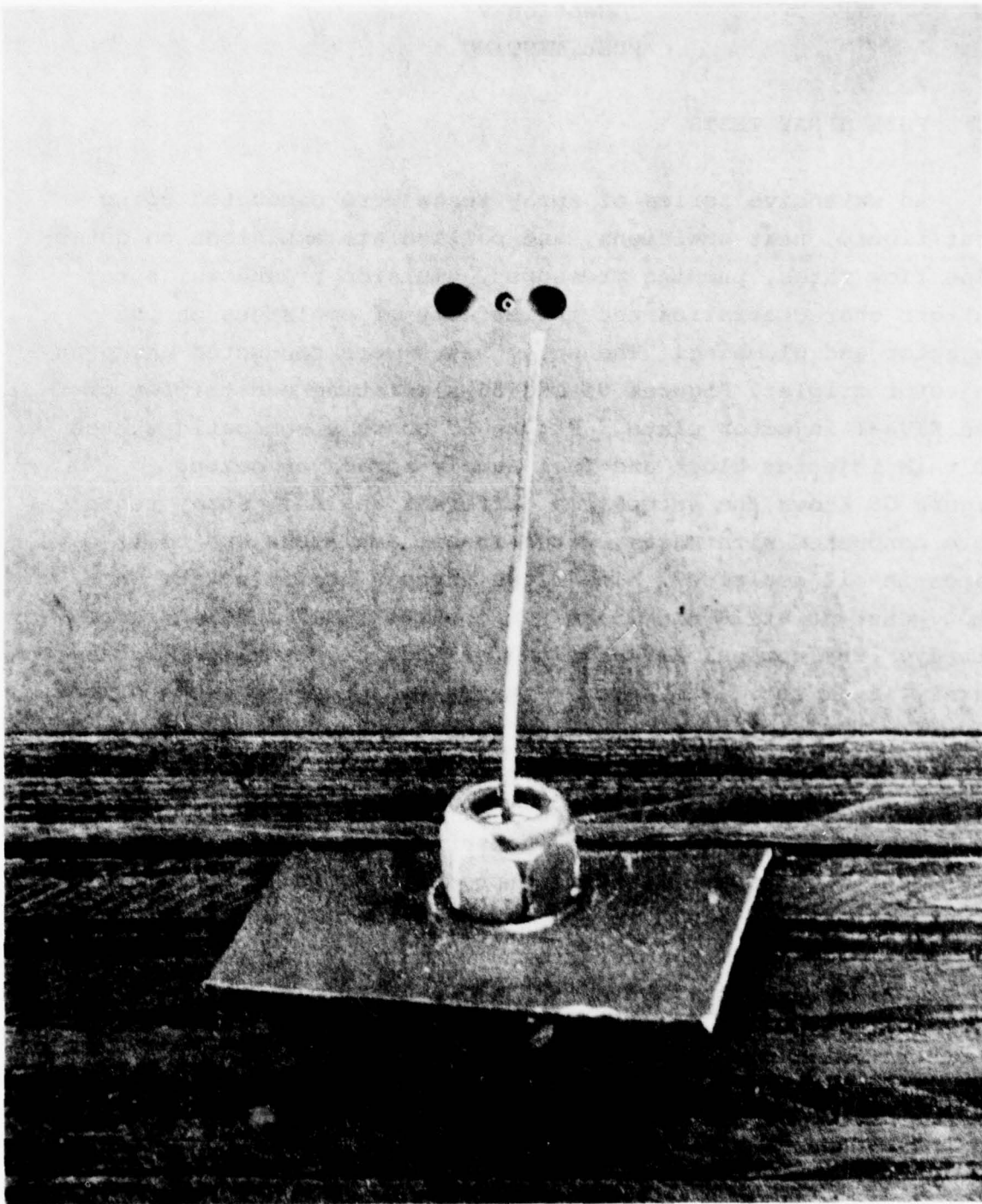


Figure 55. Simulated KIVA - I Propellant
Injector Triplet Used for
Spray Tests

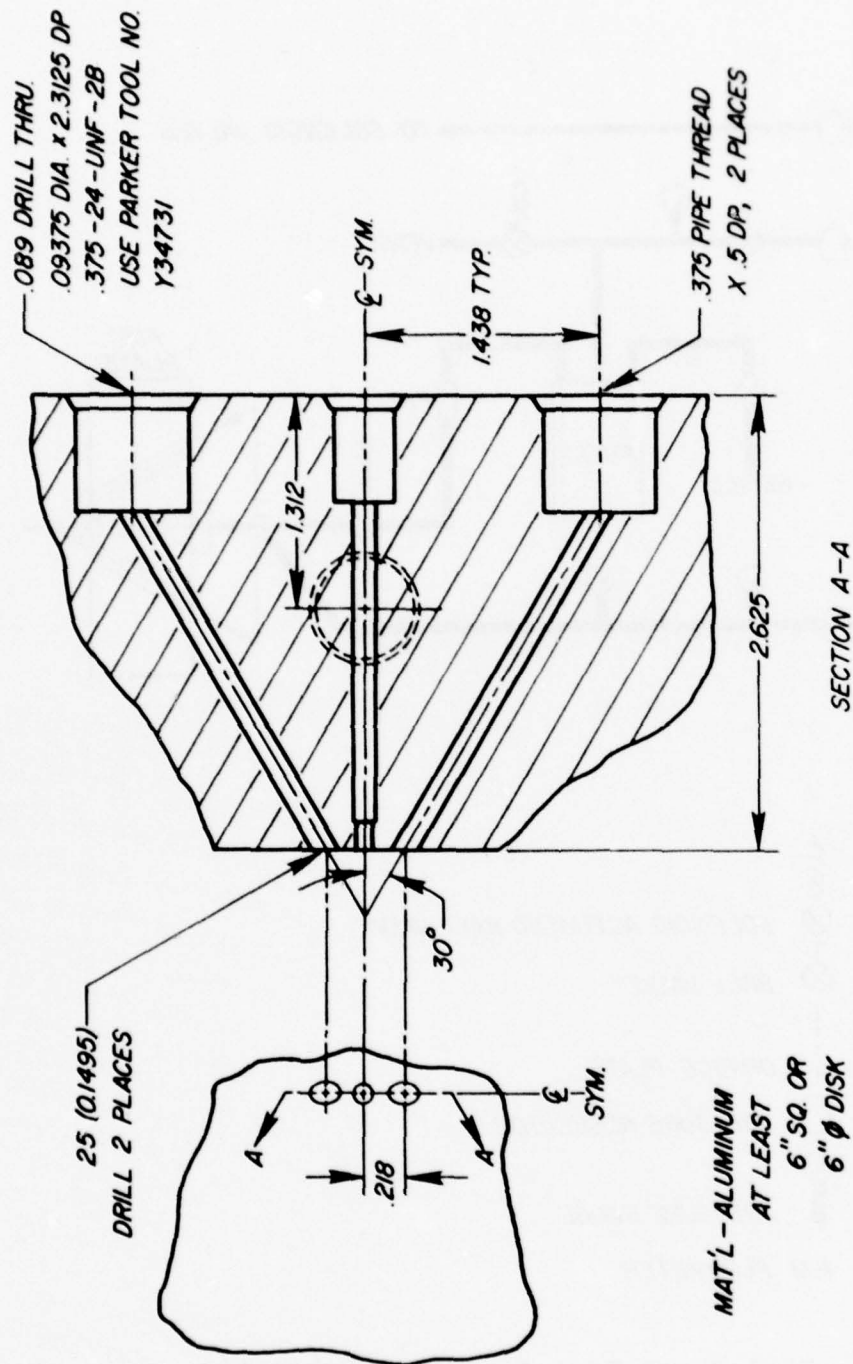


Figure 56. Injector Block Construction, Simulated
KIVA - I Propellant Injector
(Dimensions Are In Inches)

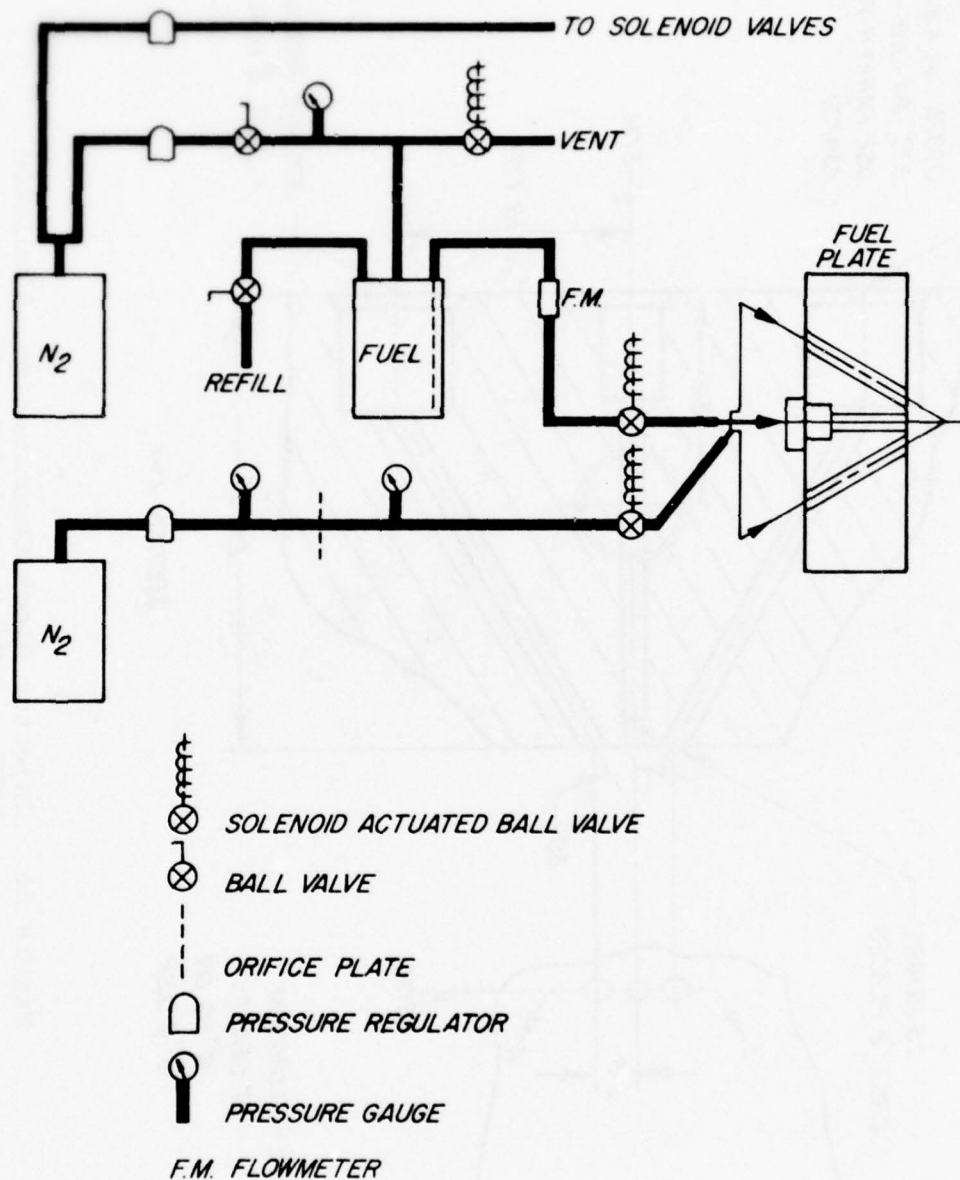


Figure 57. Fuel Spray Test Apparatus Schematic

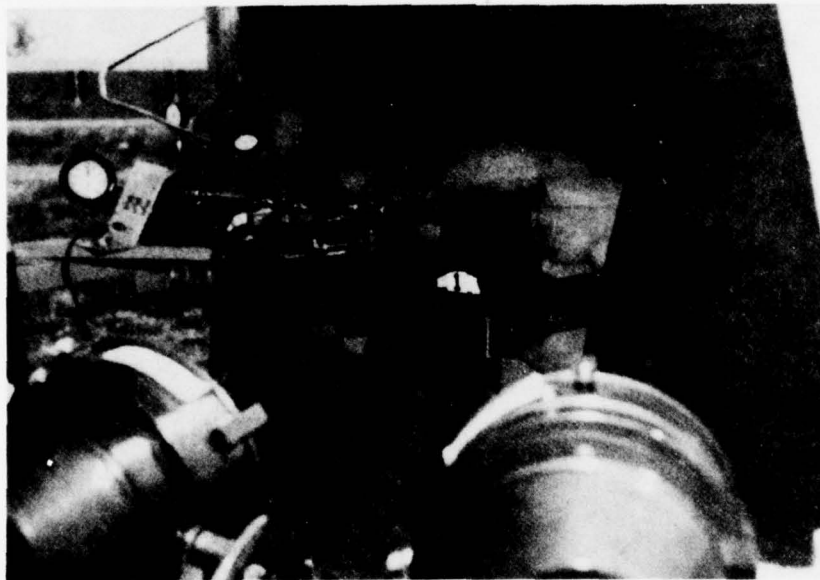
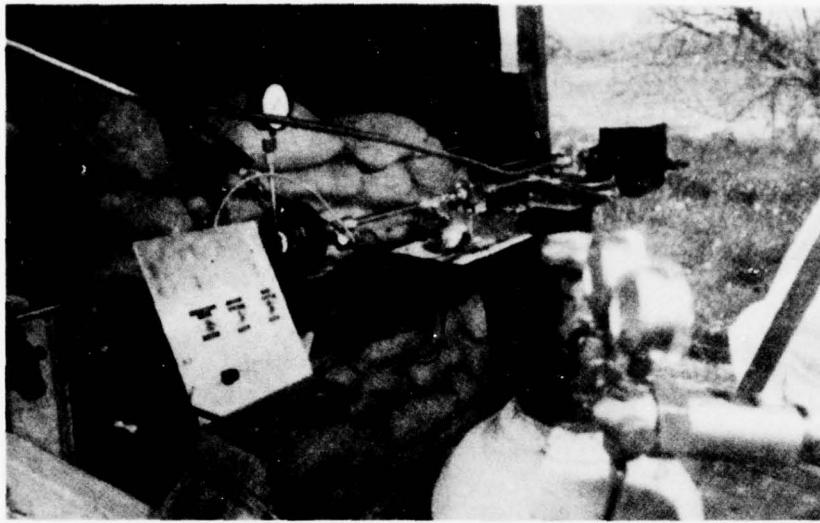


Figure 58. Fuel Spray Test Set Up

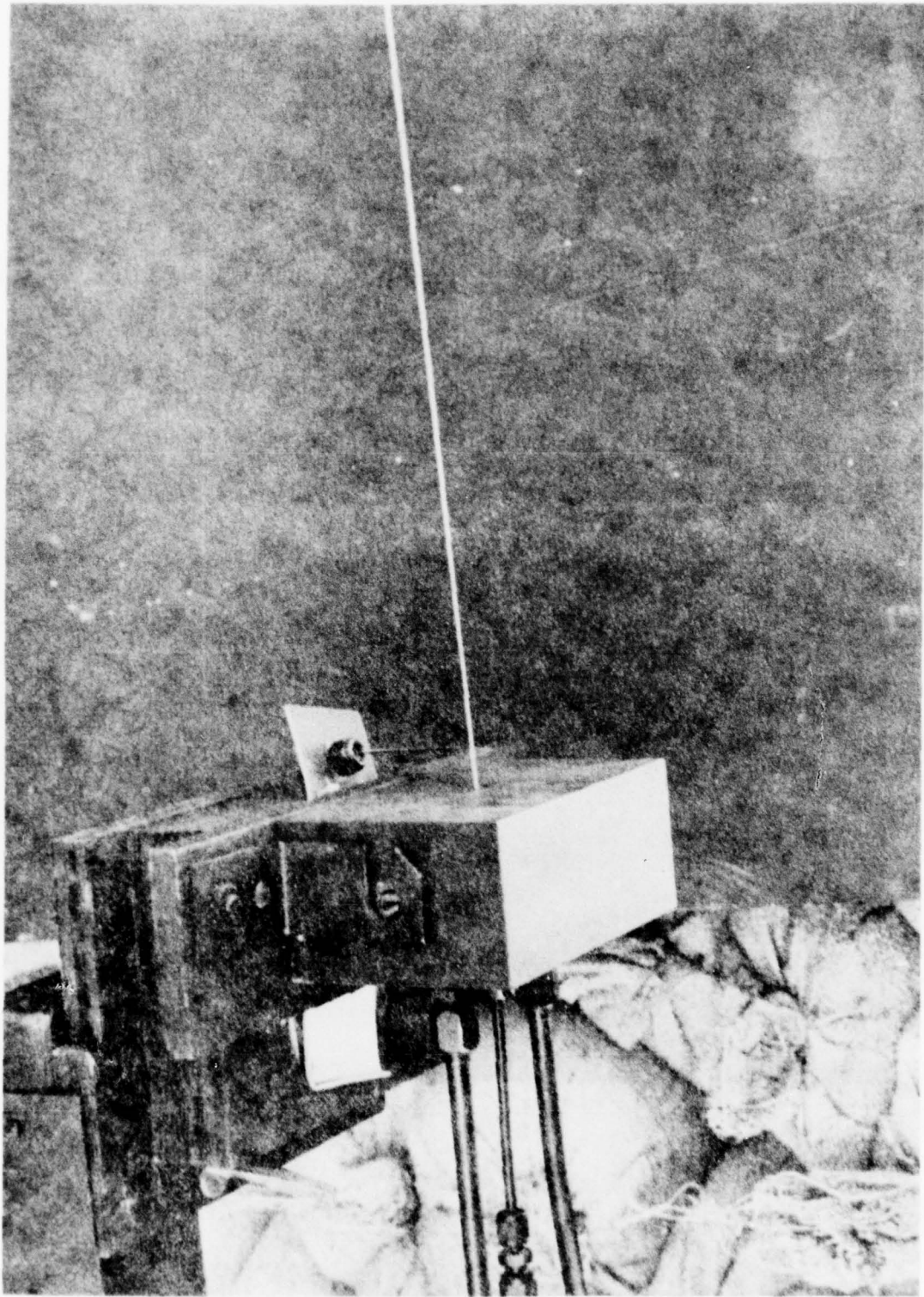


Figure 59. Water Discharged Through the Spray
Test Injector Block Without Gas Stream

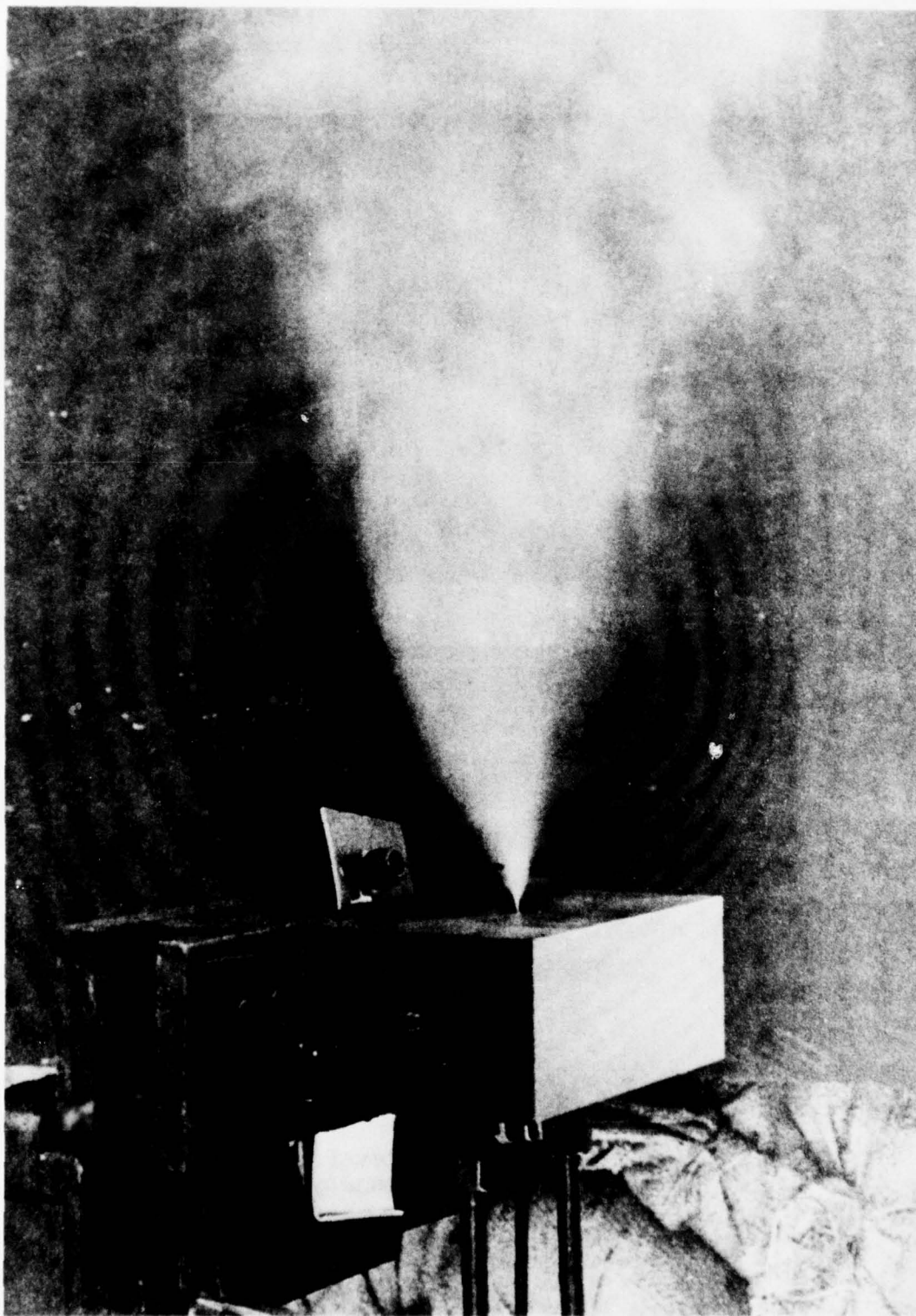


Figure 60. Water Discharged Through the Spray Test
Injector Block with Impinging Gas Stream

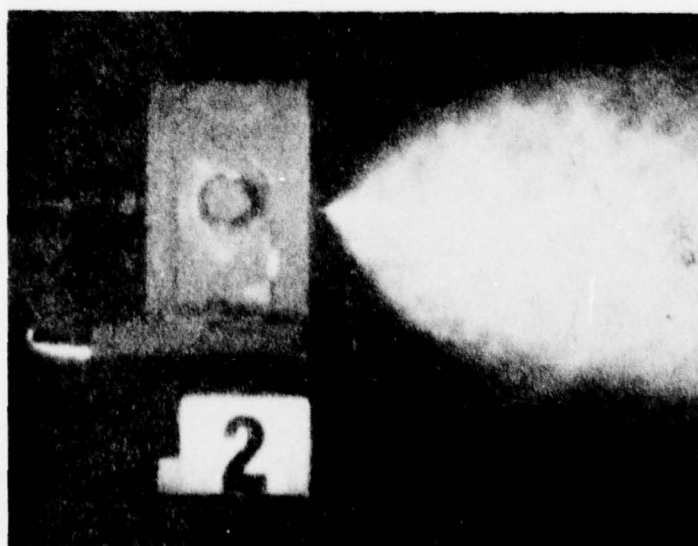
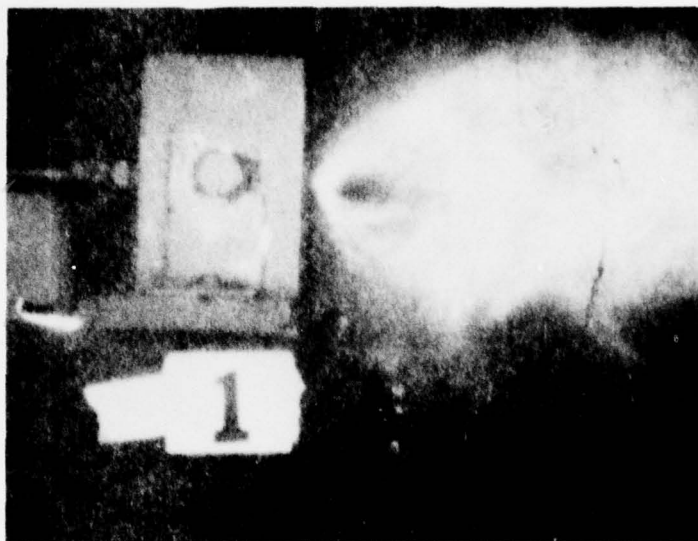


Figure 61. Neat Water Spray Pattern
-1- 0.16 id Injector 1 atm
Pressure Drop
-2- 0.084 id Injector 15 atm
Pressure Drop

- o 85% H₂O + 10% coal in 5% oil emulsion
- o 75% H₂O + 20% coal in 5% oil emulsion
- o 80% H₂O + 20% coal slurry

The emulsions listed above were observed during mixing and storage. Samples of two to five gallons were blended in a Hobart A-200 mixer. The 97/3 water-in-oil emulsion appeared thicker than the 95/5 mixture; however, the material was more unstable resulting in complete separation of the phases (water and oil) after 24 hours. The 95/5 mixture was stable over this same period of time. Beyond 24 hours of storage, oil began to appear throughout the material and remixing was necessary to restore the emulsion to its original state. The coal emulsions were more stable than the water emulsions with no separation of phases observed. A flat black film did appear on the surface of the mixture indicating a portion of the water had evaporated leaving a film of coal on the surface. The coal powder used in these emulsions was less than 44 μ m with an average particle size of 2 μ m. A straight coal-in-water slurry was mixed to observe the stability of the colloid. The 20% coal mixture began indicating separation after approximately 15 minutes. At this time a 0.32 cm thick layer of coal was observed on top of the mixture. One hour after mixing the slurry a 0.64 cm thick layer of clear water appeared below the coal layer. The coal used in this slurry was the same as described above. The rate of separation of coal and water in this slurry would necessitate some form of stirring in the fuel bottle prior to an MHD generator test. However, the slurry was stable long enough to enable a spray test to be conducted with the material at the SRL test stand.

The emulsion with no coal required the same pressure drop (16 atm) at equal flow rates as did the neat water. These pressure drops increased to 22 atm for the emulsion with the 20%

concentration of coal. This data was somewhat questionable, however, since frequent clogging of the injector did occur. Investigation of the fuel system revealed large (1600 μ m) particles lodged in the injector.

The spray pattern observed with the coal emulsions appeared similar to the spray with the neat water. The coal particles seemed to be concentrated in the lower portion of the spray which, after inspection of the injector, was attributed to misalignment of the injector. This can be seen in Figure 55. The injector was repositioned and this eliminated the nonuniform coal concentration in the spray. A sleeve was subsequently placed around the injectors to assure proper centering. Another observation made during these tests was the wetting of the faceplate just below the injector. This has also been observed on the KIVA-I faceplate.

The emulsified colloids did not affect the injectors or plumbing. In all cases to date, emulsion breakdown occurs outside the fuel system or in the injectors with no evidence of breakdown in the fuel system before entering the injectors.

An aluminum emulsion and slurry were both tested in the injector test stand. The emulsion was a 65% toluene, 30% aluminum 4% H₂O, 1% LMF-4234 mixture. The slurry was a 70% toluene-30% aluminum mixture. The aluminum powder emulsions were mixed in the combinations anticipated for use in tests with the MHD generator. A representative from Tretolite was present during the initial mixing to supervise SRL personnel and assure that proper mixing techniques were used. Although emulsions of magnesium, boron, and carbon were attempted, the lack of success indicated additional effort was required of Tretolite Division at that time to assure satisfactory emulsifier performance. As has been noted previously, toluene and JP-4 slurries of aluminum and magnesium settle rapidly and agitation of the slurries is

required in the fuel system to maintain the particles in a suspended state. For this reason a nitrogen agitation system was installed in the fuel tanks to maintain the powder in suspension during slurry testing.

Three types of tests were conducted with the fuels:

- 1) flow through the system at 1.1 kg/min
- 2) flow through the system minus injector at 8.6 kg/min
- 3) turbine flow meter calibration

The first two tests were conducted to determine the pressure drop through the injector and transmission line, respectively. The emulsions and slurries required the same pressure drops through the system. The drop across the injector was 17.0 atm and across the plumbing was 8.5 atm in all cases. In the first test with the slurry the injector clogged immediately. A sample taken after this contained a 37% concentration of aluminum. This was an indication that the solids were settling during testing despite agitation by circulating nitrogen through the slurry prior to the test. The fuel was then diluted to 25% concentration of aluminum and tested. No problems were encountered and the samples that were weighed contained a 27% concentration of aluminum. The ability to obtain a completely homogeneous mixture is questionable, however. In further tests with the emulsions and slurries, the turbine flow meter generated reliable signals when the toluene emulsion was used; however, when the toluene/aluminum emulsion or slurry was used the flow meter generated no signal. The powder in the fuel appears to jam the turbine wheel bearing and, as a result, the meter cannot produce a signal. Therefore, fuel flow monitoring was accomplished by measuring the pressure drop across the fuel line and

injector system. More information on this subject can be found in Vol II of this report.

Although it may appear that this procedure has many uncontrolled variables, once an emulsion type has been proven adaptable for use, it can be reliably duplicated by technicians with only minimal training, providing that formulation and procedural instructions are adhered to.

Since there were no adverse effects or problems with the fuel system, other than with the fuel meter, calibration tests were scheduled.

2. CALIBRATION TESTS

Calibration of the various injectors with different fuels was performed both in the injector test stand and in the full-scale KIVA-I fuel system. The injector sizes available were:

<u>Injector No.</u>	<u>I.D. (cm)</u>
1	0.157
2	0.132
3	0.104
4	0.107
6	0.084

Injector sizes 1 and 6 only were used in tests. Calibration tests were run with both sizes of injectors with neat water and water-in-oil emulsion (two formulations) as shown in Figures 62 through 65. A coal/water-in-oil emulsion was run with a size 6 injector.

Figure 66 shows the relationship of fuel bottle inlet pressure and fuel manifold or outlet pressure for various flow

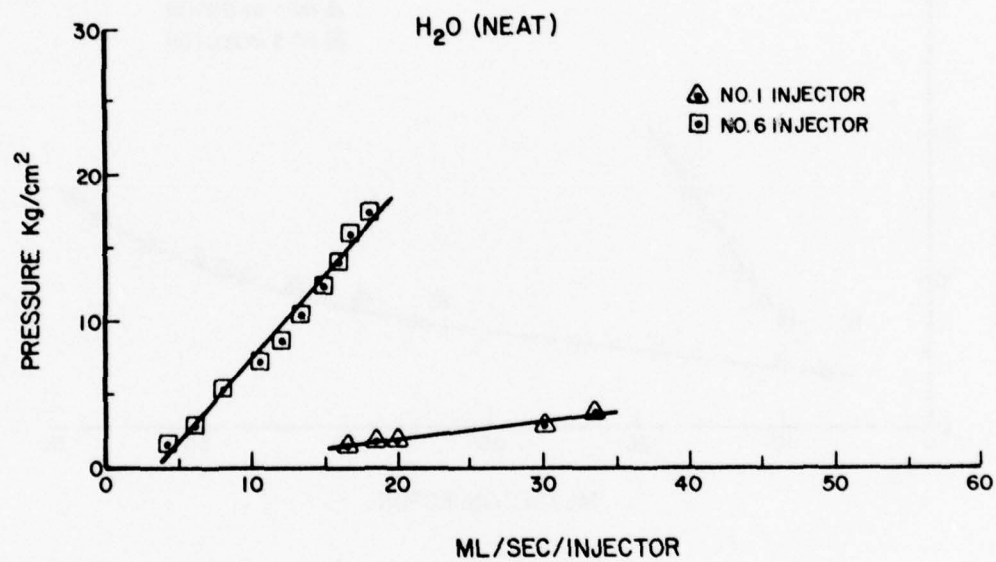


Figure 62. Neat Water Calibration Curve for KIVA - I Injectors

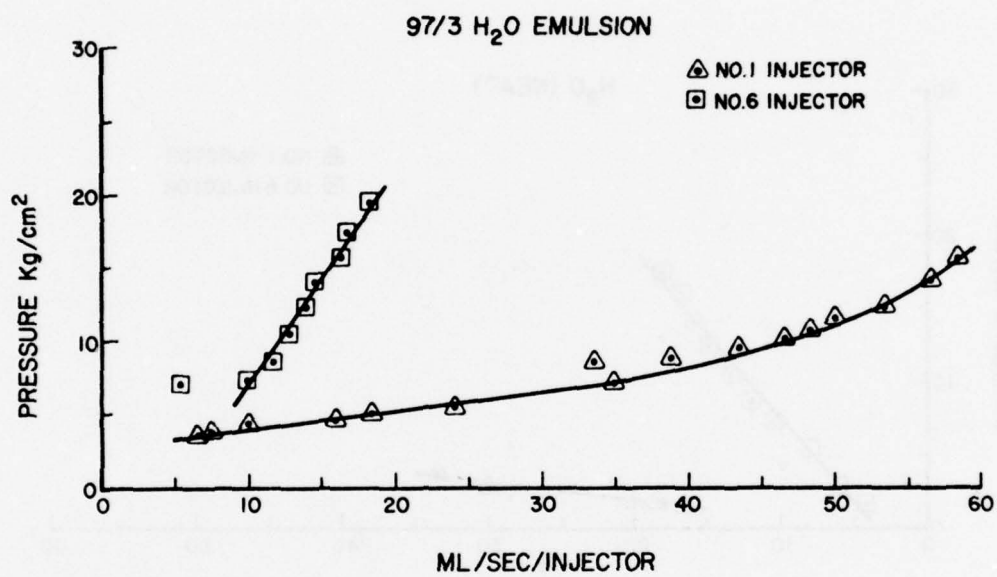


Figure 63. 97/3 H₂O Emulsion Calibration Curve for KIVA - I Injectors

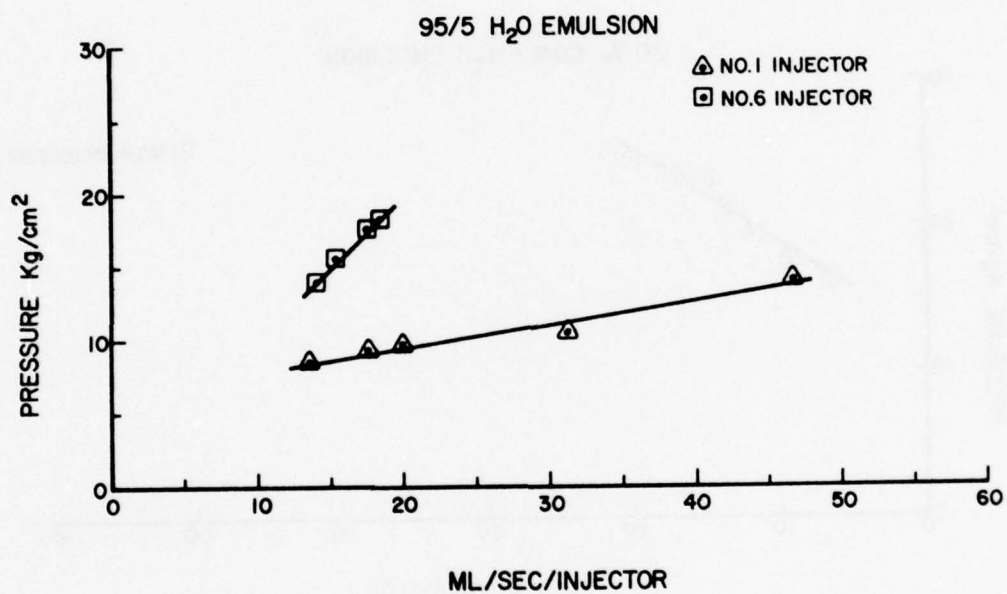


Figure 64. 95/5 H₂O Emulsion Calibration Curve for KIVA - I Injectors

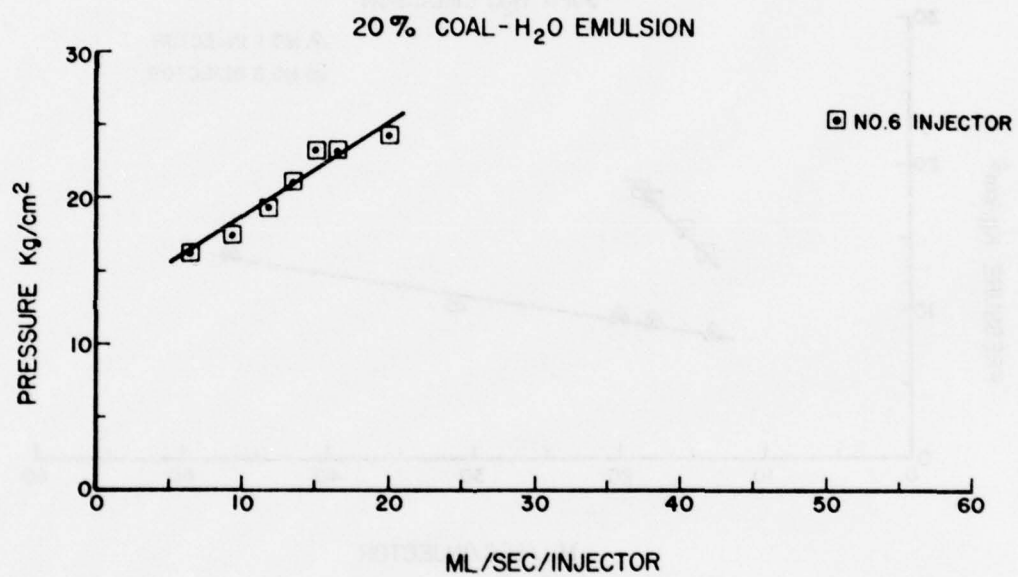


Figure 65. H₂O/20% Coal Emulsion Calibration Curve for KIVA - I Injectors

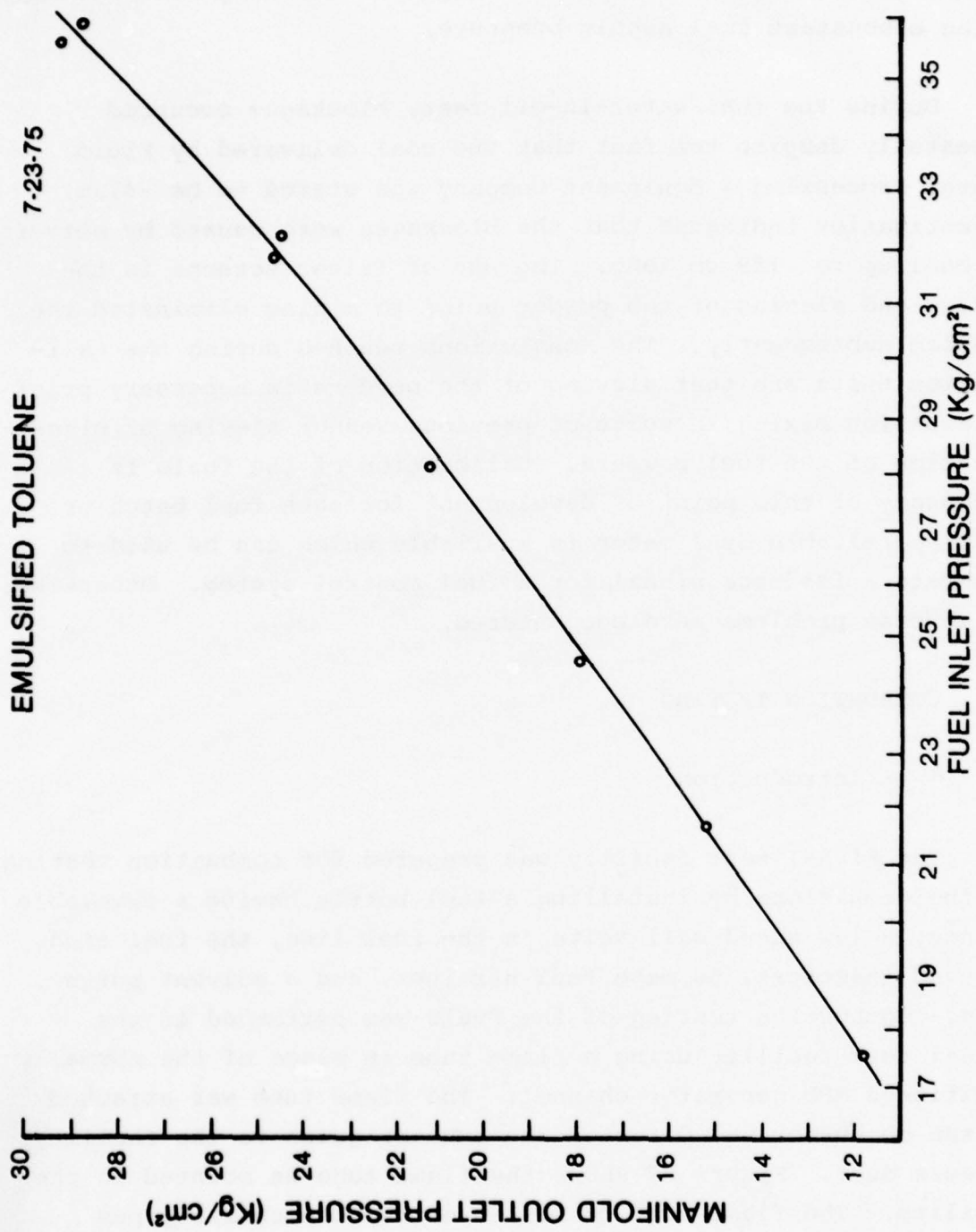


Figure 66. Fuel System Pressure Loss Curve with Emulsified Toluene

conditions through the KIVA-I fuel system. Testing was performed using a constant fuel supply pressure.

During the coal/water-in-oil test, blockages occurred repeatedly despite the fact that the coal delivered by Fluid Energy Processing & Equipment Company was stated to be $-47\mu\text{m}$. Investigation indicated that the blockages were caused by slivers of coal up to .159 cm long. The use of filter screens in the system and sieving of the powder prior to mixing eliminated the problem subsequently. The conclusions reached during the calibration tests are that sieving of the powders is necessary prior to emulsion mixing in spite of previous vendor sieving or classification of the fuel powders. Calibration of the fuels is necessary at this point of development for each fuel batch or until a reliable fuel meter is available which can be used to generate a feedback signal for a fuel control system. Otherwise, no adverse problems were encountered.

3. COMBUSTION TESTING

A. Introduction

The KIVA-I test facility was prepared for combustion testing of fuel emulsions by installing a fuel bottle having a removable flange, a low speed ball valve in the fuel line, the fuel ring, sleeved injectors, 60 mesh fuel strainer, and a solvent purge line. Combustion testing of the fuels was performed in the KIVA-I test facility using a flame tube in place of the normally positioned MHD generator channel. The flame tube was attached to the combustor and directed the exhaust gases to the facility exhaust duct. Figure 67 shows the flame tube as mounted in the facility. The flame tube consisted of two concentric pipes attached with a flange to the combustor. The space between the two concentric pipes was filled with water injected into the space through four equally spaced fittings. The water flowed

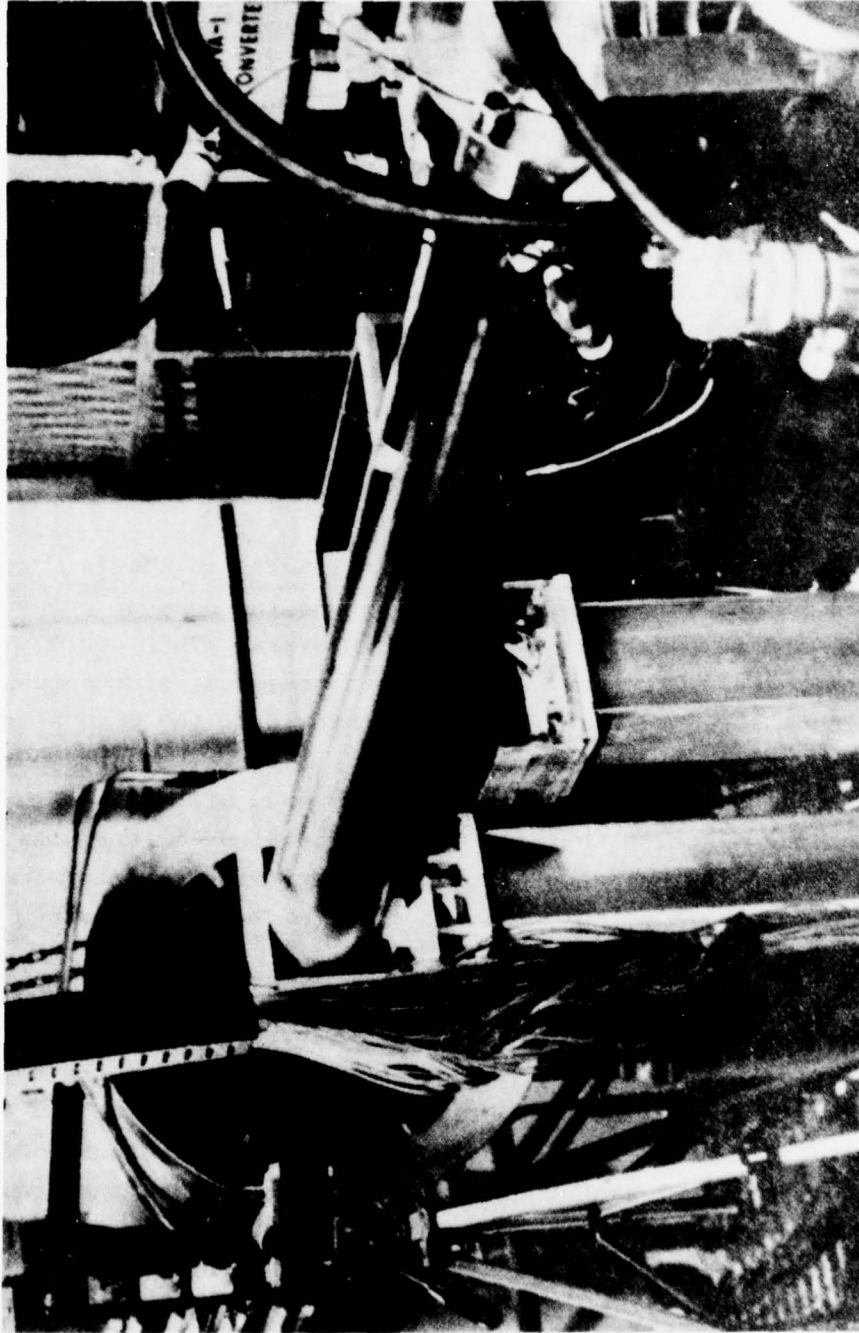


Figure 67. Combustion Test Flame Tube Exhausting into Facility Exhaust Duct

the length of the pipe and exited from the open end of the tube in a sheath. The tube was not expected to present any problems since it was previously used KIVA-I hardware.

The various fuel emulsion combinations considered, in the combustion test series, were toluene with aluminum, magnesium, and JP-4 with coal at liquid/powder concentrations of 30% solids burned at stoichiometric conditions and a total reactant mass flow rate of 0.6 kg/sec. The major objectives of the tests were study of combustor performance (pressure and coolant temperature) and the effect of metal oxide deposition on the combustor, nozzle and flame extension tube. Chamber pressure and combustor coolant temperature measured during tests with straight toluene were the baseline for comparison of the fuel emulsions.

Combustion of the colloidal fuels results in the formation of metal oxides which could be a liquid at the chamber pressures (10 atm) and temperatures (3500K) of interest. This could, therefore, cause a reduction in chamber pressure, since pressure predictions would be based upon the contents of the combustion chamber being in gaseous form. Any liquid phase present would not follow the gas laws and result in lowered pressure by creating the illusion that the chamber contained a lower reaction mass. The following calculations were performed to determine the phase of the aluminum oxide formed from burning aluminum particulates.

The vapor pressure and partial pressure of the metal oxide was calculated to determine the phase of the oxide in the combustor. The products of combustion were assumed to be from the reaction of toluene with a 30% concentration of aluminum powder and the theoretical amount of oxygen for complete combustion. Assuming complete combustion and neglecting dissociation, the reaction can be written in a simplified molal form as follows:

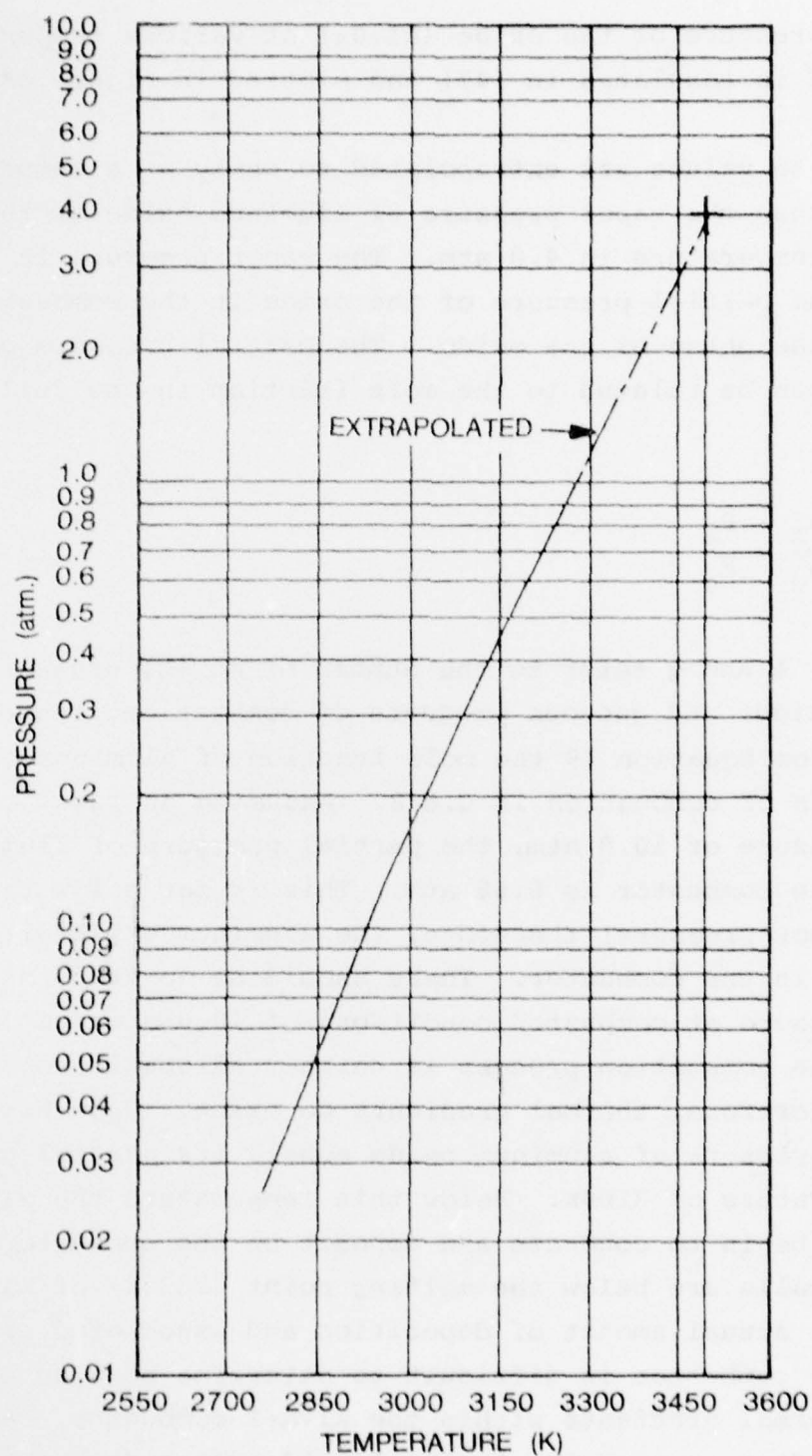


The vapor pressure of the oxide (Al_2O_3) at various temperatures up to 3250K is tabulated in [47] and plotted in Figure 68.

If these values are extrapolated to apply at a temperature of 3500K, then the vapor pressure of aluminum oxide at the combustor temperature is 4.0 atm. The vapor pressure is compared to the partial pressure of the oxide in the combustor to determine the phase of the oxide. The partial pressure of an ideal gas can be related to the mole fraction in the following manner:

$$\frac{n_A}{n_g} = \frac{P_A}{P_g} \quad (19)$$

where n , P , A and g refer to the number of moles, pressure, aluminum oxide, and gaseous products of combustion, respectively. From Equation 19 the mole fraction of aluminum oxide in the products of combustion is 0.068. Assuming an ideal combustor pressure of 10.0 atm, the partial pressure of aluminum oxide in the combustor is 0.68 atm. This is far below the 4.0 atm vapor pressure; therefore, the aluminum oxide will exist as a vapor in the combustor. There should be no drop in combustor pressure at combustor conditions of 10.0 atm and 3500K. However, the combustion process is neither adiabatic nor homogeneous; therefore, thermal gradients do exist. From Figure 68, the vapor pressure of aluminum oxide equals its partial pressure at a temperature of 3100K. Below this temperature the aluminum oxide will begin to condense and deposit on the combustor walls since the walls are below the melting point (2323K) of aluminum oxide. The actual amount of deposition and associated pressure drop in the combustor is difficult to determine because of the unknown thermal gradients within the KIVA-I combustor. Assuming all the oxide were to exist in the liquid or solid phase, however, the chamber pressure would drop by the partial pressure of the aluminum oxide, that is, 0.68 atm. The other solid additives



VAPOR PRESSURE OF ALUMINUM OXIDE

Figure 68. Extrapolated Al_2O_3 Temperature Vapor Pressure Curve

(magnesium and coal) were not analyzed because of the lack of vapor pressure data.

Following completion of the calibration tests, preparations for combustion testing were made. These included calibration of thermocouples and transducers, checking water systems, interlocks, modifying amplifier systems, reprogramming patch panels, and installation of a fuel dump system. During the final sequencing tests the fuel valve malfunctioned and was subsequently disassembled and cleaned. It was at this time that aluminum pellets were found in the fuel valve and fuel manifold. The fuel system was thoroughly flushed and the flushing fluid filtered to determine when the system was free of contamination. Sequencing tests of the programmer were completed and the first toluene/oxygen combustion test was scheduled.

B. Combustion Checkout Tests, HEF-1 and HEF-1A

The first combustion test, HEF-1, was made using neat toluene for a system checkout and baseline for comparison with other tests. The propellant mass flow was set up for 0.6 kg/sec and an O/F ratio of 3.12. In Figure 69 is seen traces of combustor cooling water discharge temperature, pilot flame chamber pressure, and main combustion chamber pressure. In the pressure curves the units are displayed at mid and full scale in kg/cm². For ease of reading, the midpoint corresponds to 100 psig and full scale is 200 psig. Seventeen seconds into a planned 60 second run, flame exiting from the flame tube was seen to take on a whitish hue and approximately 5 seconds later sparks were seen in the exhaust flame. The test was immediately terminated. Upon separating the flame tube from the combustion chamber, an area of the flame tube inner cooling wall covering 5 cm circumferentially around the inner wall and approximately 20 cm axially along the wall, centered 21 cm aft of the nozzle exit face at 3 o'clock (aft looking forward) was found to be bulged

HEF-1

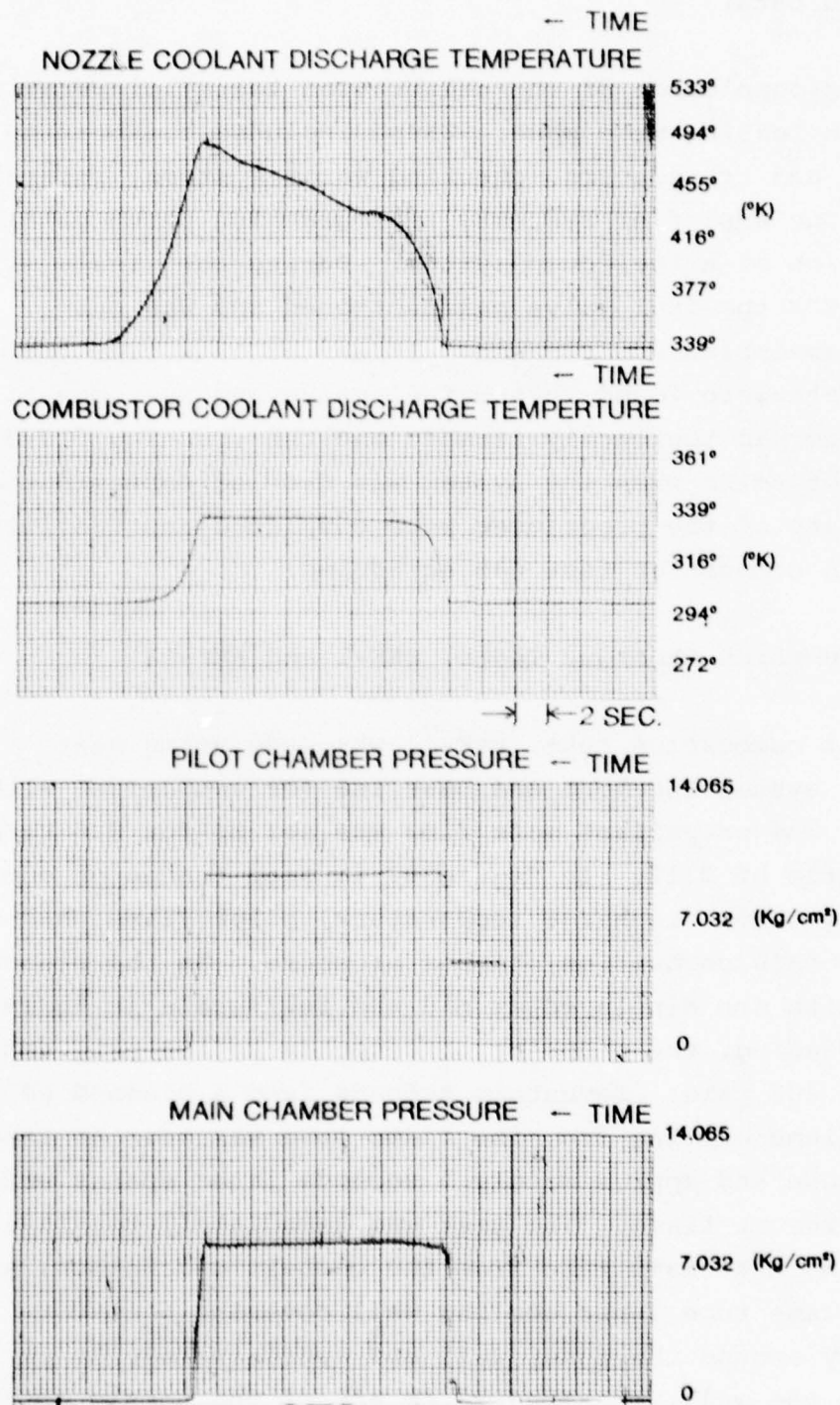


Figure 69. Combustion Check Out Test
with Flame Tube, Fuel -
Straight Toluene

into the flow about 3 cm. Inspection of this area verified that the surface was severely burned and heavily cracked. No damage of any kind to the injector plate, combustion plate, or nozzle was noted.

Considering the contamination previously found in the fuel system, the fuel manifold was suspected of being contaminated. It was subsequently removed and inspected. Several small particles of aluminum were found in the manifold, but were not large enough to have stopped fuel flow through the injectors. The manifold was flushed in a reverse direction through each fuel tube to clear what was anticipated to be a plugged tube. Two tubes were found to be severely restricted and could not be cleared either mechanically or chemically. The tubes were cut off and were found to have been welded nearly shut during original manufacture by a previous contractor. These tubes were replaced and additional flow calibration checks run to reestablish injector flow characteristics. It should be recognized at this point that although the tubes were quite restricted to the flow of an emulsion, the far lower viscosity of neat fuels allowed sufficient flow to result in essentially equal flow through all fuel tubes at the flow rates normally employed.

Failure of the flame tube is presumed to have occurred as a result of several problems. The first is a partial fuel injector tube blockage aggravated by aluminum particles contaminating the fuel system. Additionally, the flame tube rails which keep the two tubes concentric had rusted and sections had disappeared allowing the inner tube to warp and restrict the flow of water.

The flame tube was rebuilt incorporating several modifications. The first was to drill a series of 10 holes .318 cm diameter in a ring at the forward end of the flame tube. This injected approximately .2 kg/sec of water into the flame tube thereby cooling the boundary layer and reducing heating loads. Instead of axial rails being used to align the two tubes

concentrically, 4 wires were spiral wound around the inner tube, one turn within the tube length, and spot welded in place. This caused a better distribution and circulation of the cooling flow. In addition, 4 more water inlets were installed on the flame tube to supply additional water which is injected into the combustion chamber exhaust.

Initial flow tests of the flame extension tube indicated some overspray of water entering the combustion chamber. The water injection holes determined to be causing the overspray were plugged and no further problems encountered. During the flow tests it was noted that the water jacket on the flame tube was not flowing full. Upon removal of the inlet water hoses, large amounts of rust and pipe scale were found to be plugging the water jacket inlets. The contamination was removed and the water system flushed clean with no further problems with the flame extension tube. It can be assumed that this too can be considered an aggravating if not a cause factor in the flame tube failure.

The neat toluene flow curve was rerun and based on this data, Figure 70 (curve 9-4-76), the baseline combustion test HEF-1A was run using the stoichiometric O/F = 3.12. Stable combustion was established with a main combustion chamber pressure of 8.62 kg/cm² as shown in Figure 71.

The following are the combustion chamber test parameters during the run

	Chamber Pressure (kg/cm ²)	\dot{W}_f (kg/sec)	\dot{W}_{O_2} (kg/sec)	\dot{W}_{TOT} (kg/sec)	O/F
Start	8.620	0.143	0.4563	0.599	3.19
Mid-run	8.747	0.143	0.4497	0.593	3.15

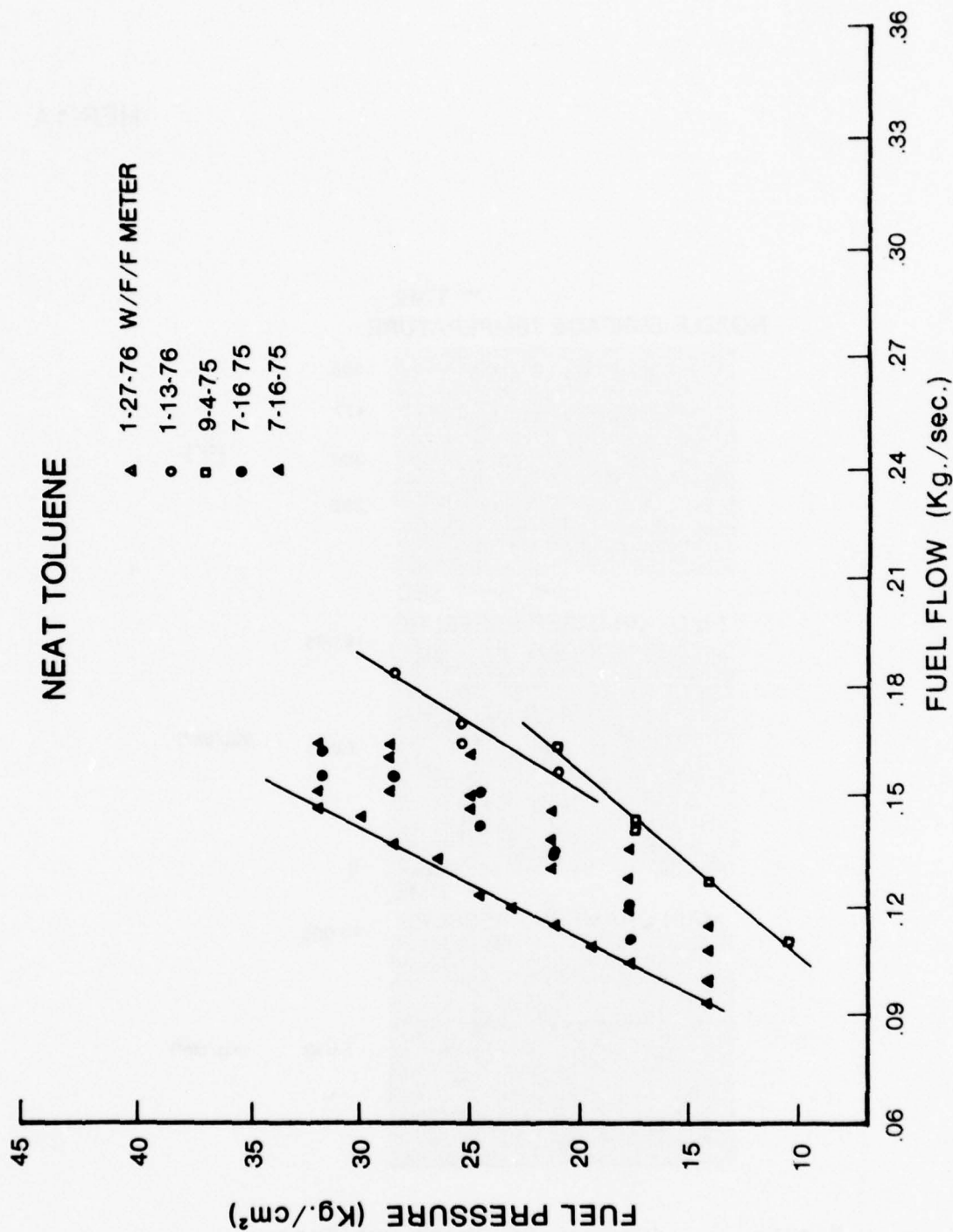


Figure 70. Straight Toluene Fuel Flow Calibration Curves

HEF-1A

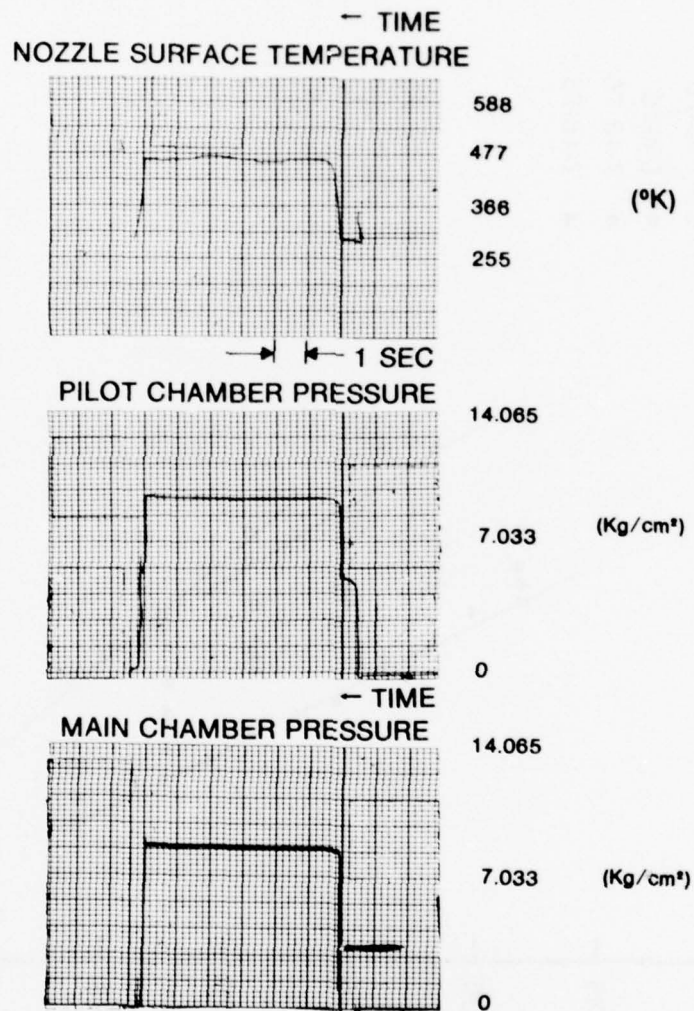


Figure 71. Combustion Check Out Test Parameters

At the end of the run chamber pressure had risen very slightly and was experiencing a $.11 \text{ kg/cm}^2$ pressure fluctuation. The test was considered a success with no hardware problems of any kind. As a result, the next test was scheduled to be of emulsified toluene with no additives to determine the combustion performance of the emulsified fuel. Figure 72 shows the results of the pre-run fuel system calibration with several attempts to duplicate points (Curve 9-8-75). As can be seen, the remixing of the fuel results in a variable flow due to differing physical characteristics. This problem was noted throughout the test program and remained as an unsatisfactory characteristic of the emulsions. It should be pointed out though, that with any particular mix, if several (2 - 3) calibration points could be obtained, a good prediction can be made of the flow characteristics of the remainder of that mix or batch of fuel. The result is that, in general, 2 to 3 points were run on subsequent calibrations. The answer to the problem is to be found in further study of the emulsion rheology to facilitate flow prediction or use of a fuel meter compatible with the emulsified particulates.

C. Emulsified Toluene Combustion Tests,
HEF-2 and HEF-3

Test Run Nos. HEF-2 and HEF-3 were made using emulsified toluene with 1% LMF 4229, 4% H_2O , and 95% toluene as constituents by weight. Run HEF-2 started smoothly with a chamber pressure of 8.972 kg/cm^2 , somewhat higher than planned. The planned O/F was 2.99.

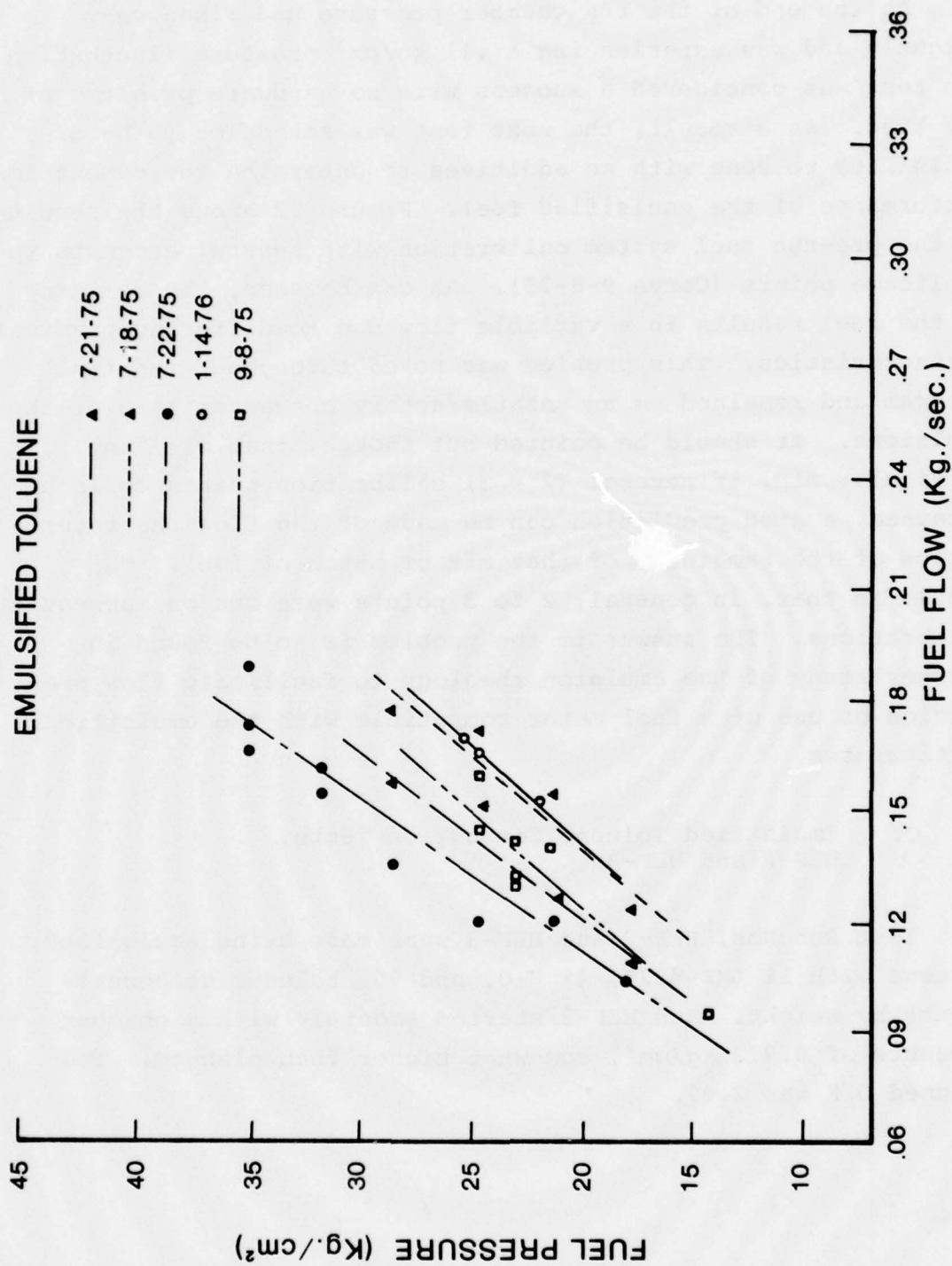


Figure 72. Emulsified Toluene Fuel Flow Calibration Curves

Chamber test parameters varied as shown in Figure 73 and below.

	Chamber Pressure (kg/cm ²)	\dot{W}_f (kg/sec)	W _{O₂} (kg/sec)	\dot{W}_{TOT} (kg/sec)	O/F
Start	8.972	0.1419	0.4664	0.608	3.286
Mid-run	9.140	0.0412	0.4618	0.603	3.27
End	9.281	0.1410	0.4618	0.603	3.275

The next test was HEF-3, run with the same fuel but with a varied O/F ratio during the run. Typical variations can be seen in Figure 74.

	Chamber Pressure (kg/cm ²)	\dot{W}_f (kg/sec)	W _{O₂} (kg/sec)	\dot{W}_{TOT} (kg/sec)	O/F
Start	9.309	0.1381	0.4488	0.587	3.25
	8.662	0.1453	0.4607	0.606	3.17

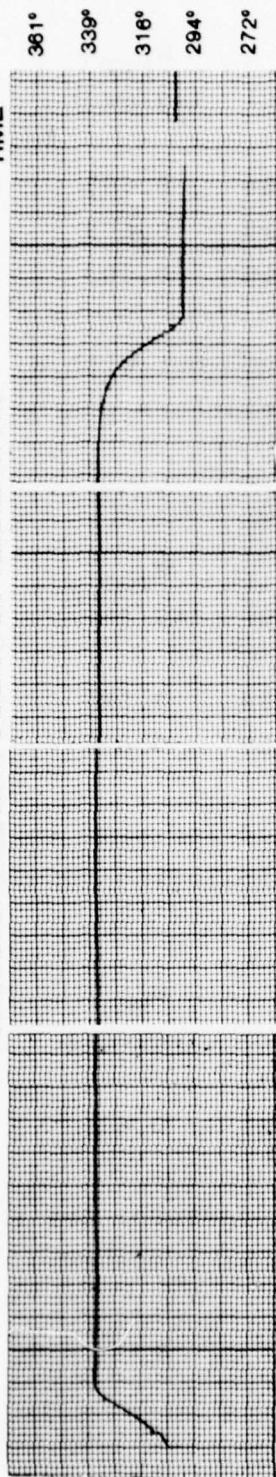
These changes took place prior to the intended increase in fuel flow. Fuel pressure was increased with the following result.

	Chamber Pressure (kg/cm ²)	\dot{W}_f (kg/sec)	W _{O₂} (kg/sec)	\dot{W}_{TOT} (kg/sec)	O/F
	8.789	0.1509	0.4601	0.611	3.05

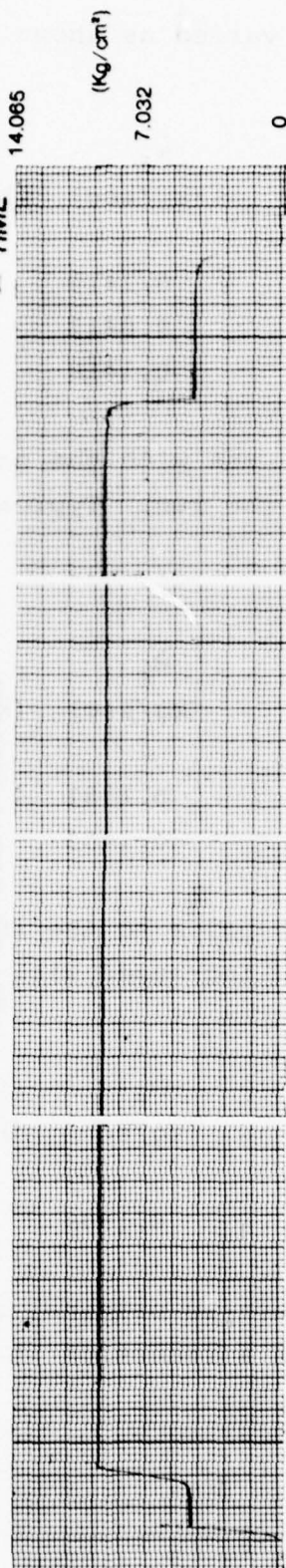
While attempting to return to original fuel pressure, the setting overshoot and resulted in a reduction in chamber pressure.

HEF-2

COMBUSTOR COOLANT DISCHARGE TEMPERATURE



PILOT CHAMBER PRESSURE



MAIN CHAMBER PRESSURE

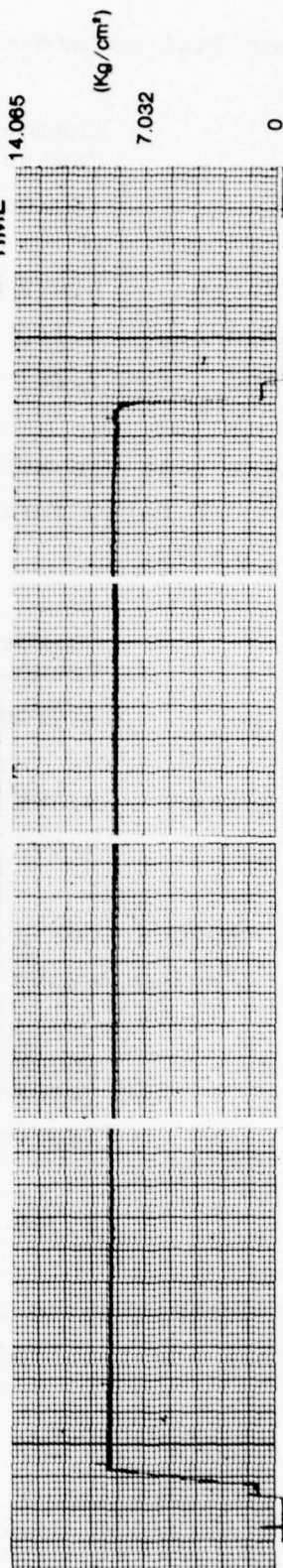
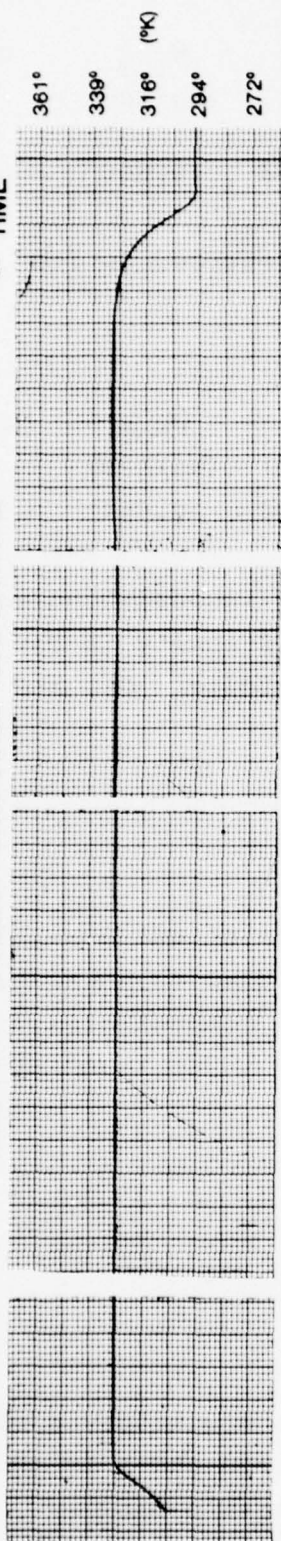


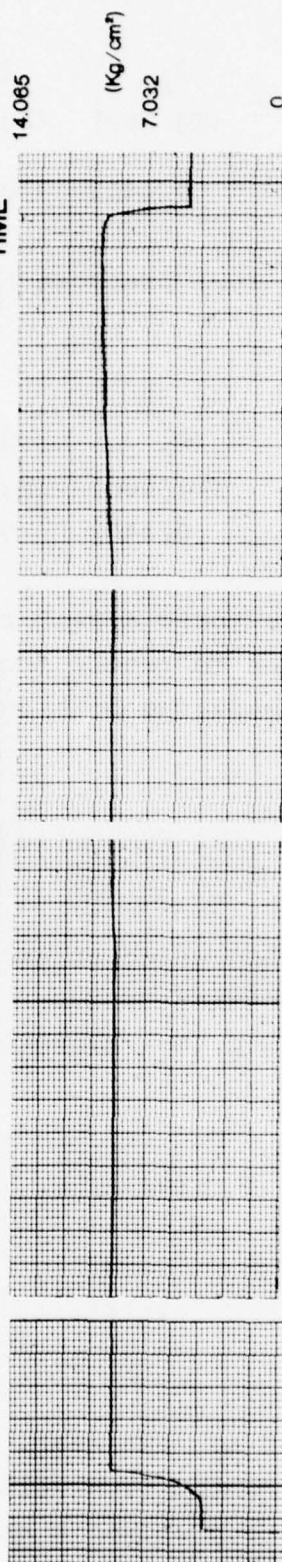
Figure 73. Combustion Test - HEF-2, Fuel - Emulsified Toluene

HEF-3

COMBUSTOR COOLANT DISCHARGE TEMPERATURE



PILOT CHAMBER PRESSURE



MAIN CHAMBER PRESSURE

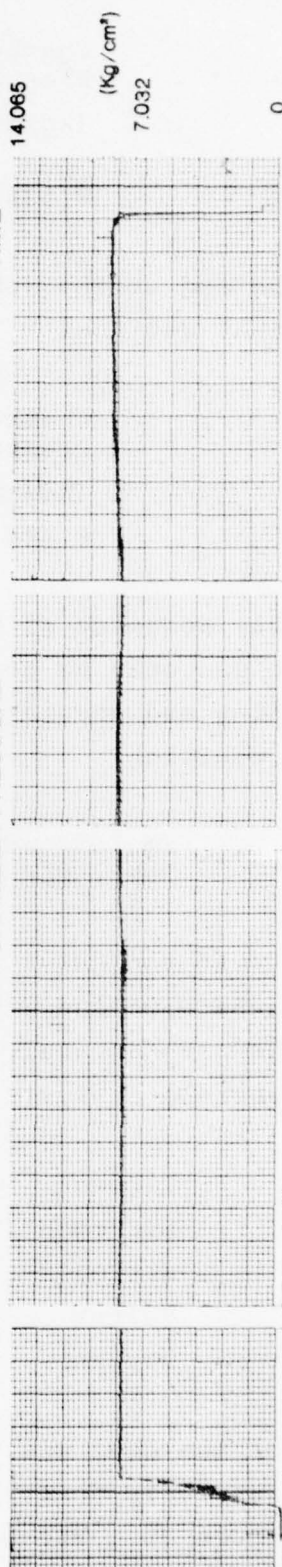


Figure 74. Combustion Test - HEF-3, Fuel - Emulsified Toluene
Variable O/F

Chamber Pressure (kg/cm ²)	\dot{W}_f (kg/sec)	\dot{W}_{O_2} (kg/sec)	\dot{W}_{TOT} (kg/sec)	O/F
8.550	0.1412	0.4588	0.660	3.25

By the end of the run the fuel pressure had returned to its original setting.

Chamber Pressure (kg/cm ²)	\dot{W}_f (kg/sec)	\dot{W}_{O_2} (kg/sec)	\dot{W}_{TOT} (kg/sec)	O/F
8.648	0.1452	0.4588	0.604	3.16

In this sequence of events there appear to be inconsistencies which can only be concluded to result from difficulty in controlling and accurately measuring both the oxidizer, O₂, and the fuel emulsion.

D. Emulsified JP-4/Coal Combustion Test, HEF-4

Test run HEF-4 was made using an emulsion of 62% JP-4, 30% coal, 6% H₂O, and 2% emulsifier EM-23D. The coal used was bituminous with an analysis of 6.9% ash and 93.1% combustibles. Combustible analysis was:

Carbon	76.5%
Hydrogen	4.9%
Nitrogen	1.5%
Sulfur	1.18%
Oxygen	8.9%

All of the coal was sieved to -325 mesh. The emulsion was mixed as previously described and the flow calibration chart is shown in Figure 75. The entire run showed a very stable chamber

FUEL EMULSION CALIBRATION

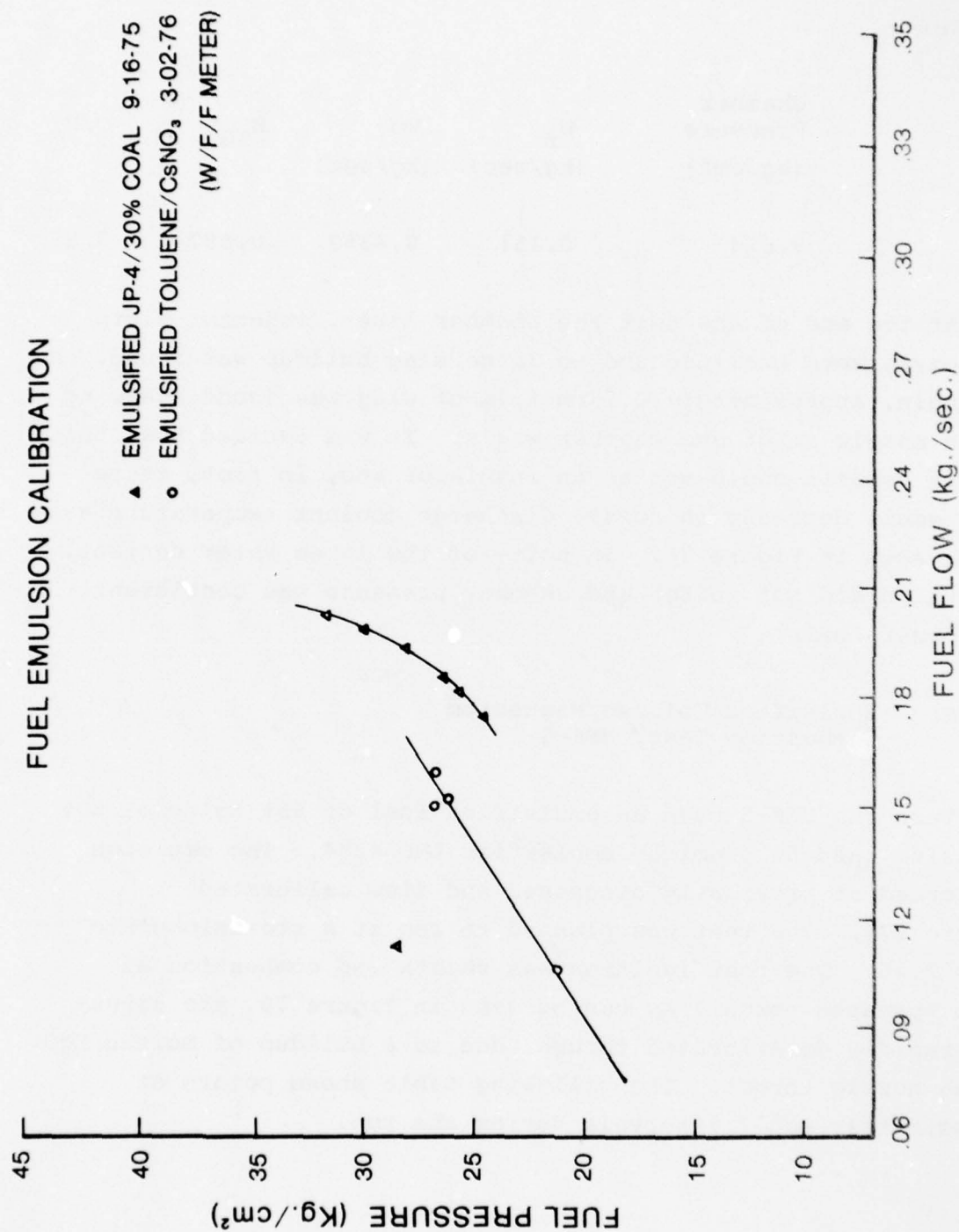


Figure 75. Fuel Calibration Curves for Coal and CsNO₃ Seed Particle Additives

pressure after a slow start of combustion on a planned O/F = 2.90 test.

Chamber Pressure (kg/cm ²)	\dot{W}_f (kg/sec)	\dot{W}_{O_2} (kg/sec)	\dot{W}_{TOT}	O/F
9.014	0.151	0.4359	0.587	2.89

At the end of the test the chamber liner, injector plate and nozzle were examined and no large slag buildup was found. A very thin, approximately 0.25mm film of slag was found adhering to the nozzle inlet and chamber walls. It was decided that this type of deposit could act as an insulator and, in fact, there was a small decrease in nozzle discharge coolant temperature as can be seen in Figure 76. In spite of the large water content, combustion did not suffer and chamber pressure was consistent with other fuels.

E. Emulsified Toluene/Magnesium
Combustion Test, HEF-5

Test run HEF-5 used an emulsified fuel of 65% toluene, 30% magnesium, and 5% premixed emulsifier LMF-4234. The emulsion was formed as previously discussed and flow calibrated (Figure 77). The test was planned to run at a stoichiometric O/F = 2.26. The test ignition was smooth and combustion at first appeared normal. As can be seen in Figure 78, the situation rapidly deteriorated though, due to a buildup of molten MgO in the nozzle throat. The following table shows points at approximately equal intervals during the run.

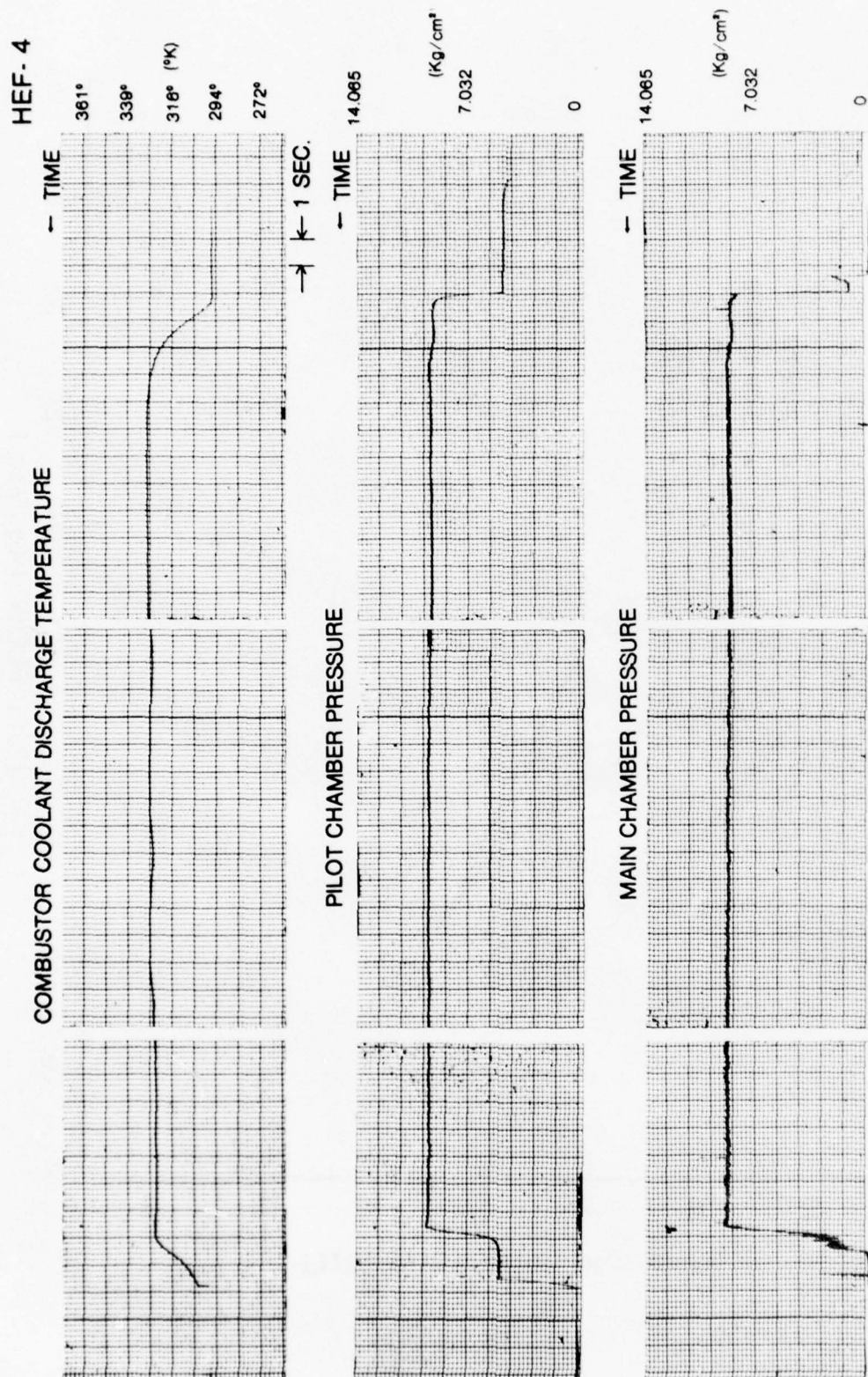


Figure 76. Combustion Test Run - HEF-4, Fuel - Emulsified JP-4 62%, Coal 30%

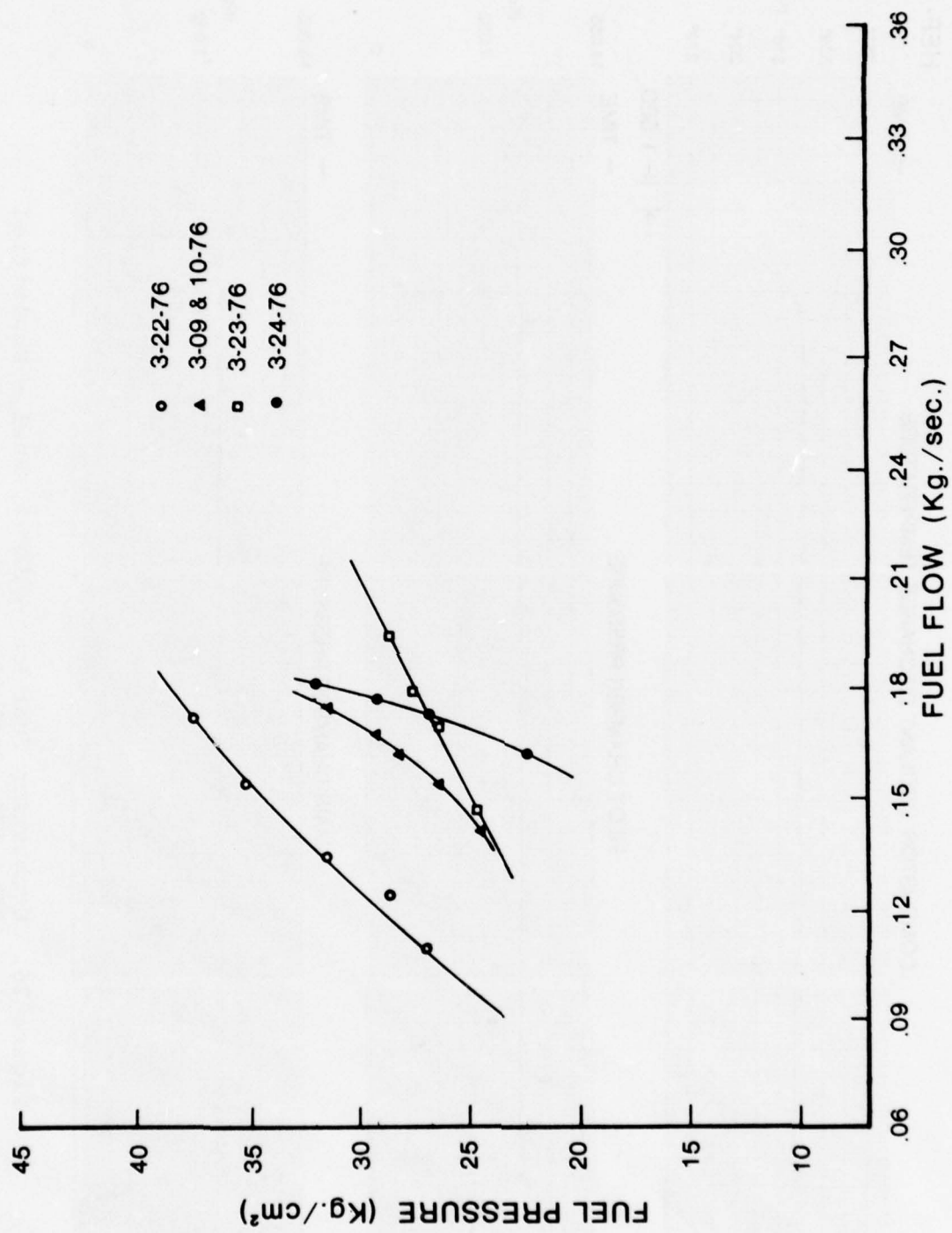


Figure 77. Calibration Curves for Emulsified Toluene/Magnesium

HEF-5

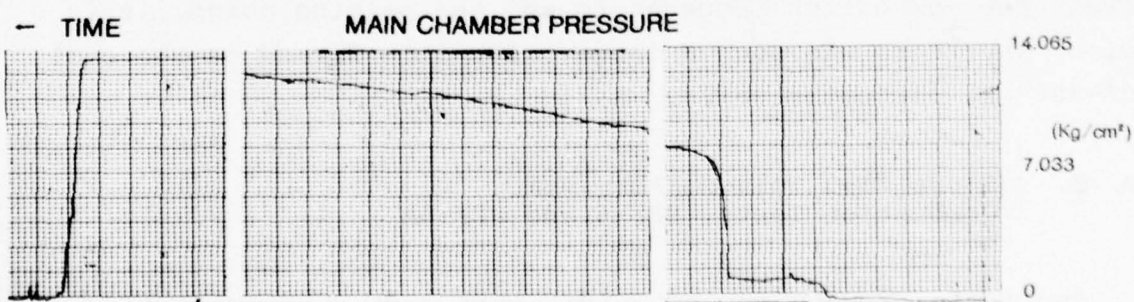
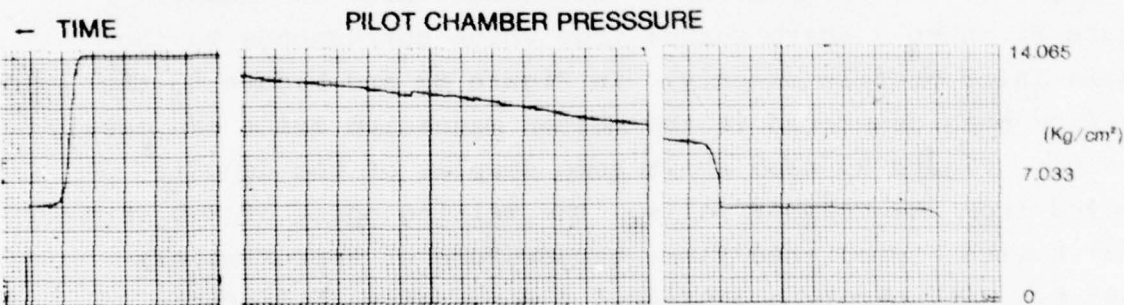
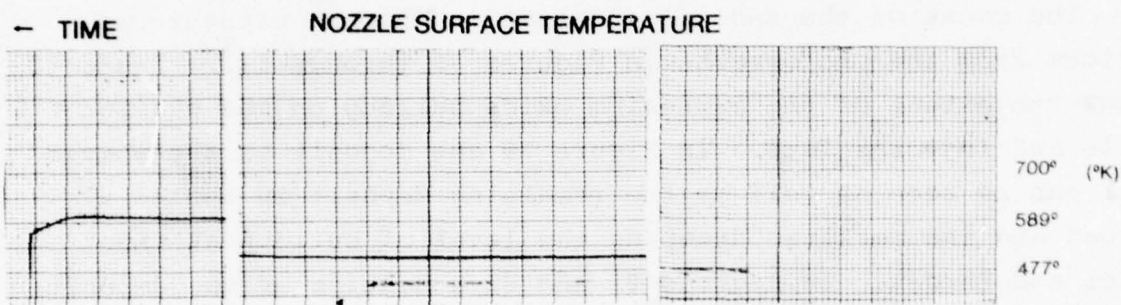
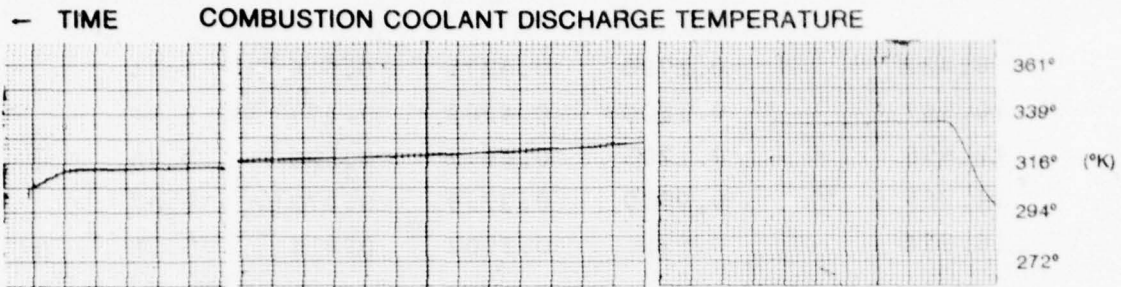


Figure 78. Combustion Test Run - HEF-5, Fuel - Emulsified Toluene 65%, Magnesium 30%

Chamber Pressure (kg/cm ²)	Fuel (kg/sec)	Oxidizer (kg/sec)	Total Mass (kg/sec)	O/F
8.437	0.1790	0.4371	0.616	2.44
10.547	0.1500	0.4267	0.577	2.84
12.656	0.1205	0.4077	0.528	3.38
14.765	0.0930	0.3790	0.472	4.07
16.874	0.635	0.3502	0.414	5.51

The cause of the radical increase in chamber pressure is obvious from the photographs in Figures 79 through 83. Figure 80 shows the extent of the magnesium oxide buildup on the chamber walls and injector face. In Figure 79 the deposit on the nozzle face can be seen as well as the remaining deposit in the nozzle throat and the markings denoting the level of buildup at the inlet and throat. In Figures 81 and 82 a section of the deposit removed from the lower part of the nozzle inlet is shown. Figure 81 shows a sharp curved edge which corresponds to the nozzle inlet profile exactly. In Figure 82 and Figure 83 the new flow path generated in the molten magnesium oxide can easily be seen. Figure 83 also shows some samples of the deposit removed from the chamber walls. The melting point of MgO is 3073° K with a predicted flame temperature of approximately 3400° K. With barely a 300°-400° K temperature difference between the combustion temperature and the melting point, it is obvious why there was such a large oxide film formed on the cool 400°-500° K, combustor walls.

F. Emulsified Toluene/Aluminum Combustion Tests, HEF-6 and HEF-6A

Two tests of aluminum emulsions were made subsequent to completely cleaning the combustion chamber and nozzle of deposits formed during Test HEF-5. The aluminum emulsion was made with 65% toluene, 30% aluminum, 5% LMF-4234 using the procedure

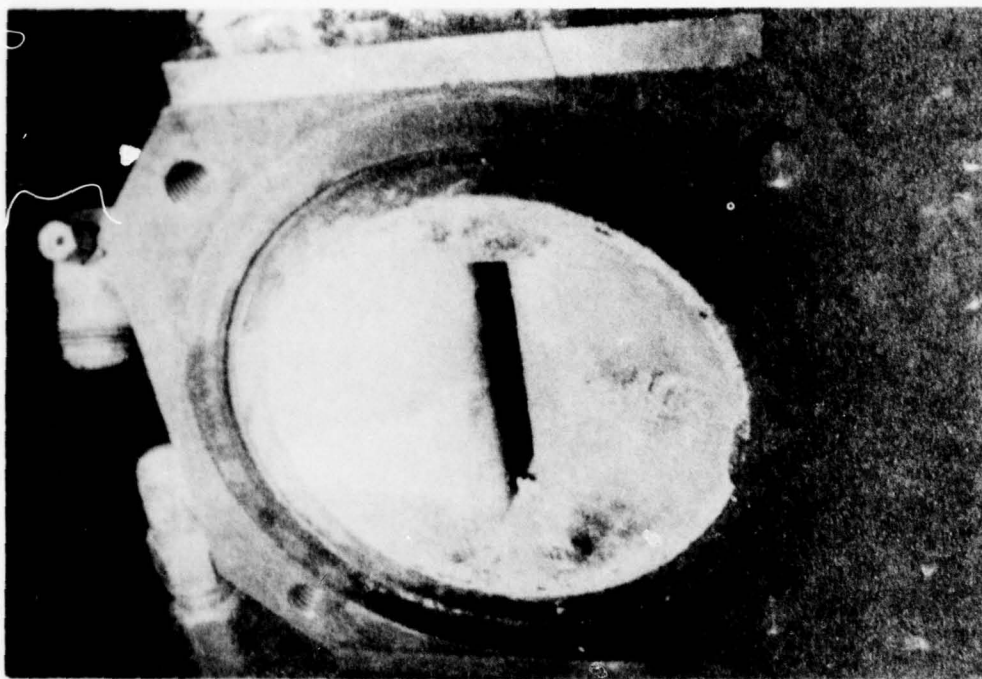


Figure 79. Combustion Nozzle Inlet

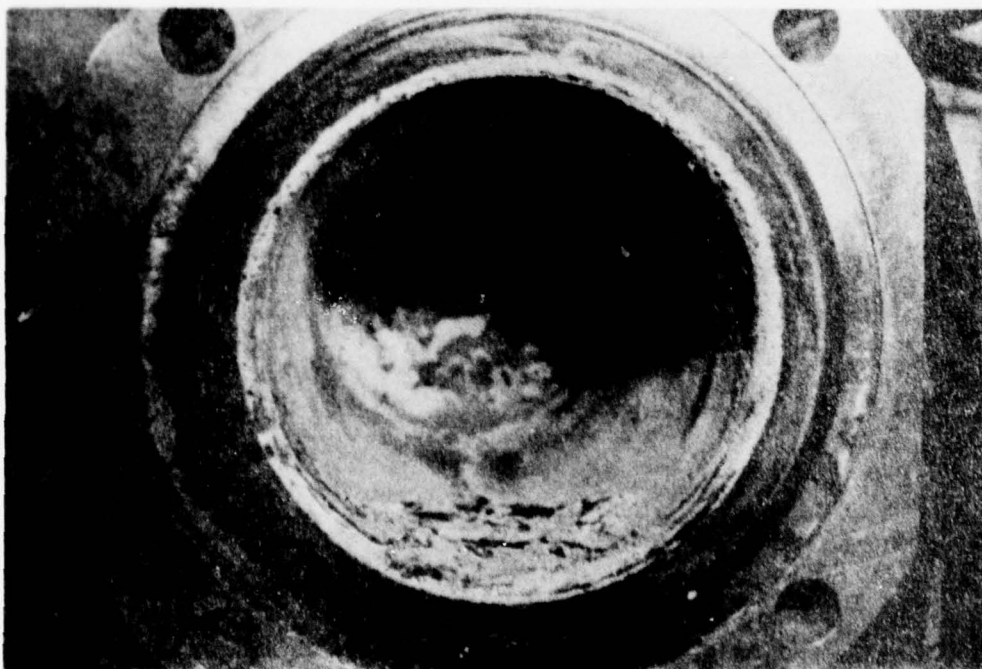


Figure 80. Combustion Chamber and Injector Plate - Note Magnesium Oxide Deposits on Walls and Injector Plate Face - Deposit Flakes at Bottom Were Broken Loose During Disassembly

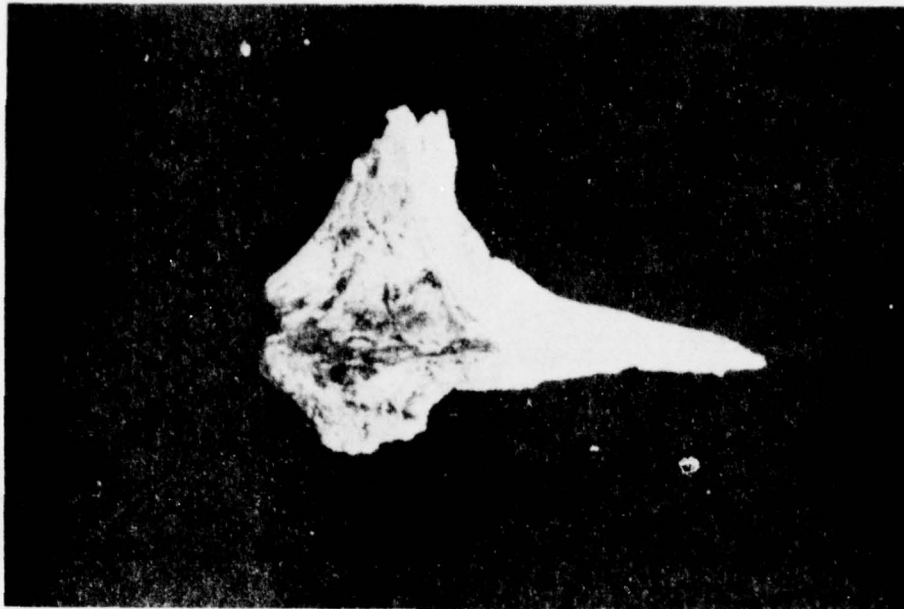


Figure 81. Magnesium Oxide Deposit Removed From Combustor Nozzle Inlet, Nozzle Contact Surface Shown With Nozzle Cross-section Facing Out

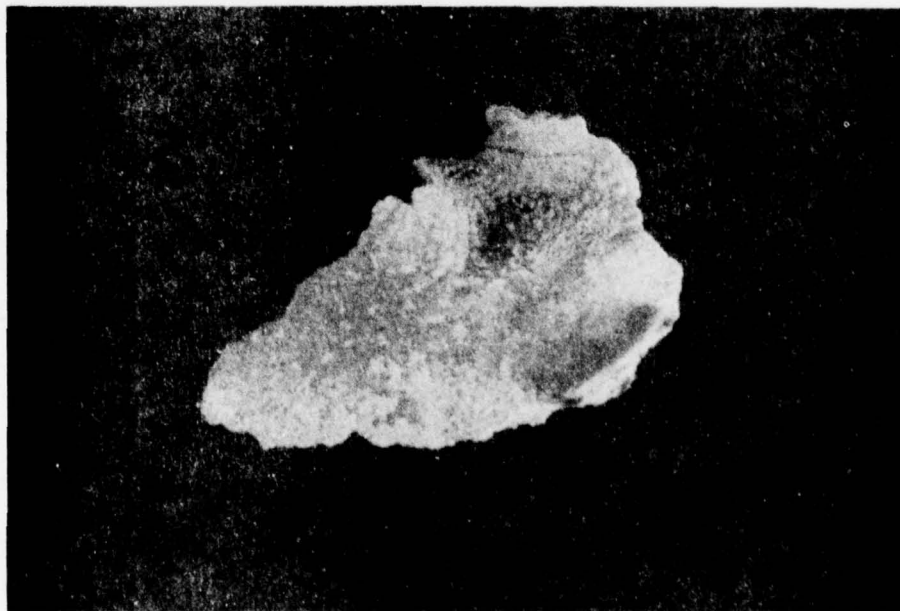


Figure 82. Magnesium Oxide Deposit Removed From Combustor Nozzle Inlet, Gas Flow Surface Facing Out



Figure 83. Magnesium Oxide Deposit Flakes Removed From Combustion Chamber Walls and Deposit Chip Removed From Nozzle Inlet - Gas Flow Surface on the Chip is Up and Flow Direction is Left to Right as Gas Enters the Nozzle Convergent Section

already described. The fuel system was calibrated with this fuel as shown in Figure 84. Test runs HEF-6 and HEF-6A were both made using the same fuel batch. Test run HEF-6 started with a planned stoichiometric O/F = 2.36. Run parameters were as shown below:

Chamber Pressure (kg/cm ²)	\dot{W}_f (kg/sec)	\dot{W}_{O_2} (kg/sec)	\dot{W}_{TOT} (kg/sec)	O/F
8.760	0.1746	0.4244	0.599	2.43
7.495	0.1944	0.4296	0.624	2.21

As can be seen in Figure 85, the minimum chamber pressure encountered, combustion became rough and pressure fluctuations of 0.703 kg/cm² were noted, combustion was unsteady for approximately two seconds after which time chamber pressure steadied and gradually increased to a final level of 8.606. At a point a few seconds prior to shutdown the conditions were:

Chamber Pressure (kg/cm ²)	\dot{W}_f (kg/sec)	\dot{W}_{O_2} (kg/sec)	\dot{W}_{TOT} (kg/sec)	O/F
8.339	0.1761	0.4281	0.604	2.43

At the end of the run the chamber and nozzle were inspected and found to have a heavy buildup of alumina on the chamber walls although none was noted in the nozzle inlet or throat. The effect of the alumina layer buildup on the combustor walls can be seen in the decreasing combustor coolant discharge temperature averaging 20-25° K cooler than normal. Although it seems unlikely from an intuitive standpoint, the deposits had the appearance of having deposits of unburned aluminum. It was decided that run HEF-6A with an increased O/F = 2.38 be made immediately upon completion of chamber and injector

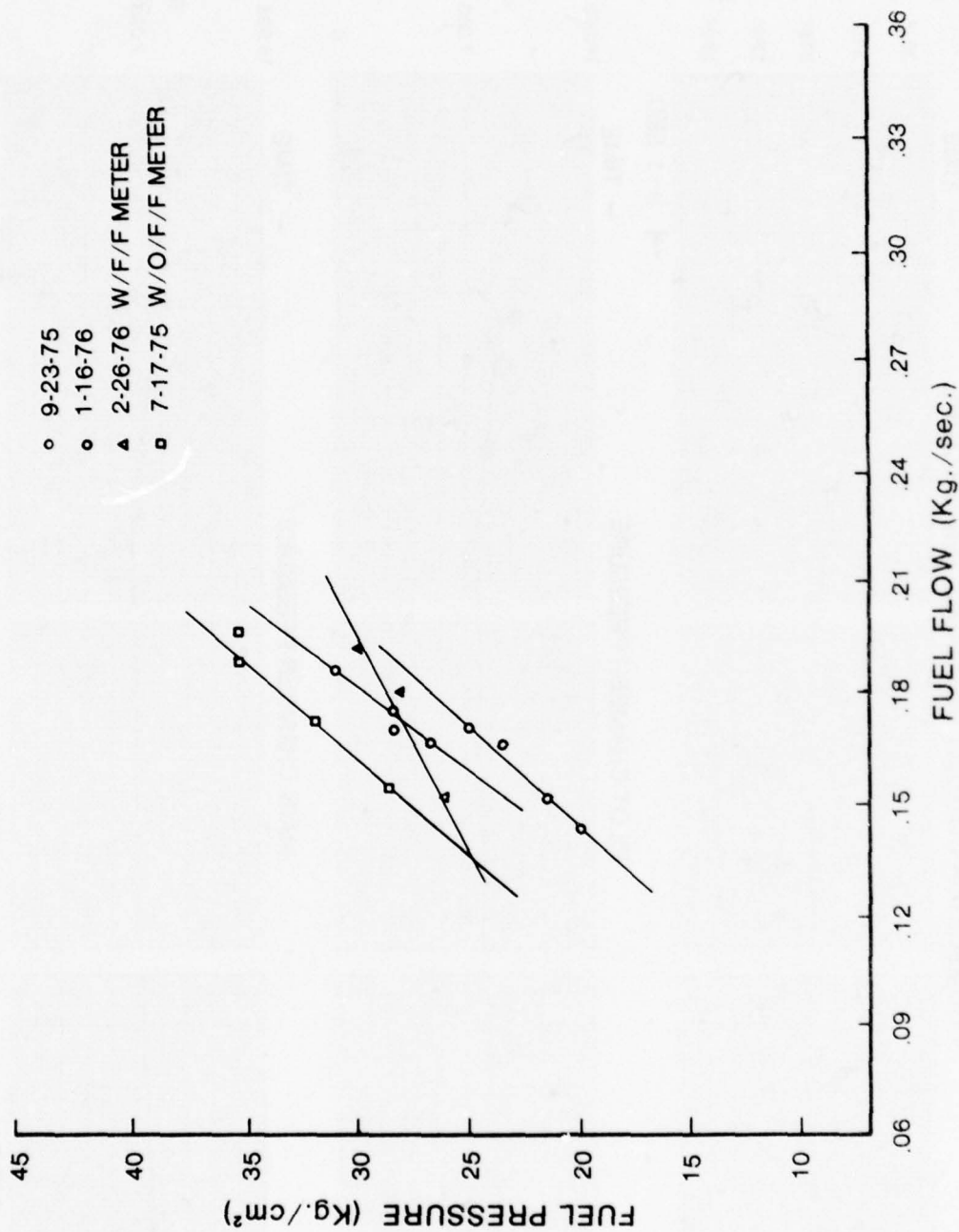
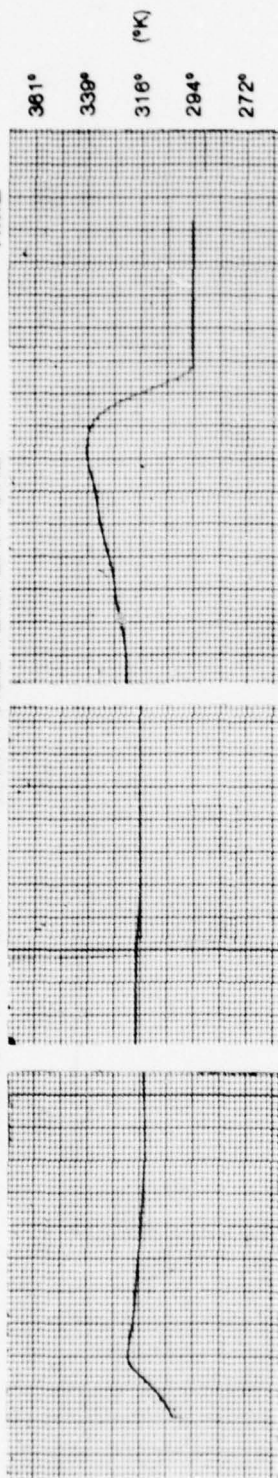


Figure 84. Calibration Curves For Emulsified Toluene/Aluminum

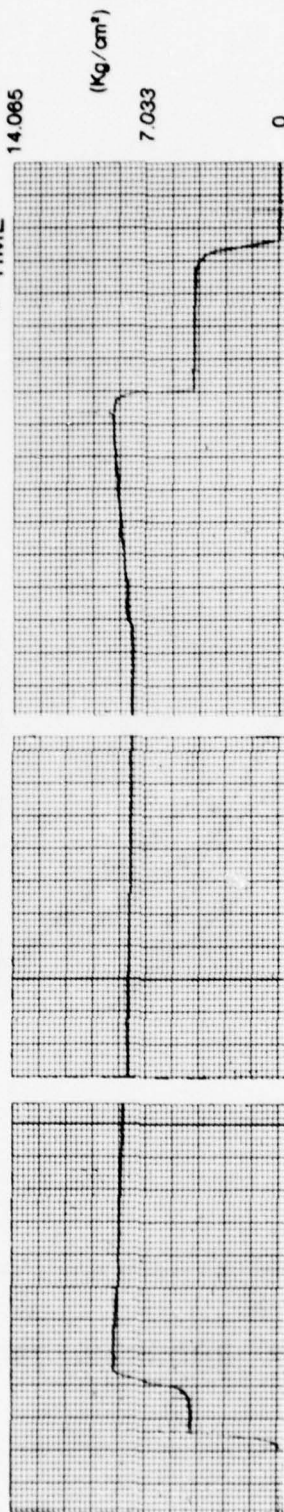
HEF-6

COMBUSTOR COOLANT DISCHARGE TEMPERATURE



→ 1 SEC.

PILOT CHAMBER PRESSURE



MAIN CHAMBER PRESSURE

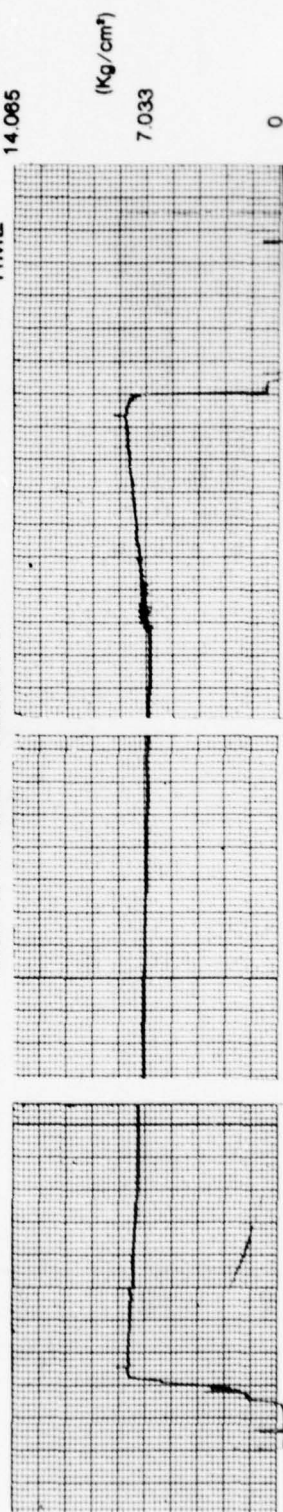


Figure 85. Combustion Test - HEF-6, Fuel - Emulsified Toluene 65%, Aluminum 30%

cleanup. This run was of 30 second duration due to a limited fuel supply remaining. Test run HEF-6A started at a chamber pressure of 8.353 kg/cm².

The run parameters were:

Chamber Pressure (kg/cm ²)	\dot{W}_f (kg/sec)	\dot{W}_2 (kg/sec)	\dot{W}_{TOT} (kg/sec)	O/F
8.353	0.1676	0.4424	0.610	2.64

In Figure 86 we see that after approximately five seconds of uneven chamber pressure the burning became rough with 0.98 kg/cm² pressure fluctuations which lasted with decreasing intensity for approximately 13 seconds. At this time chamber pressure rose steadily up to the point of scheduled shutdown at which time the calculated conditions were:

Chamber Pressure (kg/cm ²)	\dot{W}_f (kg/sec)	\dot{W}_{O_2} (kg/sec)	\dot{W}_{TOT} (kg/sec)	O/F
8.184	0.1707	0.4422	0.613	2.59

Upon disassembly of the chamber only a light dusty coat of alumina was observed on the chamber walls and nozzle inlet. A few small areas of thin buildup were noted on the injector plate in the region of the injectors. This test also showed a marked decrease in combustor coolant discharge temperature despite the fact that the coating was quite thin.

Once again a result of this test was an indication of either poor fuel flow control, oxygen flow control, or both. At this point, combustion tests were discontinued and power testing was started since there were no major problems which were not

HEF-6A

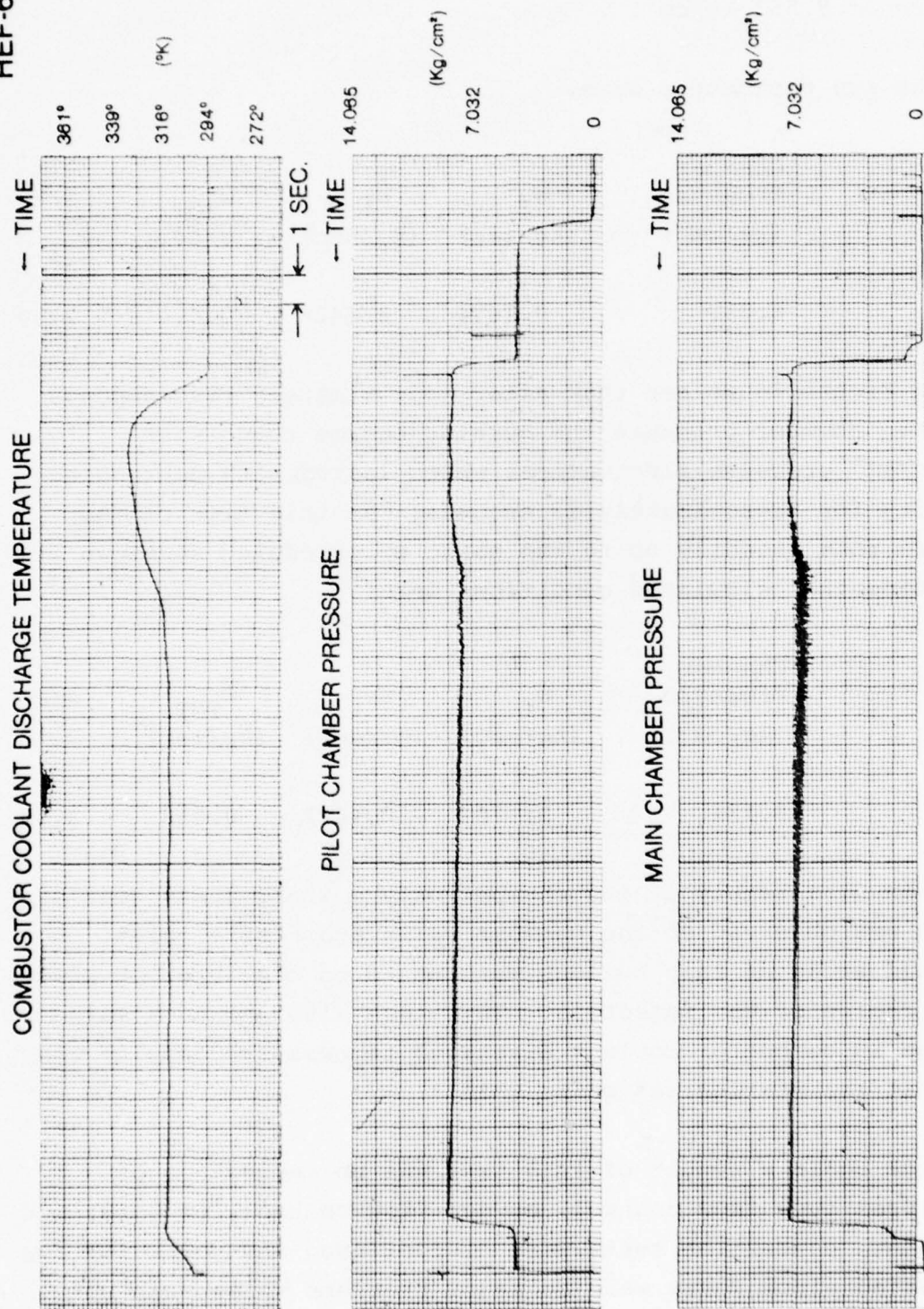


Figure 86. Combustion Test - HEF-6A, Fuel - Emulsified Toluene 65%, Aluminum 30%

solved through modification of procedures or equipment. Although fuel metering remains a troublesome area, it was felt that the metering technique used was sufficiently accurate to justify proceeding with power testing with the MHD channel.

4. MHD GENERATOR POWER TESTING

A. Introduction

During this phase of the fuels testing, a total of 30 tests were run using the KIVA-I water cooled 45° diagonally conducting wall MHD generator channel shown in Figure 87 installed in the test stand. Figure 88 shows the control room setup with the exception of oscilloscopes and computer tape recording units.

B. MHD Channel Checkout Test With Toluene, HEF-7

Test run HEF-7 was run as a checkout of the entire system with the exception that the magnet was pulled back from the channel as shown in Figure 87 for the purpose of observation. The channel was run with liquid toluene fuel and oxygen at a stoichiometric O/F ratio of 3.13. The test was scheduled to run 10 seconds and no seed was injected. The test was completed with no generator problems but due to a data recording malfunction no data was taken. The test was rescheduled and run as test run HEF-7A. Figure 89 shows the toluene fuel calibration curve. The repeat test was again made with an O/F ratio of 3.13 and a total propellant flow of 0.6 kg/sec. Figure 90 shows traces of pilot chamber pressure, main combustion chamber pressure, and chamber H₂O exit temperature. The chamber pressure is considerably lower than the anticipated 10.34 kg/cm². The pressure as can be seen after a very slightly rough start remained stable at approximately 8.16 kg/cm². The pilot flame came on smoothly and burned for 5 sec prior to main chamber

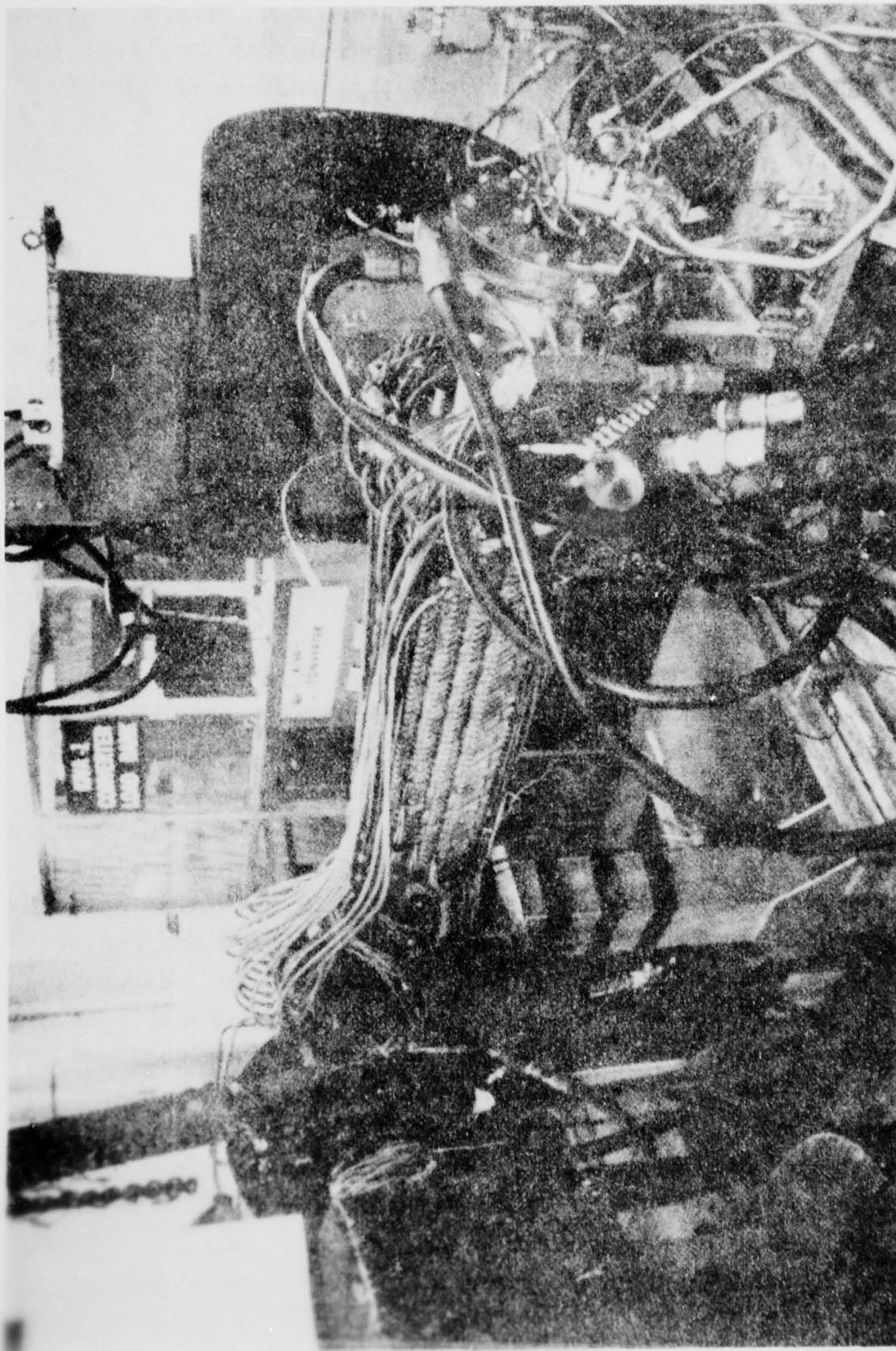


Figure 87. KIVA - I Water Cooled, 45°, Diagonally
Conducting Wall, MHD Generator

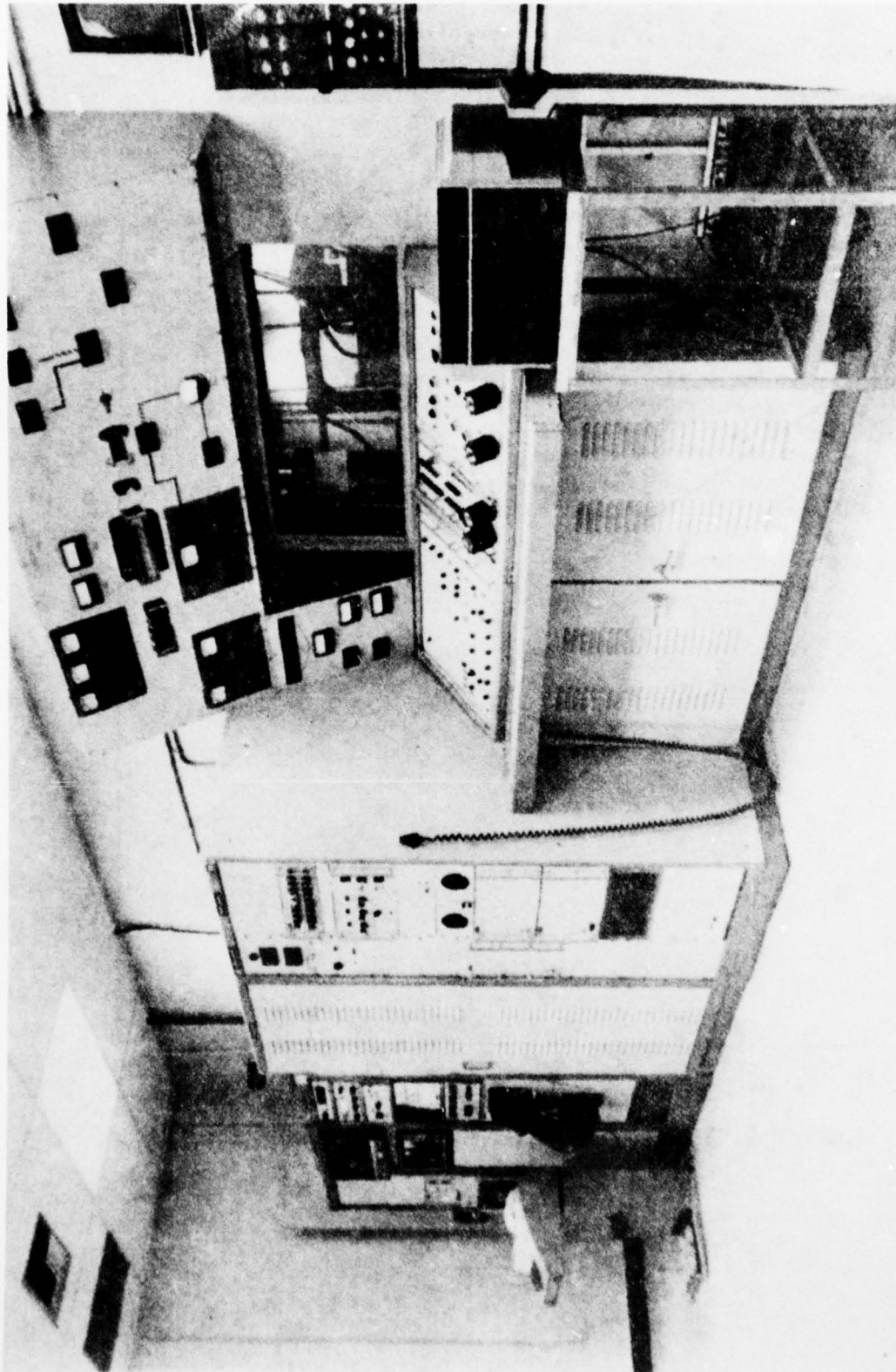


Figure 88. KIVA - I MHD Generator Control Room

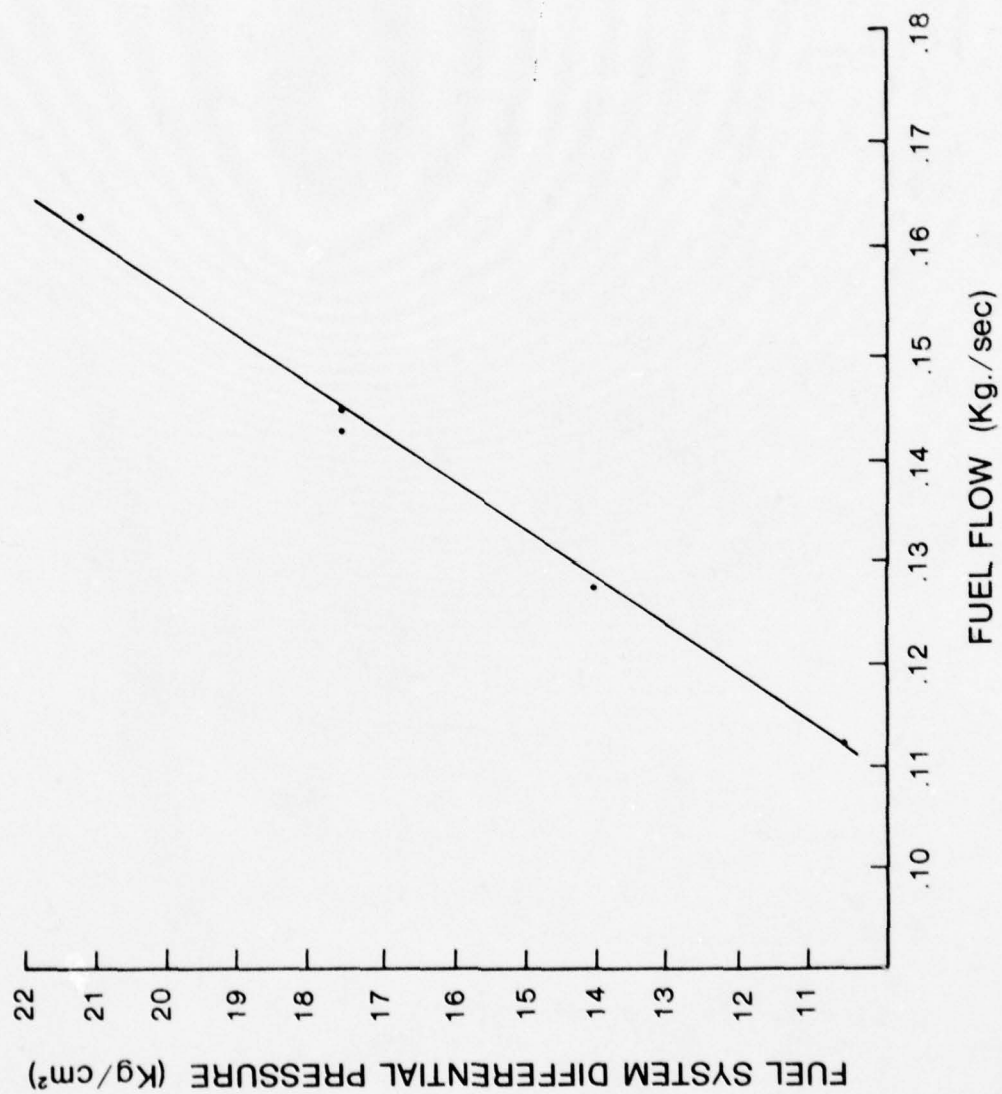


Figure 89. Neat Toluene Fuel Flow Calibration Curve

HEF-7A

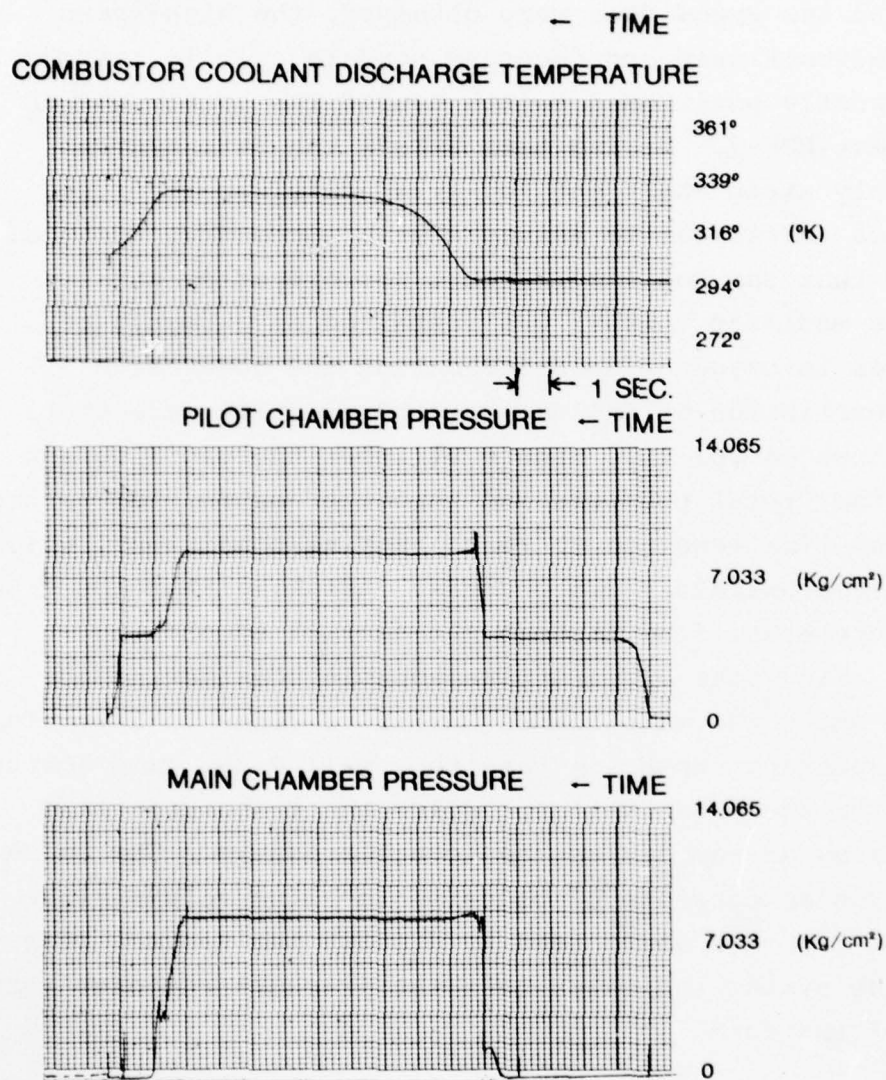


Figure 90. MHD Generator Check Out Test - HEF-7A, Fuel - Neat Toluene, Modified .772cm, Oxidizer Venturi Installed

initiation. The slight increase in main chamber pressure prior to main chamber ignition indicates the opening of the oxygen valves prior to the fuel valves. Combustor water exit temperature was stable and showed no abnormalities. A normal shutdown took place at the preset time. Although during this test, strip chart and low speed data were obtained, the high-speed data system malfunctioned and recorded no data. It is assumed that an incorrectly positioned switch caused the total loss of data during test HEF-7. During test HEF-7A the data systems cycled, but only strip chart and low-speed data was recorded. These data were sufficient to assure that a successful test had been made and that the modified venturi was operating as expected. The modified venturi was installed as a result of inconsistencies in oxygen flow noted during the combustion tests. The description of the venturi modification, checkout, and use are shown in Vol II. Figure 91 shows the oscillograph trace of oxidizer total pressure and throat pressure. Of particular note is the time required to reach choking conditions, which appears to be approximately 2.5 seconds. Assuming that the time required to accelerate flow through the venturi to choking conditions is this great appears unreasonable considering the rapidity with which the main chamber pressure rises to operating levels. The apparent answer is that the small 0.102 cm diameter throat static pressure tap will not allow the transducer line pressure to decay as rapidly as the actual pressure. The solution to the problem consists of reducing the line volume since an increase in tap size would tend to distort the venturi flow. Analysis of the system indicated that the pressure response rate equation is of the form

$$\dot{P} = -k_0 \left[(P^\beta - P_s^\beta) P^\beta \right]^{1/2} \quad (20)$$

By substituting the appropriate values for k , α , and P_s , \dot{P} can be integrated to find the time for response by numerical

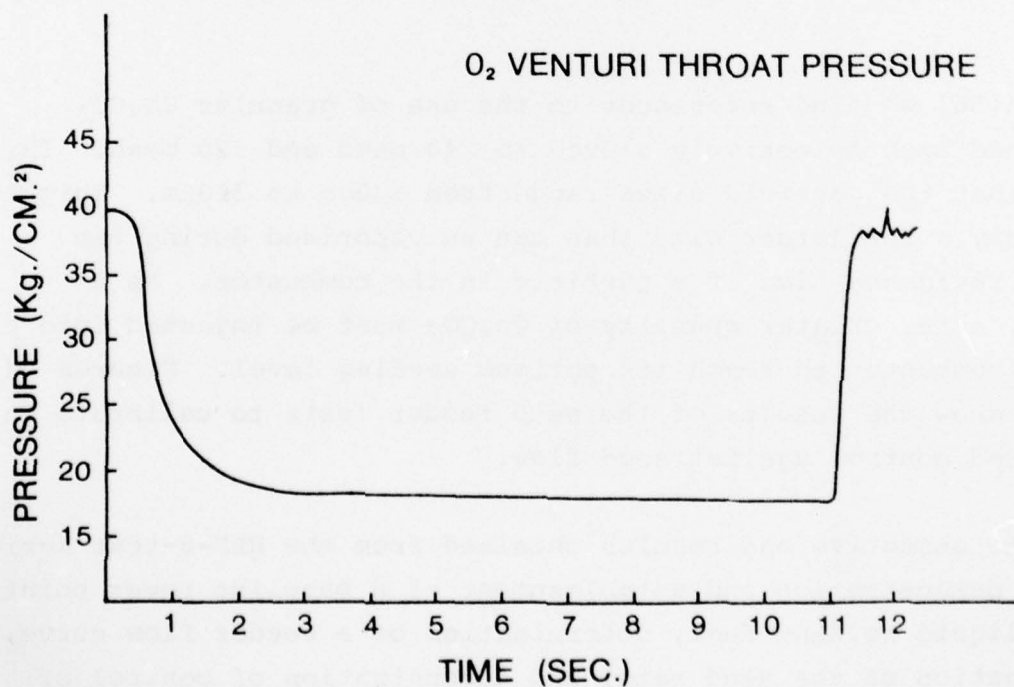
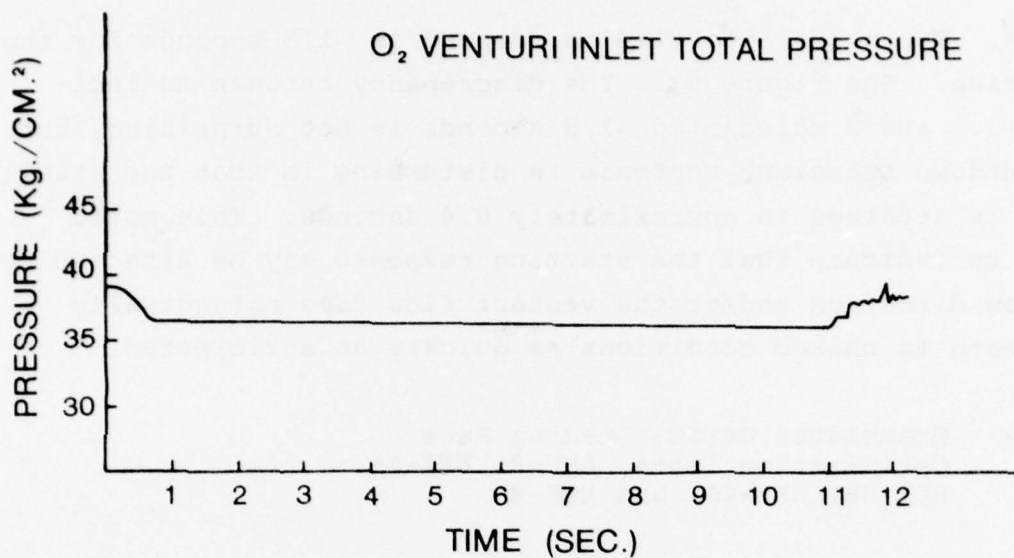


Figure 91. 0.772 Diameter Oxidizer Venturi (Modified)
Total Pressure and Throat Static Pressure

methods. The calculated time to respond is ~ 1.5 seconds for the ideal case. See Figure 92. The discrepancy between an indicated ~ 2.5 and a calculated ~ 1.5 seconds is not surprising, but the shutdown transient response is disturbing in that the stabilization is attained in approximately 0.4 seconds. This would appear to indicate that the starting response may be affected by the flow direction and/or the venturi flow does not actually accelerate to choked conditions as quickly as anticipated.

C. Granulated Cs_2CO_3 Seeding Rate
Optimization Tests, HEF-8, HEF-8A,
HEF-8B, HEF-8C, and HEF-8D

Test run HEF-8 was the first test scheduled to produce power. Prior to this test, the calculated values for the ballast resistors were connected as shown in Table 3.

Figure 93 shows a diagram of the generator electrical connections.

In [56] we find references to the use of granular Cs_2CO_3 which had been selectively sieved to >40 mesh and <20 mesh. This means that the particle sizes range from $830\mu\text{m}$ to $360\mu\text{m}$. This is obviously a far larger size than can be vaporized during the $10\mu\text{sec}$ residence time of a particle in the combustor. As a result, a far greater quantity of Cs_2CO_3 must be injected into the KIVA-I combustor to reach its optimum seeding level. Figures 94 and 95 show the results of the seed feeder tests to calibrate the seed feed control against seed flow.

The objective and results obtained from the HEF-8-test series were: demonstration and establishment of a baseline power point using liquid toluene fuel, determination of a seeder flow curve, optimization of the seed rate, and demonstration of control of oxygen flow rate.

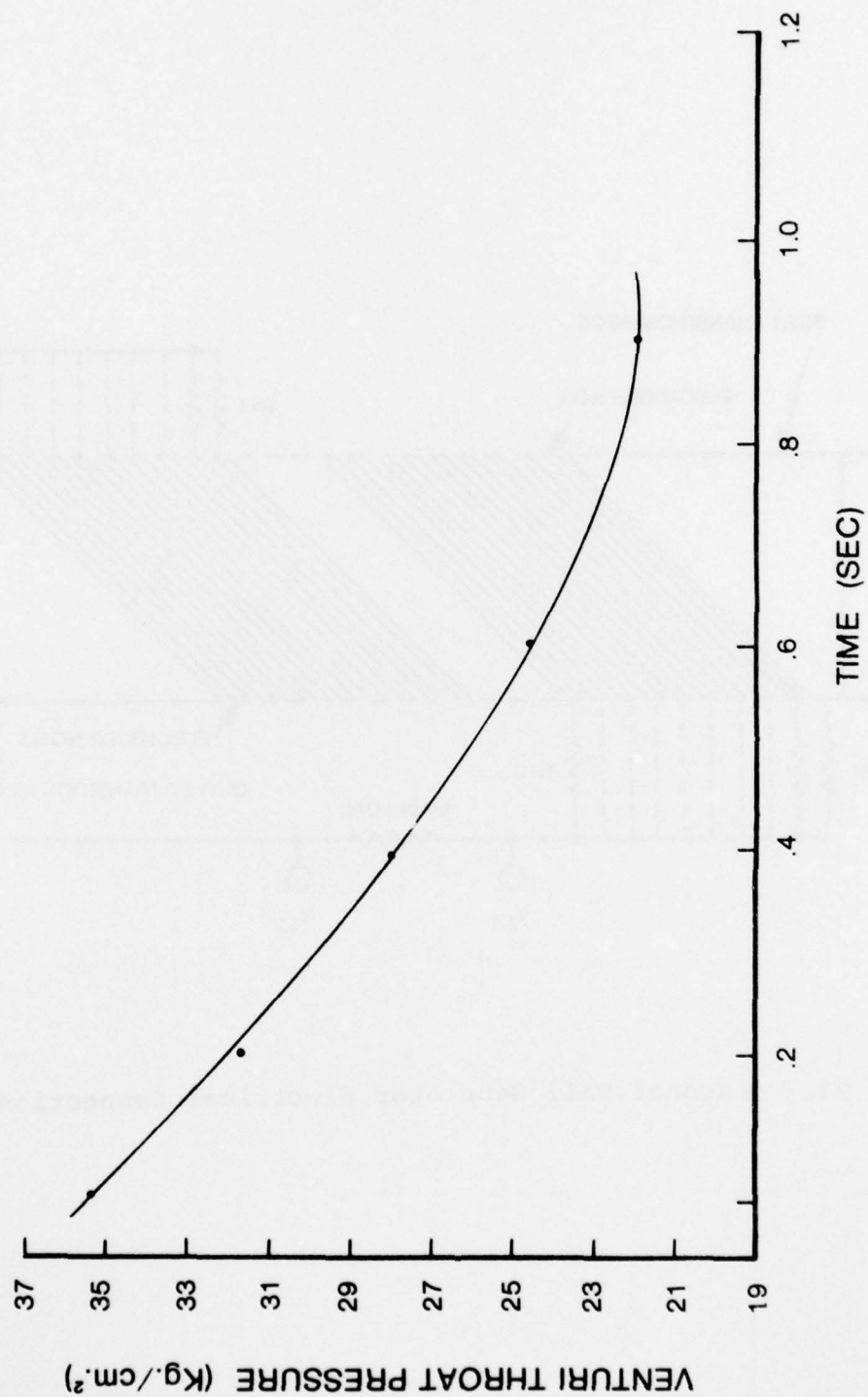


Figure 92. Calculated Pressure Decay For O₂ Venturi Throat Pressure Line

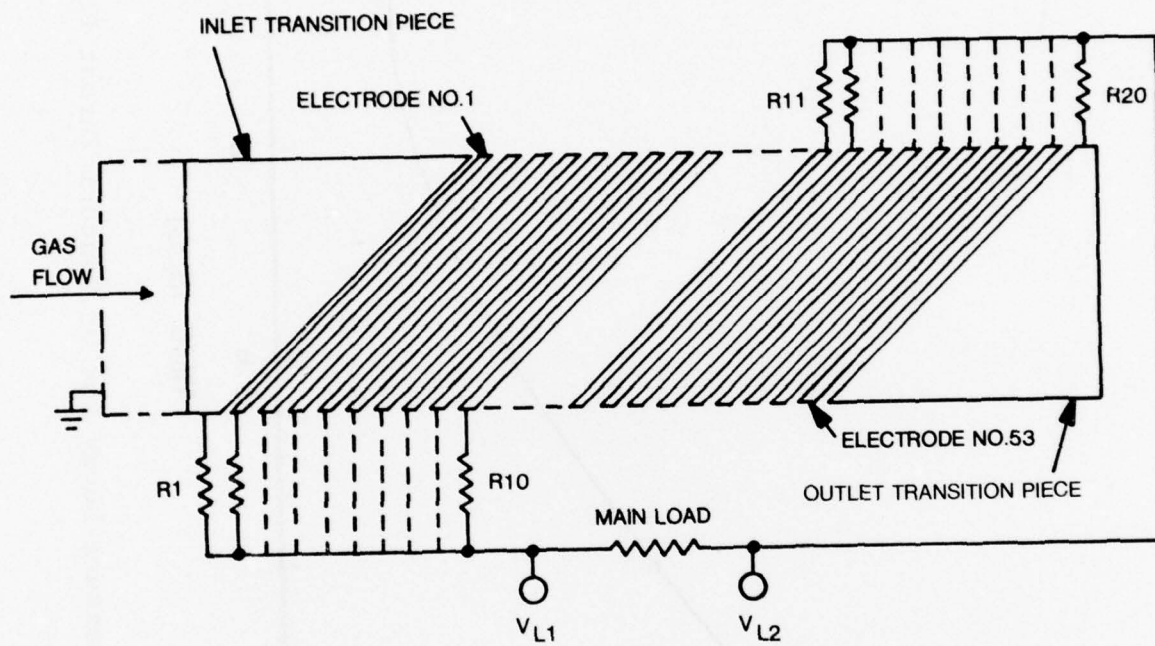


Figure 93. Diagonal Wall Generator Electrical Connections

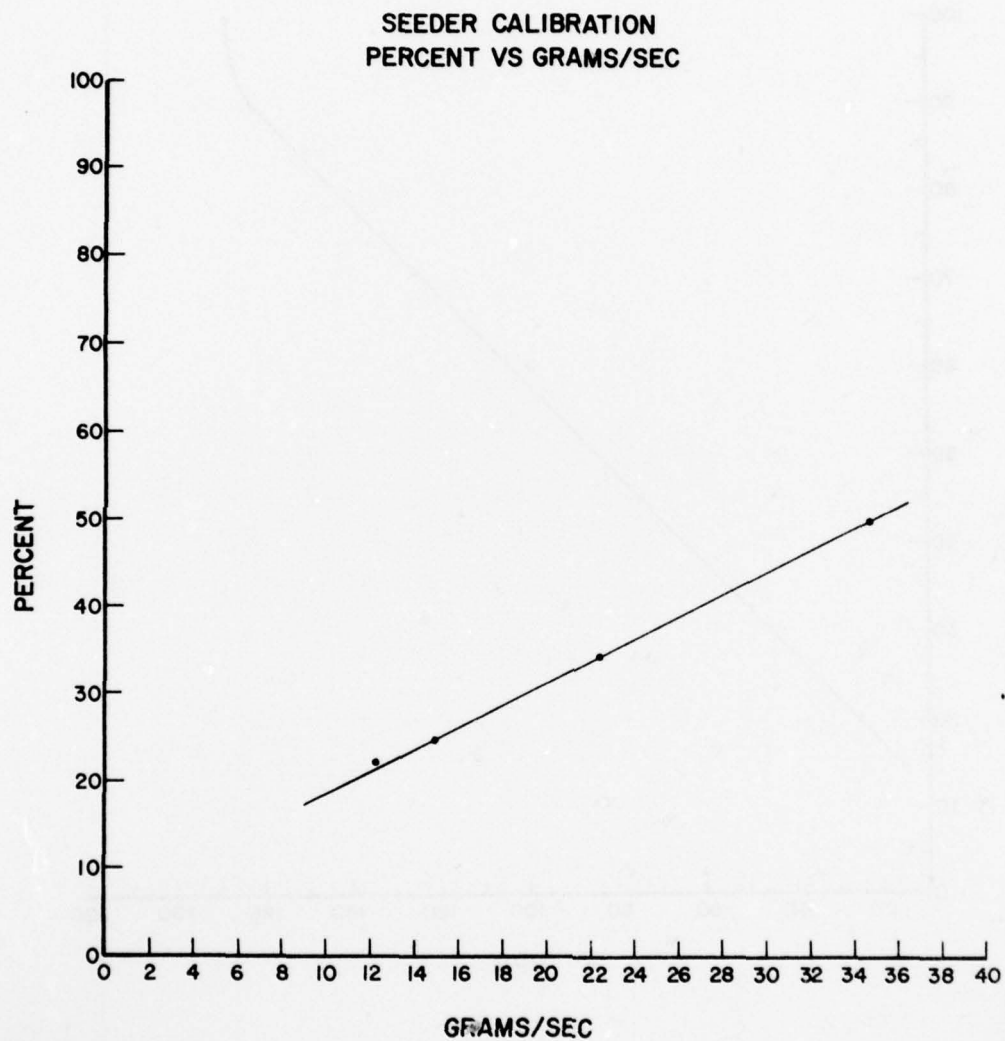


Figure 94. Seeder Calibration For Seed Classified
>20 But <40 Mesh, Percent of Full Scale
Setting Vs. Seed Flow

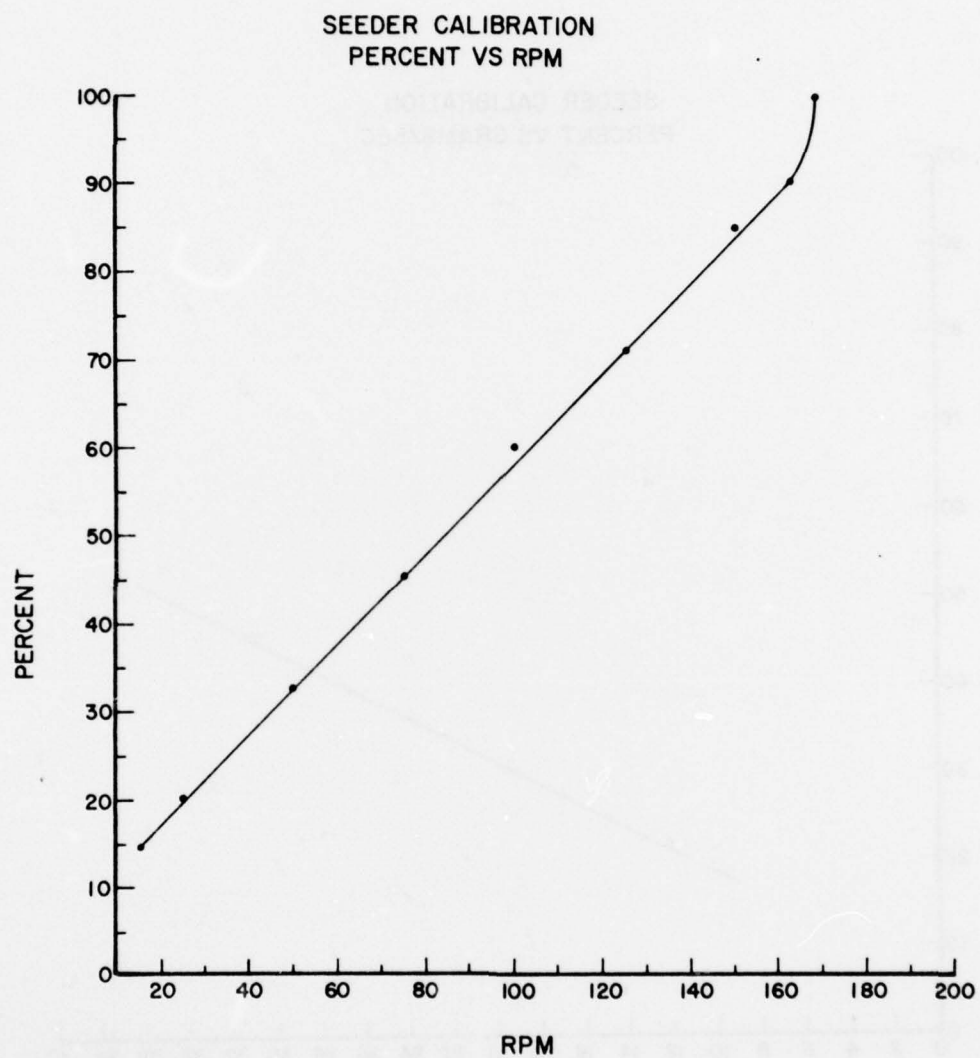


Figure 95. Seeder Calibration, Percent of Full Scale Setting Vs. Seed Wheel RPM

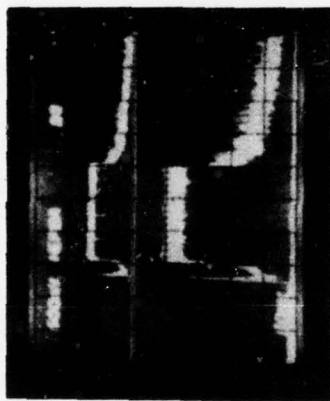
TABLE 3. BALLAST RESISTOR VALUES FOR
DIAGONAL WALL CHANNEL

Electrode No.	Effective Single Resistor Value (ohms)
1	10.5
2	9.40
3	8.10
4	6.90
5	5.70
6	4.45
7	2.94
8	1.53
9	0.260
46	0.290
47	1.49
48	3.10
49	4.60
50	6.17
51	7.60
52	9.10
53	10.8
Outlet Transition Piece	12.2

In each of the five power tests (8, 8A, 8B, 8C, 8D), a pre-measured amount of Cs_2CO_3 seed was placed in the seed hopper. During the tests the seeder was run at a speed estimated to exhaust the seed supply prior to the end of combustion. In this manner, by measuring the time of seed injection through use of the voltage curve as measured by an oscilloscope, the time averaged seed rate can be determined.

In the description of this and subsequent tests voltage, current, and power produced will be described using various terms. The term "peak indicated" means that this is the highest value of the parameter described, i.e., current, voltage, to be seen in the photographic oscilloscope traces. "Average" means the arithmetic mean of the noise band shown in the photographic oscilloscope traces. The term "peak recorded" refers to the highest value recorded by the data system which samples data channels at a regular interval and as such may or may not pick up the true peak.

Test run HEF-8 was set up for a 15 sec run. The fuel calibration for toluene is shown in Figure 89. Seed flow rate was set for 0.072 kg/sec (8.7% Cs) with a 10 sec seed flow period. The magnet current was set to 725 A to produce a peak field of 2.3 tesla. The load across V_{L_2} to V_{L_1} (see Figure 93) was set to 10 Ω . During the start sequence the seed feeder motor momentarily started, dumping a portion of the seed into the oxidizer line. This caused a high seed surge at start-up and a short powered portion of the run. In all other respects the run was normal, although again the high speed data system malfunctioned. The powered portion of the run was too short and seed feed rate was too high to obtain usable power data. As a result, test run HEF-8A was made after installing a sequencer circuit lockout on the seed feeder motor. The circuit lockout was maintained until a normal start occurred. The test was completely successful except for the continued absence of high speed data. To compensate for the possible lack of high speed data, the low speed data system had been programmed to sample the load voltage four times during a scan. Figure 96 shows an oscilloscope trace of the power meter voltage and power meter current. The run was a nominal 15 second test. As may be seen, the seeder feed starts approximately one second after the start of combustion. This can be determined by the initial voltage spike which is caused by a burst of residual seed dust or powder remaining in the



TIME →

RUN NO. HEF-8A

FUEL: NEAT TOLUENE

SEED: Cs-5.0% OF PROPELLANT (35.9 gm./sec. Cs_2CO_3)

PROPELLANT: 0.55 Kg./sec. O/F: 2.98

LOAD: 10 OHM

SCALE: TOP TRACE - 1000 VOLTS/CM. BOTTOM TRACE - 33.33 AMPS/CM.

TIME: 2 SEC./CM.

Figure 96. Powermeter Current & Voltage
Oscilloscope Trace

AD-A060 156

SYSTEMS RESEARCH LABS INC, DAYTON OH AEROSYSTEMS RESE--ETC F/G 21/4
HIGH ENERGY MHD FUELS DEVELOPMENT PROGRAM.(U)
APR 78 R E ECKELS

F33615-75-C-2043

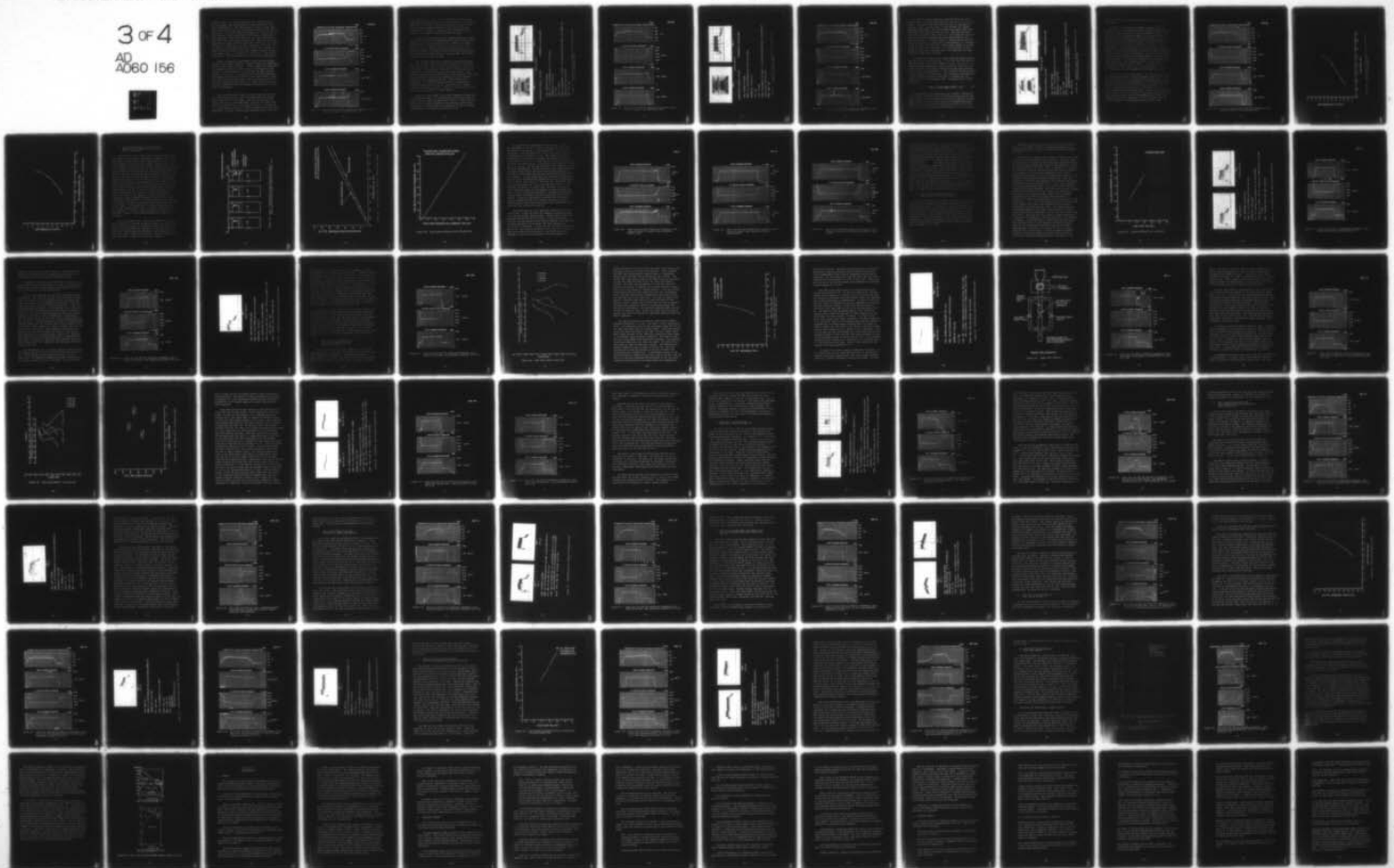
UNCLASSIFIED

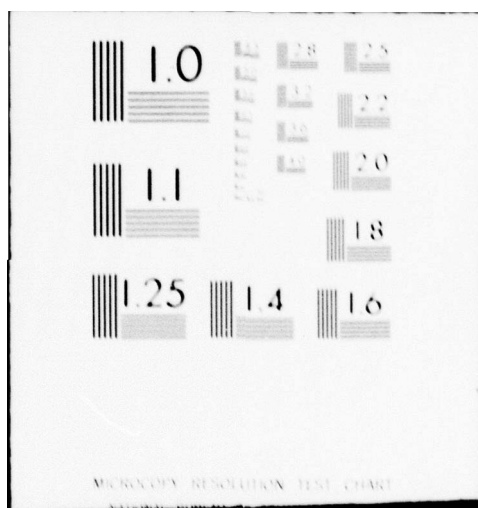
AFAPL-TR-78-10

NL

3 of 4

AD
A060 156





oxidizer lines. The run was made with 215.4 gms of Cs_2CO_3 in the seed hopper and a seed feed motor speed setting of 0.50. This corresponds to a feed gear speed of 83 rpm. Actual seed time can be seen to last for six seconds resulting in an average seed rate of 35.4 gm/sec which corresponds to a Cs seed rate of 5.0% based on a propellant flow of 0.55 kg/sec. The highest dc power parameter values recorded by the low speed data system were 1348 volts, 121.2 amps, and 167.6 kw. Note that the power measurement is taken from the power meter and not $P = IV$. Mean voltage and current were, as seen in Figure 96, 1300 volts, and 125 amps for a calculated mean power of 162.5 kw. During the power extraction portion of the test, chamber pressure averaged 8.105 kg/cm² with a 1 σ variation of .057 kg/sec. The oxidizer flow averaged .415 kg/sec with a 1 σ variation of .0020 kg/sec.

Figure 97 shows the oscillograph traces of pilot chamber pressure, main chamber pressure, chamber coolant exit temperature, and O₂ venturi throat pressure. In this figure it is noted that the combustion pressure at start rose to 9.99 kg/cm² or very nearly the target pressure of 10.34 kg/cm² (10 atm) and then dropped to 8.3 kg/cm². At ignition the initial fuel flow rate was probably essentially on target as was the O/F ratio. Note that the actual propellant rate is low (.55 kg/sec) and the O/F is 2.98 as opposed to the target 3.13. After ignition the fuel nozzle ΔP decreased due to the chamber pressure and as a result fuel flow decreased.

Test run HEF-8B was a repeat of run 8A with the exception of Cs seed time and rate. Test run HEF-8B lasted 15 seconds with a seed time of 9.4 seconds. The test was started with 198 gms of Cs_2CO_3 in the seed hopper resulting in a mean usage rate of 21.1 gm/sec with a seed motor setting of .34 resulting in a feeder speed of 52 rpm. Cs seed was then 3.0% of the total propellant. The peak recorded power parameters were 1336 volts,

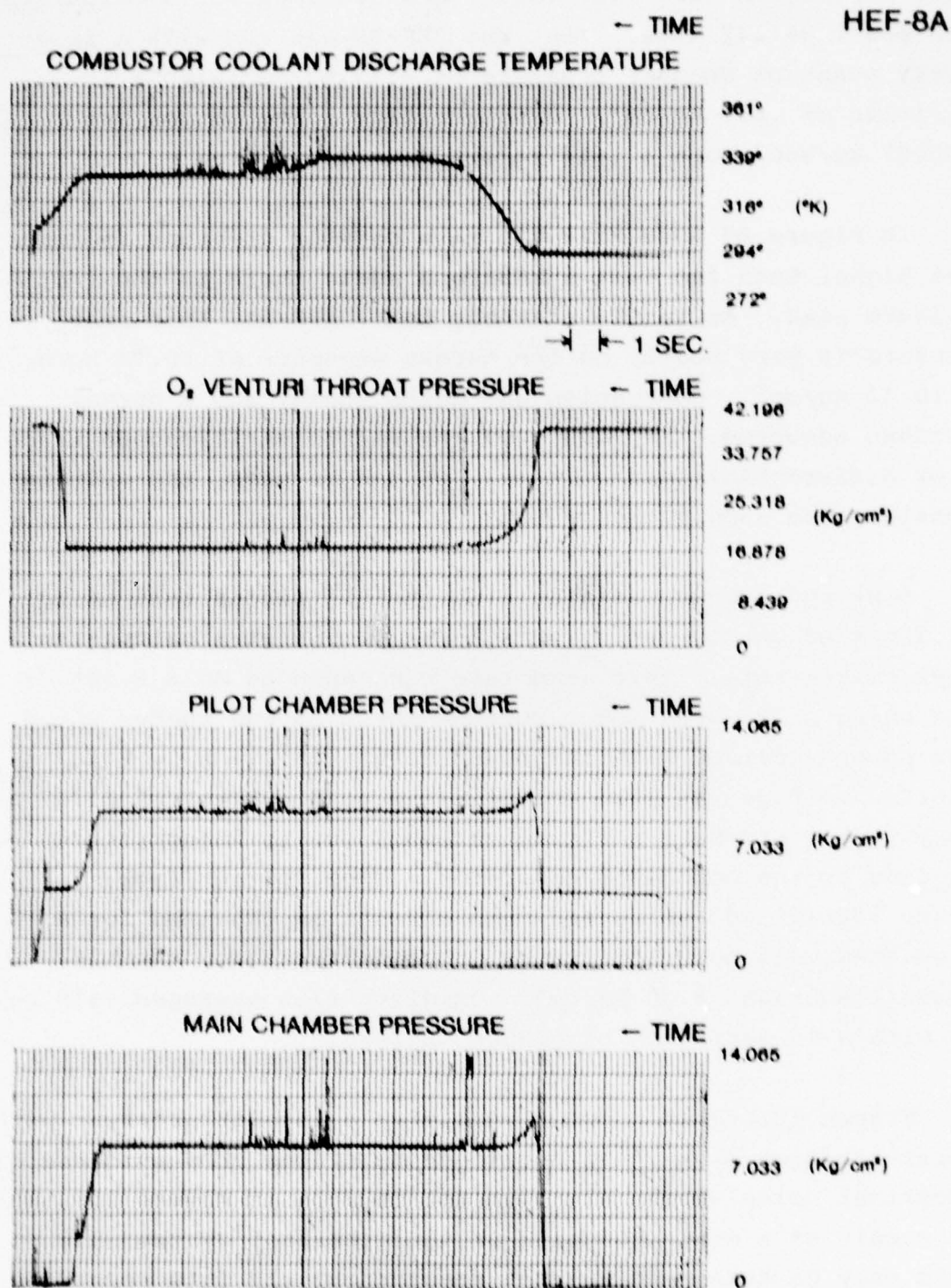


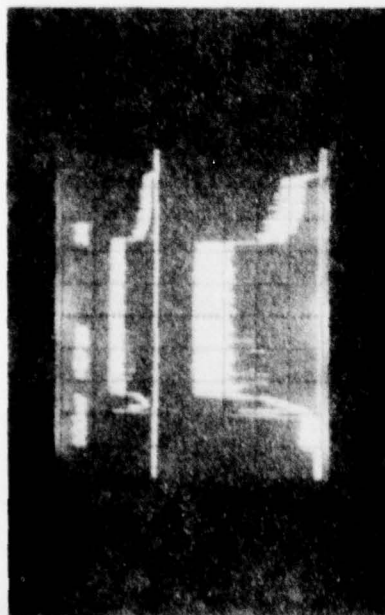
Figure 97. Power Test Run HEF-8A Combustion Parameters, Fuel - Straight Toluene, Load Resistance 10Ω

117.4 amps, and 175.6 kw. From Figure 98 the indicated mean power parameters were 1250 volts, and 114 amps for a calculated mean power of 142.5 kw. Test run HEF-8B was run with a relatively constant chamber pressure of 8.25 kg/cm^2 with a 1σ variation of $.057 \text{ kg/cm}^2$. Oxidizer flow 1σ variation was 0.00087 kg/sec about a $.414 \text{ kg/sec}$ mean flow rate.

In Figure 99 note that the main chamber pressure is somewhat higher than for Test HEF-8A and again there is the initial pressure peak. As in the previous test, HEF-8A, this peak pressure is very nearly on the target pressure of 10.34 kg/cm^2 at 10.13 kg/cm^2 . Combustion was quite steady and a normal shutdown occurred. In Figure 98 the second oscilloscope trace is of differential load voltage. As can be seen, the voltage signature has some noise or hash.

Test run HEF-8C was also a nominal 15 second test using 141.7 gms of Cs_2Co_3 during an 8.9 sec period at a calculated 15.92 gm/sec rate. This seed rate corresponded to a 2.38% Cs rate using a .25 seed motor setting for a 35 rpm feeder speed. Peak power recorded with the power meter was 174 kw. Peak recorded voltage was 1313 volts with a peak current of 117.7 amps. These parameters were shifting somewhat due to intermittent chugging of the combustor/generator. Mean voltage from Figure 100 is 1200 volts and mean current is 104 amps for a calculated mean power of 125 kw. During the test, chamber pressure averaged 8.30 kg/cm^2 . Oxidizer flow averaged $.415 \text{ kg/sec}$ with a 1σ variation of 0.0004 kg/sec .

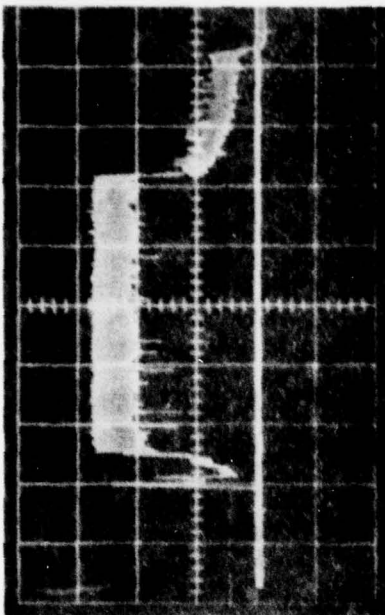
Figure 101 again shows a very stable chamber pressure with a post-ignition peak. All oscilloscope traces show evidence of electrical noise which, although not obvious in Figure 100, was the result of a minor chugging of the generator system which could only be heard and was not recorded by any data recording system except as intermittent electrical noise.



TIME --

RUN NO. HEF-8B

POWER METER CURRENT & VOLTAGE



TIME --

DIFFERENTIAL LOAD VOLTAGE

FUEL: STRAIGHT TOLUENE

SEED: Cs - 3.0% OF PROPELLANT (21.1 gm./sec. Cs_2CO_3)

PROPELLANT: 0.55 Kg/sec.

O/F: 2.99

LOAD: 10. OHM

SCALE: POWERMETER: TOP TRACE - 1000 VOLTS/CM. BOTTOM TRACE - 33.33 AMPS/ CM.

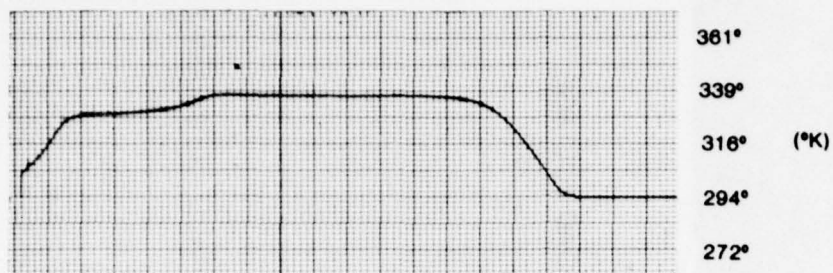
LOAD VOLTAGE: 500 VOLTS/CM.

TIME: 2 SEC./CM.

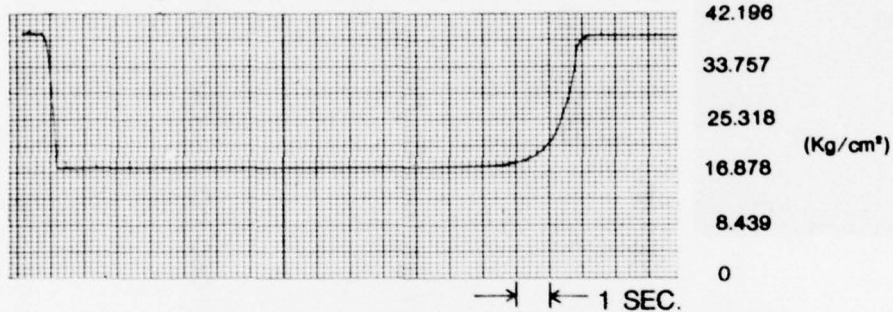
Figure 98. Powermeter Current, Voltage and Differential Load Voltage Oscilloscope Trace

HEF-8B

COMBUSTOR COOLANT DISCHARGE TEMPERATURE — TIME



O₂ VENTURI THROAT PRESSURE — TIME



PILOT CHAMBER PRESSURE — TIME



MAIN CHAMBER PRESSURE — TIME

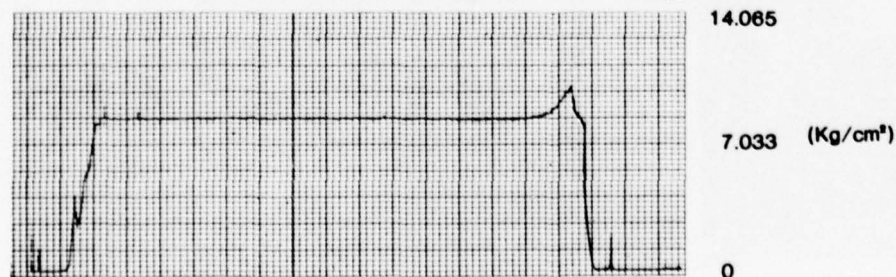
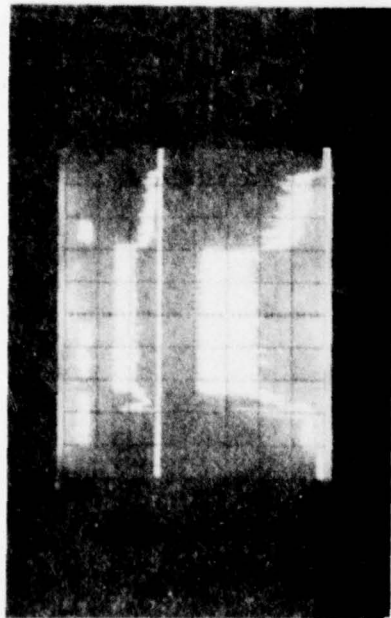


Figure 99. Power Test Run HEF-8B Combustion Parameters, Fuel - Straight Toluene, Load Resistance 10Ω



TIME →

RUN NO. HEF-8C

POWER METER CURRENT & VOLTAGE

FUEL: STRAIGHT TOLUENE

SEED: Cs - 2.28% OF PROPELLANT (15.9 gm./sec. Cs_2CO_3)

PROPELLANT: 0.55 Kg./sec.

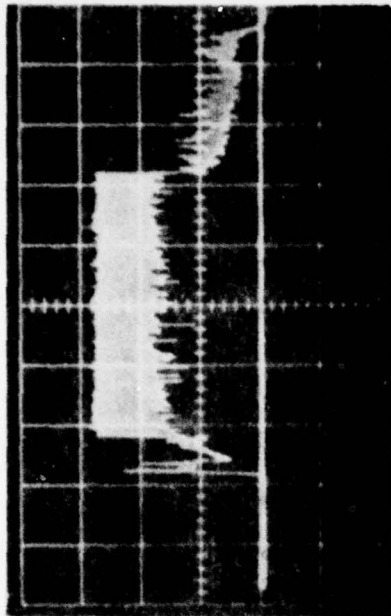
O/F: 2.94

LOAD: 10. OHM

SCALE: POWERMETER TOP TRACE - 1000 VOLTS/CM. BOTTOM TRACE - 33.33 AMPS/CM.

LOAD VOLTAGE: 500 VOLTS/CM.

TIME: 2 SEC./CM.



TIME →

DIFFERENTIAL LOAD VOLTAGE

Figure 100. Powermeter Current, Voltage and Differential Load Voltage Oscilloscope Trace

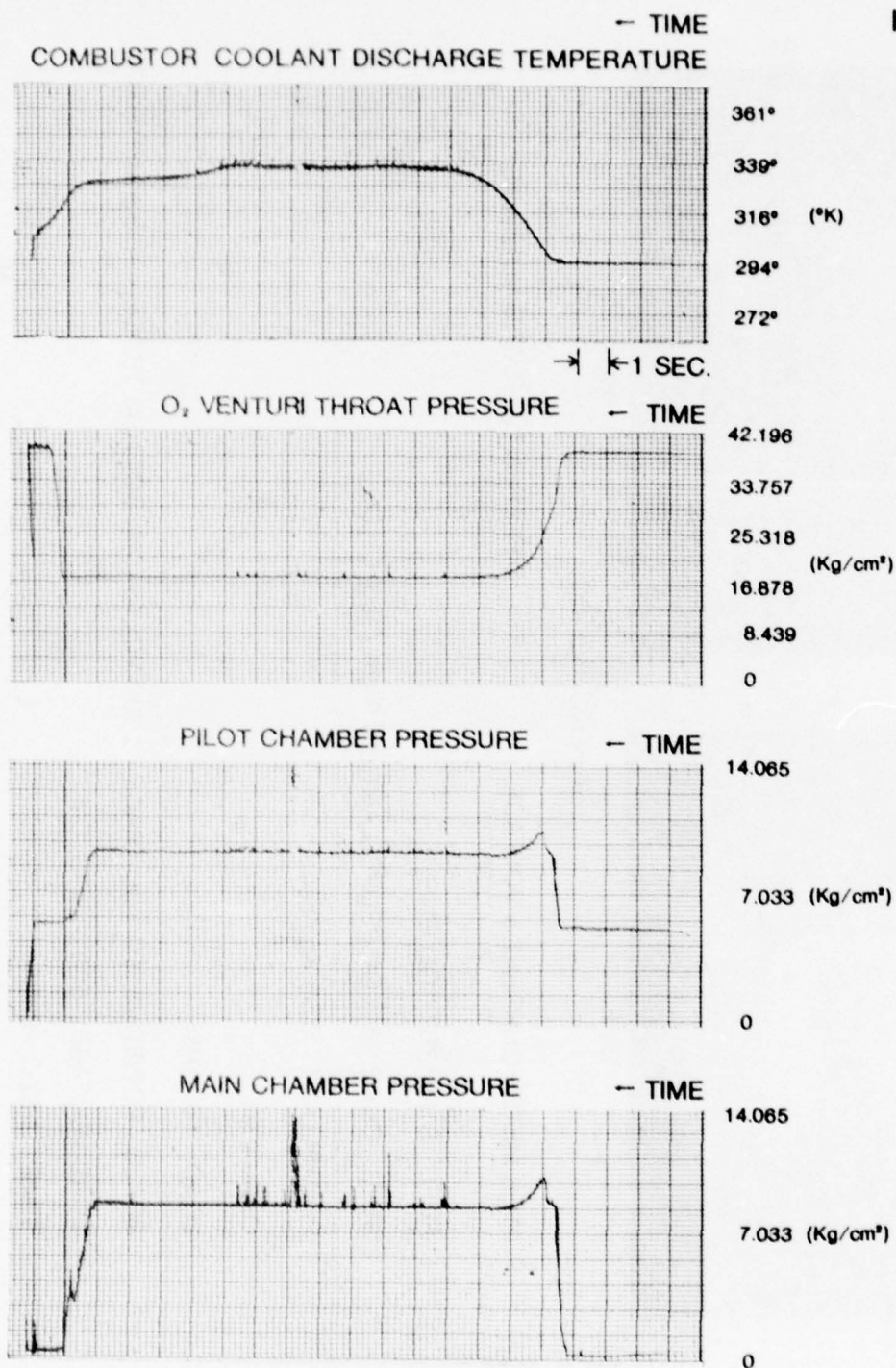


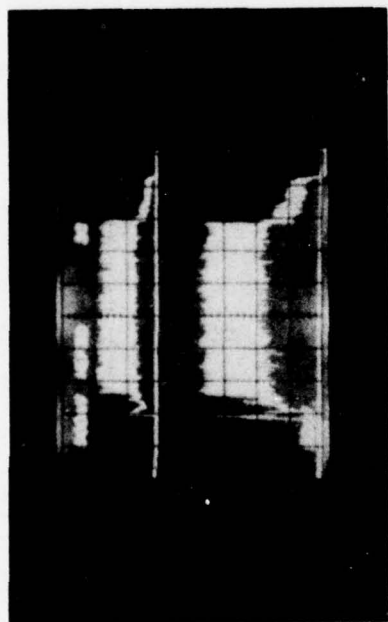
Figure 101. Power Test Run HEF-8C Combustion Parameters, Fuel - Straight Toluene, Load Resistance 10Ω

In test run HEF-8D there was increased electrical noise. The test was a 15 second test with 127.6 gms Cs_2CO_3 in the seed hopper. The seed feeder delivered seed for 10.7 seconds at a setting of 22%. The mean rate of seed flow was 11.9 gm/sec although the momentary rate was probably much larger than this. The seeder gear speed averaged 29.7 rpm. The peak recorded power meter parameters were 1350 volts, 100.5 amps and 132.4 kw, none of which were recorded during the same recording cycle. From Figure 102 it is obvious that the voltage and current were both oscillating at a steady rate of approximately 8.5 cycles/sec. As may be seen, peak indicated voltages were roughly 15 to 1600 volts with a mean of 1100 volts. The load indicated current peaked at very nearly 130 amps with a 94.0 amp mean for a mean calculated load power of 103 kw.

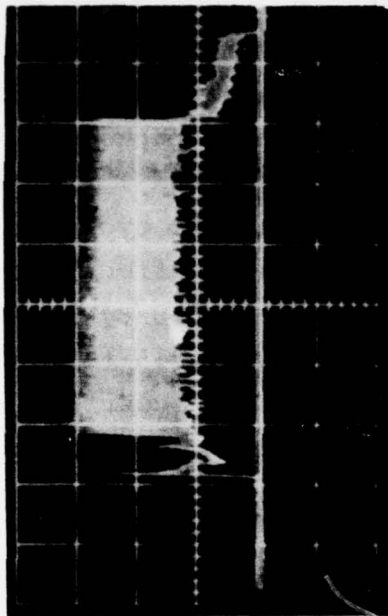
As previously noted, little usable data was obtained during the test due to electrical noise. It is felt that the source of this noise lies in the heavy surges of current through the load resistors hence generating a large oscillating electrical field which induces an oscillating voltage having the same frequency in all of the instrumentation. A low flow rate of seed can result in pulsed injection of the seed. This occurs as seed contained in the toothed gear type of feed wheel is dropped into the oxygen flow in an intermittent mode. The pulse rate is determined by:

$$f = \frac{N(\text{No. of seeder gear teeth}) \times \text{rpm}}{60} \quad (21)$$

The E01 seeder gear feed wheel has 12 teeth. Examination of the seeder tachometer data by arbitrarily rejecting the very high and very low rpm data points results in a series of seeder speed points with a very small population standard deviation. The mean is 42.26 rpm and the standard deviation is 0.65 rpm. Calculation of the resulting pulse frequency is 8.45 cycles per



TIME →



TIME →

RUN NO. HEF-8D

POWER METER CURRENT & VOLTAGE

DIFFERENTIAL LOAD VOLTAGE

FUEL: STRAIGHT TOLUENE

SEED: Cs - 1.72% OF PROPELLANT (11.9 gm./sec. Cs_2CO_3)

PROPELLANT: 0.55 KG./SEC.

O/F: 3.00

LOAD: 10 OHM

SCALE: LOAD VOLTAGE - 500 VOLTS/CM. POWERMETER TOP TRACE - 1000 VOLTS/CM.

POWERMETER BOTTOM TRACE - 33.33 AMPS/CM.

TIME: 2 SEC./CM.

Figure 102. Powermeter Current, Voltage and Differential Load Voltage Oscilloscope Trace

second or essentially the exact frequency observed in the data trace noise.

In Figure 103 the trace of chamber pressure shows the effect of an 8.5 Hz electrical signal synchronized with the same frequency signal appearing in the pilot chamber pressure trace as well as in the combustion chamber coolant temperature. Obviously it is impossible for the KIVA-I system to heat and cool at the frequency indicated, hence the signal must be generated by an oscillating or pulsating dc signal in the generator load. One interesting effect does appear in closer observation of the coolant trace. As soon as power generation ceases, as indicated by cessation of the noise signal, the mean temperature signal starts to decrease. This effect can be seen in corresponding traces of coolant temperature in runs 8A, 8B, and 8C although it cannot be so closely tied to cessation of power generation. The interesting effect is that there is no corresponding chamber pressure change. Although this test produced very little useful data, the implications of the data are interesting from the standpoint of ac power generation.

Using the preceding test results, the effectiveness of the seed has been evaluated. Figure 104 shows a plot of log of Cs flow as a percent of total propellant vs average power. As may be seen, the last three test points lie on a straight line and the first test point lies above the line indicating that the rate of increasing effectiveness of the seed at 5% was not as great as between the last three tests. Figure 105 is a plot of log avg power vs log of Cs flow as a percent of total propellant. This figure indicates that at approximately 6% Cs flow, the maximum power will be developed. It also indicates that the rate of increase of power beyond 5.0% Cs flow is minor.

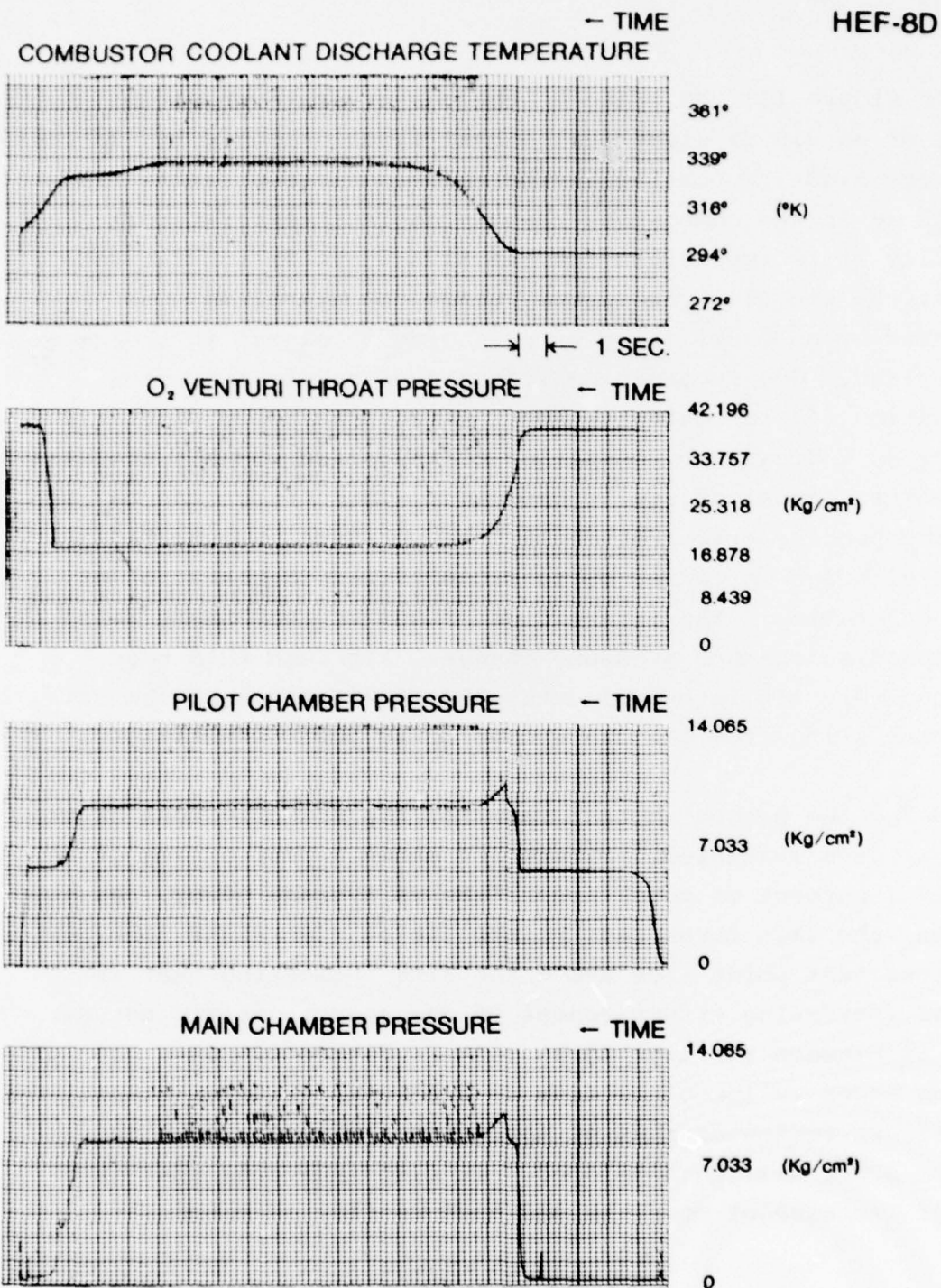


Figure 103. Power Test Run HEF-8D Combustion Parameters, Fuel - Straight Toluene, Load Resistance 10 Ω

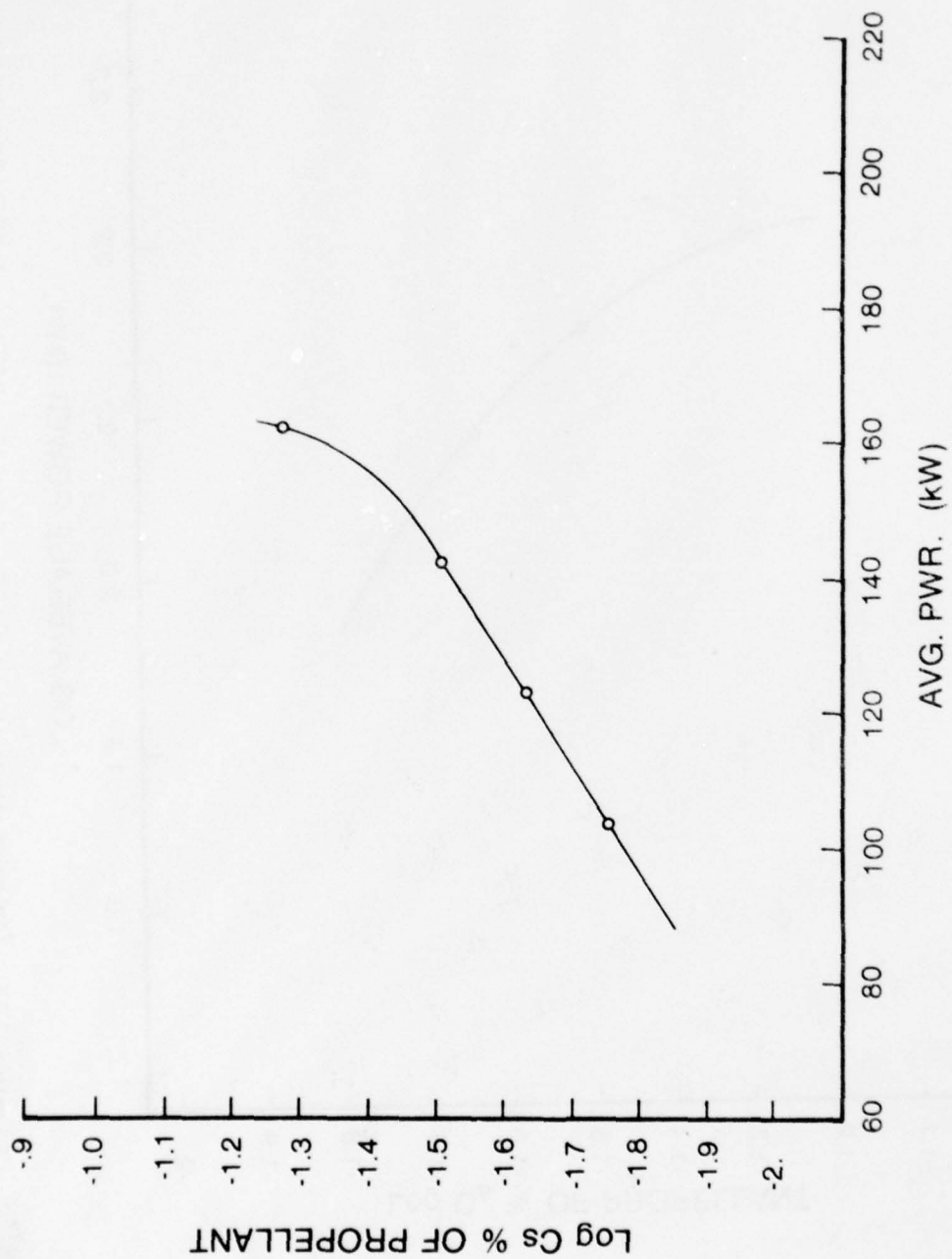


Figure 104. Effectiveness of Granulated Cs_2CO_3 Seed in the KIVA - I MHD Generator

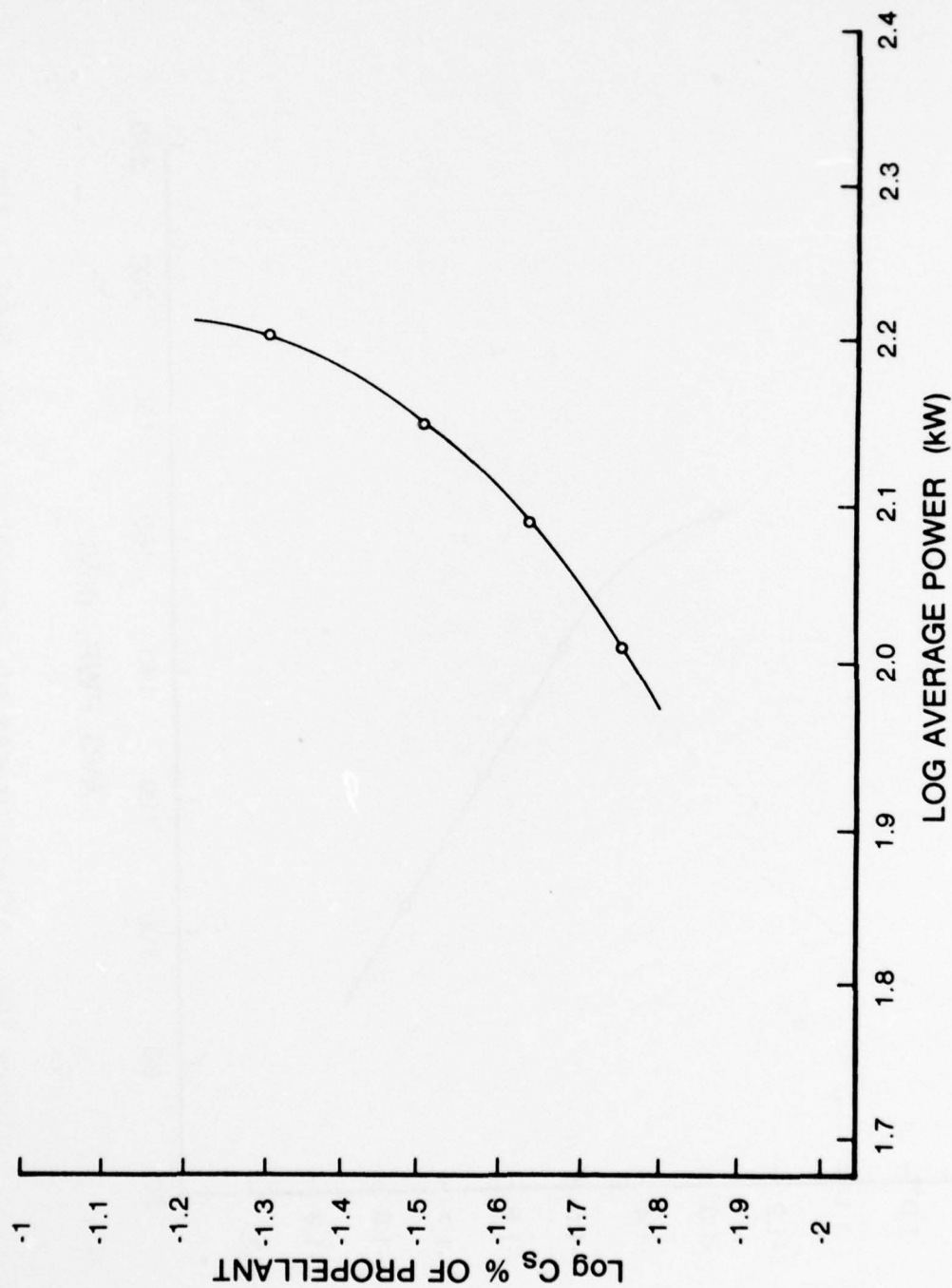


Figure 105. Effectiveness of CsCO_3 Seed In KIVA - I MHD Generator

D. Neat Toluene Baseline, O/F Optimization,
and Load Switch Checkout Tests, HEF-9,
HEF-9A, and HEF-9B

The next test series, HEF-9, 9A, 9B, was intended to determine ideal O/F ratio and to operate the channel for the first time with a load switching system installed by USAF/APL. The load switching circuit diagram is shown in Figure 106. The load switches consisted of four aircraft engine starter solenoids, each connected in parallel with the existing hand-operated knife switches, all but one of which were to be left open during test starts. The figure also shows the electrolytic capacitors connected in parallel with the switches to prevent arcing as the switches are opened. Prior to this test series a new oxygen venturi was installed to allow passage of more oxidizer at lower inlet total pressure. This venturi was designed with the same flow lines as previously used venturis except that the throat diameter was 0.926 cm. A 0.102 cm throat static tap was provided to determine the existence of choking conditions. Figure 107 indicates the required initial static conditions required to obtain scheduled operating conditions based upon calibration. Additionally, the pressure regulator was examined to determine the cause of low oxygen flow rates during the HEF-8 series tests. It was found that a cracked control pressure fitting was leaking sufficiently to prevent attainment of design flow although a relatively high percentage of control was available. Repair of the fitting allowed full control of the regulator.

Prior to the HEF-9 test a new type of turbine flow meter was installed in an attempt to achieve better fuel flow measurements. This flow meter was designed to operate in flowing slurries and was mounted as required in a vertical section of fuel line. The toluene flow calibration curve with fuel flow meter installed is shown in Figure 108. Further discussion of this fuel meter is found in the operations manual.

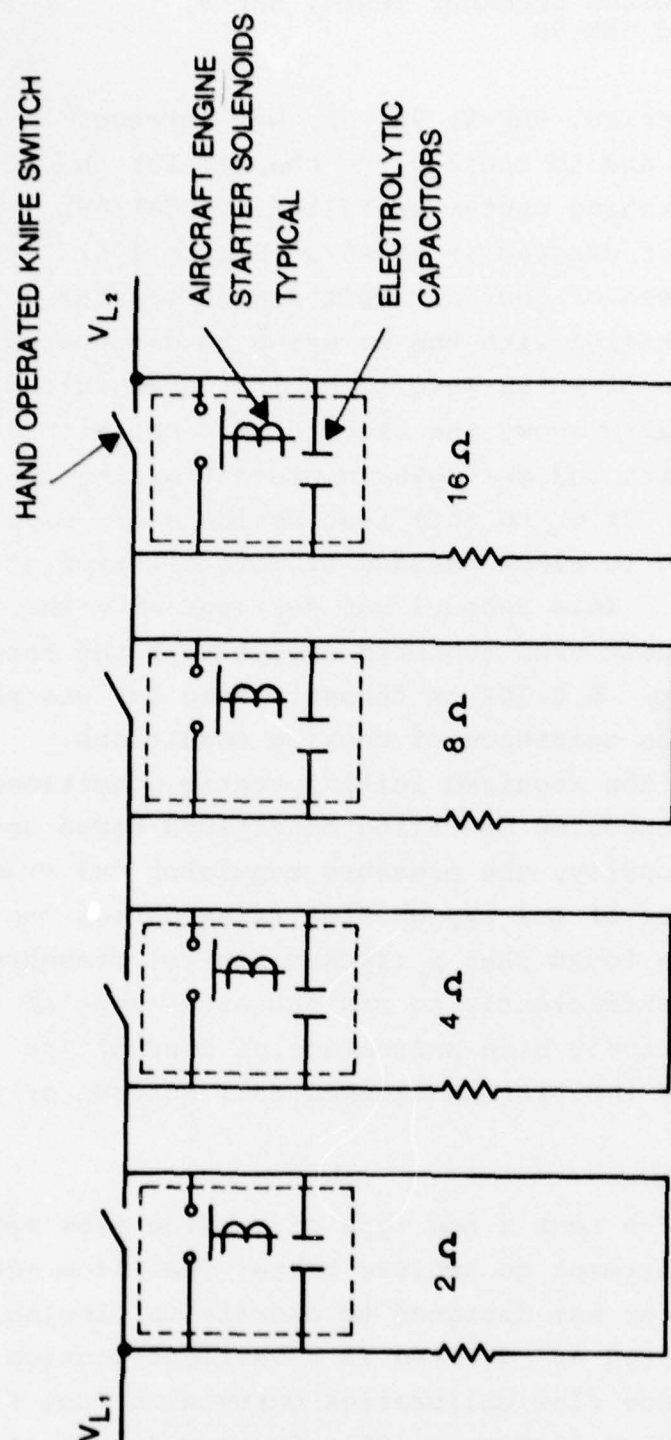


Figure 106. KIVA - I MHD Generator Load Resistance Schematic -
Early Load Switching Systems Shown Within Dashed Line

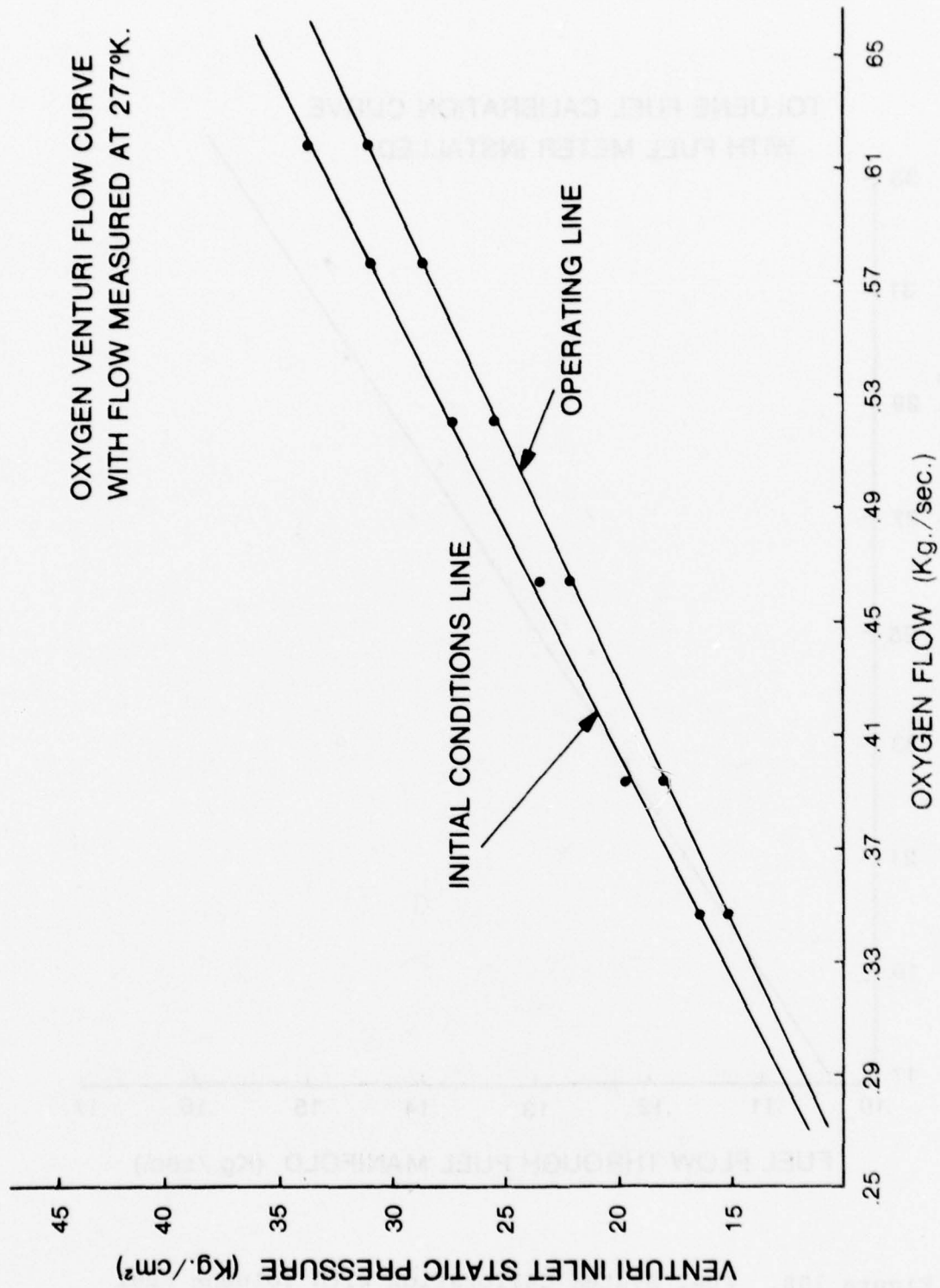


Figure 107. Oxygen Venturi Flow Curve for 0.926cm Throat Venturi

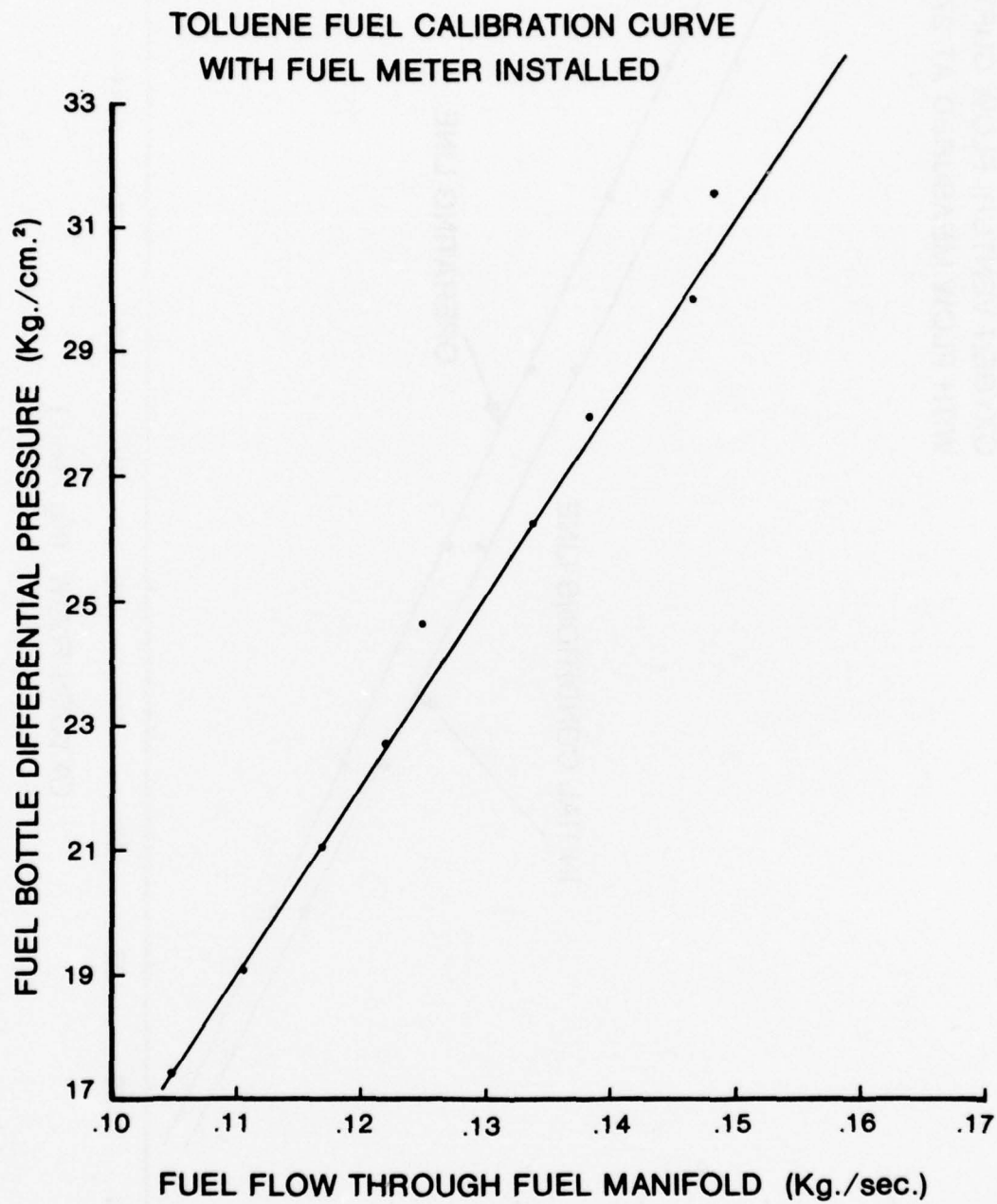


Figure 108. Fuel System Calibration with Toluene Fuel

Test run HEF-9 was scheduled to last 20 sec. Cs_2CO_3 was programmed to run for 15 sec at a 29.4 gm/sec flow rate. The magnet was to operate at 725A developing 2.3 Tesla at the field peak. Load resistances of 6Ω , 8Ω , 10Ω , and 12Ω were to be interchanged at intervals of 3 sec. The propellant flow was scheduled to be 0.6 kg/sec of toluene and oxygen; O/F was to be varied from 3.2 to 3.0. In Figure 109 we see that the combustor operated in a normal manner. The ignition peak combustor pressure was 11.25 kg/cm^2 . No data was obtained on the combustor coolant discharge thermocouple. During the test little power generation was observed and at the end of the test both data and seed remaining in the hopper verified that the seed drive motor had not operated. It was assumed that the seed motor switch had not been turned on and HEF-9A was immediately run as an exact duplicate of HEF-9. The results of this test were exactly the same as previously obtained. Figure 110 shows the results of the combustor operation. As may be seen, the data is nearly an exact duplicate except for the absence of start-up electrical noise. Again, no power was generated. Residual seed and data indicated that the seeder feed motor once again had failed to operate. Extensive investigation revealed that the seeder control program card had a bad contact which was repaired. Numerous manual tests proved the system to be operational once again and test HEF-9B was scheduled.

Test HEF-9B was set up to duplicate conditions in the previous tests. Figure 111 shows the combustor operating parameters with the normal ignition peak. Pressure during this test decayed from the peak to 8.72 kg/cm^2 . As O/F was varied, indicated by the varying venturi throat pressure, the combustion pressure decreased to 8.44 kg/cm^2 and then increased to 8.79 kg/cm^2 at shutdown. During start-up the load switches were set to 6Ω . The load was switched to 8Ω as ignition took place. When seed started, the load was at a 10Ω value and a peak voltage of 1410 volts was recorded, which corresponds to a

HEF-9

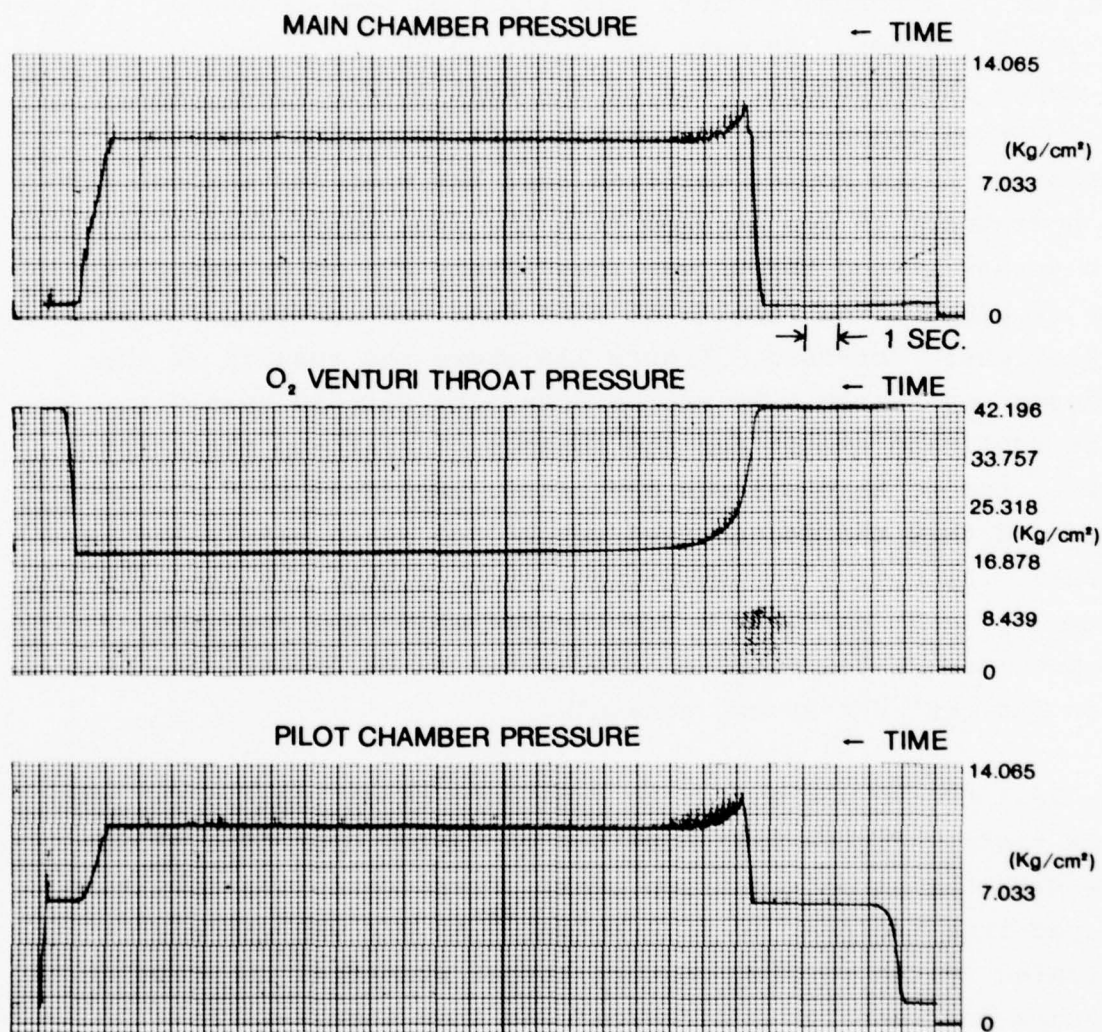


Figure 109. Power Test Run HEF-9 Combustion Parameters, Fuel - Straight Toluene, Variable Load Resistance, Seeder Failed

HEF-9A

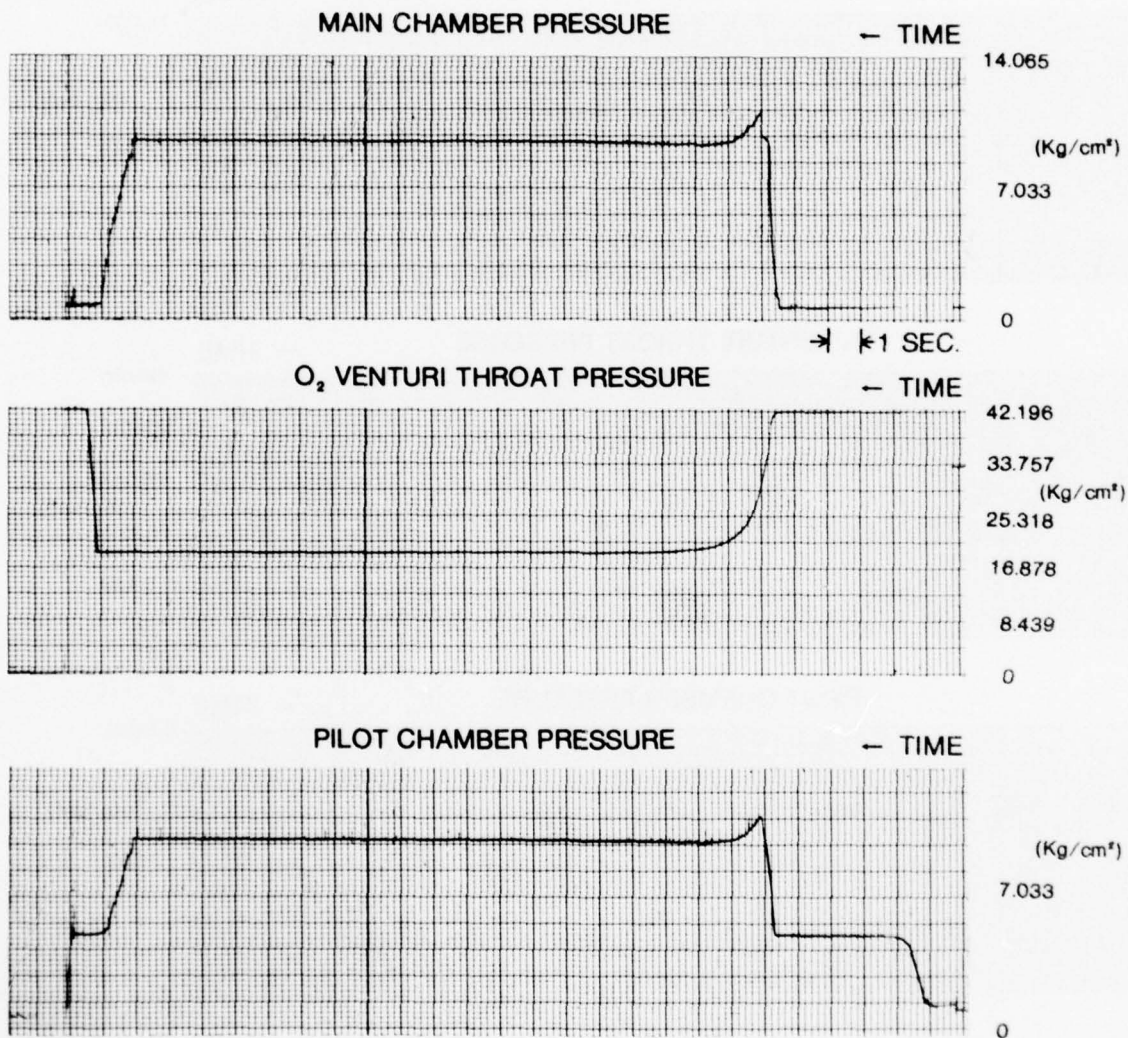


Figure 110. Power Test Run HEF-9A Combustion Parameters, Fuel - Straight Toluene, Load Resistance Variable, Seeder Failed

HEF-9B

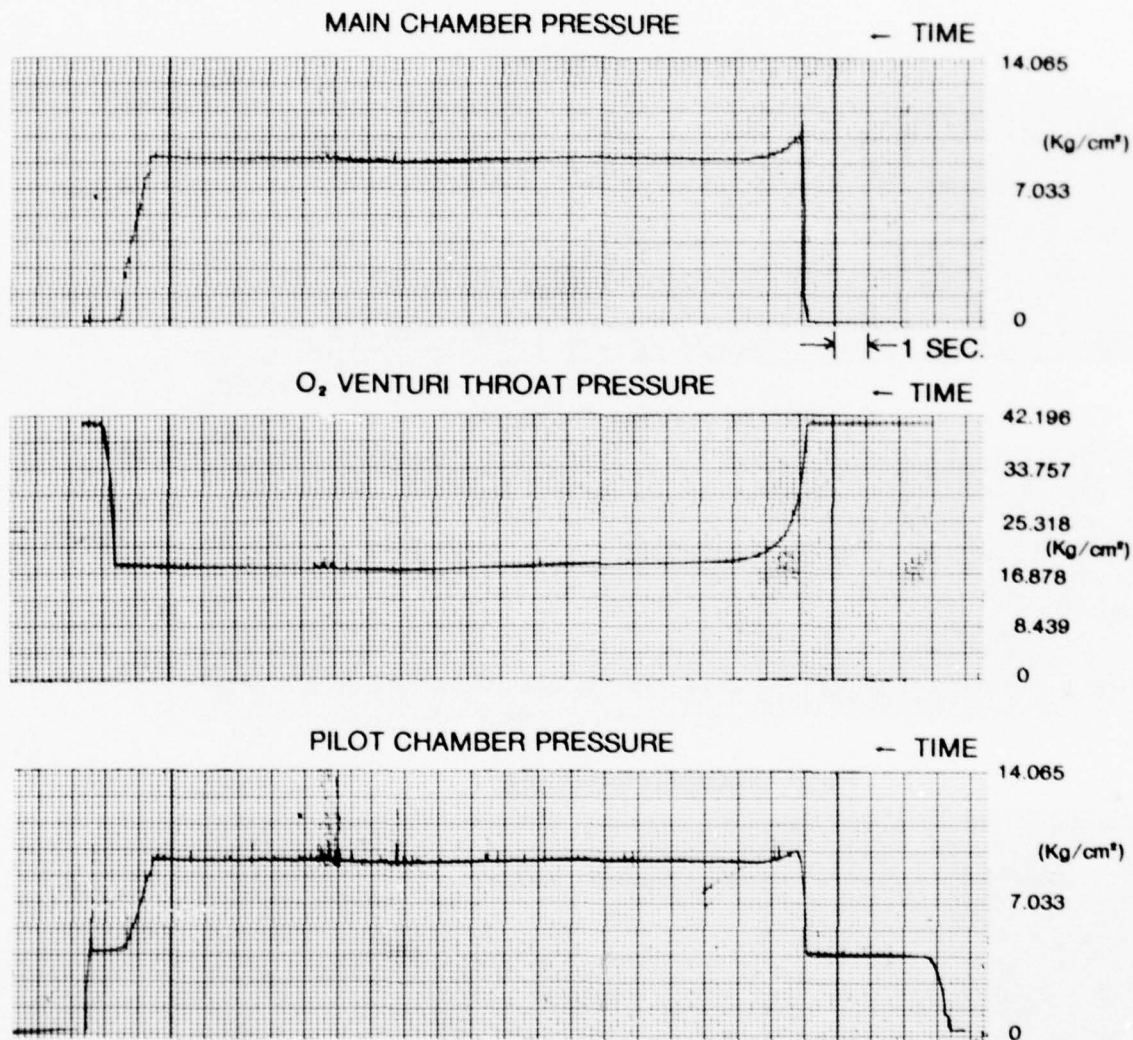


Figure 111. Power Test Run HEF-9B Combustion Parameters, Fuel - Straight Toluene, Load Resistance Variable, Load Shorted

calculated power of 198.8 kw. As the load was switched to 12 Ω (reference Figure 106), it is necessary to close the 2.0 Ω switch and open the 4 Ω switch. At this point, the first failure occurred with explosive destruction of the 4 Ω load capacitor and fusing of the solenoid. The other solenoids were subsequently burned and other capacitors were burned as the switching sequence progressed. As a result, only one power point was obtained and it was decided that future load switching would include only one resistance change consisting of shorting one resistor rather than trying to open any switches while current is flowing. During the time period that the 10 Ω load was in place, fuel flow was calculated to be 0.142 kg/sec with an oxidizer flow of 0.464 kg/sec resulting in a calculated total propellant flow of 0.606 kg/sec and an O/F ratio of 3.27. The seed flow rate was nominally 29.4 gm/sec for a 3.7% Cs seed rate. The O/F was 0.07 or 2% higher than the planned starting point. The average power generated during this point was 184.3 kw. Based on the average power the result was .31 M J/kg.

E. Toluene Emulsion Power Tests With
Load Switching, HEF-10 and HEF-10A

The next test series was planned to determine the relative power production capability of emulsified toluene using the Petrolite emulsifier. A variable O/F and two resistance load switching was also planned. The test conditions for the runs were to be a 0.6 kg/sec propellant flow using oxygen and 96% toluene emulsion. The planned O/F was to be nominally 3.04 starting at 3.10 and decreasing to 2.90. The seed feeder was programmed to deliver 29.4 gm/sec of Cs_2CO_3 for 6 sec during the 10 sec runs and the magnet was set to produce a maximum field intensity of 2.3 tesla.

The toluene emulsion was mixed using 1% LMF 4229 emulsifier, 3% H₂O, and 96% toluene. The mixing procedure was as previously described. Figure 112 shows the fuel flow calibration curve.

The first test, HEF-10, was run with a fixed O/F ratio and a fixed 10Ω load to simplify test procedures. Data was taken on all systems, including the high speed data recording system, but the high speed system which must be programmed for a fixed run time started 10 sec early. This is assumed to be caused by an electrical transient generated during the start-up preliminary sequencing. It was found subsequently that, while a technician was checking out the 110V electrical operation of an otherwise disconnected work bench mounted relay, with each operation of the relay the computer's A-D converter was stepped through its recording channels one at a time. As a result of the early recording start only 1 to 2 sec of start transient power generation was recorded. The fact that this was a computer problem is verified by the normal start of low speed data. Note that the oscilloscope trace, Figure 113, is manually triggered at the start of low speed data recording. In Figure 113 is shown the oscilloscope trace of differential load voltage ($V_{L_2} - V_{L_1}$). The peak voltage observed on the oscilloscope appears to be 1600 volts although the peak voltage recorded on low speed data was 1392V. The average from the oscilloscope appears to be 1400V. Based on this, the peak power generated was approximately 256 kw, and the average power was 196 kw. Observing the load voltage a gradual increase to a maximum at the midpoint of the test and then a slow decrease is apparent. During the test no intentional control changes were made and both O/F and \dot{M} remained relatively constant. Based on the average power developed, the specific power developed was .323 MJ/kg at an average O/F of 3.17 and propellant flow of 0.603 kg/sec. The main combustion chamber pressure in Figure 114 shows the typical ignition peak of 10.27 kg/cm² and quickly dropping off to 8.72 kg/cm². The

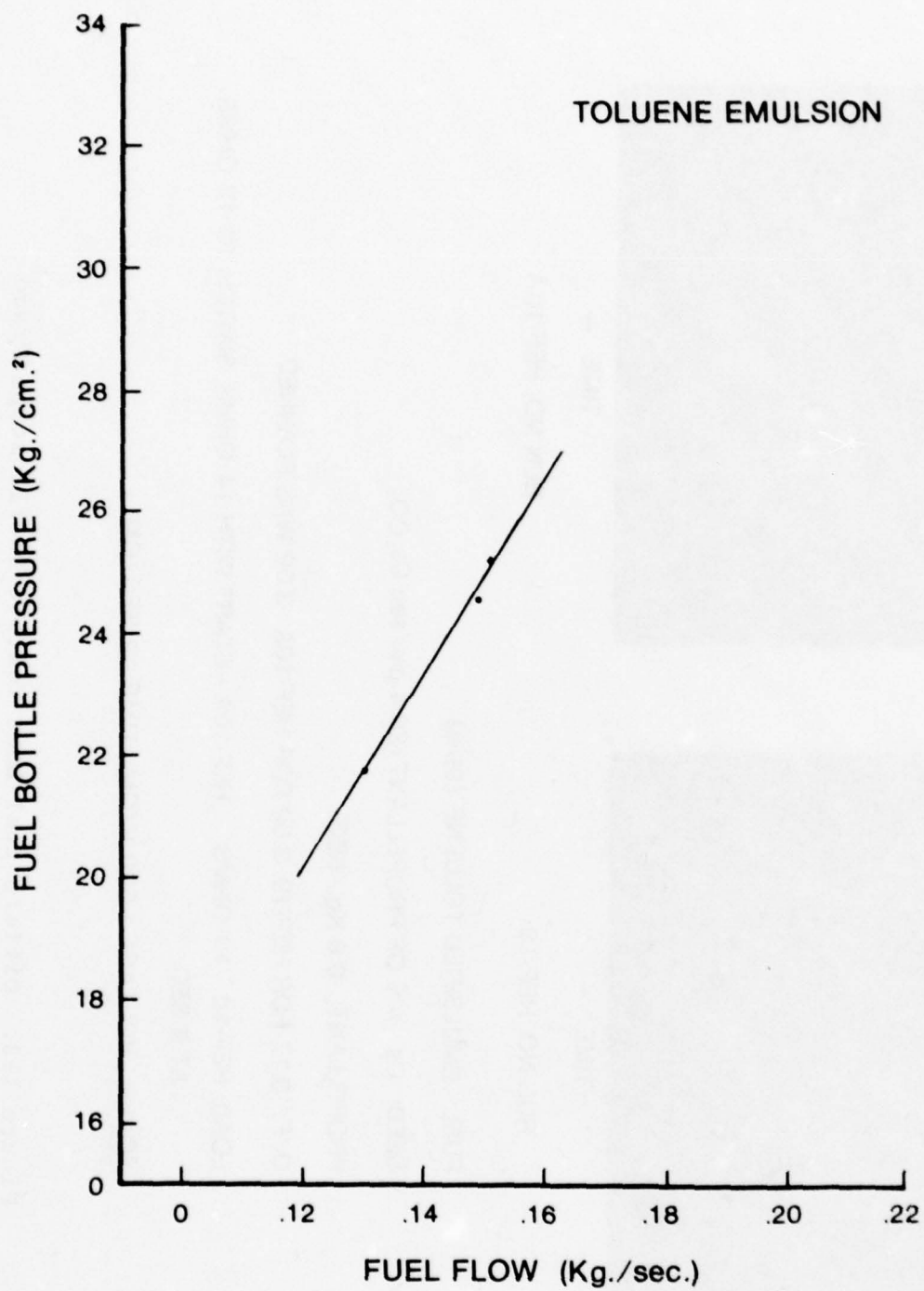
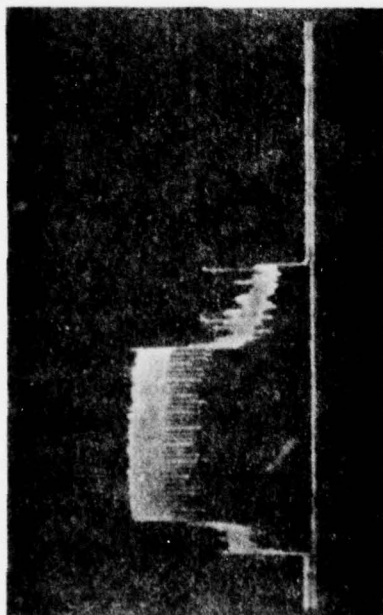
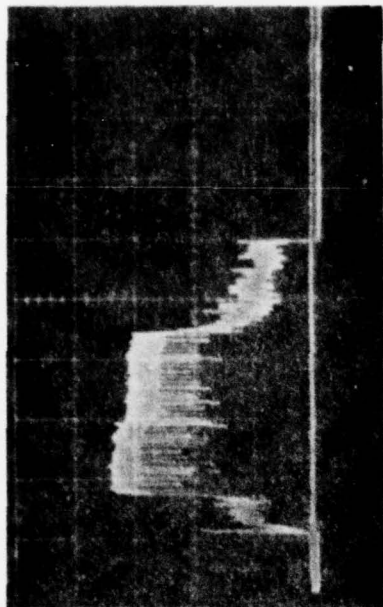


Figure 112. Toluene Emulsion Fuel Calibration



TIME →

RUN NO. HEF-10



TIME →

RUN NO. HEF-10A

FUEL: EMULSIFIED TOLUENE (96%)

SEED: Cs - 4% OF PROPELLANT (29.4 gm/sec Cs_2CO_3)

PROPELLANT: 0.6 Kg./SEC.

O/F: 3.17 FOR HEF-10, 3.09 FOR HEF-10A 3.02 WAS PLANNED.

LOAD: HEF-10 - 10 OHMS HEF-10A - START WITH 14 OHMS, SWITCH TO 12 OHMS
AT 6 SEC.

SCALE: VOLTAGE - 500 V/CM., TIME - 2 SEC/CM.

Figure 113. Differential Load Voltage Oscilloscope Trace

HEF-10

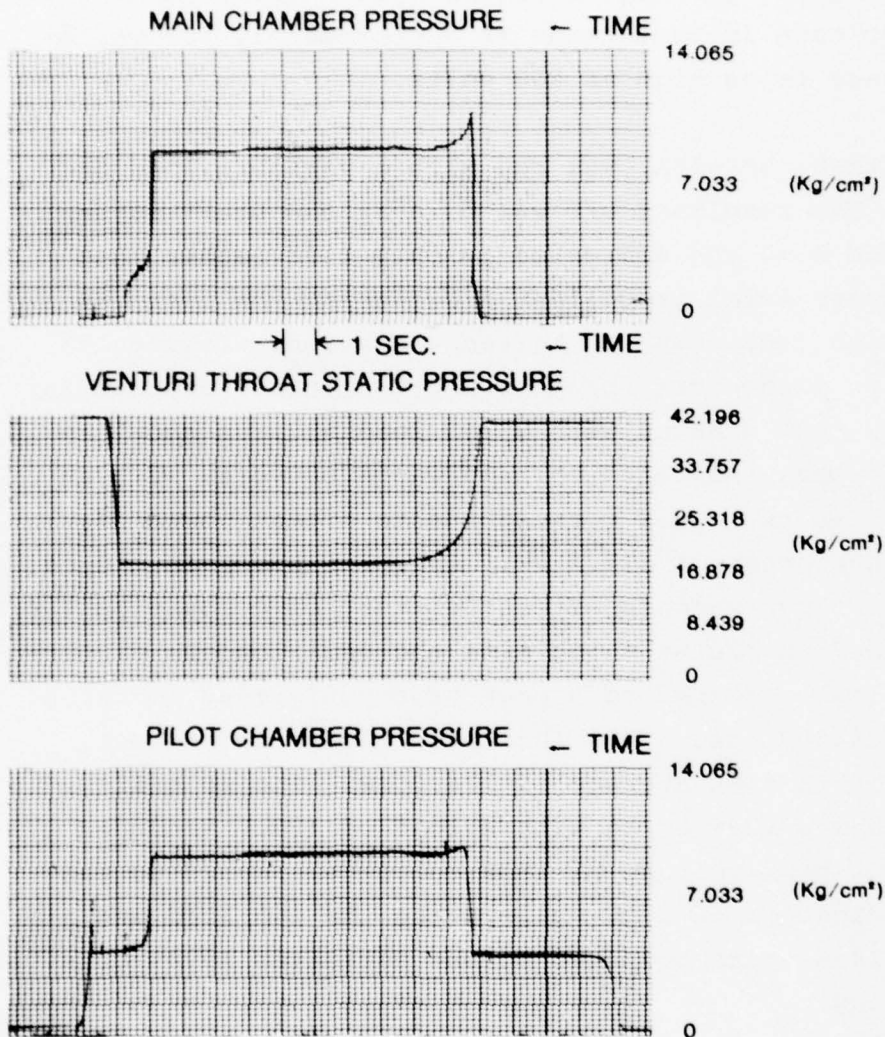


Figure 114. Power Test Run HEF-10 Combustion Parameters, Fuel - Emulsified Toluene, Load Resistance 10Ω

combustion pressure trace then indicates a slight increase in pressure of 0.14 kg/cm^2 with a gradual decrease back to the initial value at the point where seeding was stopped.

In Figure 113 note the noise level which is typical of all power tests using the granulated Cs_2CO_3 seed. The peak-to-peak noise signal voltage in most cases is approximately 500 volts and in some cases is as high as 850 volts.

The next test, HEF-10A, was run with a variable load and variable O/F. The resultant O/F was 3.14 at the start rather than the planned 3.10 and decreased to only 3.05 rather than 2.90. The average total propellant flow during the test was 0.608 kg/sec with less than $.01 \text{ kg/sec}$ variation. Figure 115 shows combustion parameters for test HEF-10A to be very similar to HEF-10. The test started with a 14Ω load and, as shown in Figure 113, the peak indicated voltage was 1700 volts with an average of 1575 volts. This corresponds to a peak power of 206.4 kw and an average of 177.2 kw. Specific power developed was $.291 \text{ MJ/kg}$. Four seconds after the start of combustion the load was switched to 12Ω at which time the oscilloscope differential load voltage dropped to a peak of roughly 1590 volts and an average of 1445 volts. This indicates a calculated peak power of 210.7 kw and an average of 174.0 kw. The specific power developed was $.286 \text{ MJ/kg}$ with a load of 12Ω . Recorded data indicated a peak voltage of 1638 volts as opposed to the oscilloscope indication of 1700 while using the 14Ω load and a peak recorded 1496 volts compared to the estimated 1590 volts with the 12Ω load.

Test HEF-10B was run in a similar manner to HEF-10A except that midway through the test the load was switched from 10Ω to 8Ω . A minor problem occurred during this test as seen in Figure 116. The combustion chamber was either initiated early or the data systems were late in starting. As a result, the

HEF-10A

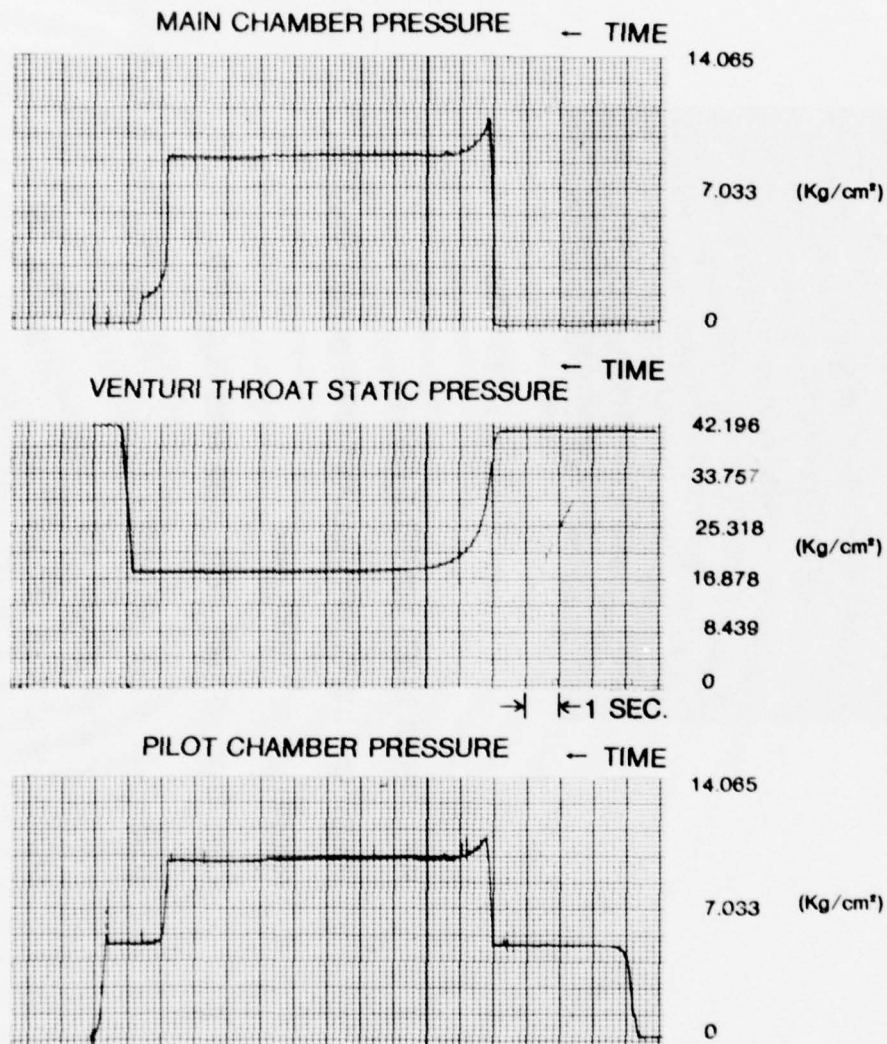
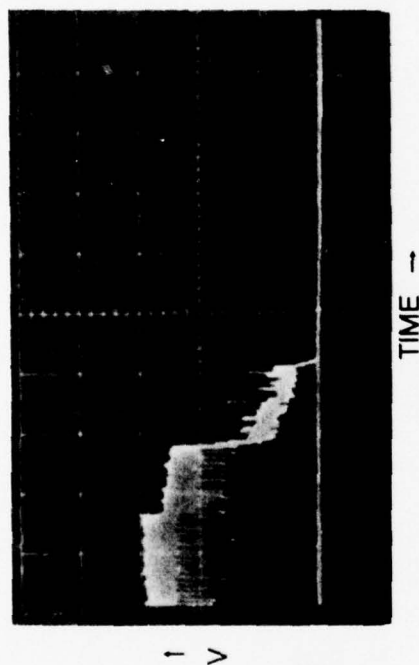


Figure 115. Power Test Run HEF-10F Combustion Parameters, Fuel - Emulsified Toluene, Load Resistance Variable 14Ω to 12Ω



TIME →

RUN NO. HEF-10B

FUEL: EMULSIFIED TOLUENE (96%)

SEED: Cs - 4% OF PROPELLANT (29.4 gm/sec Cs_2CO_3)

PROPELLANT: 0.6 Kg./sec.

O/F: 3.09 FOR HEF-10B; 3.02 WAS PLANNED.

LOAD: HEF-10B START WITH 10 OHMS, SWITCH TO 8 OHMS AT 3 SEC.
(EARLY IGN. AT - 2. SEC.)

SCALE: VOLTAGE - 500 V/CM., TIME 2 SEC/CM.

Figure 116. Differential Load Voltage Oscilloscope Trace

oscilloscope did not record the start of combustion although the majority of the power data was recorded. Combustion started with a mass flow of 0.612 kg/sec and O/F of 3.11 the mass flow dropped to .611 kg/sec as the O/F dropped to 3.09, an insignificant change. Maximum indicated differential load voltage with the 10 Ω load was 1500 volts resulting in a peak power of 225 kw and an average voltage of 1350 volts for an average power of 182.3 kw. The specific power produced was .298 MJ/kg with the 10 Ω load. The load was switched to 8 Ω with slightly more than 2 seconds of powered time remaining. During this time the peak indicated voltage was 1325 volts for a peak power of 219.5 kw. The average differential load voltage, as seen in Figure 116 was 1150 volts for an average power of 165.3 kw. The specific power produced was .271 MJ/kg with the 8 Ω load.

In Figures 114, 115, and 117 we can see for the first time an actual pressure change with the start of power production (seed initiation) and the end of power generation (seed off). All three tests, HEF-10, 10A, 10B, have quite similar combustor pressure traces. The minimal O/F ratio change is evident observing the venturi throat pressure which changes insignificantly during the runs after reaching steady state conditions. Figure 118 indicates the generator load line for the HEF-10 fuel test series. No difference in power produced by the toluene emulsion can be observed when comparing to the neat toluene tests.

F. Emulsified Toluene/CsNO₃ Seed
Power Tests, HEF-11, HEF-11A,
HEF-11B and HEF-11C

The next test series involved combustion of emulsified toluene and CsNO₃. The CsNO₃ was purchased in crystalline form with random size distribution. The CsNO₃ was milled in a roller ball mill. The mill jug was one-half filled with dense Al₂O₃ milling rollers 1.9 cm dia and 1.9 cm long. The space

HEF-10B

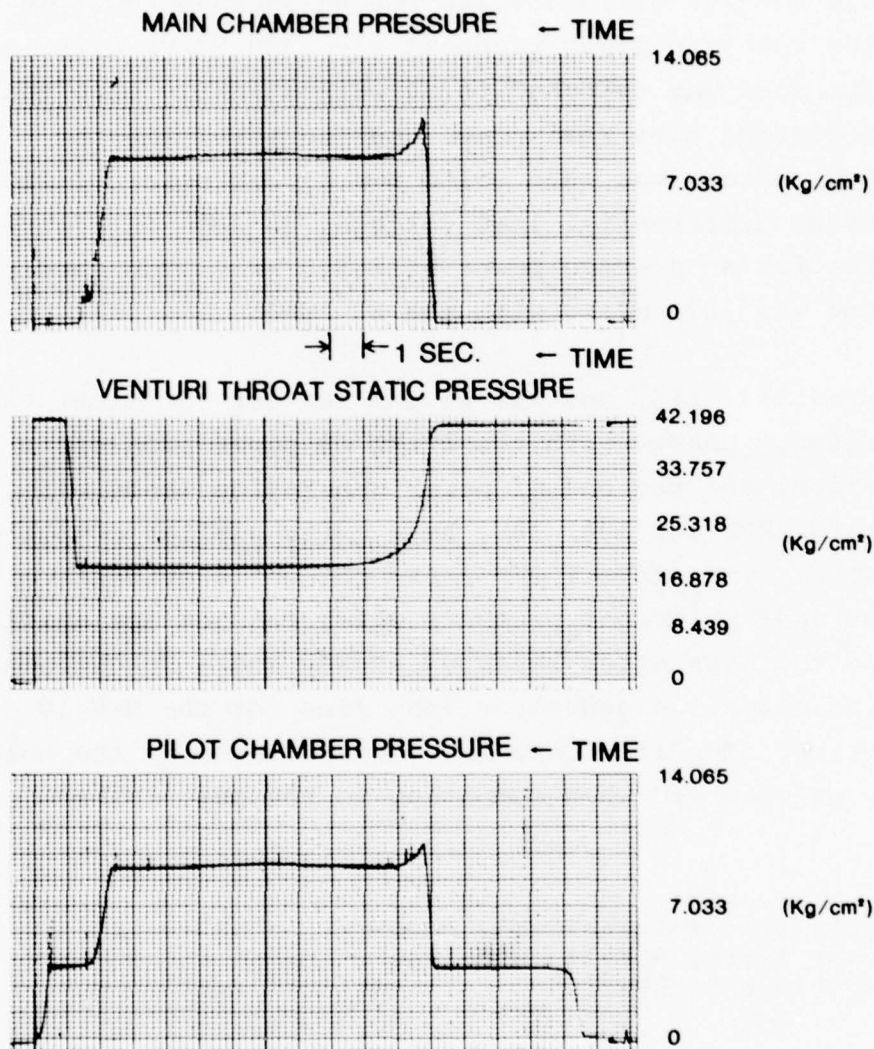


Figure 117. Power Test Run HEF-10B Combustion Parameters, Fuel - Emulsified Toluene, Load Resistance Variable 10Ω to 8Ω

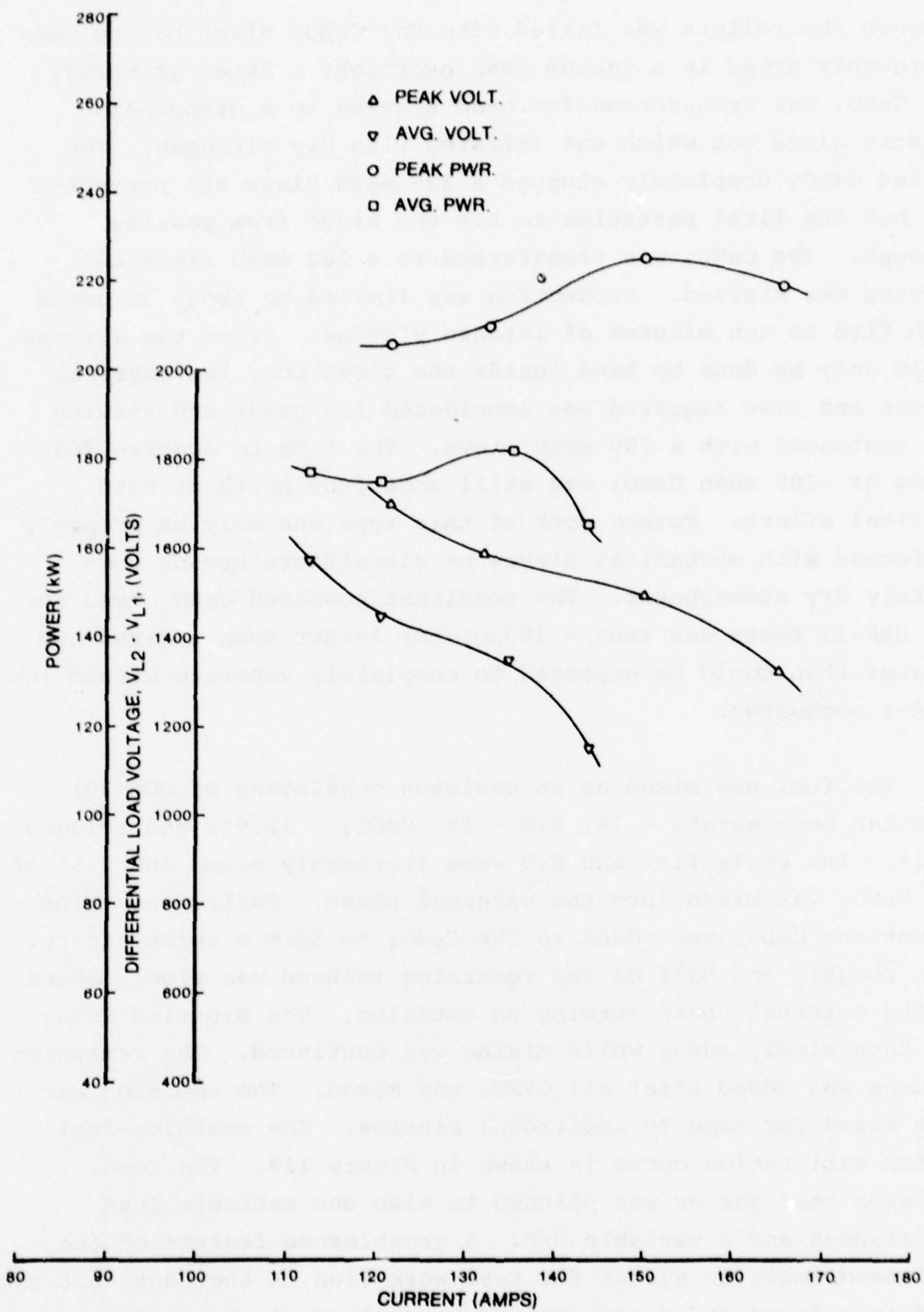


Figure 118. Test Series HEF-10 Load Line

between the rollers was filled with the CsNO_3 after having been thoroughly dried in a vacuum oven overnight. After grinding, the CsNO_3 was transferred for hand sieving to a disposable plastic glove box which was inflated with dry nitrogen. The milled CsNO_3 completely clogged a 325 mesh sieve and prevented all but the first particles to hit the sieve from passing through. The CsNO_3 was transferred to a 200 mesh sieve and sieving was started. Production was limited to about 30 grams each five to ten minutes of intense sieving. Since the sieving could only be done by hand inside the glove box, the physical effort and time required was considered too great and sieving was continued with a 100 mesh sieve. The time to acquire 1650 grams of -100 mesh CsNO_3 was still some four hours of hard physical effort. Future work of this type can only be properly performed with mechanical sieves or classifiers having completely dry atmospheres. The resultant powdered CsNO_3 used for the HEF-11 tests was thus - 150 μm , far larger than desired and greater than could be expected to completely vaporize within the KIVA-I combustor.

The fuel was mixed as an emulsion consisting of POE(20) sorbitan monolaurate - 1%, H_2O - 2%, CsNO_3 - 12.9%, and toluene - 84.1%. The emulsifier and H_2O were thoroughly mixed and 0.5% of the CsNO_3 was mixed into the external phase. Sufficient toluene to wet the CsNO_3 was added to the CsNO_3 to form a thick slurry. Then roughly one-half of the remaining toluene was slowly added to the external phase forming an emulsion. The slurried CsNO_3 was then slowly added while mixing was continued. The remaining toluene was added after all CsNO_3 was mixed. The emulsion was then mixed for some 10 additional minutes. The emulsion-fuel system calibration curve is shown in Figure 119. The seed emulsion test series was planned to also use variable load resistances and a variable O/F. A troublesome feature of the fuel-seed emulsion system for test work lies in the fact that the seed is a fixed and predetermined percentage of the fuel which eliminates the possibility of varying seed rate independently

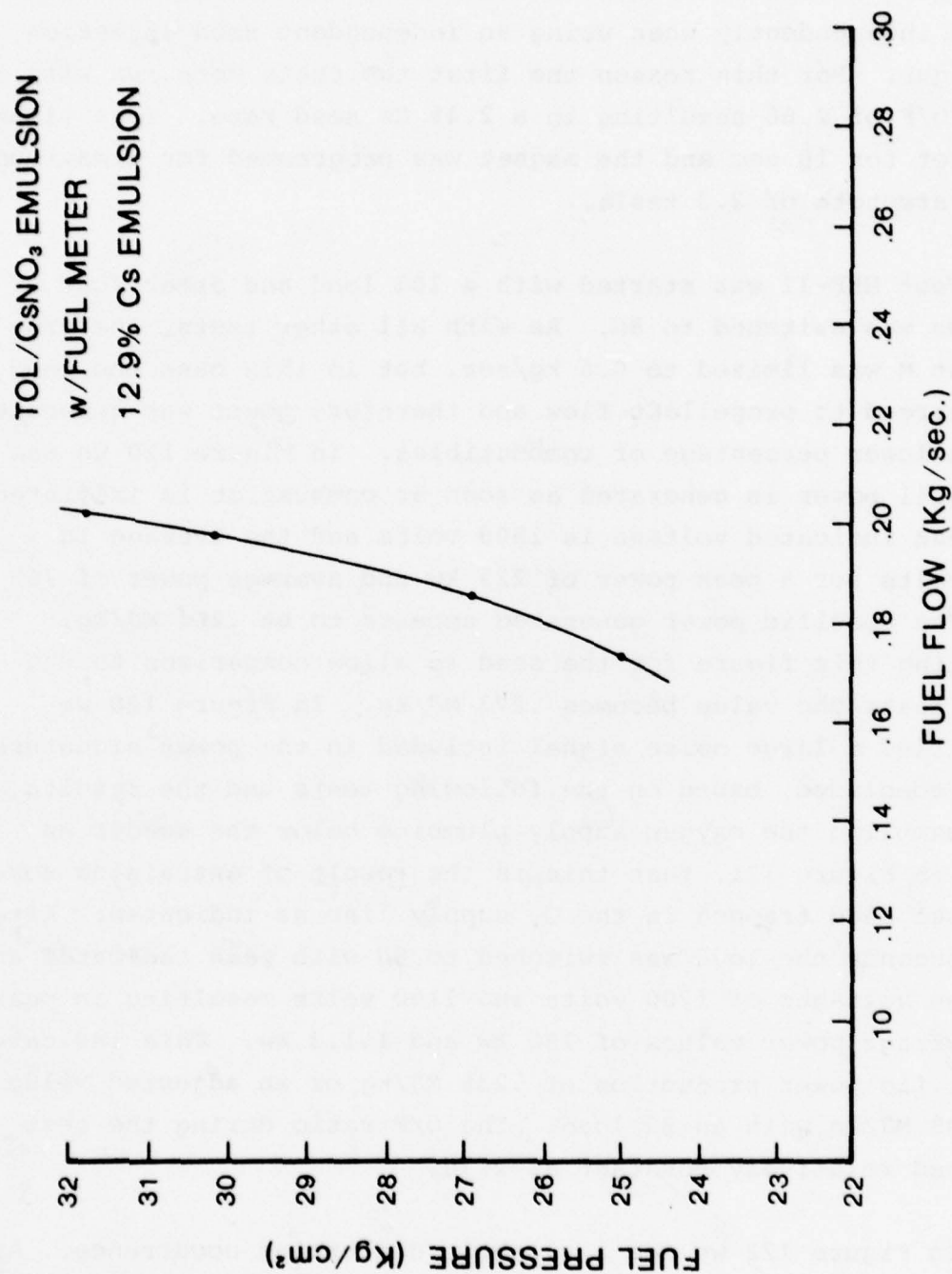
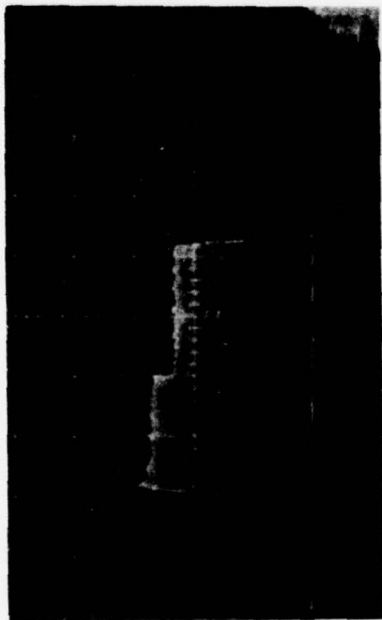


Figure 119. Fuels System Calibration Curve with Emulsified
Toluene and CsNO₃ Seed Fuel

from the O/F mixture. The seed rate changes with a varying O/F when using a fuel-seed emulsion but O/F and seed rate can be varied independently when using an independent seed injection technique. For this reason the first two tests were run with a fixed O/F of 2.66 resulting in a 2.4% Cs seed rate. Test times were set for 10 sec and the magnet was programmed for a maximum field strength of 2.3 tesla.

Test HEF-11 was started with a 10Ω load and after four seconds was switched to 8Ω . As with all other tests, the propellant \dot{M} was limited to 0.6 kg/sec, but in this case the seed was charged to propellant flow and therefore power was generated with a lower percentage of combustibles. In Figure 120 we see that full power is generated as soon as combustion is initiated. The peak indicated voltage is 1500 volts and the average is 1300 volts for a peak power of 225 kw and average power of 169 kw. The specific power generated appears to be .264 MJ/kg. Adjusting this figure for the seed to allow comparison to the other tests the value becomes .273 MJ/kg. In Figure 120 we still find a large noise signal included in the power signature. It is concluded, based on the following tests and the results of disassembling the oxygen supply plumbing below the seeder as shown in Figure 121, that this is the result of entraining some residual seed trapped in the O_2 supply line as indicated. After four seconds the load was switched to 8Ω with peak indicated and average voltages of 1200 volts and 1100 volts resulting in peak and average power values of 180 kw and 151.3 kw. This indicates a specific power production of .236 MJ/kg or an adjusted value of .245 MJ/kg with an 8Ω load. The O/F ratio during the test remained relatively constant at 2.70.

In Figure 122 we see a slightly disturbing occurrence. At test start plus 0.9 sec, where the test start is indicated by opening of the pilot flame valves, the pilot chamber pressure rises to 4.5 kg/cm^2 indicating a strong pilot flame. At start



TIME →

RUN NO. HEF-11



TIME →

RUN NO. HEF-11A

FUEL: TOLUENE/CsNO₃ EMULSION (84.1/12.9)

SEED: Cs-2.4% OF PROPELLANT (12.9% OF FUEL-CsNO₃)

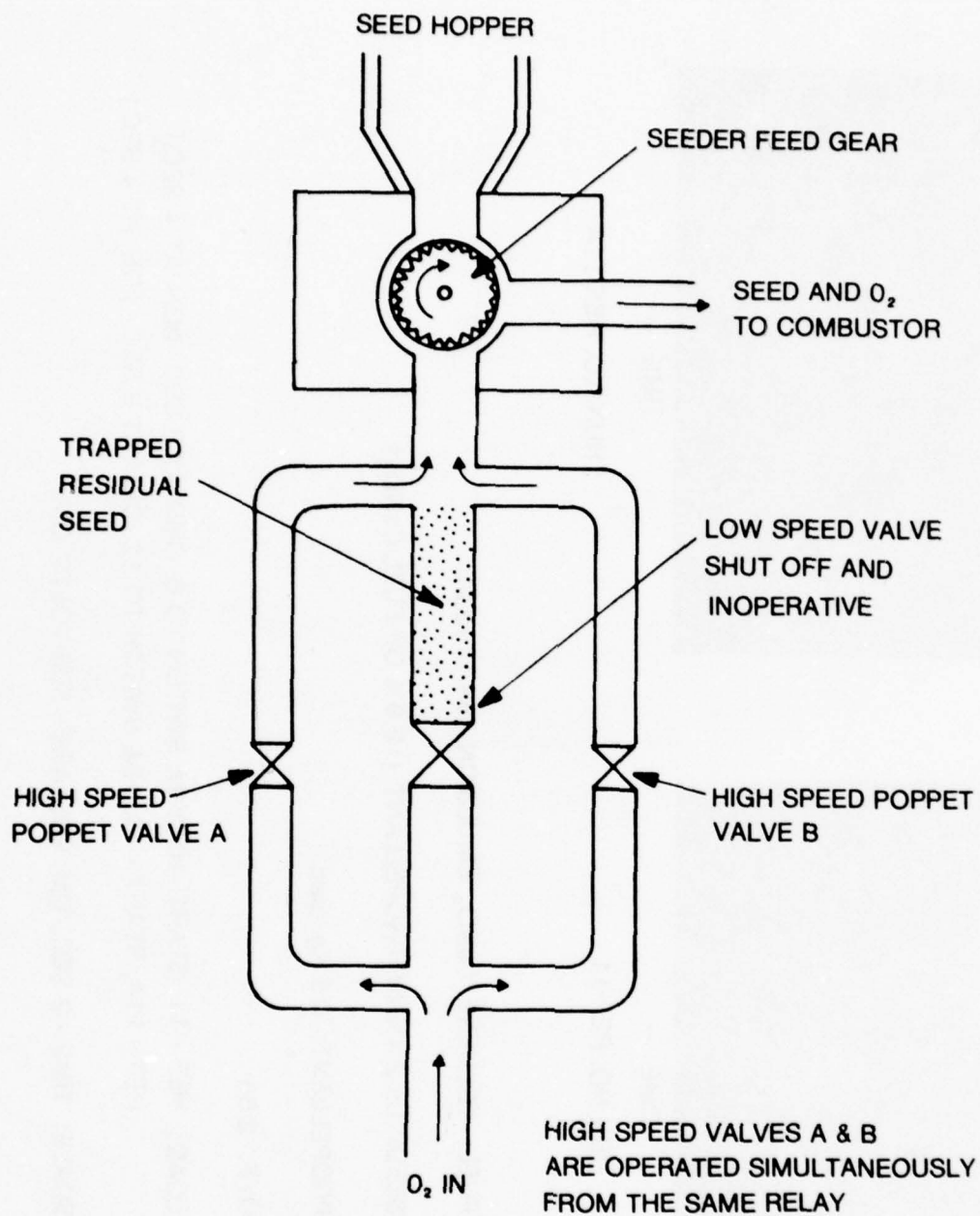
PROPELLANT: 0.6 Kg./sec.

O/F: 2.66

LOAD: HEF - 11; START - 10 OHM, SWITCH TO 8. OHM AT 8 SEC. (IGN. AT 4 SEC.)
HEF - 11A; START - 14.0HM, SWITCH TO 12. OHM AT 8 SEC. (IGN. AT 4 SEC.)

SCALE: TIME - 2 SEC./CM. VOLTAGE - 500 VOLTS/CM.

Figure 120. Differential Load Voltage Oscilloscope Trace



SEEDER FEED SCHEMATIC

Figure 121. Seeder Feed Schematic

HEF-11

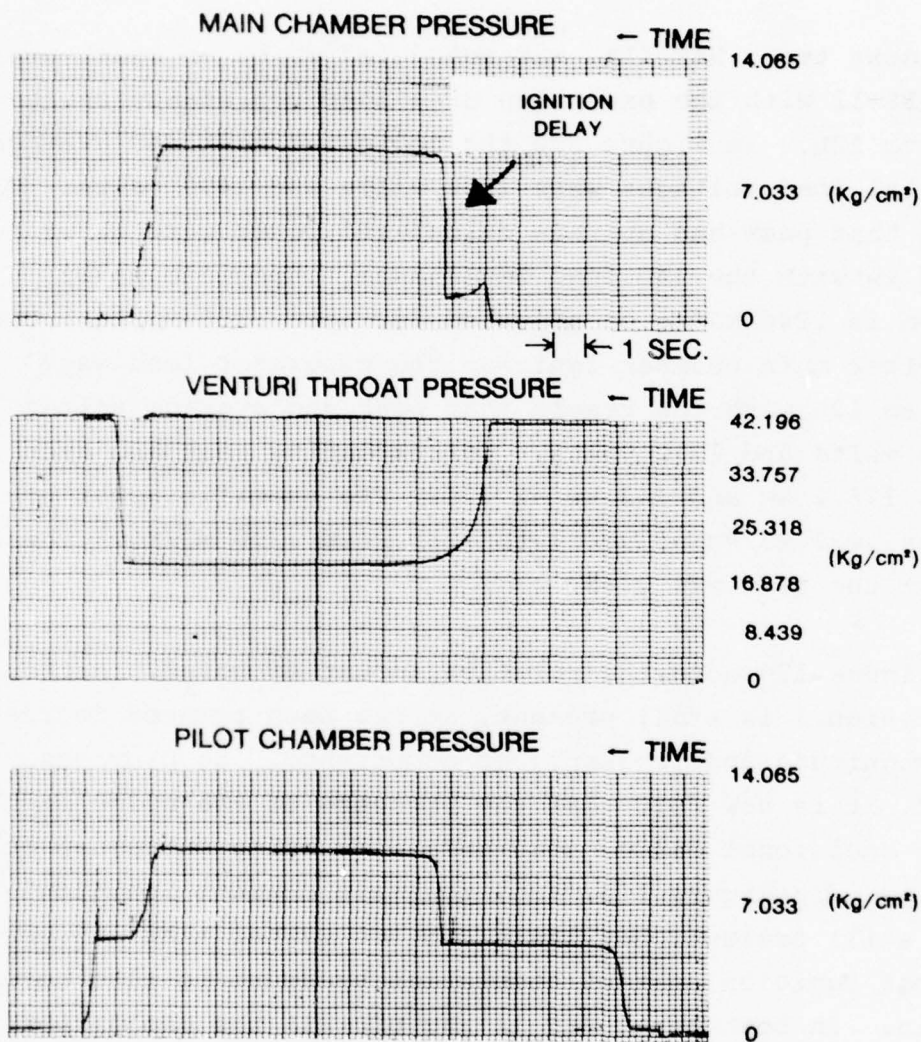


Figure 122. Power Test Run HEF-11 Combustion Parameters, Fuel - Emulsified Toluene/CsNO₃, Load Resistance Variable 10Ω to 8Ω

plus 5.3 sec the O₂ valves are seen to open, evidenced by the venturi throat pressure drop. This is normally immediately followed by main chamber ignition. Instead we find a slight increase in pressure to a peak, a pressure decay for 1.2 sec and then ignition. There appears to be a slight step in the main chamber pressure at test sequence initiation plus 11.5 sec but this follows the resistance change by one full second.

The next test, HEF-11A, was scheduled to be an exact duplicate of HEF-11 with the exception of a load resistance change from 14 Ω to 12 Ω . In Figure 120 the indicated peak and average differential load voltages were 1600 volts and 1490 volts. This indicates that peak and average calculated power were 182.9 kw and 158.6 kw with the 14 Ω load resistance. Specific power production is .246 MJ/kg or adjusted for seed .255 MJ/kg. Four seconds after main chamber ignition the generator load was switched to 12 Ω with the result that peak and average voltage were 1450 volts and 1310 volts. Corresponding peak and average power was 175.2 kw and 143 kw at 12 Ω . The specific power generated was .222 MJ/kg or corrected for seed .230 MJ/kg. The O/F throughout the test was 2.68.

In Figure 120 note the relative amount of noise. Although the noise signal is still present, it has been reduced noticeably both in magnitude and frequency of occurrence. As previously mentioned, it is now felt that the presence of the noise signal is due to occasional CS₂CO₃ seed particles being entrained in the O₂ flow. In Figure 123, too, the main chamber ignition delay is still present, but lasts 0.5 sec rather than 1.5 sec. The typical ignition peak of combustion pressure is also noted once again. In both tests HEF-11 and HEF-11A the combustion pressure is relatively stable at approximately 9.14 kg/cm.

In attempting to draw a load line we find that the data has too much scatter. A similar result occurs when the specific power is plotted vs load resistance (Figure 125). The first

HEF-11A

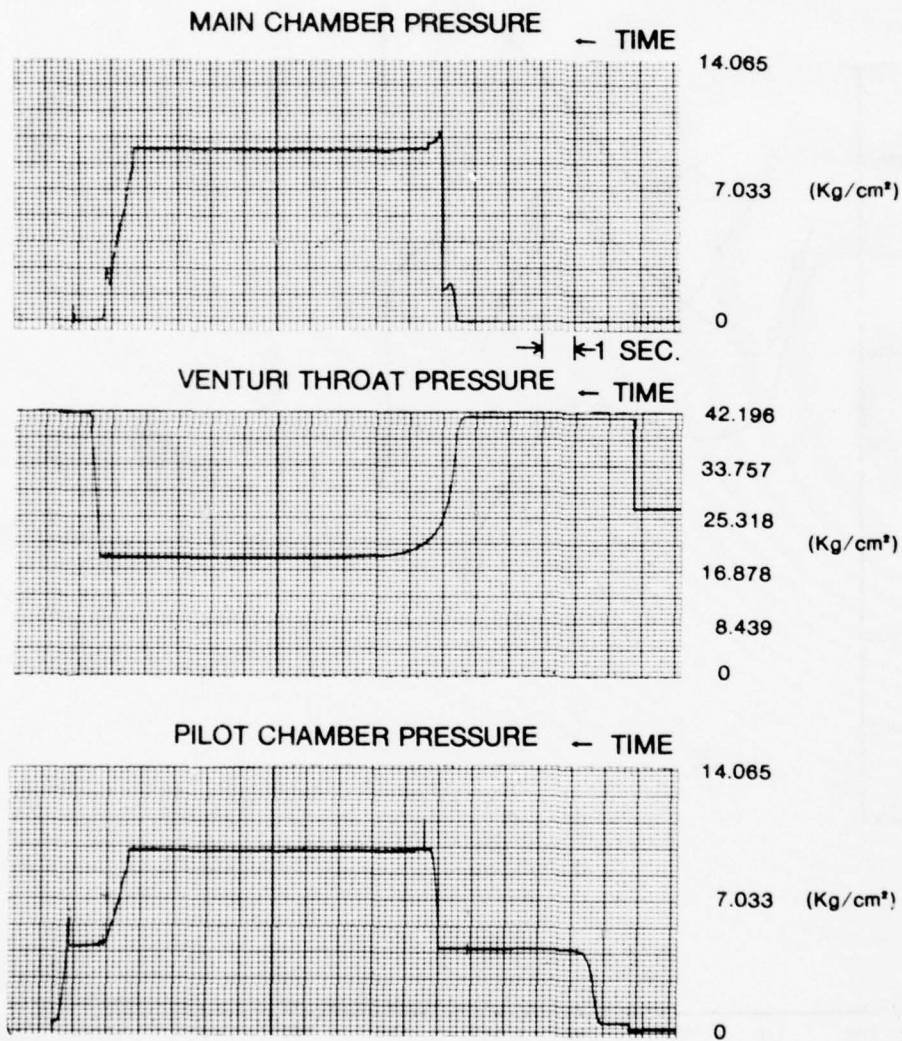


Figure 123. Power Test Run HEF-11A Combustion Parameters, Fuel - Emulsified Toluene/CsNO₃, Load Resistance Variable 14Ω to 12Ω

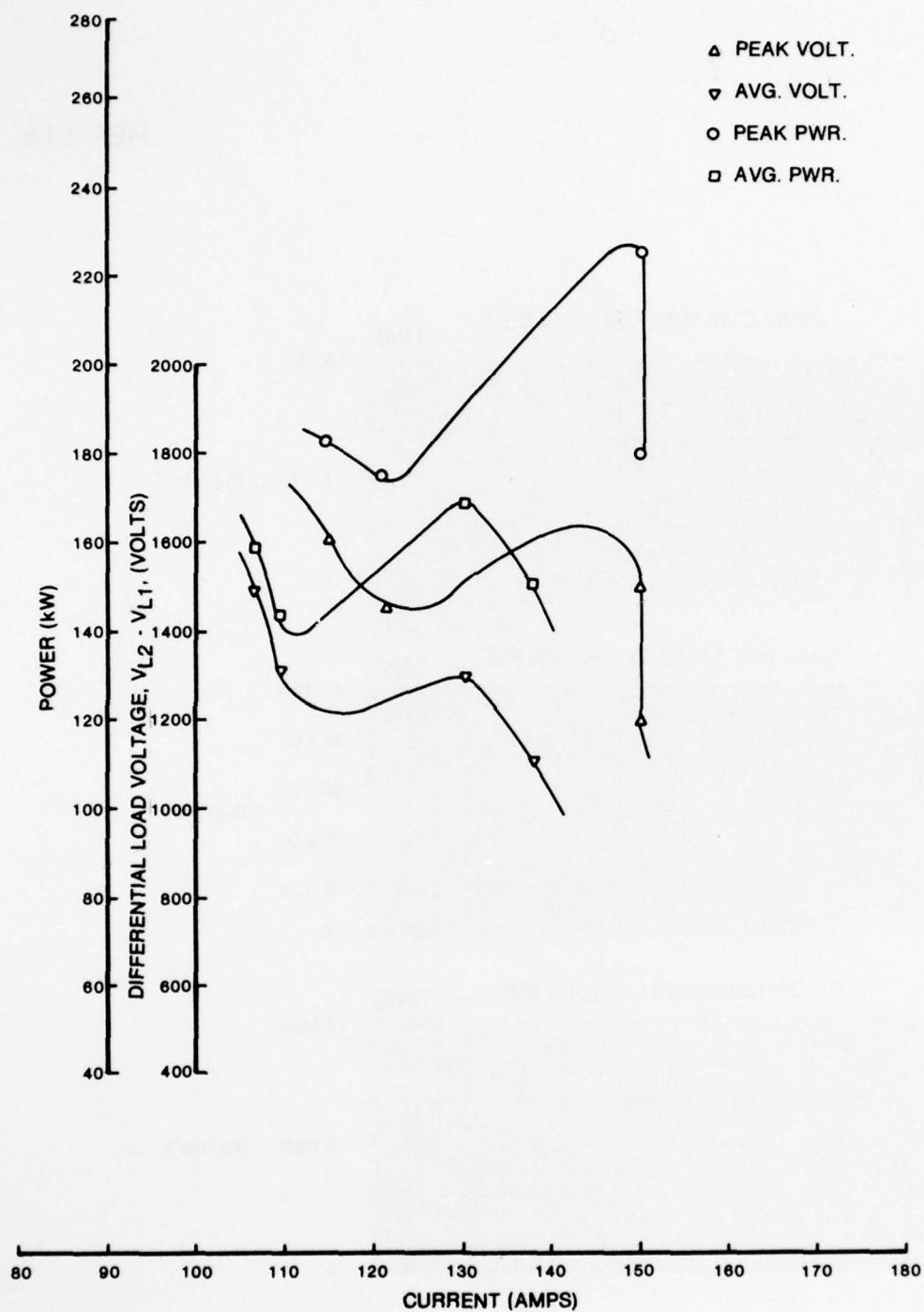


Figure 124. Test Series HEF-11, 11A Load Line

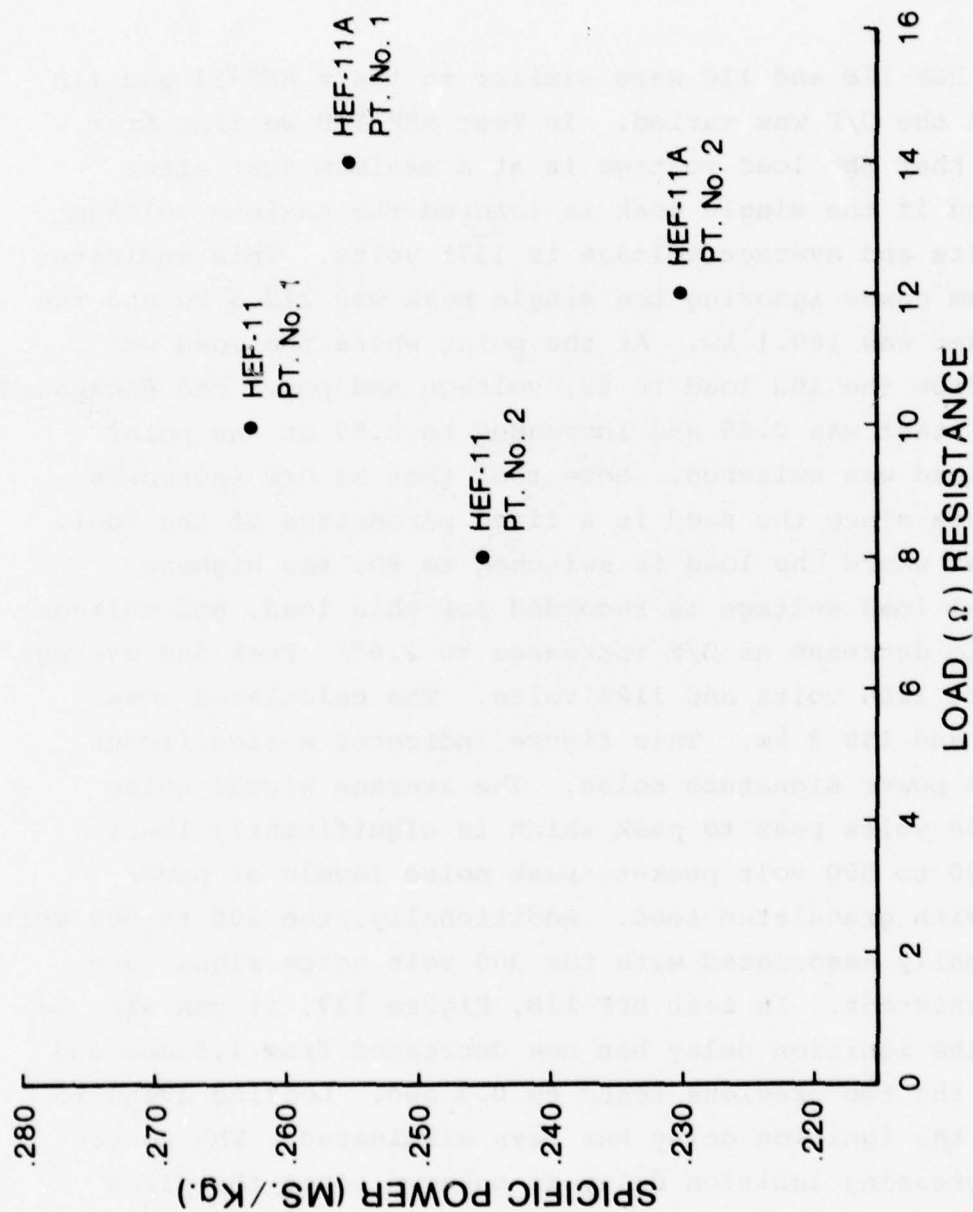
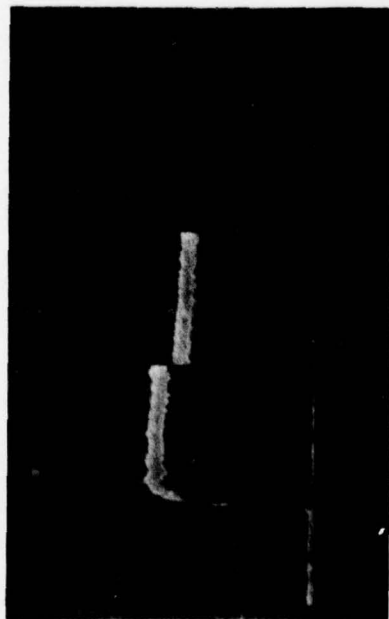


Figure 125. Test Series HEF-11, 11A Specific Power

point in each run has the highest specific power regardless of load resistance. This seems to indicate degradation in channel performance as a test progresses although channel performance degradation is not readily apparent by simply observing the power signature.

Tests HEF-11B and 11C were similar to tests HEF-11 and 11A except that the O/F was varied. In Test HEF-11B we find from Figure 126 that the load voltage is at a maximum just after ignition and if the single peak is ignored the maximum voltage is 1475 volts and average voltage is 1375 volts. This indicates that maximum power ignoring the single peak was 217.5 kw and the average power was 189.1 kw. At the point where the load was switched, from the 10 Ω load to 8 Ω , voltage and power had decreased. O/F at the start was 2.55 and increased to 2.57 at the point where the load was switched. Note too, that as O/F increases Cs% decreases since the seed is a fixed percentage of the fuel. At the point where the load is switched to 8 Ω , the highest differential load voltage is recorded for this load, and voltage continues to decrease as O/F increases to 2.67. Peak and average voltage were 1200 volts and 1125 volts. The calculated power was 180 kw and 158.2 kw. This figure indicates a significant decrease in power signature noise. The average signal noise range is 150 volts peak to peak which is significantly lower than the 300 to 500 volt peak-to-peak noise levels of power generated with granulated seed. Additionally, the 300 to 500 volt spikes normally associated with the 300 volt noise signal are nearly nonexistent. In test HEF-11B, Figure 127, it can also be seen that the ignition delay has now decreased from 1.5 sec and 0.5 sec in the two previous tests to 0.3 sec. Looking ahead to Figure 128 the ignition delay has been eliminated. The source of this decreasing ignition delay is unknown since the pilot chamber pressure indicates a strong ignition flame prior to starting oxygen and fuel flow into the main combustion chamber. Subsequent to completion of this test program, the fuel control



TIME —

RUN NO. HEF-11B



TIME —

RUN NO. HEF-11C

FUEL: TOLUENE/CsNO₃ EMULSION (84.1/12.9)

SEED: Cs - 2.5% OF PROPELLANT (12.9% OF FUEL — CsNO₃)

PROPELLANT: 0.6 Kg./sec.

O/F: VARYING FROM 2.50 TO 2.70 AT A STEADY RATE

LOAD: HEF-11B; START - 10. OHM, SWITCH TO 8. OHM AT 8.1 SEC. (IGN. AT 3.4 SEC.)

HEF - 11C; START - 14 OHM, SWITCH TO 12. OHM AT 8.4 SEC. (IGN. AT 3.2 SEC.)

SCALE: TIME - 2 SEC./CM. VOLTAGE - 500 VOLTS/CM.

Figure 126. Differential Load Voltage Oscilloscope Trace

HEF-11B

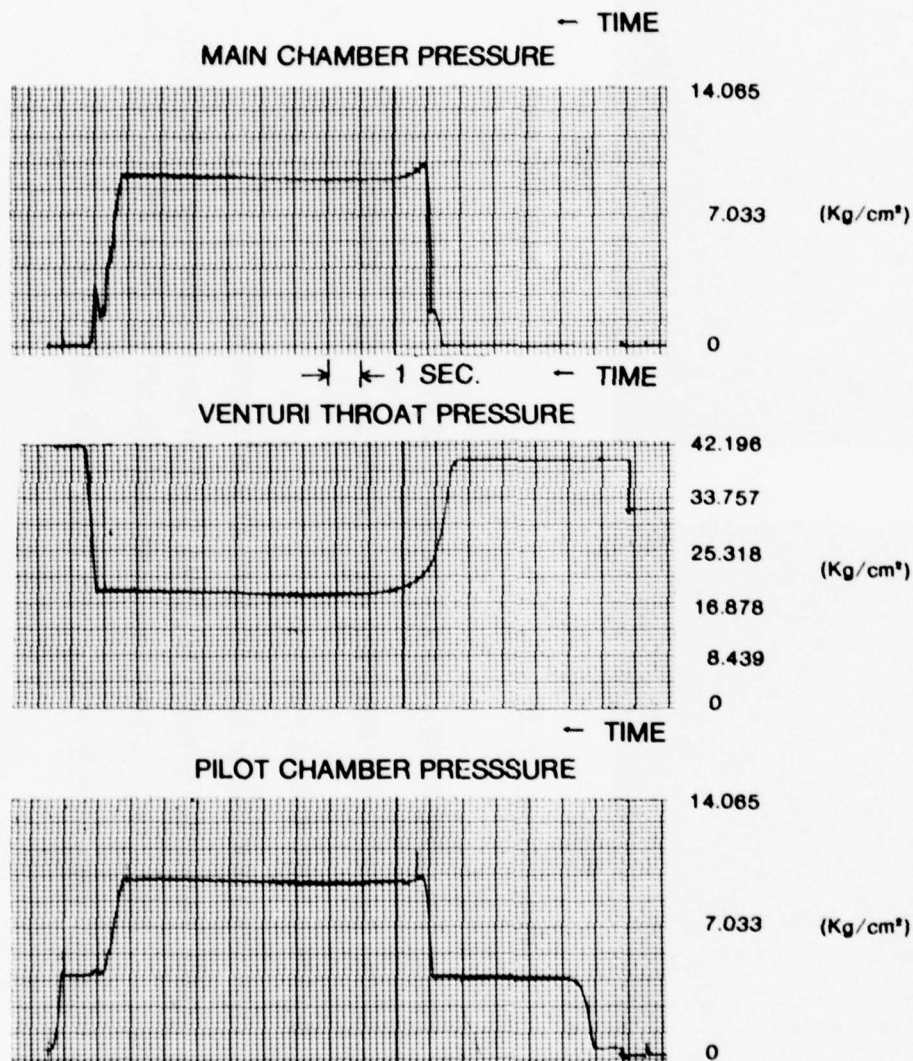


Figure 127. Power Test Run HEF-11B Combustion Parameters, Fuel - Emulsified Toluene/CsNO₃, Load Resistance Variable 10Ω to 8Ω

HEF-11C

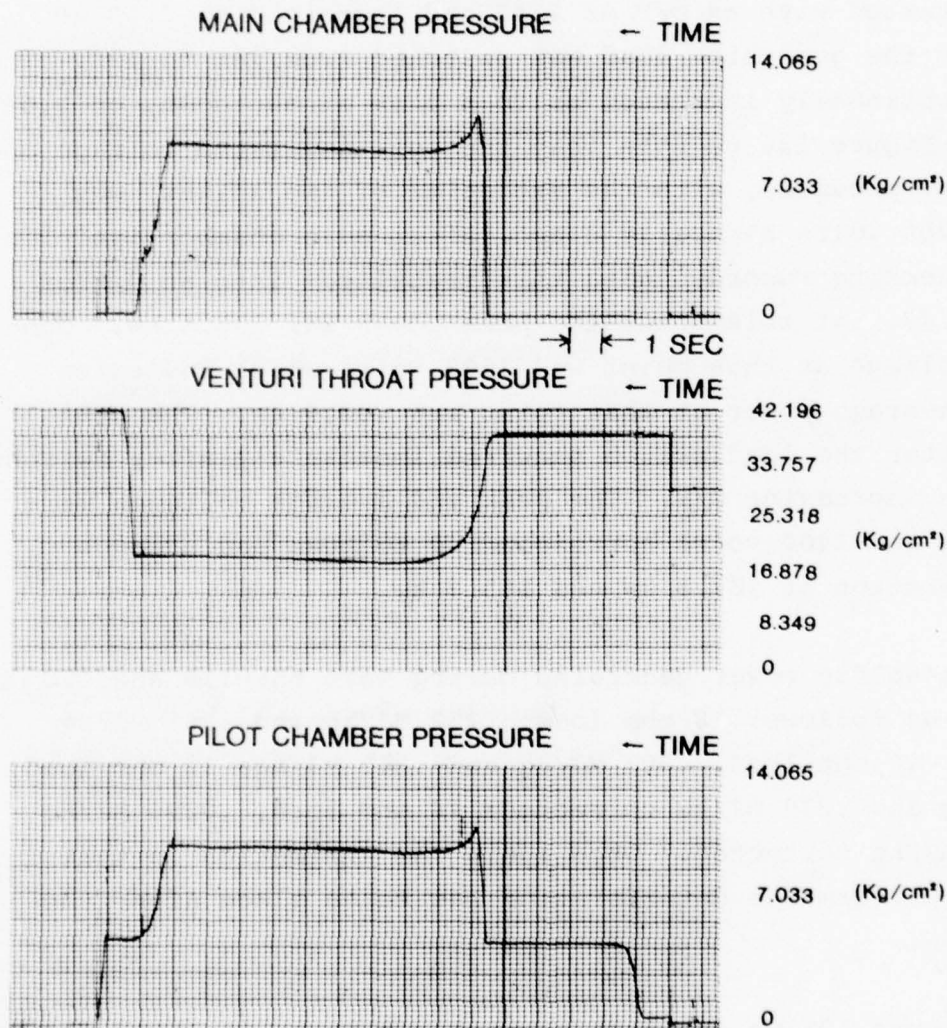


Figure 128. Power Test Run HEF-11C Combustion Parameters, Fuel - Emulsified Toluene/CsNO₃, Load Resistance Variable 14Ω to 12Ω

valve was found to be malfunctioning and is a plausible explanation although no evidence of this was found during this test program.

Test HEF-11C was run with a variable O/F and variable resistance. Since the O/F ratio of 2.55 at start-up was the best power O/F of Test HEF-11B, the starting O/F for HEF-11C was started lower in an attempt to point out the peak O/F. Test HEF-11C started with an O/F of 2.45 and increased to 2.53 at which time the generator load was switched from 14Ω to 12Ω . The O/F was continually increased on to a peak at shutdown, of 2.64. Observing Figure 126 we note that the peak indicated voltage and hence power produced, with the exception of two spikes, was roughly 1700 volts at nearly 3 sec. after main chamber ignition. By crosschecking recorded data this translates into an O/F of roughly 2.47. At this point the peak power was 206.4 kw. The average voltage at this point was 1600 volts which indicates that the average power at that point was 182.9 kw. The peak voltage after the load switch occurred immediately after switching due to the increasing O/F. The peak and average voltages were 1500 volts and 1400 volts corresponding to peak and average power generation of 187.5 kw and 163.3 kw.

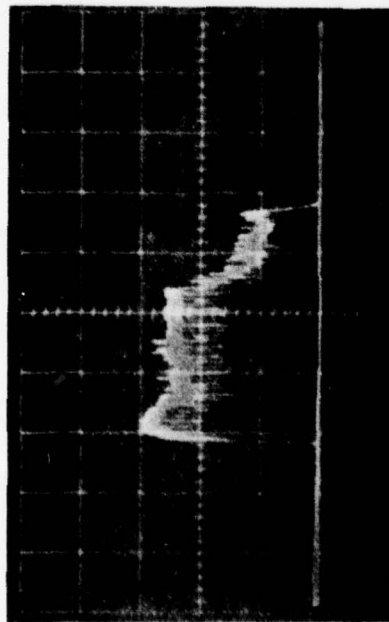
The specific power generated during Test HEF-11B and 11C tests was as follows: 8 ohm load, .252 MJ/kg and .261 MJ/kg corrected; 10 ohm load, .303 MJ/kg and .315 MJ/kg; 12 ohm load, .260 MJ/kg and .270 MJ/kg corrected; 14 ohm load, .0296 MJ/kg and .308 MJ/kg corrected. Once again the indication is that generator performance deterioration has taken place after the load change.

In Figure 128 we see that there has been no ignition delay and that after the initial pressure peak at ignition the chamber pressure rose steadily from 8.72 kg/cm^2 . The changing O/F is indicated by an increasing O_2 venturi throat pressure.

This series of tests has indicated that use of small particle seed can greatly reduce the MHD power generation noise signature when compared to the use of granulated seed. The use of the fine particles in an emulsion then creates two advantages. First, as demonstrated, a low noise signature which might be further reduced by $<10\mu\text{m}$ seed particles and, secondly, the emulsion technique produces a homogeneous distribution of seed particles throughout the fuel and subsequently a relatively homogeneous plasma while using less total seed than required by the granulated seed system.

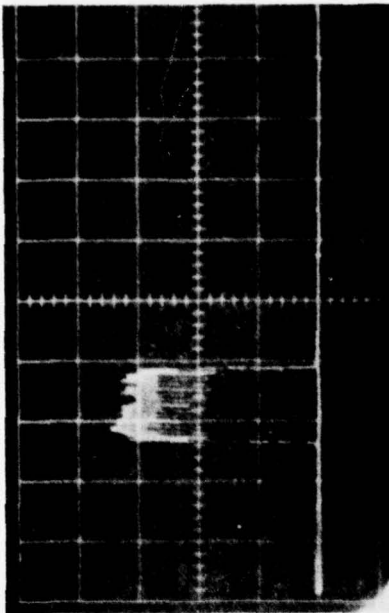
G. Emulsified Toluene/Aluminum
Power Tests, HEF-12 and HEF-12A

The next test series, HEF-12 and 12A were the first power tests of emulsified toluene and aluminum. The emulsion was formed in the same manner as that used in the combustion tests. The percentages were: LMF-4234 - 5%, aluminum - 30%, and toluene - 65%. The scheduled conditions were: variable O/F starting at 2.25 gradually changing to 2.45. The seed was granulated Cs_2CO_3 injected with the O_2 stream at the rate of 29.4 gm/sec. A variable load starting with 10Ω and changing to 8Ω midway through the 10 sec run was planned. Magnet power was scheduled for a peak field of 2.3 Tesla. Observing Figure 129 Test HEF-12 started 2 sec late when seed had begun to be injected. The same thing is more obvious in Figure 130 comparing O_2 venturi pressure with combustion pressure. Normal operation allows the data system to start followed one second later by pilot chamber ignition. Five sec into the run, after 4 sec of pilot burning, the oxygen and fuel valves open. One second after the fuel valve and oxygen valves open, or 6 sec after start, seeding is started. In this case the seeding was initiated before combustion started due to the 2 sec delay in combustion. A strong pilot flame was available on schedule; therefore, the combustion delay is unexplained except for a valve malfunction as discovered during a test series subsequent to this program. At



TIME —

RUN NO. HEF-12



TIME —

RUN NO. HEF-12A

FUEL: TOLUENE/ALUMINUM EMULSION (67/30)

SEED: Cs - 4.% OF PROPELLANT (29.4 gm/sec Cs_2CO_3 ADDED WITH O_2)

PROPELLANT: 0.6 Kg./sec.

O/F: 2.35 AVERAGE FOR HEF-12 2.53 FOR HEF-12A

LOAD: HEF-12; START -10. OHM, SWITCH TO 8. OHM AT 7 SEC. (DELAYED IGN. AT 5.6 SEC.)

HEF-12A; START - 14. OHM, SWITCH TO 12. OHM AT 8 SEC. (DELAYED IGN. AT 5.2 SEC,
BLOWOUT AT 8.2 SEC.)

SCALE: TIME - 2 SEC./CM. VOLTAGE - 500 VOLTS/CM.

Figure 129. Differential Load Voltage Oscilloscope Trace

HEF-12

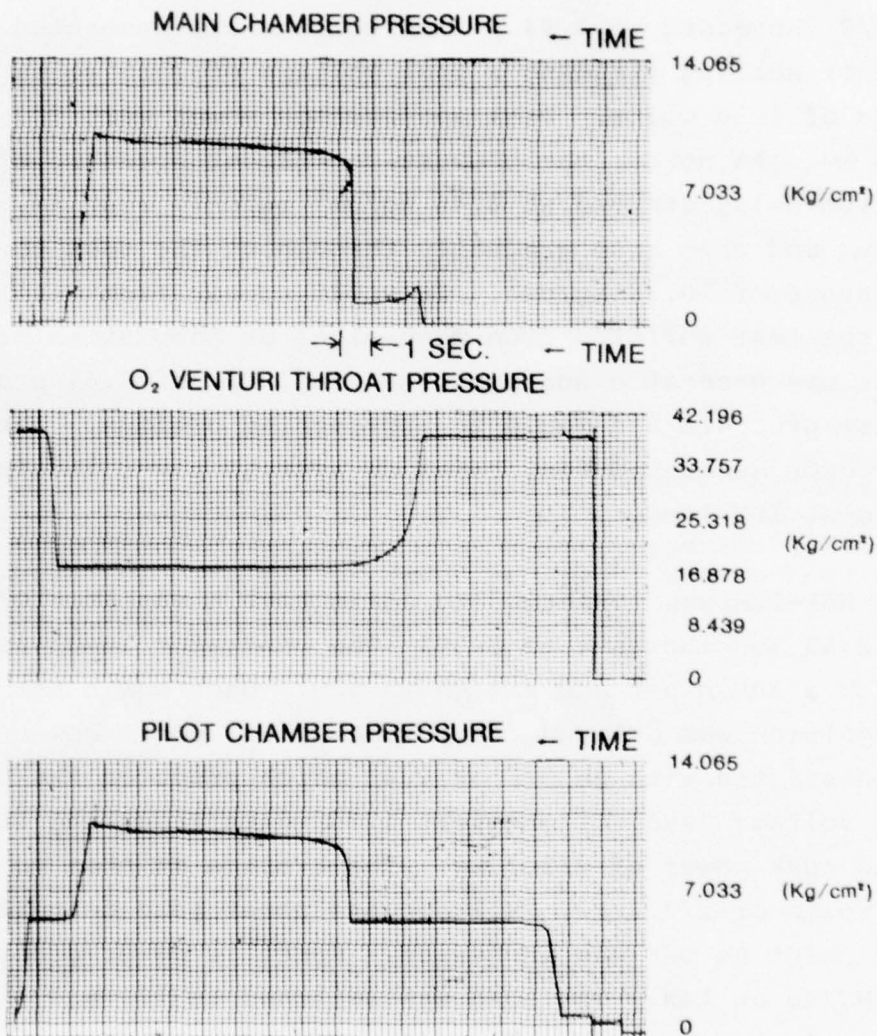


Figure 130. Power Test Run HEF-12 Combustion Parameters, Fuel - Emulsified Toluene/Aluminum, Load Resistance Variable 10Ω to 8Ω

ignition the O/F ratio was 2.30 rather than the starting O/F of 2.24. As combustion started the O/F was changing rapidly resulting in a change in O/F from 2.30 to 2.38 during the one second of power generation with a 10 Ω load. The peak indicated voltage was 1500 volts with an average of 1425 volts. Hence the calculated peak power was 225 kw and average was 203 kw. The load was switched to 8 Ω and the combustion pressure continued to rise as O/F increased to 2.44. Peak voltage was generated at cessation of seeding yielding a peak voltage of 1325 volts and an average of 1250 volts. Peak and average power were 219.5 kw and 195.3 kw. As noted, the combustion chamber pressure after the ignition delay started at 8.44 kg/cm² quickly rose to 9.28 kg/cm² and then rose gradually throughout the test to a final pressure of 10.13 kg/cm². It would appear from this that although the test suffered from mechanical or combustion problems, good power was generated and that the final O/F of 2.44 produced the highest pressure and would be approaching optimum. The specific power generated was, based on average power levels, .326 MJ/kg at 10 Ω load.

Test HEF-12A was scheduled to again have a variable O/F but start at 2.40 and increase to 2.60. The generator load was programmed for a 14 Ω start and switch to 12 Ω . Once again main combustion ignition was delayed, this time by 1.3 sec. Power generation started with an O/F of 2.48 which produced the highest indicated voltage level of the test 1725 volts resulting in a calculated peak power of 212.5 kw. The average at that point was 1575 volts or 177.2 kw. Voltage and power both decreased from that point as O/F was increased. Specific power generated was .280 MJ/kg at 14 Ω . The load was switched to 12 Ω and almost immediately fuel exhaustion was suffered. As can be seen in Figure 129 it is impossible to determine the exact point of load shift. Recorded data indicates two voltage readings prior to fuel lean blowout. The highest of the two values was 1318 volts for a calculated power of 144.8 kw. Post-test investigation

HEF-12A

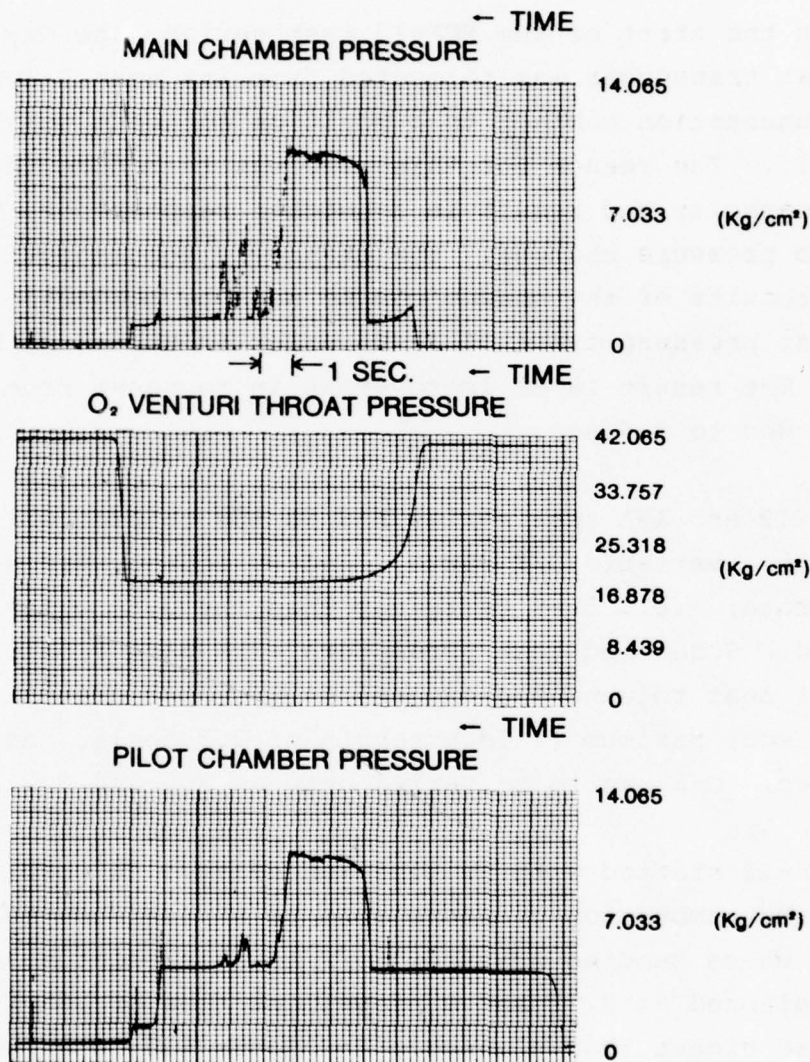


Figure 131. Power Test Run HEF-12A Combustion Parameters, Fuel - Emulsified Toluene/Aluminum, Load Resistance Variable 14Ω to 12Ω - Fuel Exhaustion at 8.2 Seconds

revealed considerable fuel on the tank walls and slumping around the fuel delivery tube. Figure 131 indicates an increase in combustion pressure from 9.85 kg/cm^2 as O/F increased to 2.58.

H. Neat Toluene Repeat Power Test
with Variable O/F and Load Switching,
HEF-13 and HEF-13A

Prior to the start of the HEF-13 test series, the oxygen venturi throat transducer was relocated from its normal location in the instrumentation cabinet to a position adjacent to the venturi itself. The reason for this move was to reduce the signal line capacity and result in a quicker response of the transducer to pressure changes. The change is documented in Vol II, but results of the change can be seen by comparing the venturi throat pressure trace of tests prior to HEF-13 with Figure 132. The result is an improvement in response from some two to three sec to 0.6 sec.

The HEF-13 and 13A test series had as its objective: operation with a variable O/F ratio, load switching, and a higher seed rate; i.e., 5.6% Cs rather than the 3.8% which had been utilized. Scheduled test parameters were mass flow of 0.6 kg/sec of neat toluene and oxygen, 44.1 gm/sec granulated Cs_2CO_3 for 7 sec, maximum field strength of 2.3 tesla, and a run time of 10 sec. O/F was to be varied between 3.0 and 3.2.

Test HEF-13 started with no ignition delay. As seen in Figure 132, the combustion pressure rose to a peak decayed to 10.27 kg/cm^2 where seeding started. O/F at this point was higher than planned at 3.51 and a propellant flow of .64 kg/sec which was also higher than planned. In Figure 133 both peak and average voltage increase toward the end of the 10Ω load portion of the run at which time the peak indicated and average voltage were 1480 volts and 1360 volts where O/F was 3.56. This indicates peak and average power were 219 kw and 185 kw as the O/F

HEF-13

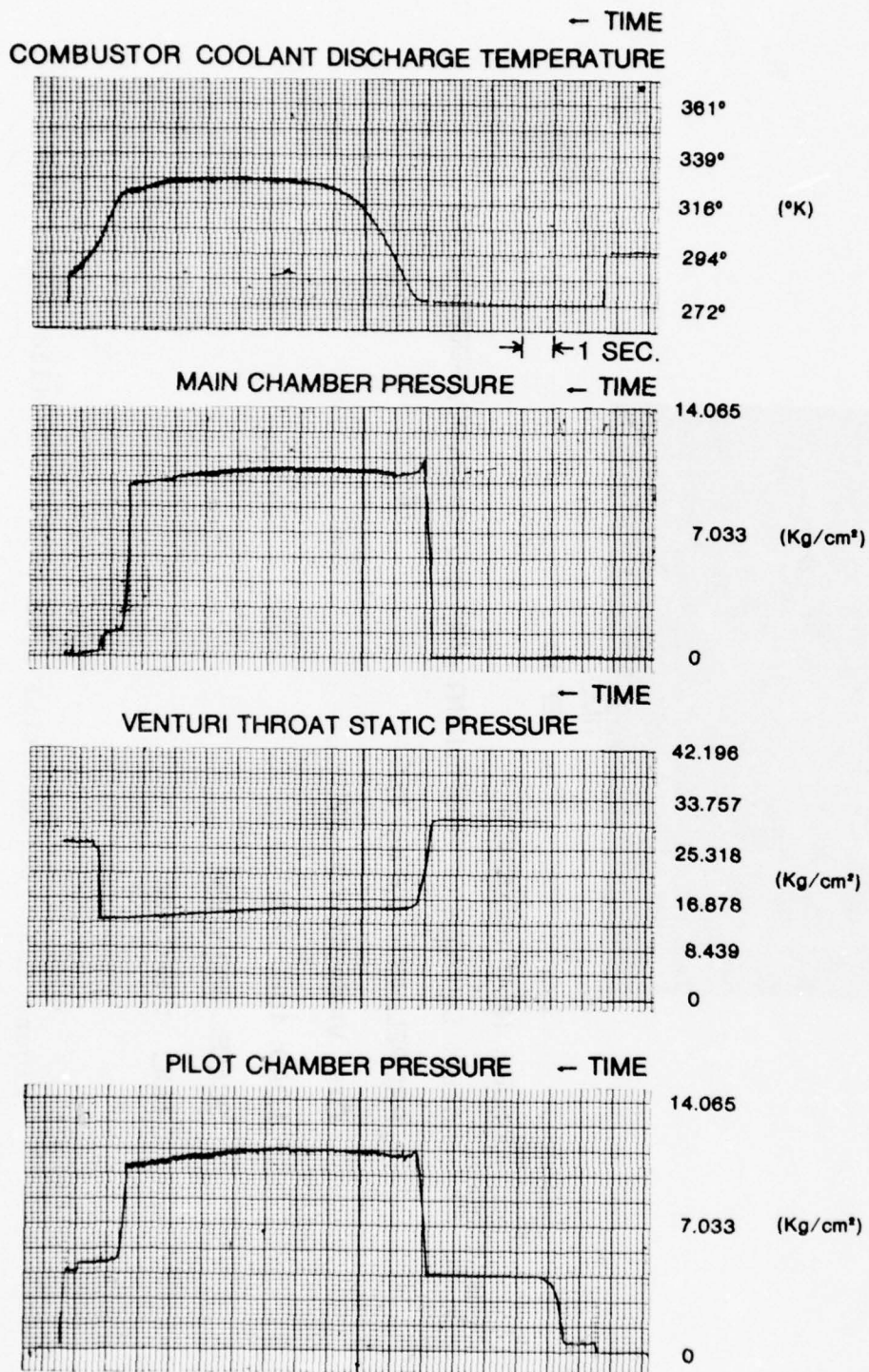
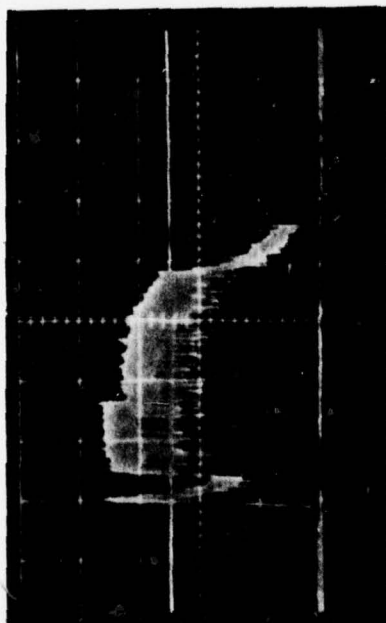


Figure 132. Power Test Run HEF-13 Combustion Parameters, Fuel - Straight Toluene, Load Resistance Variable 10Ω to 8Ω



TIME →

HEF-13

FUEL: NEAT TOLUENE

SEED: Cs - 5.6% OF PROPELLANT (44.1 gm/sec Cs_2CO_3 ADDED w/ O_2)

PROPELLANT: 0.6 Kg/SEC.

O/F: VARIABLE 3.0 ~ 3.2

LOAD: $10\Omega \rightarrow 8\Omega$

SCALE: 400 V/CM.

TIME: 2 SEC/CM.

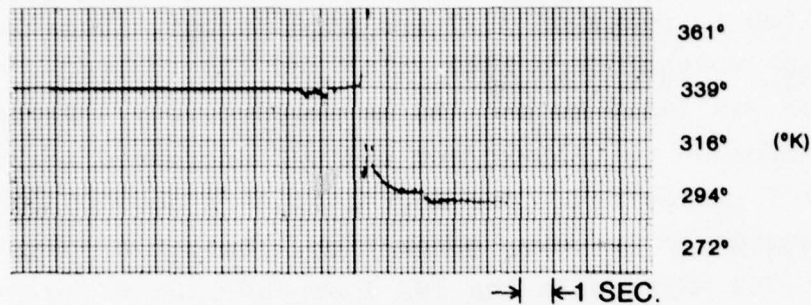
Figure 133. Differential Load Voltage Oscilloscope Trace

increases and \dot{M} increased slightly to .643 kg/sec. At this point, combustor pressure had increased to 10.5 kg/cm². After the load switch to 8 Ω the O/F and combustor pressure both continued to climb to peaks of 3.57 and 10.6 kg/cm². Peak indicated and average voltage were 1340 volts and 1200 volts. Calculated power was 224.5 kw and 180 kw respectively. Beyond this point \dot{M} decreased to .615 kg/sec and O/F decreased to 3.33 as better control was gained. The decreases were accompanied by corresponding decreases in power generation. Specific power generation was .288 MJ/kg with the 10 Ω load and .281 MJ/kg.

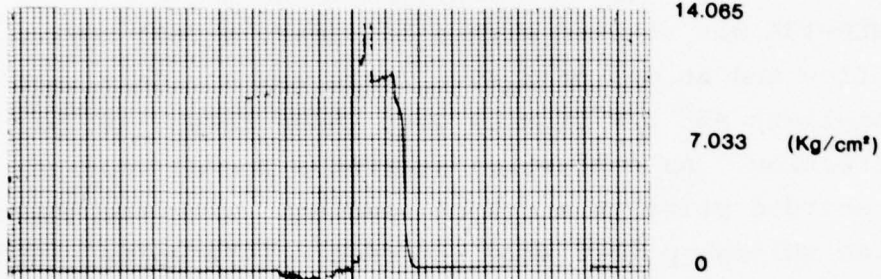
Test HEF-13A was started with a 14 Ω load, a .611 kg/sec propellant flow and an O/F of 3.46. There was no ignition delay and the propellant and O/F figures were those taken just prior to seed initiation. As combustion started a normal voltage spike was recorded prior to start of seeding. With the start of seeding three voltage points were recorded: 1052 volts, 1550 volts, and 1588 volts. Note here that the recorded voltage generally runs at or slightly below the average indicated voltage. No meaningful oscilloscope data was received. After the first three voltage points were recorded, arcing destroyed the records as seen in Figure 134 where the amplifiers either were burned up or were incapacitated. Subsequent investigation revealed that an arc had jumped from the diffuser across 4 in. of phenolic insulation block to the channel coolant exhaust manifold, through the T/C in that manifold, into the control room via the T/C lead and then to the T/C reference junction. The T/C reference junction thermal insulation (fiberglass) as well as operating components were completely destroyed. Essentially no fiberglass remained in the reference junction. The current continued through the reference junction to the amplifier drawer, on to the dc transducer power supply, to the O₂ temperature T/C and O₂ supply line. It then arced two to three inches from the O₂ supply line to a water supply valve and dissipated itself in the ground. During this time the only abnormality

HEF-13A

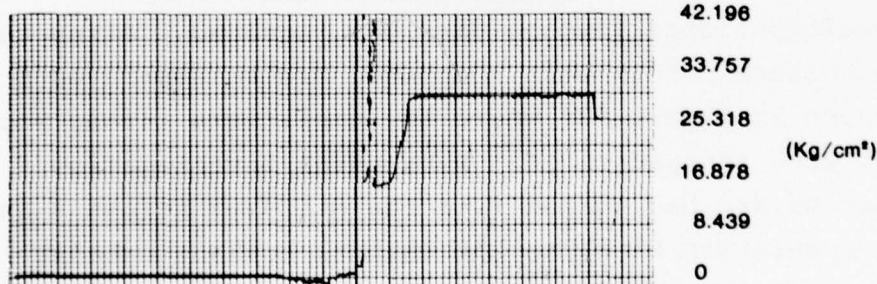
— TIME
COMBUSTOR COOLANT DISCHARGE TEMPERATURE



MAIN CHAMBER PRESSURE — TIME



— TIME
VENTURI THROAT STATIC PRESSURE



PILOT CHAMBER PRESSURE — TIME

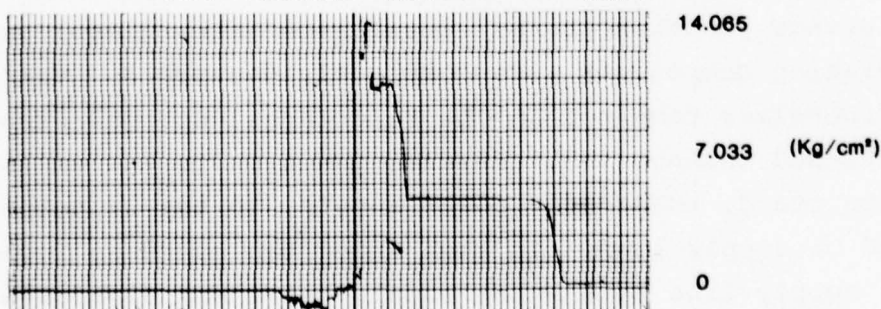


Figure 134. Power Test Run HEF-13A, Fuel - Straight Toluene, Load Resistance Variable 14Ω to 12Ω - Arcing Destroyed Instrumentation

noted in addition to loss of all instrumentation was several small flashes as the instrumentation amplifier I.C. chips were burned out. With the loss of instrumentation the test was aborted.

I. Neat Toluene Repeat Test With
Variable O/F, HEF-14 and HEF-14A

After three weeks of considerable effort the instrumentation was repaired and Tests HEF-14 and 14A were scheduled. These tests were scheduled as duplicates of the HEF-13 series. Test HEF-14 started normally with an O/F of 3.27 and propellant flow of .604 kg/sec. In Figure 135 we see that this resulted in a combustion pressure of 9.28 kg/cm² which rose to 9.49 although O/F and \dot{M} remained constant. In Figure 136 we see that the peak indicated voltage was 1280 volts and average voltage was 1120 volts. These values indicate peak and average power produced of 163.8 kw and 125.4 kw with the 10 Ω load. Although \dot{M} was decreased from 0.606 kg/sec at the load switch point to 0.597 kg/sec at test end, with an accompanying O/F decrease from 3.30 to 3.20, there was no decrease in combustor pressure and peak and average voltages were 1120 volts and 1000 volts respectively. These values yield calculated powers of 156.8 kw and 125.0 kw. The specific power generated was .207 MJ/kg for the 10 Ω load and .209 MJ/kg with an 8 Ω load. These values are considerably lower than expected and should have indicated generator problems.

Test HEF-14A was started with a 14 Ω load and a slightly low \dot{M} of .585 kg/sec. The low \dot{M} and O/F of 3.18 was reflected in a slightly low combustor pressure of 9.56 kg/cm², seen in Figure 137, which remain nearly constant through the test. At test end pressure had only risen to 9.63 kg/cm² while O/F had not changed appreciably. Peak indicated voltage with the 14 Ω load was 1500 volts while average voltage shown in Figure 136 was 1360 volts. Corresponding power was 160.7 kw and 132.1 kw. When the load was switched to 12 Ω , the peak and average values became 1370 volts

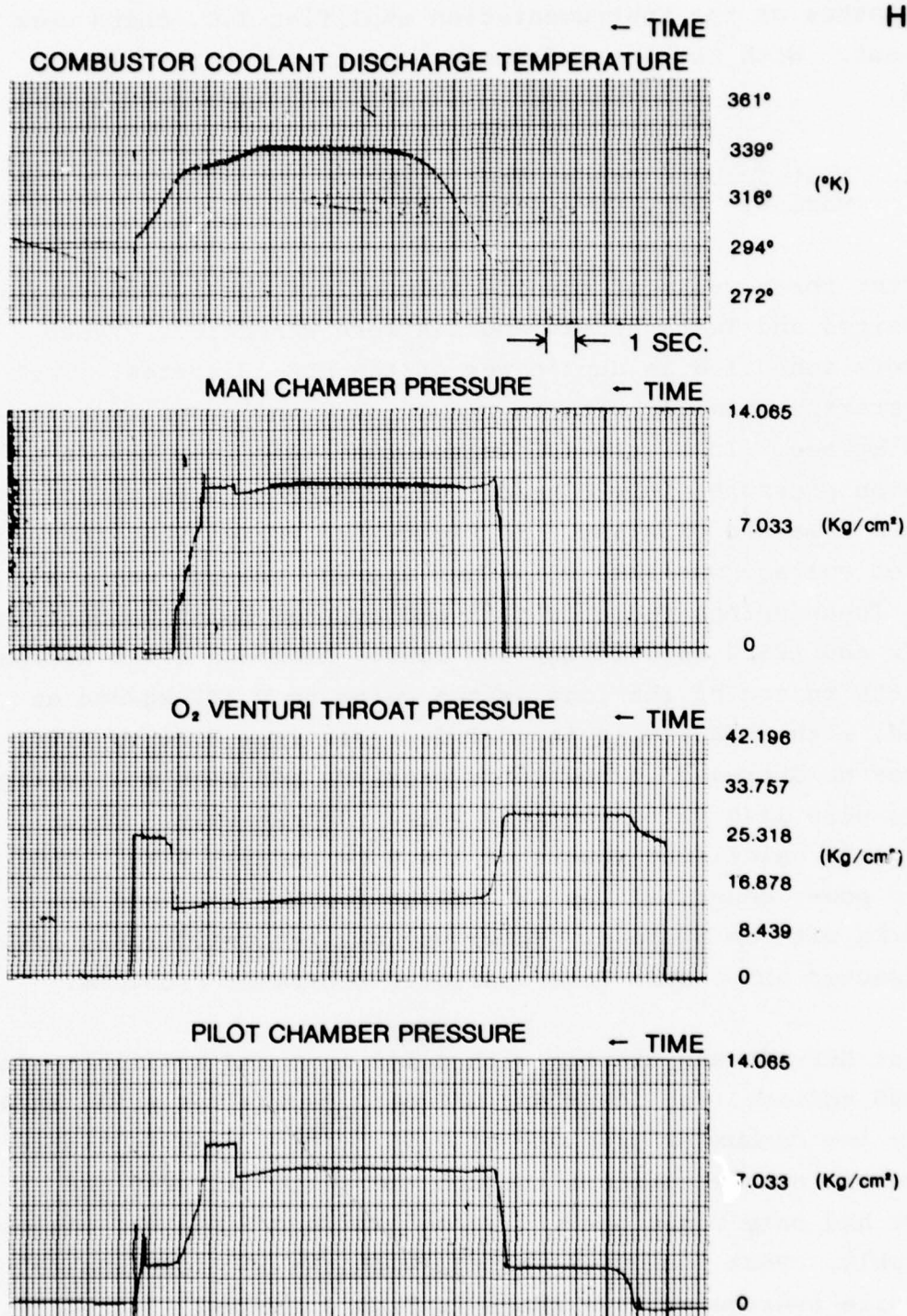
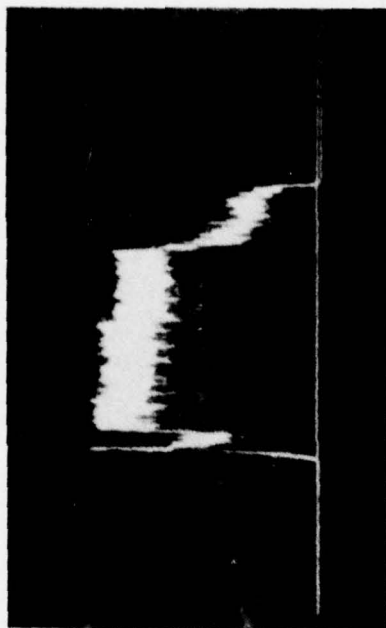


Figure 135. Power Test Run HEF-14 Combustion Parameters, Fuel - Straight Toluene, Load Resistance Variable 10Ω to 8Ω



TIME →
HEF-14



TIME →
HEF-14A

FUEL: STRAIGHT TOLUENE

SEED: Cs - 6% OF PROPELLANT (44.1 gm/SEC. Cs_2CO_3 ADDED WITH O_2)

O/F: HEF-14 = 3.27, HEF-14A = 3.18

LOAD: HEF-14 STARTED WITH 10Ω AND CHANGED TO 8Ω AT 9.2 SEC.

HEF-14A STARTED WITH 14Ω AND CHANGED TO 12Ω AT 9.9 SEC.

SCALE: TIME - 2 SEC./CM VOLTAGE - 400 V/CM.

Figure 136. Differential Load Voltage Oscilloscope Trace

HEF-14A

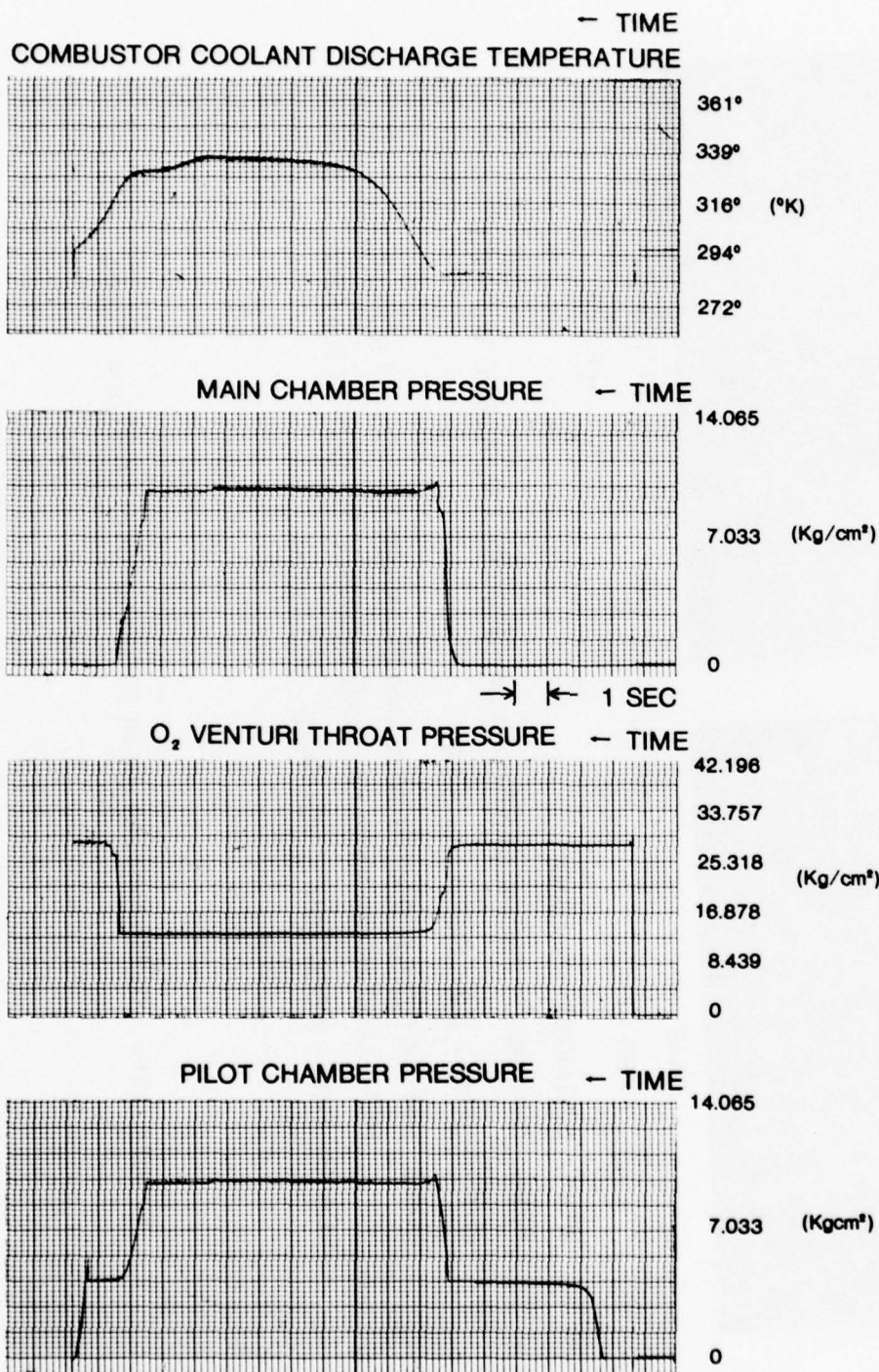


Figure 137. Power Test Run HEF-14A Combustion Parameters, Fuel - Straight Toluene, Load Resistance Variable 14Ω to 12Ω

and 1200 volts. Power generation values calculated from these voltage levels were 149.0 kw and 120.0 kw. Specific power generation was .226 MJ/kg for the 14 Ω load and .205 MJ/kg with a 12 Ω load. Again these are very low values.

J. Emulsified Toluene/CsNO₃ Seed Repeat Test
With Increased Seed Flow Rate, HEF-15 and
HEF-15A

Test series HEF-15 and 15A were planned to retest the CsNO₃ seed emulsions with a higher (4% Cs) seed percentage, variable O/F ratio and load switching. Test parameters were: $\dot{M} = 0.6$ kg/sec, nominal O/F = 2.50 varying between 2.4 and 2.5, magnetic peak field of 2.3 tesla, and run time of 10 sec. Test HEF-15, as seen in Figure 138, started after a 0.5 sec ignition delay. Combustion pressure was quite low at the start, 6.75 kg/cm², and although pressure rose throughout the test, pressure was quite unstable. Indicated \dot{M} was .62 kg/sec at an O/F of 2.17. The extremely low combustion pressure appears to indicate that the fuel and total mass flow calculated from the calibration curve are in error, as would be the O/F. It is believed that the fuel flow was considerably below that indicated. Observing Figure 139 we find a radically varying voltage and thus variable power level. The power and voltage tended to increase as chamber pressure rose, which is logical, but after the load was changed to 8 Ω the power and voltage stabilized and gradually decreased as chamber pressure stabilized but continued to increase. Peak indicated voltage is 820 volts with the 10 Ω load corresponding to a 67.2 kw peak power. Average voltage and power are 720 volts and 51.8 kw. After the load change, the values become 840 volts and 88.2 kw peak. Average values are 760 volts and 72.2 kw. Specific power values were .084 MJ/kg, 10 Ω load and .142 MJ/kg with an 8 Ω load.

As a result of the unusually low power production during this test, it was considered that damage to the channel had

HEF-15

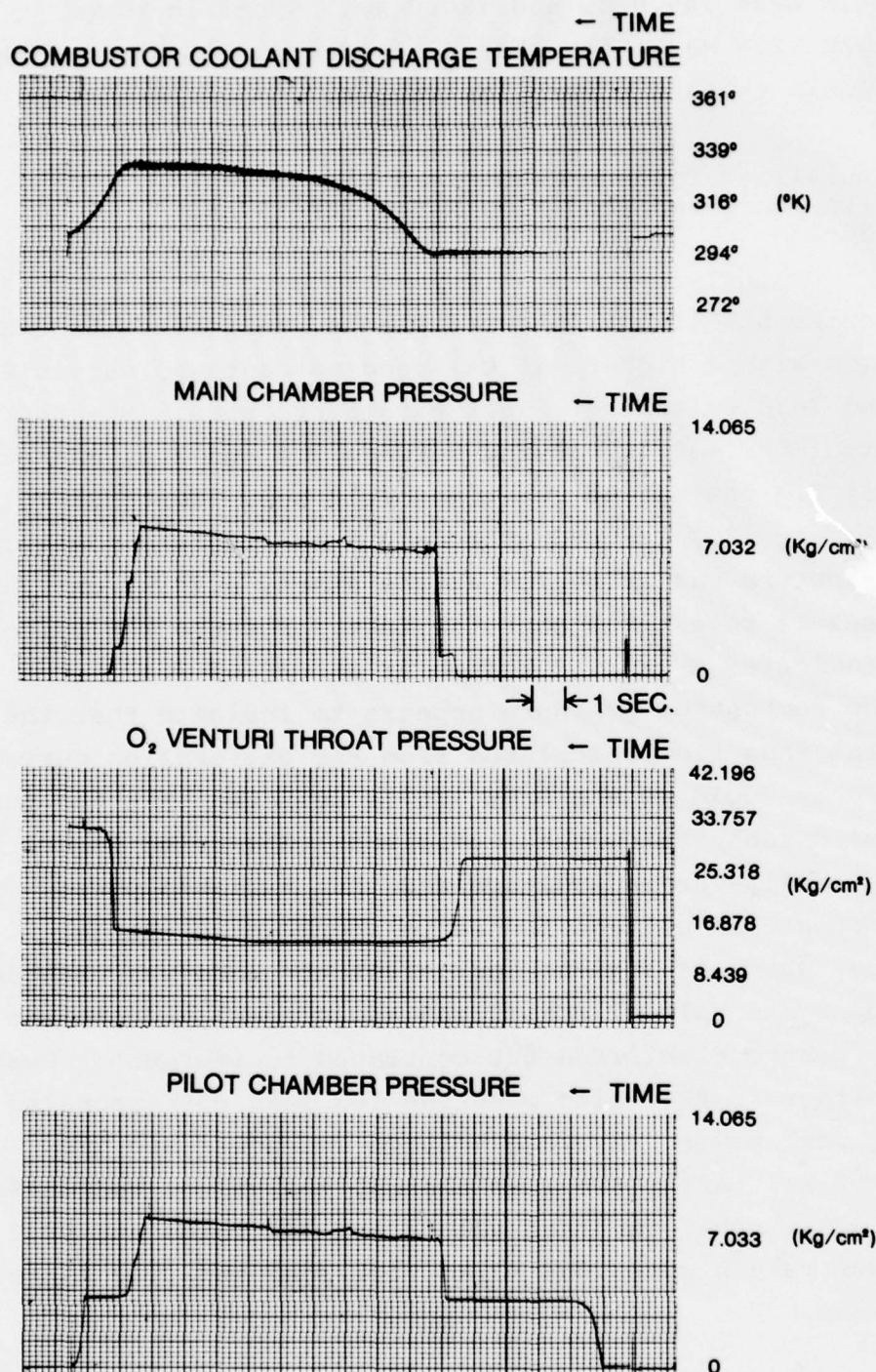


Figure 138. Power Test Run HEF-15 Combustion Parameters, Fuel - Emulsified Toluene/CsNO₃ (4% Cs), Load Resistance Variable 10Ω to 8Ω



TIME --
HEF-15



TIME --
HEF-15A

FUEL: TOLUENE/CsNO₃ EMULSION

SEED: CsNO₃ 19% OF FUEL Cs 4% OF PROPELLANT

PROPELLANT: 0.6 Kg/SEC.

O/F: 2.4 → 2.5

LOAD: HEF-15 START — 10Ω CHANGE TO 8Ω AT 7.6 SEC.

HEF-15A START — 14Ω CHANGE TO 12Ω AT 9.0 SEC.

SCALE: 400 V/CM.

TIME: 2 SEC./CM.

Figure 139. Differential Load Voltage Oscilloscope Trace

occurred. Two tests of channel integrity were made. First, the channel interelectrode resistance was measured using a high voltage (1500 Vdc) source. The leakage current was found to be within normal limits and the interelectrode insulation was therefore assumed to be intact. Next the combustion chamber igniter pilot chamber was removed and a borescope was inserted through the chamber ignition port and on through the nozzle to allow close proximity visual inspection of the electrodes. No damage was noted and hence it was assumed that there were no problems with the channel itself. As events were ultimately to reveal, this assumption was incorrect but no reason is known for the high interelectrode resistance with the insulation damage eventually found.

Test HEF-15A started similarly to HEF-15 although the ignition delay was decreased. Combustion pressure was somewhat unstable and tended to decrease from 8.16 kg/cm^2 as seen in Figure 140. In Figure 139 the peak indicated voltage occurred at 0.3 sec after the start of combustion and was variable but continuously decreasing throughout the test while the chamber pressure increased after the load change to 8.72 kg/cm^2 . Peak 14Ω load voltage was 1360 volts corresponding to 132 kw. Mean voltage varied considerably, but the average was approximately 1080 volts indicating a power dissipation of 83.3 kw. After the load was changed, once again the combustion pressure stabilized as did the voltage signature. Peak voltage was 1200 volts indicating a power dissipation of 120 kw. The maximum average voltage and power were 1000 volts and 83.3 kw. Specific power generated was .132 MJ/kg at 14Ω and .126 MJ/kg.

K. Neat JP-4 Fuel Power Baseline
Test, HEF-16 and HEF-17

The test series HEF-16 and HEF-17 were intended to establish a baseline for neat JP-4 fuel power production. The test parameters were programmed as follows: $\dot{M} = 0.6 \text{ kg/sec}$, granulated

HEF-15A

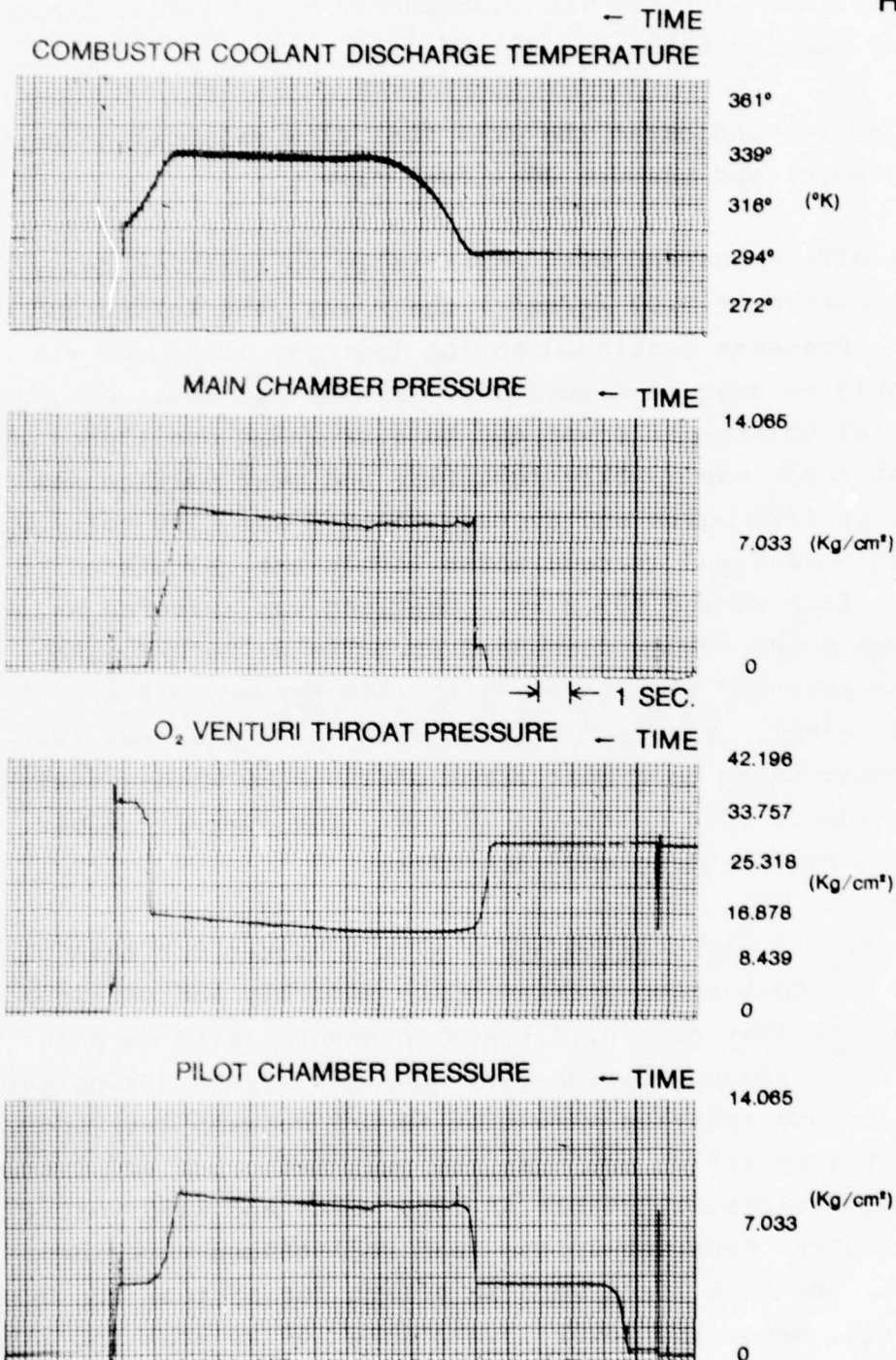


Figure 140. Power Test Run HEF-15A Combustion Parameters, Fuel - Emulsified Toluene/CsNO₃ (4% Cs), O/F Variable from 2.4 to 2.5, Load Resistance Variable 14Ω to 12Ω

Cs_2CO_3 seed at the rate of 29.4 gm/sec for 12 sec, run time = 15 sec. Maximum magnetic field intensity = 2.3 tesla, nominal O/F = 3.49 varying between 3.45 and 3.55.

Figure 141 indicates the JP-4 fuel flow calibration curve used to predict and measure JP-4 fuel flow.

Test HEF-16 started with essentially no ignition delay at a chamber pressure of 9.07 kg/cm². The \dot{M} was .456 kg/sec and O/F was 3.45. Pressure continued at the ignition level and was quite stable as seen in Figure 142. Figure 143 does not indicate initial voltage or power due to a grounded oscilloscope lead. The fault was quickly rectified and peak voltage was indicated as 1280 volts and average voltage was 1180 volts with a 10 Ω load. Peak and average power levels are calculated to have been 163.8 kw and 139.2 kw. The load was switched and the voltage and power values decreased steadily as \dot{M} , O/F, and combustion pressure all increased to .645 kg/sec, O/F = 4.16, and 10.13 kg/cm². The peak voltage with an 8 Ω load was 1120 volts corresponding to a peak power of 156.8 kw with a maximum average value of 1000 volts and 125 kw. The specific power generated was .306 MJ/kg and .204 MJ/kg.

Test HEF-17 was started again with a higher O/F than planned and lower \dot{M} . Combustion started quite smoothly and continued throughout the test at a 9.14 kg/cm² pressure level as seen in Figure 144. \dot{M} varied between .584 and .587 kg/sec during the test with an accompanying variation in O/F between 3.61 and 3.71. In Figure 145 we see that the peak indicated and average voltage were relatively stable at 1300 volts and 1180 volts. Since during the test set-up the load resistances were incorrectly set, the same loads were in effect during test run HEF-17 as in HEF-16, hence the power levels were 169 kw peak and 139.2 kw average with the 10 Ω load. When the load was switched to 8 Ω , the peak and average voltage were 1120 volts and 1020 volts. As

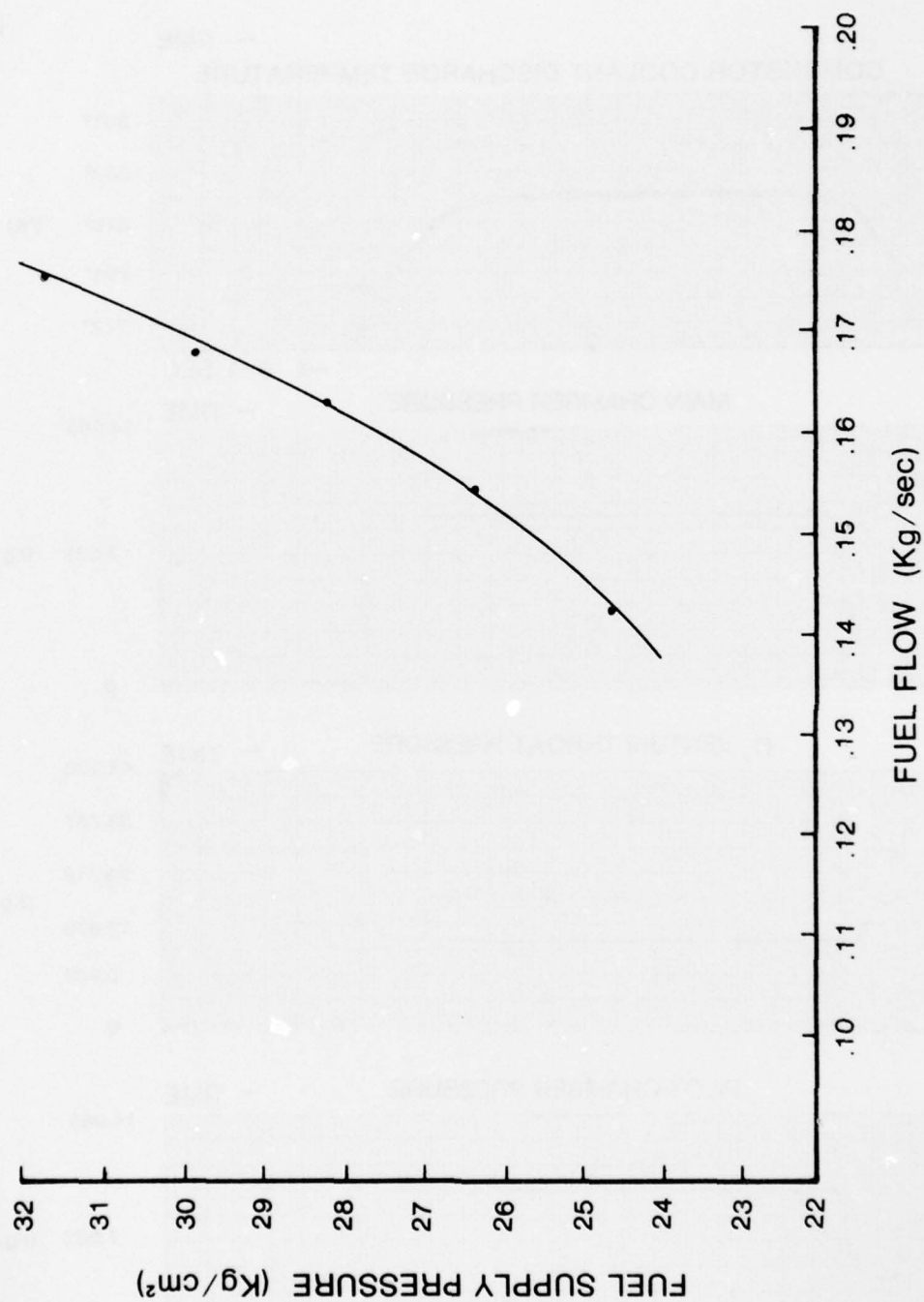


Figure 141. Fuel Flow Calibration Curve

HEF-16

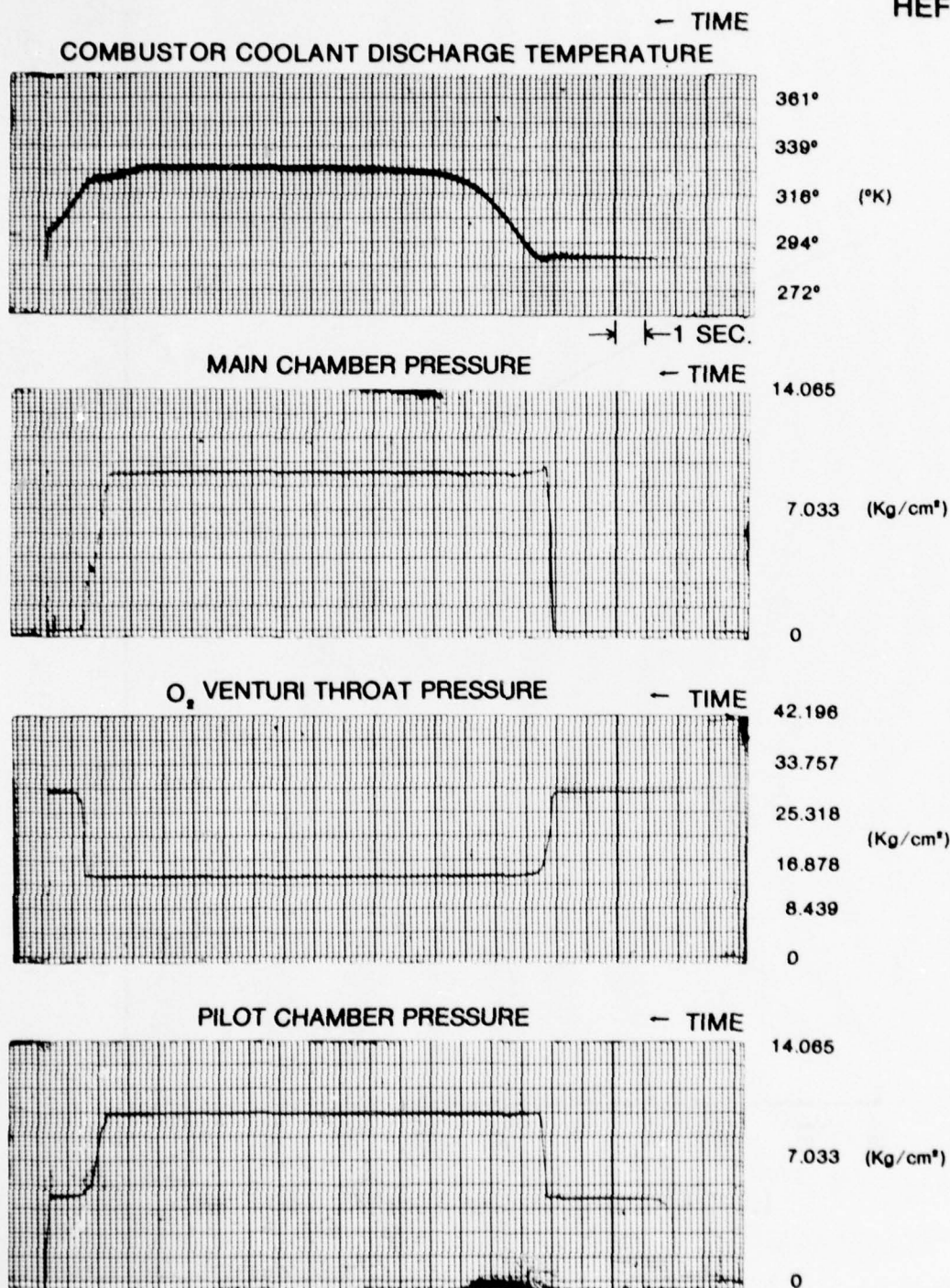
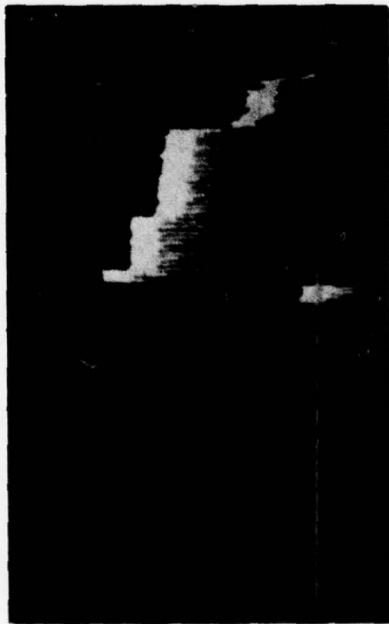


Figure 142. Power Test Run HEF-16 Combustion Parameters, Fuel - Neat JP-4, O/F Variable from 3.45 to 3.55, Load Resistance Variable 10Ω to 8Ω



TIME --
HEF-16

FUEL: NEAT JP-4

SEED: Cs - 4% OF PROPELLANT (29.4 gm/sec Cs_2CO_3 ADDED w/O)

PROPELLANT: 0.6 Kg/SEC.

O/F: 3.45--3.55

LOAD: 10Ω CHANGED TO 8Ω AT 13 SEC.

SCALE: 400 V/CM.

TIME: 2 SEC./CM.

NOTE: SCOPE INPUT
GND'ED FIRST
PART OF RUN LIFTED @ 5.5 CM.

Figure 143. Differential Load Voltage Oscilloscope Trace

HEF-17

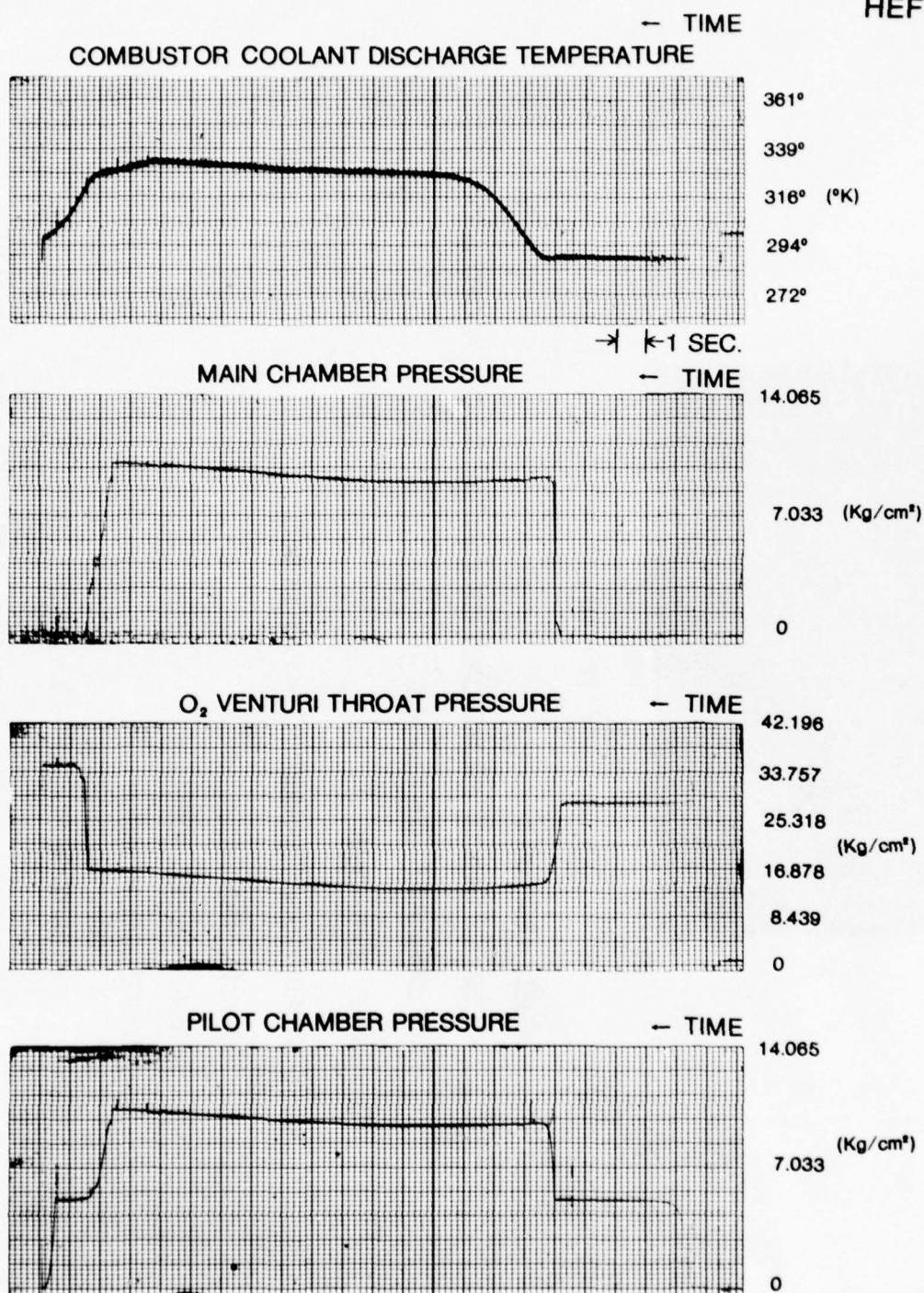
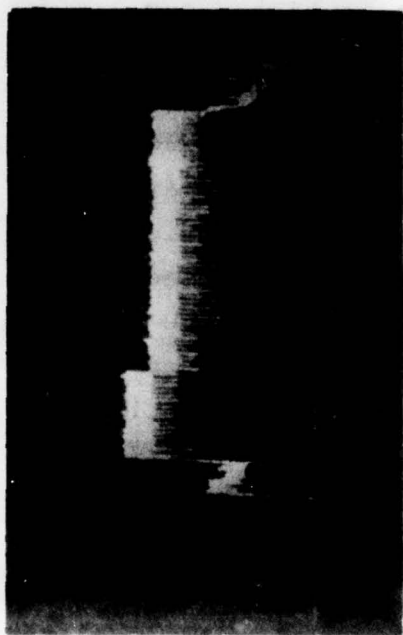


Figure 144. Power Test Run HEF-17 Combustion Parameters, Fuel - Neat JP-4, O/F Variable from 3.61 to 3.71, Load Resistance Variable 10Ω to 8Ω



TIME →
HEF-17

FUEL: NEAT JP-4

SEED: Cs - 4% OF PROPELLANT (29.4 gm/sec Cs_2CO_3 ADDED w/ O_2)

PROPELLANT: 0.6 Kg/SEC.

O/F: 3.61→3.71

LOAD: 10Ω CHANGED TO 8Ω AT 8 + SEC.

SCALE: 400 V/CM.

TIME: 2 SEC./CM.

NOTE: CAPACITOR CONNECTED ACROSS LOAD DURING FINAL 4
SEC OF OPERATION

Figure 145. Differential Load Voltage Oscilloscope Trace

can be seen, the peak and average power was very stable at 156.8 kw and 130.1 kw. Specific power generated was .238 MJ/kg at 10 Ω load and .222 MJ/kg at 8 Ω . This is compared with .306 MJ/kg and .204 MJ/kg at essentially the same conditions during Test HEF-16.

L. Emulsified Toluene/Aluminum Power
Test With Increased O/F, HEF-18 and HEF-18A

The purpose of test series HEF-18 and 18A was to evaluate the toluene-aluminum emulsion as a fuel at a higher O/F ratio than used previously; i.e., 2.86 vs 2.35. During these tests a fixed O/F ratio would be used and variable generator loading. The test parameters were: $\dot{M} = 0.6$ kg/sec, O/F 2.86, 29.4 gm/sec of granulated Cs_2CO_3 for 12 sec, run time = 15 sec, maximum magnetic field intensity = 2.3 tesla. Figure 146 indicates the emulsified toluene/aluminum fuel calibration curve used. Test 18 was started normally with an O/F of 2.74 and \dot{M} of .550 kg/sec, both of which were slightly low. This resulted in a combustor pressure as seen in Figure 147 of 8.30 kg/cm². Combustion was relatively stable and although \dot{M} increased during the run by only .007 kg/sec, O/F increased to 2.90 and combustor pressure increased to 8.93 kg/cm². The test ran quite smoothly and stopped on the programmed schedule. Peak indicated and average voltage with the 10 Ω load were 1280 volts and 1140 volts as seen in Figure 148. Power was calculated to be 163.8 kw peak and 130 kw average. The load was shifted to 8 Ω and the peak indicated and average voltage were 1120 volts and 1040 volts. Indicated peak and average power generated was 156.8 kw and 135.7 kw. Specific power generation was .236 MJ/kg with the 10 Ω load and .243 MJ/kg with the 8 Ω load.

Test HEF-18A was planned to duplicate HEF-18 with the exception of using 14 Ω and 12 Ω generator loads. During the start of the test ignition was accompanied by a sharp explosive crack sounding much the same as a rifle report. Observing

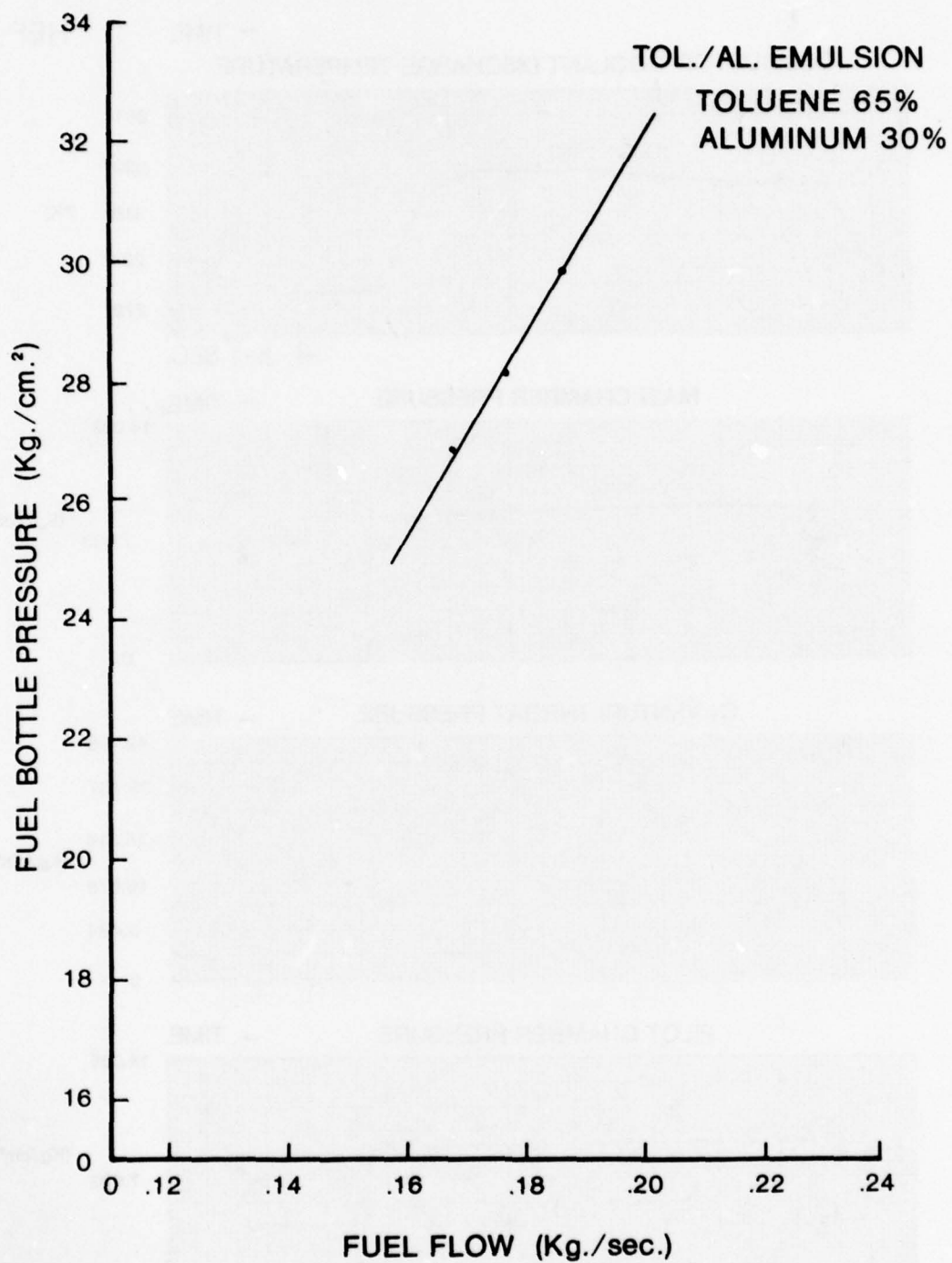


Figure 146. Fuel System Calibration Curve for Emulsified Toluene/Aluminum Fuel

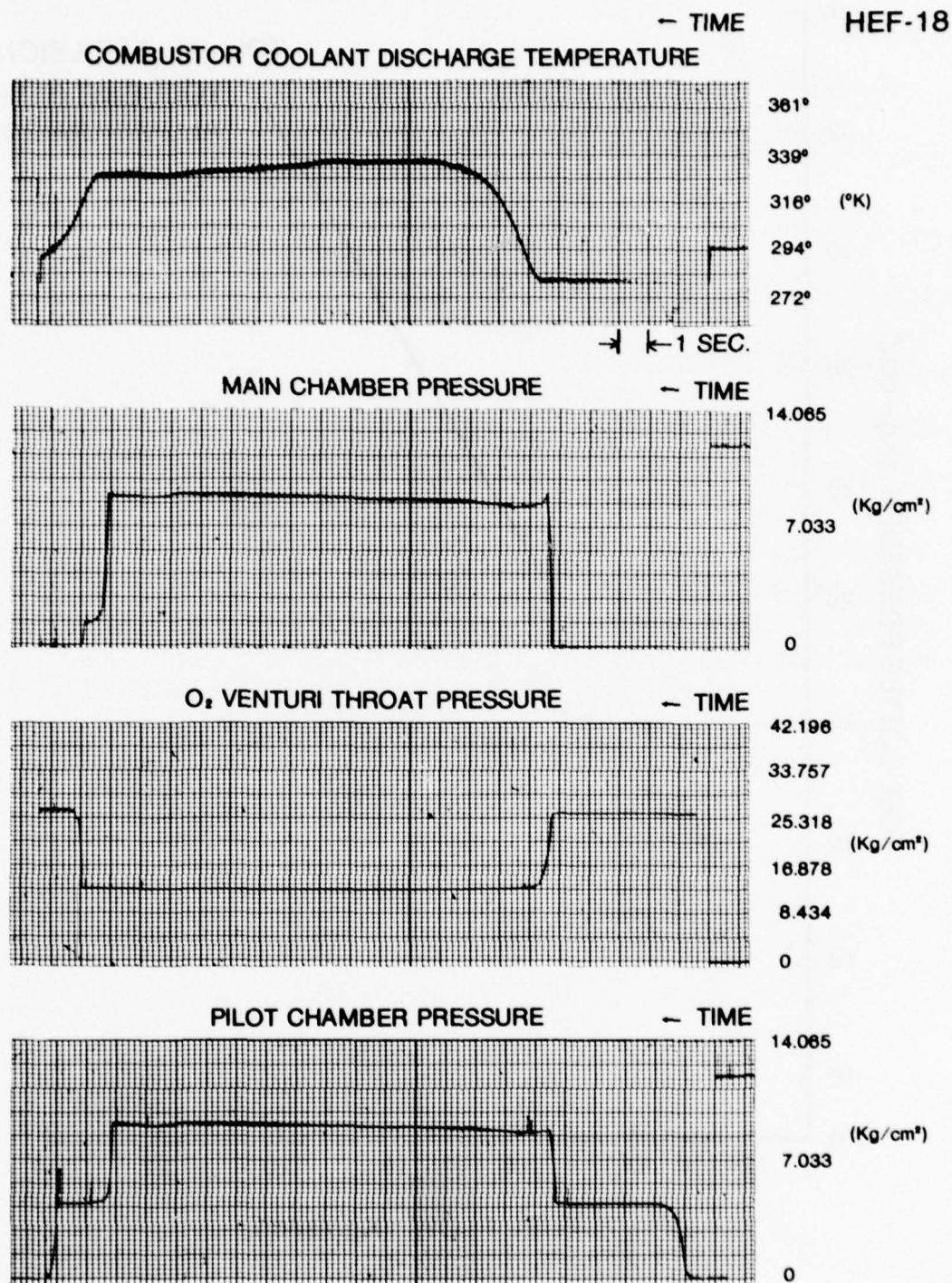
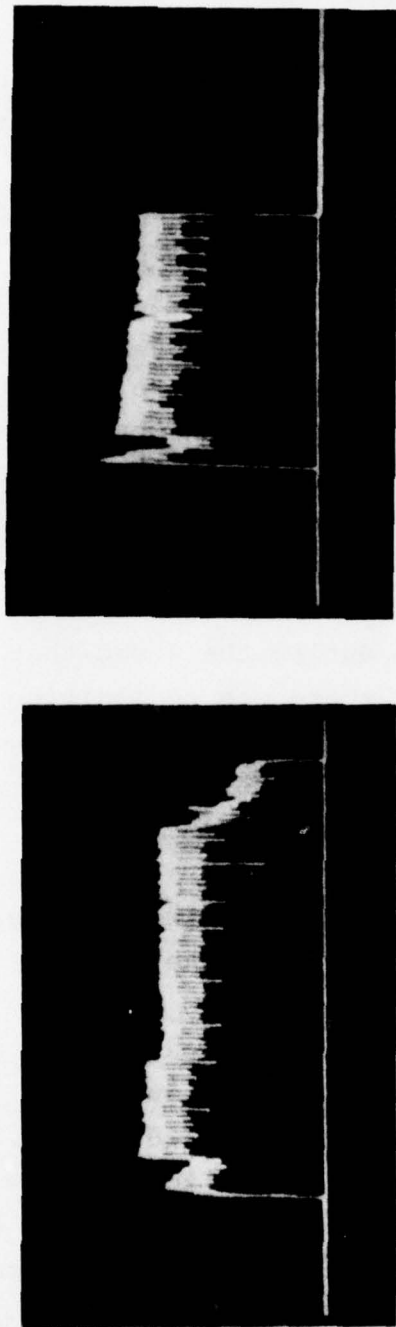


Figure 147. Power Test Run HEF-18 Combustion Parameters, Fuel - Emulsified Toluene/Aluminum, O/F Variable 2.74 to 2.90, Load Resistance Variable 10 Ω to 8 Ω



TIME →
HEF-18

TIME →
HEF-18A

FUEL: EMULSIFIED TOLUENE 6%/ALUMINUM 30%
 SEED: Cs - 4% OF PROPELLANT (29.4 gm/SEC Cs_2CO_3 WITH O_2)
 PROPELLANT: 0.6 Kg/SEC.
 O/F: HEF-18, 2.74 TO 2.90
 HEF-18A, START 2.82
 LOAD: HEF-18 START AT 10Ω CHANGED TO 8Ω AT 8.6 SEC.
 HEF-18A START AT 14Ω CHANGED TO 12Ω AT 9.8 SEC.
 SCALE: 400 V/CM.
 TIME: 2 SEC./CM.

Figure 148. Differential Load Voltage Oscilloscope Trace

Figure 149 it was found that the pilot chamber did not light until 5.6 sec into the test start, at that point and both the oxygen and fuel valves had been open approximately 0.1 to 0.2 sec. In spite of the explosive start the indicated ignition peak pressure was minimal and relatively stable though gradually increasing combustion pressure was maintained. At approximately five to six sec after ignition a diffuser cooling water leak was detected and the test was aborted. Post-test examination indicated that the sharp pressure rise had stressed the diffuser sidewall bolts sufficiently to allow coolant to leak between the side walls and cover plate. The combustor injection plate was removed to examine the combustor walls, but no damage was found. Only a light dusty coating of Al_2O_3 covered the chamber walls. Upon removal of the O_2 lines light carbon deposits were found back to the seeder and slight discoloration of the Cs_2CO_3 seed was noted. It is felt that the only explanation is in the O_2 -ethane pilot light mixture filling the combustion chamber and perhaps backing up the O_2 supply lines during the 4 sec that the pilot valves should have been open and there was no ignition spark. The diffuser bolts were replaced, the coolant passages were pressure checked, and the rest of the generator system was reassembled for further testing.

When test HEF-18A had started, the mass flow was .55 kg/sec and the O/F was 2.82 producing a combustor pressure of 8.58 kg/cm² at the start of power production. Although pressure increased, the voltage and power dissipation decreased from a peak indicated of 1400 volts to 1300 volts, see Figure 148. The average voltage decreased from 1280 volts to 1200 volts. This means that peak power decreased from 140 kw to 120.7 kw and average power from 116 kw to 103.9 kw. The voltage and power remained relatively constant after the load switch from 14 Ω to 12 Ω with peak and average voltages of 1240 volts and 1160 volts. The corresponding power production was 128.1 kw and 112.1 kw. Specific power was, considering the high voltage end

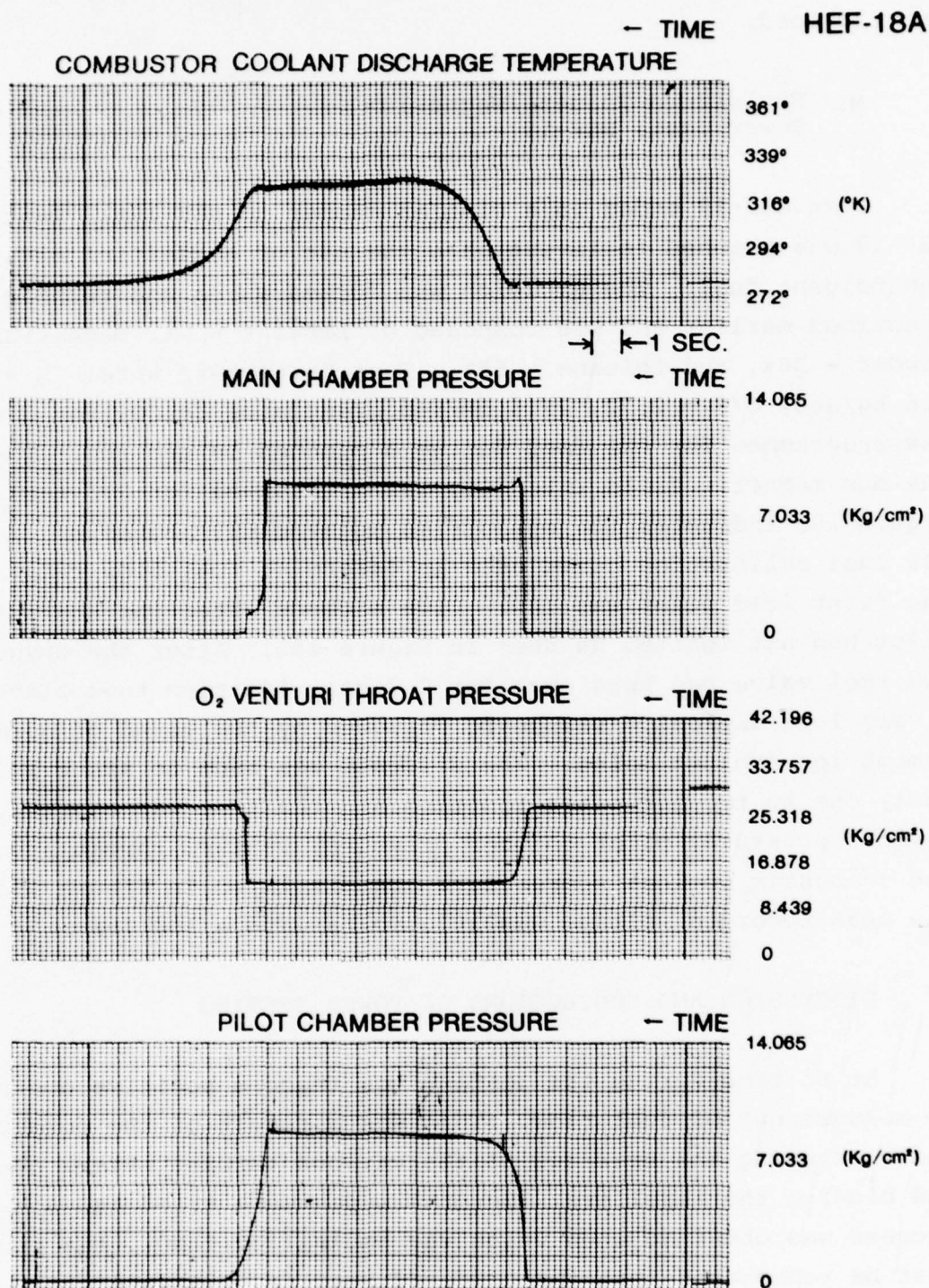


Figure 149. Power Test Run HEF-18A Combustion Parameters, Fuel - Emulsified Toluene/Aluminum, O/F at Start 2.82, Load Resistance Variable 14Ω to 12Ω

of the curve, .213 MJ/kg with the 14 Ω load and .202 MJ/kg with the 12 Ω load.

M. Emulsified Toluene/Magnesium
Power Test, HEF-19

Test HEF-19 ended in a similar manner to HEF-18A. Test HEF-19 was planned to investigate the use of emulsified magnesium and toluene fuel. The emulsion was formed using the technique described earlier and was composed of LMF4234 - 5%, magnesium powder - 30%, and toluene - 65%. Test parameters were: \dot{M} = 0.6 kg/sec, O/F = 2.72, 29.4 gm/sec granulated Cs_2CO_3 for 7 sec was programmed for the seed during a planned 10 sec run. The maximum magnetic field intensity was programmed for 2.3 tesla. Figure 150 indicates the emulsified toluene 65%/magnesium 30% fuel calibration curve used to determine fuel flow rate. The first load point was 10 Ω . Five seconds after the start the pilot had not ignited as seen in Figure 151. After the oxygen and fuel valve had been open for 2.2 sec, ignition took place. A very loud explosion was heard followed by the sound of normal combustion exhaust noise. The diffuser was seen to start leaking badly one to two sec after ignition and the test was aborted. Chamber pressure, pilot chamber pressure, venturi throat pressure, and combustor coolant temperature are displayed in Figure 151. The peak recorded voltage was 1073 volts with a 10 Ω load.

5. DISCUSSION AND CONCLUSIONS OF POWER TESTING

At no time during the testing was there a positive control or measurement of fuel flow. This was a result of the powdered fuels entering the bearings of the various turbine meters used and binding the impellers. Several types were tried and some success was obtained when using the emulsified CsNO_3 , but it must be remembered that the powdered seed in this case was sieved to -100 mesh or 150 μm . This is too large a particle to enter the bearings and hence the system works until enough

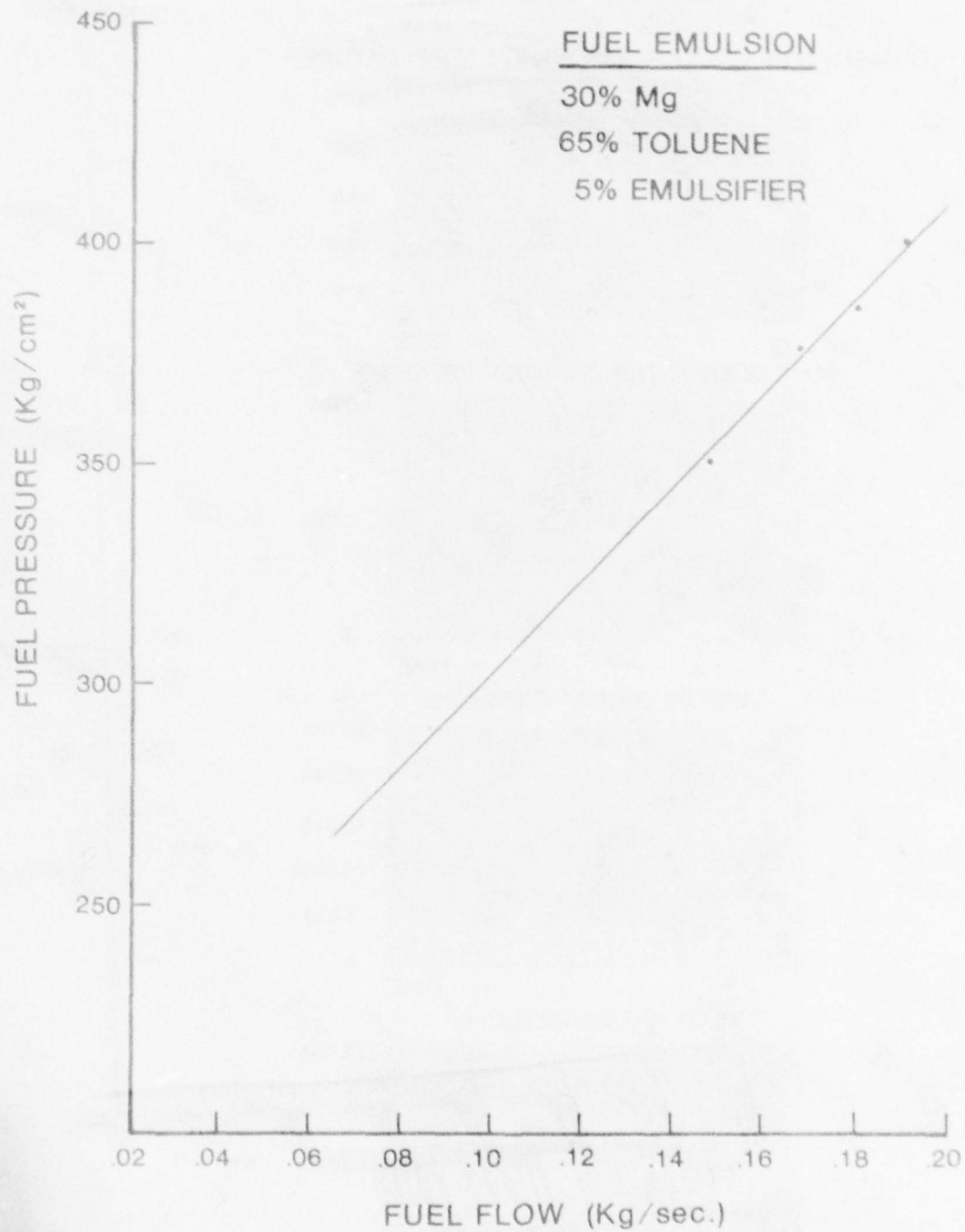


Figure 150. Fuel System Calibration Curve for Emulsified Toluene/Magnesium Fuel

HEF- 19

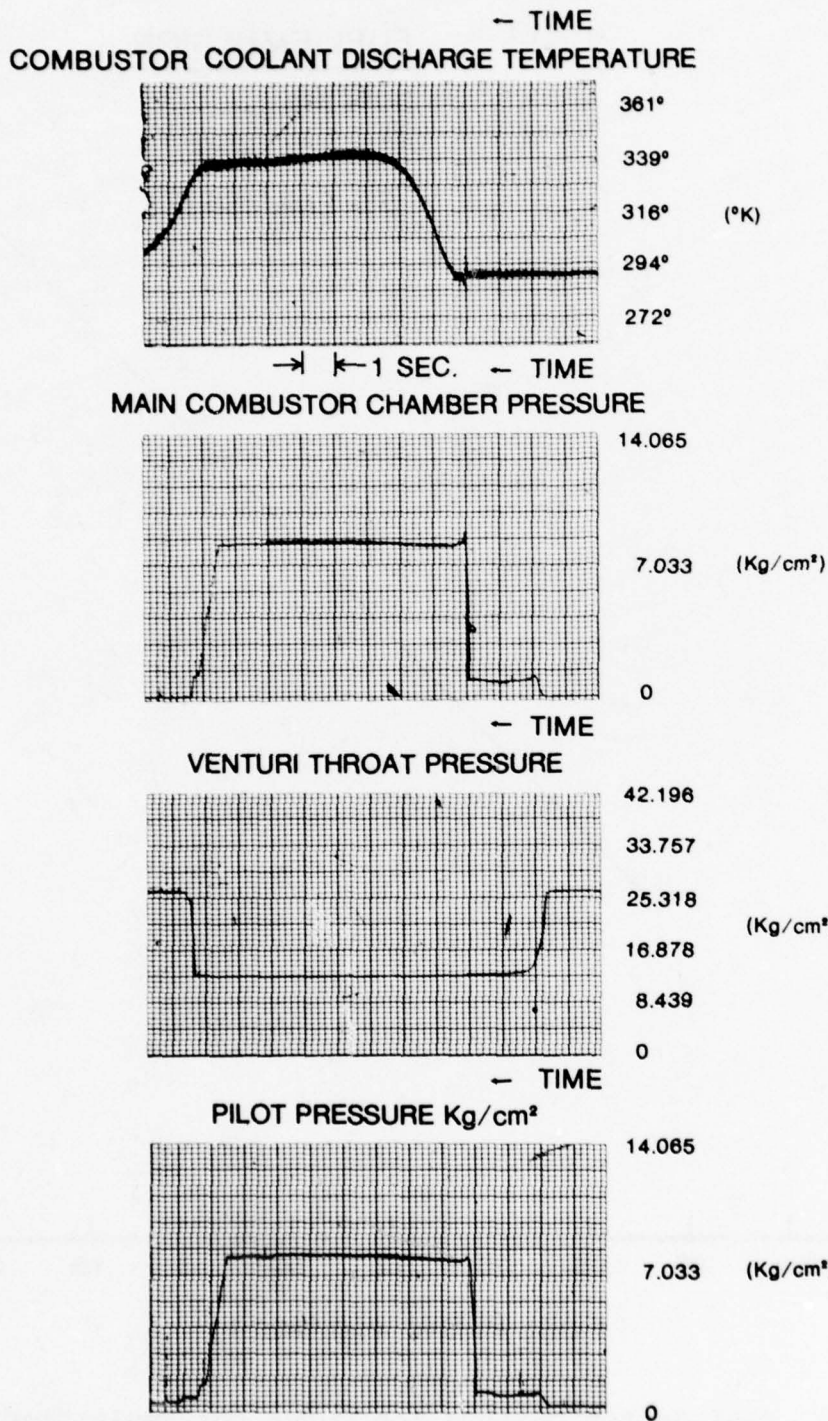


Figure 151. Power Test Run HEF-19 Combustion Parameters, Fuel - Emulsified Toluene/Magnesium, O/F at 2.72, Load Resistance 10Ω

smaller particles will still accumulate and bind the bearings. As a result, flow control, measurements, and calculation of specific power generated can only be considered to be better than guessing.

Initially the flow of oxygen was suspect, but although accurate rapid control was not possible, accurate measurements were made after modifying the venturi and test procedure.

The seeded fuel performed quite well, reducing power signature noise by at least 30% and removing nearly all of the large voltage spikes. The use of smaller particle seed should improve performance even further.

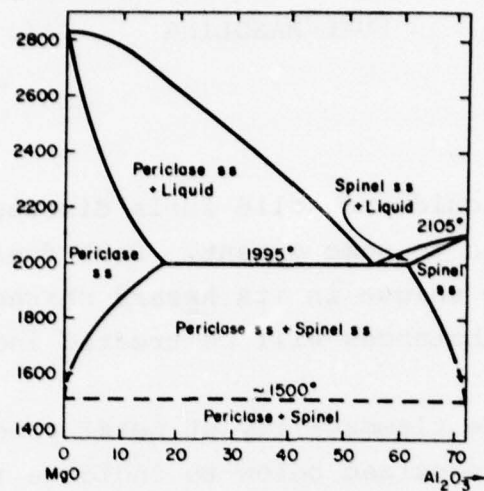
The use of aluminum powder emulsified into the fuel did appear to increase specific power, but although the numbers have been presented they are suspect since the mass flow measurements are suspect. The use of powdered metal additives also makes closer demands on O/F tolerances with the result that the techniques used here are not nearly accurate enough or easy enough to control. The use of magnetic flow meters is one possibility but with the use of waterless emulsions they become ineffective. Magnetic resonance meters have been investigated and have been found to be unusable with the metallic additives. Sonic meters are possible techniques for measurement. Further study of emulsion rheology and flow characteristics through venturis could prove to be quite productive.

It is apparent that the use of small particle seed and metallic particle additives can improve MHD power production. The use of emulsification techniques solve the problem of suspending these materials in a carrier fuel satisfactorily but create control and measurement problems which must be investigated further.

The KIVA-I combustion chamber has a relatively long residence time for the products of combustion, ~ 10 m sec. This characteristic, in conjunction with the high melting temperatures of some high energy fuel products of combustion, results in precipitation and solidification of a varying thickness slag layer in the combustion chamber. The fact that slag is deposited is not necessarily an adverse situation, since the slag layer acts as an insulator and reduces heat loading, but a building which starts to block the nozzle could never be construed as favorable. Obviously it would be desirable to control the slag layer thickness. The simplest means of controlling the slag layer thickness is melting temperature control of the slag.

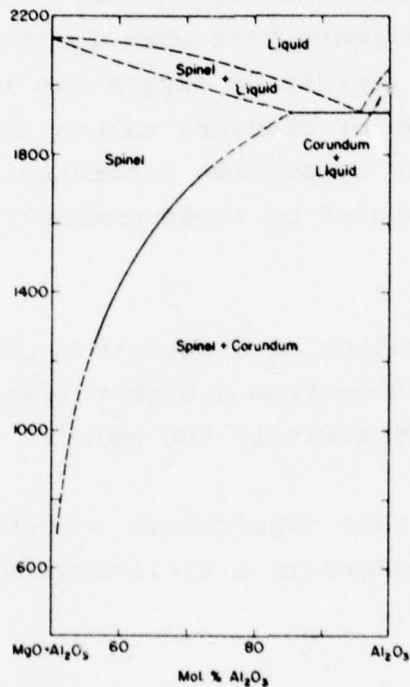
The result of mixing two or more materials is generally a reduction of the melting temperature of the resulting mixture to less than that of either constituent alone. The implication is clear that the use of binary or ternary eutectic compounds could be an effective means of slag layer control. Observing Figure 152 it can be seen that the addition of a small amount of Mg to Al thus forming MgO in the combustion chamber to mix with Al_2O_3 would decrease the resultant liquidus temperature of the $\text{MgO-Al}_2\text{O}_3$ mixture when compared to that of Al_2O_3 alone. Such an addition too, might result in a more stable burning fuel in the combustion chamber if the Atlantic Research Studies[15] previously mentioned are correct. The result might well be a higher output fuel, due to better combustion, and one with fewer slagging problems than would be encountered when using either Mg or Al alone as additives. A similar result might be expected when used with boron and facilitate the use of high boron content fuels.

MgO-Al₂O₃



System MgO-MgO-Al₂O₃.

A. M. Alper, R. N. McNally, P. G. Ribbe, and R. C. Doman, *J. Am. Ceram. Soc.*, 45 [6] 264 (1962).



System MgO-Al₂O₃-Al₂O₃.

After Della M. Roy, Rustum Roy, and E. F. Osborn, *J. Am. Ceram. Soc.*, 36 [5] 149 (1953).

Figure 152. MgO - Al₂O₃ Phase Diagrams Showing Eutectic Points

Section VI

FUEL HANDLING

1. GENERAL

The various liquid and solid fuels discussed here are all hazardous substances to some extent. Each fuel has characteristics which can be unique in its hazard character; therefore, each of the fuel substances will be treated individually.

Findings on the flammability of metal powders by the Bureau of Mines[52] are synopsized below to indicate the hazardous nature of metal powders.

Tests of different kinds on small piles or layers of powder to determine conditions under which they would ignite have been made. These tests indicate that when ignited in a pile the powders will burn as rapidly as oxygen can reach them but will not produce explosions or pressure unless the pile is disturbed in some manner, either by outside intervention or because of energy and force liberated by rapid combustion of considerable quantities of powder.

Minimum concentration of dispersions of powders in air needed to permit ignition from a high-voltage, low-energy spark ranged from 20 to approximately 500 gm/m³.

The wall temperature required in a heated furnace to ignite dispersions of the powders in air; zirconium excepted, ranges from 315° C to 900° C.

The minimum energy required for ignition by spark of dispersions of a number of powders is so small as to be insignificant in practice. If the ignition temperature is reached there can hardly fail to be sufficient energy for ignition.

There is a wide range of values for pressure development and rate of development. The highest pressure was measured during the explosion test of a magnesium-powder dust cloud, when a value of 5.06 kg/cm^2 was recorded. The maximum rate of pressure rise in this test was nearly $351 \text{ kg/cm}^2 \text{ sec}$ and only 0.016 second elapsed between the ignition of the dust cloud and the instant when the maximum pressure was reached. Obviously an explosion of this intensity would result in complete destruction of equipment and plant structure. Carefully designed relief vents of large area located very close to the ignition source might reduce the pressure and destruction somewhat, but they could not possibly entirely prevent damage in such a rapidly developing explosion.

The metals listed in what is believed to be a fair arrangement of decreasing order of inflammability are: zirconium, magnesium and its alloys, aluminum, and titanium, being the most hazardous, reduced and carbonyl iron, manganese, zinc, silicon, tin, and antimony form an intermediate group. Cadmium, copper, chromium, lead, and milled iron have a low order of inflammability and explosibility.

A wide range of behavior was found in tests made to determine the inflammability of dispersions of the powders in atmospheres of reduced oxygen content. Carbon dioxide was used as the diluent for air in a series of tests. Titanium, zirconium, and magnesium and its alloys all ignited in pure carbon dioxide. The maximum allowable oxygen content of the atmosphere ranged from 3 to 18 percent with a number of the other metals. When nitrogen was used, the permissible oxygen content was higher, and no dispersion ignited in pure nitrogen by spark ignition in these tests. Helium, when used as a diluent gas allowed only slightly higher oxygen content than nitrogen but not sufficiently so to justify its use in other than special cases.

In a number of explosion tests several powders developed strong pressure in nitrogen-air mixtures containing only 1 or 2% more oxygen than the amount that would have prevented ignition altogether.

Some of the tests have a bearing on fire hazards. The minimum ignition temperature of quiescent layers of dust in general are below the ignition temperature of dispersions but there are exceptions. Minimum energy required for ignition of dust layers is minute indeed in the case of a number of the powders.

Quiescent layers of zirconium, magnesium, and magnesium alloys burned vigorously in commercial carbon dioxide and nitrogen when heated sufficiently. Aluminum, titanium, chromium, copper, iron, lead, manganese, silicon, tin, and zinc reacted in some manner in one or the other of these gases provided that their temperature was raised sufficiently.

2. MAGNESIUM POWDERS

The following are some of the recommendations of the National Fire Protection Association in handling, storage, and fire protection for magnesium powder.

Burning magnesium powder produces a flame temperature of about 3900°C. Such fires cannot be extinguished by the application of water, carbon dioxide, foam, carbon tetrachloride or other common fire extinguishing agents. Application of these materials may greatly intensify the burning or cause violent explosions.

Fine magnesium powder can be readily ignited by a spark, flame, or frictional heat sufficient to raise its temperature to about 482°C. When ignited while in suspension in air it

will explode violently. The high pressure developed and the very rapid rate of pressure rise emphasize the importance of adopting all possible protective measures wherever magnesium powder is processed or handled.

Note: The U.S. Bureau of Mines reports that milled magnesium powder has an explosibility index greater than 10, in common with aluminum powder, thorium and thorium hydride powders, titanium powder, uranium and uranium hydride powders, and zirconium powder. It requires 40 millijoules of energy to ignite a dust cloud and as little as 0.8 millijoules to ignite a static layer. The minimum ignition temperatures for a dust cloud and static layer are 538°C and 427°C respectively. Minimum explosive concentration in air is 25 gm/m³.

In areas where powders are processed or handled all electrical wiring and equipment shall conform to the National Electrical Code, NFPA No. 70. All areas of buildings where powders are used shall be considered Class II Division 1 locations under Articles 500 and 502 of the National Electrical Code.

Attention should be specifically directed to the requirements of the National Electrical Code, NFPA No. 70 for the location of transformers, type and location of motors, generators, and their control equipment, cables, fuses, circuit breakers, conduits and lights of all types.

Grounding machinery to remove static electricity produced in powder manufacture and collection is vital for safety. It should be thoroughly done according to Recommended Practice on Static Electricity, NFPA No. 77, for all machinery, fans, ducts, screens, collectors, and other equipment.

Ignition of magnesium powder can be prevented in laboratory apparatus when argon, neon, or helium are used to create an

inert atmosphere. Practical and economic problems have limited their use in commercial operation. Nitrogen gives partial protection, but it will react directly with magnesium when the source of ignition is strong. Carbon dioxide reacts readily with magnesium and should not be used. It is necessary, therefore, to give particular attention to the elimination of all possible sources of ignition, and the following general recommendations and requirements covering ignition hazards have been prepared to supplement the rules listed.

Hot air heating should not be employed. The stirring action of a forced hot air heating system might easily be dangerous as it would keep the fine dust in suspension. Heating by easily cleaned steam or hot water coils is satisfactory and safe.

Only minimum-sparking tools shall be used in cleaning, repairing or adjusting magnesium powder equipment. Tool materials that collect static charges should be avoided. Friction must be avoided or minimized.

The principal precaution to observe in storing magnesium powder is to avoid storage in open bins or other open containers and to limit the storage in any one area to the smallest feasible amount.

Note: This places no restriction upon the storage of magnesium powder in sealed containers regarding quantity or distance insofar as the explosion hazard is concerned. Precautions should be observed with regard to the fire hazard involved.

Magnesium powder shall be kept free of water or moisture.

Magnesium powder shall be protected against any form of heat capable of raising the temperature to the ignition point.

Finely divided magnesium being stored for short periods shall be kept in closed containers to protect it against possible ignition.

The finished product shall be packed in cans, drums, or moisture-proof containers which can be closed to prevent accidental spilling during handling.

All containers in which magnesium is stored shall be plainly labeled.

Fire protection for magnesium powder is largely a fire prevention problem. Small magnesium powder fires can be extinguished but no satisfactory method of extinguishing large fires is known. It is essential, therefore, that magnesium powder fires be detected in the incipient stage and the proper extinguishing procedure followed.

Burning magnesium powder cannot be extinguished by the application of water, carbon dioxide, foam, carbon tetrachloride or common fire extinguishing agents. These materials when applied to a magnesium fire may stimulate the burning and can cause a strong explosion. To avoid the possibility of extinguishers of the type mentioned being used by persons unfamiliar with the hazard, it is recommended that all such extinguishers be excluded from areas in which magnesium fires may occur.

Sprinkler systems should not be installed in buildings where magnesium powder constitutes an important hazard.

Violent disturbance of a magnesium powder fire by the application of extinguishing agents, drafts of air, or movement

of the surface on which the fire is burning shall be avoided. Magnesium powder propelled into the air under such conditions will explode violently.

Small fires in dry magnesium powder can be controlled by carefully spreading dry graphite, dry magnesium foundry flux or clean dry cast iron chips on and around the fire. If air reaches the fire through this covering the magnesium will continue to burn and the mass may remain hot for a long time.

Other effective extinguishing agents for magnesium fires are marketed as proprietary compounds. These are generally in powder form and are applied by means of scoops, shovels, tubes or specially designed distributing apparatus. Their use is generally limited to fires of small or moderate size which can be approached closely enough to permit the proper manual application of the extinguishing medium.

It should be noted here that magnesium burns with an intensely blinding white light making the exact location of even a very small fire difficult to pinpoint without welding type goggles. The application of such fire fighting or retardant materials is therefore greatly hampered.

Extinguishing a magnesium powder fire may be a very dangerous undertaking because of the possibility of an explosion occurring when burning powder is disturbed. For this reason many operators prefer to seal a magnesium fire in the room in which it originates and allow it to burn itself out.

Good housekeeping is essential and all possible precautions shall be taken to insure safe operation.

Smoking materials, lighters and matches shall be prohibited.

Special clothing for employees in magnesium powder handling plants is recommended. Employees clothing should be easily removable, kept clean and free from powder. Leather or other smooth clothing from which the dust can be brushed off readily may be worn. Smooth canvas or denim suits can be made fire retardant by treatment with chemicals. Clothing made from fibers known to accumulate static charges, such as silk, nylon, etc. should be prohibited. Clothing should be made with non-ferrous snap fasteners and should be made without pockets or cuffs. Wearing of woolen or fuzzy outer clothing should be prohibited. Shoes worn by employees or anyone entering powder buildings should have nonsparking soles and heels fastened with wooden pegs, copper nails, or adhesive. The wearing of shoes with exposed steel parts shall be prohibited.

Inhalation of magnesium particles $<10\mu\text{m}$ represents a serious lung damage hazard and hence the use of fine filter dust masks are necessary.

3. ALUMINUM POWDERS

Conditions similar to magnesium powders exist with aluminum powders and the same recommendations hold true. Rules to be recognized are as follows:

Avoid any condition that tends to suspend or float powder particles in the air.

Avoid every possible action that generates static electricity, creates a spark, or otherwise results in reaching the ignition temperature.

Where generation of static electricity may occur, utilize every means to minimize it and dissipate it to avoid a spark discharge.

Take steps to limit the size of a fire or explosion and to hold any resulting damage to the very minimum.

Soft, fine bristled push brooms and lightly oiled sawdust are recommended for cleaning dusty floors. (Standard explosion-proof vacuum cleaners have caused fires which were believed to result from static.)

Locate electric motors and as much electrical equipment as possible outside operating rooms. Only lighting and control circuits should be in operating rooms. All electrical equipment must meet the National Codes for explosion-proof installations. This includes flashlights, portable power tools, and other devices.

Use NO nonconductive material for handling or containing aluminum powders. Use only nonsparking metal scoops for handling powder. The handling should be slow and deliberate to hold dusting to a minimum.

Use nonsparking metals wherever possible.

Machinery used in mixing operations should be equipped with outboard dust-proof bearings which should be kept well lubricated. Excessive temperature rise in any part should call for an immediate shutdown. If a shaft or other part should freeze on a bearing surface, no attempt should be made to loosen the part by force (by a hammer blow, for example).

Use liberal applications of a heavy grease on all exposed ring or bevel gears to minimize the danger from aluminum powder-containing materials.

Any bearings on machines inside operating rooms should be well protected by good seals.

All employees should wear conductive shoe soles and heels, or special anti-static boots which will effectively ground each person.

All floors and walls up to a height of 3 feet should be coated with a conductive nonsparking material. ("Ceilcrete B" is a conductive floor coating made by Ceilcrete Company, Inc., 4832 Ridge Road, Cleveland, Ohio.) (Conductive rubber coating material is available from Goodall Rubber Company, Whitehead Road, Trenton, N. J.)

Three types of suitable nonsparking, conductive floors are: (1) magnesite flooring installed over a wood or concrete base with properly grounded metal grids placed beneath the floor surface; (2) emulsified asphalt composition flooring with a conductive aggregate, also laid over grounded metal grids; and (3) industrial graphite tile made of a conductive mastic, the edges of the tile being melted together with a hot iron on installation to provide a continuous conductive surface. No metal grid is required, the tile itself being grounded at several points.

All metal in the buildings must be grounded. This includes not only the machines and equipment itself but also all metal window and door frames, structural beams and other elements. Such grounding connections should be bonded and regularly checked for resistance.

All movable equipment such as drums, containers, and scoops must be grounded at all times by use of clips and flexible ground leads.

Do not use wooden or fiber containers. Use only properly grounded metal containers. When employed with a conductive floor, they will permit more rapid dissipation of static charges.

After pouring or scooping powder from one machine or container into another, be sure to allow the powder to remain at rest for a period of time during which the static charges may dissipate themselves. Considerable time may be required for fine flake powders. Likewise, mixers should be allowed to rest for a period before removing the mixture, permitting static charges to be dissipated or conducted to the ground. A simple electroscope can be used to determine when a mixture is free of static charges.

Keep all drums sealed. Both flake and granular aluminum powders are shipped in sealed drums with fully removable heads. Store these unopened in a separate area wherever possible. If stored with such chemicals as nitrates or others of similar character, a fire from any cause would present a most serious problem.

Whenever a drum of aluminum powder is opened for loading or inspection, it should be closed and resealed as quickly as possible. This not only assures greater safety against fire from external cause but prevents water entrance from the air. In one instance, a sealed drum of flake powder withstood an explosion and subsequent fire without ignition of the contents of the drum.

All containers in work areas should likewise be closed and sealed. Only those in actual use should be open at any time.

A minimum of aluminum powder should be in operating rooms, the balance being kept in outlying approved storage areas.

Note: The pressure rise of an aluminum dust explosion is extremely rapid and necessitates large relief areas if they are to be effective.

Keep powder DRY. Water from any source, even condensate on equipment, will at times cause a reaction liberating hydrogen.

All equipment should be so located that the operator has a free path to an outside door without a mixing bench, mixer, or other object being between him and the door.

It is true that dry sand, carefully placed to cover a pile of burning aluminum powder, will smother the flame. But in the excitement attending such a fire, there is great danger that the sand will be thrown or shoveled onto the mass, throwing the powder into the air. There have been several cases where relatively harmless fires were changed into serious fatal explosions in this manner.

Consequently, the safer and more prudent rule is to instruct employees to walk out of the building.

NEVER USE ORDINARY FIRE EXTINGUISHER, WATER, CARBON TETRACHLORIDE, FIRE FOAM, CARBON DIOXIDE, OR SIMILAR EXTINGUISHING AGENTS ON ALUMINUM POWDER FIRES. Furthermore, a fine spray of water from a stirrup pump, such as used by civilian defense workers on incendiary bombs, should NEVER be used on aluminum powder fires. DO NOT HAVE FIRE EXTINGUISHERS AVAILABLE WHERE ALUMINUM POWDER IS STORED OR USED. As previously mentioned, their use can turn a small fire into a disastrous explosion.

AD-A060 156 SYSTEMS RESEARCH LABS INC DAYTON OH AEROSYSTEMS RESE--ETC F/G 21/4
HIGH ENERGY MHD FUELS DEVELOPMENT PROGRAM. (U)
APR 78 R E ECKELS F33615-75-C-2043

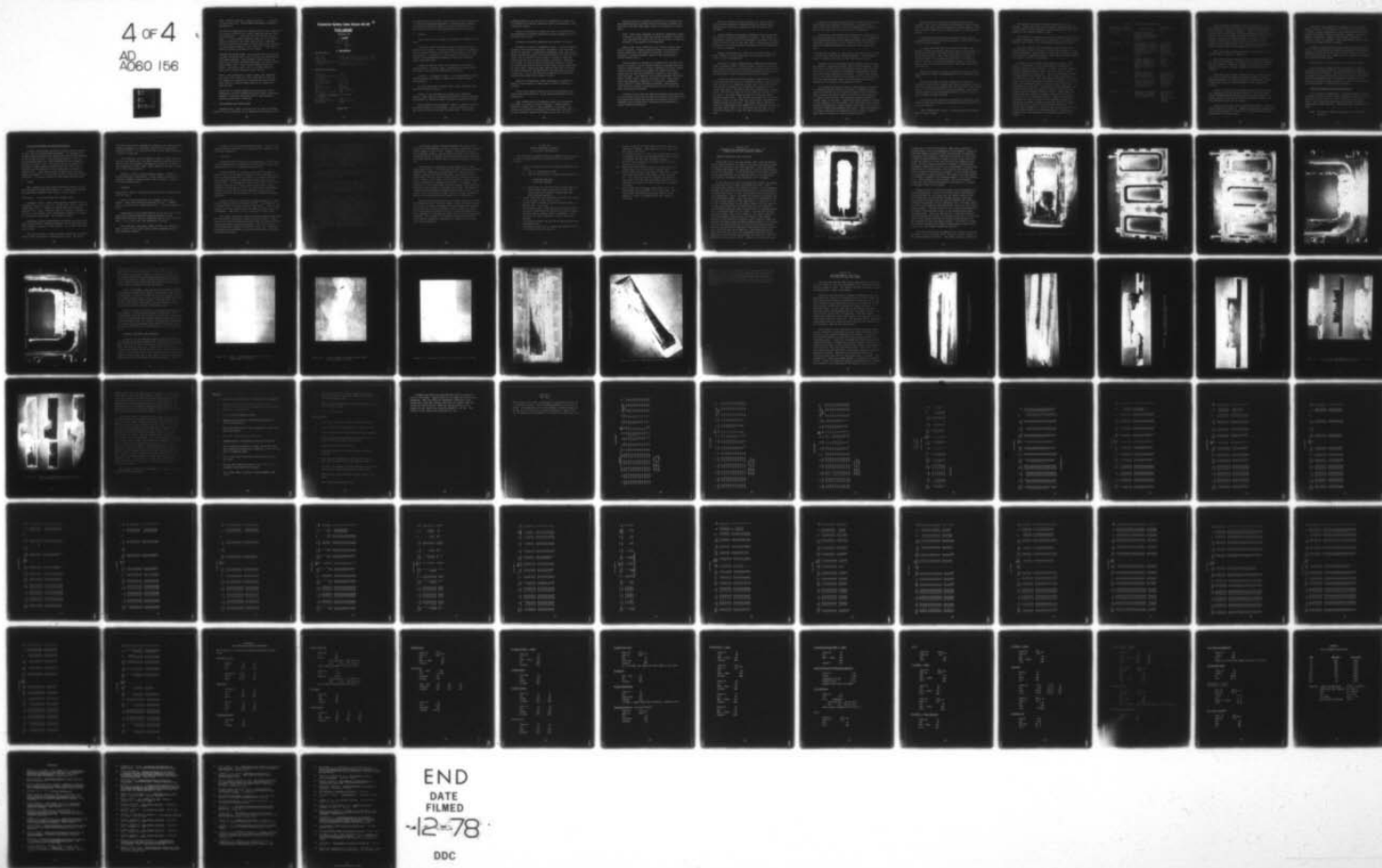
UNCLASSIFIED

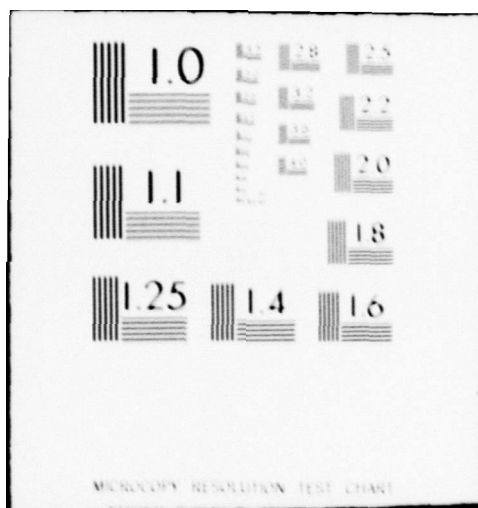
AFAPL-TR-78-10

NL

4 of 4

AD
A060 156





RULE: Wherever possible, isolate the fire . . . then let it burn itself out. DO NOT EXPOSE PERSONNEL IN TRYING TO EXTINGUISH IT.

The ignition temperature of aluminum dust is very indefinite. It has been reported that a photo flash bulb has set off a dust explosion . . . even when the bulb did not crack or burst. It is of utmost importance that local fire departments be informed of the above precautions. Also they should be provided with maps or charts showing the location of any aluminum powders or other chemicals. Such charts should be readily available at all times.

CLOTHING AND LOCKER ROOMS: The clothing worn by operating personnel should be kept clean and free from aluminum dust by frequent washing. Many companies supply shirts and slacks to both male and female employees, the slacks being made without cuffs. These clothes should be made of cotton. Avoid any nylon, silk, or silklike materials which might possibly generate static charges.

There is the possibility of great danger when employees wear their work clothes to their homes before changing. For instance, a spark from a cigarette may easily cause fatal burns to a person whose clothing is filled with aluminum dust.

Inhalation of aluminum powders having particles $<10\mu\text{m}$ represents a serious respiratory hazard; hence, dust masks capable of filtering such particles or self-contained breathing apparatus is required.

4. MISCELLANEOUS FUEL PARTICULATES

Although boron, carbon, and coal are not nearly as susceptible to fire or explosion as are magnesium and aluminum, these

Chemical Safety Data Sheet SD-63

TOLUENE

ADOPTED MAY, 1956

1. NAMES

Chemical Name: Toluene
Common Name: Toluene
Toluol
Methylbenzene
Formula: $C_6H_5CH_3$

2. PROPERTIES

2.1 GRADES AND STRENGTHS

Reagent Grade (Not more than 1°C distillation range, incl. 110.6°C)
Nitration Grade (Not more than 1°C distillation range, incl. 110.6°C)
Industrial Grade (Not more than 2°C distillation range, incl. 110.6°C)
Industrial Grade for Use in Paint,
Varnish, Lacquer, etc. (Distillation Range: 107.5°C to 112.5°C)
90/120 Grade (Distillation Range: 100°C to 150°C)

2.2 PROPERTIES AND CHARACTERISTICS

Physical State Liquid
Explosive Limits 1.27 to 7.0
(per cent by volume in air)
Flash Point 4.4°C (40°F)
(closed cup)
Autoignition temperature 552°C (1026°F)
Boiling Point (pure). 110.6°C (231°F)
Color Clear
Corrosivity Noncorrosive
Melting Point (pure). -95°C (-139°F)
Odor Aromatic, benzene-like
Specific Gravity @ 20°C (68°F). 0.866
(Water = 1)
Vapor Concentration in Saturated.
Air @ 25°C (77°F) and 760 mm
pressure 3.68% (36,800 ppm)
Vapor Density (air = 1) 3.14
Vapor Pressure 25°C (77°F). 28 mm Hg (0.541 psia)
Threshold Limit 200 ppm

Figure 153.

all represent serious hazards and should be treated accordingly. If operating procedures applicable to magnesium and aluminum are adopted as standard practice with all particulate fuel additives the safety of such operations cannot be questioned.

5. TOLUENE

Liquid fuels can be equally as dangerous as powdered solid fuels.

Industrial grade and 90/120 toluene contain significant quantities of benzene. The 90/120 grade may contain as much as 25% and this may result in as much as 50% benzene in the vapor concentration. Information on the hazards of benzene is contained in the Manufacturing Chemists' Association chemical safety data sheet SD-2.

Industrial hazards result from inhalation of excessive concentrations of toluene vapor, prolonged skin contact with the liquid, and liquid contamination of the eyes.

Toluene is a flammable liquid. Fire extinguishers include carbon dioxide, dry chemical, vaporizing liquids and foam extinguishers.

At room temperature, toluene emits vapors which may form explosive mixtures with air.

Toluene is not regarded as a highly toxic chemical. However, under certain circumstances exposures may be hazardous and measures to minimize exposure should be routinely followed.

Acute exposures cause headache, nausea, giddiness and loss of consciousness in this sequence. Local irritative effect upon the nose, throat and eyes has been noted. Acute toxic

symptoms generally are the result of inhalation of vapor, and if exposures are extreme, death may ensue from paralysis of the respiratory center.

Chronic intoxication is known to exist in instances where concentrations of toluene exceed the current threshold limit of 200 parts per million.

No specific warning properties are ascribed to toluene.

Toluene is a Class II flammable liquid. It emits flammable vapors at room temperatures which, diffused in air, may form explosive mixtures. It should be remembered, also, that toluene vapors are more than three times the weight of air and they may "flow" and be ignited by open flames or sparks at locations remote from the site at which toluene is handled. Therefore, all sources of ignition must be eliminated from the area and all welding and cutting should be done under careful supervision and only after a permit has been obtained from the fire chief or safety supervisor and approved by the supervisor in charge of the area. Gas or oil-fired units should be eliminated or isolated from areas where toluene is used.

Under no circumstances should employees be permitted to smoke or carry matches in areas where toluene is stored or handled.

Electrically powered heating and lighting equipment may cause fires and explosions, as may sparks generated by static electricity.

High concentrations of hazardous vapors are discharged from open or partially closed containers. Open equipment should be avoided, but if such equipment is necessary, the working area should be protected with mechanical ventilation to prevent hazardous vapors from escaping into the work area.

General ventilation should be sufficient to maintain work-room concentrations of toluene below the maximum allowable concentration (200 ppm) when these rooms are occupied for 8 hours daily.

Note: Ventilation necessary to maintain atmospheric concentrations of toluene below the maximum allowable concentration precludes the possibility of the existence of explosive mixtures in the general room atmosphere.

Sparks from static electricity will ignite toluene vapor and air mixtures. Toluene flowing through a line generates static electricity, and effective grounding of the line is necessary to prevent possible ignition (See NFPA pamphlet, "Static Electricity.")

Before toluene is poured or discharged from one metal container to another, the two vessels should be grounded and electrically interconnected. All metal surfaces with which toluene comes in contact should be grounded and bonded with heavy copper wire so that the resistance to ground is not greater than five ohms. This applies to all metal equipment and piping such as tanks, mixers, stills, and pipe lines. Where drive belts are necessary, conductive "V" belts are recommended. Pulley and drive shafts should be grounded. Nonconductive drive belts are liable to accumulate an electric charge and their use should be avoided.

Toluene is not a serious industrial health hazard when its use is properly controlled through the application of engineering principles and workers are provided with proper protective equipment and are effectively instructed and supervised in proper handling procedures.

Safety in handling toluene depends, to a great extent, upon the effectiveness of employee education, proper safety instructions, intelligent supervision and the use of safe equipment.

Workers should be thoroughly informed of the hazards that may result from improper handling of toluene. They should be cautioned to prevent spills and thoroughly instructed regarding proper action to take in case they occur. Each employee should know what to do in an emergency and should be fully informed as to first aid measures.

Workers should know the locations of safety showers, eye baths, bubbler drinking fountains, or the closest source of water for use in emergencies.

Cup-type or rubber framed goggles, equipped with approved impact resistant glass or plastic lenses, should be worn whenever there is danger of toluene coming in contact with the eyes. Goggles should be carefully fitted by adjusting the nose piece and head band to ensure maximum protection and comfort.

Industrial Canister Type Gas Masks, equipped with full face pieces and approved by the U.S. Bureau of Mines, fitted with the proper canister for absorbing toluene vapor, will afford protection against concentrations of toluene not exceeding 2% by volume when used in accordance with the manufacturer's instructions. The oxygen content of the air must not be less than 16% by volume. The masks should be used for relatively short exposure periods only. They may not be suitable for use in an emergency since, at that time, the actual vapor concentration is unknown and may be very high. The wearer must be warned to leave the contaminated area immediately on detecting the odor of a harmful vapor; this is an indication that the mask is not functioning properly or that the vapor concentration is too high.

Chemical Cartridge Respirators may be used to avoid inhaling disagreeable but harmless concentrations of toluene vapor. These respirators, however, are not recommended for protection where toxic quantities of toluene may be encountered.

Sustained or intermittent skin contact with liquid toluene may produce dermatitis at the site of contact. It is imperative that contaminated clothing be removed promptly and laundered or thoroughly dried before re-use. Affected areas of the body should be washed thoroughly with soap and water (except the eyes).

Clothing made of rubber or other impervious material may be worn to protect the body against toluene splashes. These garments must be cleaned inside and out each time they are used.

Suitable fire extinguishing agents include carbon dioxide, dry chemical, vaporizing liquids, and foam extinguishers. Water spray can be used to control unconfined toluene fires but ordinarily it is not effective for complete extinguishment unless the surface area involved is very small. In open tank toluene fires, solid hose streams tend to scatter the liquid and spread the fire, whereas water spray cools the burning surface and excludes air to control or extinguish the fire.

All precautions must be taken to guard against health and fire hazards wherever toluene is handled. Nonsparking tools should be used and the area should be posted with NO SMOKING or other appropriate warning signs as required by the operation. If leaks or spills occur, only properly protected personnel should remain in the area. Leaking containers should be removed to the outdoors or to an isolated, well ventilated area, and the contents transferred to other suitable containers. All spills should be flushed away promptly with water. Excessive quantities of toluene should not be permitted to enter drains or sewers where there is danger of vapors becoming ignited.

Before drums are opened they should be supported and grounded. The latter can be done by fastening a screw clamp to the rim of the drum, and connecting this clamp through No. 4 AWG extra flexible copper wire to a water pipe or to any permanent ground.

Drums should be opened with nonsparking tools and the fittings should never be struck with tools or other hard objects which may cause sparking.

To remove the body plug from a drum of toluene, the operator should wear goggles and use a bung or plug wrench. He should place the bung up, stand to one side, and face away during the operation. After the plug starts to loosen, it should be given not more than one full turn. If internal pressure exists, it should be allowed to escape to the atmosphere. Then only should the operator loosen the plug further and remove it.

When filled drums or other containers are stored indoors, they should be stored in noncombustible, well ventilated structures.

When filled drums or other containers are stored in separate storage rooms, trapped floor drains should be provided. The floors should be pitched to the drains and the latter should lead to a safe location and be properly trapped. Only those persons properly protected should attempt to clean up areas in which toluene has been spilled.

All storage areas should be provided with automatic sprinklers or some other adequate extinguishing system desirable for interior storage.

Other combustibles, acids, or oxidizing materials should not be stored nearby.

The storage of toluene in glass containers is to be avoided. Safety cans with pouring outlets equipped with tight-fitting caps or valves normally closed by springs and with fire baffles in the outlets should be used.

The disposal of toluene by burning or discharge by drainage to natural waterways should only be conducted in accordance with Federal, state and/or local regulations regarding pollution.

Provision must be made to prevent toluene spills from entering public sewers or drains in sufficient amounts to cause explosion hazards. Connections to such sewers or drains should be provided with separator boxes or other approved means whereby the entry of toluene is precluded.

Toluene is not a highly toxic chemical; however, under certain circumstances it can be hazardous and measures to minimize exposures are necessary. Toluene is readily absorbed from the gastrointestinal tract, the lungs, and to a small extent, through the intact skin. Part of the absorbed toluene is eliminated in the expired air, but a large percentage is excreted in the urine. The only industrial hazards of significance result from inhalation of excessive concentrations of the vapor, prolonged skin contact with the liquid, and liquid contamination of the eyes. In high vapor concentrations, such as may be encountered in tanks or partially closed vessels, toluene exerts a powerful narcotic action. Under these conditions and with sustained exposure, death may ensue from paralysis of the respiratory centers. Vapors in subnarcotic concentrations, but in excess of the maximum allowable concentration (200 ppm), produce varying but usually transitory manifestations of central nervous system disturbance. The liquid, when splashed into the eyes, may produce opacities and corneal burns unless it is removed promptly. Dermatitis is produced only after repeated or sustained contact with the liquid.

TABLE 4. TOLUENE VAPOR RESPONSES

Toluene Vapor Concentration	Time of Exposure	Probable Response	Probable After Effects
50-100 ppm	8 hr	No serious effects. Slight drowsiness and possibly slight headache in the unconditioned workers.	None.
200 ppm (MAC)	8 hr	Unconditioned workers may complain of fatigue, some muscular weakness and burning, itching or "crawling" skin. There may be complaints of headache and some nausea.	Unconditioned workers may complain of fatigue of short duration and a few may suffer restless sleep.
300-400 ppm	8 hr	Varying degrees of fatigue and headache. Varying degrees of muscular weakness, mental confusion and slight incoordination.	Fatigue lasting several hours and insomnia.
600 ppm	3 hr	Marked fatigue and mental confusion, exhilaration, headache, and dizziness.	Fatigue and weakness lasts several hours. There may be complaints of nausea and nervousness. Many suffer headache.
	8 hr	Definite mental confusion, considerable incoordination and staggering gait.	
800 ppm	3 hr	Nausea and pronounced confusion. Considerable incoordination and staggering gait.	Nervousness and fatigue may last several days. There may be marked insomnia.

Common subjective responses, such as recognition of odor and irritation of the eyes and nose, cannot be relied upon as warning signs of excessive exposure. Olfactory fatigue and tolerance occurs early and conditioned operators usually do not perceive the odor or mildly irritative processes. The simple effects on the central nervous system, such as persistent headache, giddiness or undue fatigue are, however, useful criteria for the identification of concentrations of toluene in excess of safe limits for prolonged periods of exposure.

There have been no reports of death attributable to the ordinary use of toluene in industry.

Toxic manifestations resulting from a single exposure will vary with the atmospheric concentration of toluene encountered and the duration of exposure. Table 3 indicates the probable response of humans to various atmospheric concentrations of toluene.

Acute exposures of short duration and at infrequent intervals can be tolerated without irreversible damage. However, sustained exposure to concentrations of toluene which produce narcosis may result in fatal paralysis of the respiratory centers.

Contact of the skin with liquid toluene will often result in a temporary burning stinging sensation. Occasional accidental contamination of the skin with the liquid presents no serious hazard if the affected areas are washed promptly with soap and water until free of toluene.

Contact of the eyes with liquid toluene results in burns of varying degrees of severity. Immediate flushing of exposed eyes with copious quantities of water for 15 minutes minimizes the possibility of serious injury.

Continuous daily exposures to concentrations of toluene vapors in excess of 200 ppm may give rise to a clinical picture of chronic toluene intoxication. Such cases may show varying degrees of fatigue, general nervousness, insomnia, and loss of appetite and weight. However, upon complete cessation of exposure - which is indicated - such individuals, usually, soon regain their normal levels of health.

Frequent or sustained skin contact with liquid toluene may result in the development of dermatitis because of the defatting properties of toluene as well as its local irritative action. Protective creams are not a substitute for avoidance of excessive skin contact by other means.

Sensitization to liquid toluene is not known to occur.

First aid will ordinarily only be required in cases of ingestion or narcosis resulting from inhalation of very high concentrations of toluene. The need for first aid treatment for exposures involving body contact with the liquid is remote and conceivably necessary only in instances of submersion or in cases of prostration where inhalation of vapors is facilitated by clothing which is saturated with toluene.

First Aid Treatment For Toluene Ingestion

Call a physician immediately. Vomiting should be induced promptly by giving a pint or more of warm salt solution (2 table-spoonfuls of table salt to a pint of water) or warm soapy water. Have the patient stick his finger down his throat if necessary to induce vomiting. Keep the patient comfortable and warm.

NOTE: Do not give anything by mouth to an unconscious patient.

First Aid Treatment For Toluene Inhalation

A worker who has been overcome by toluene must be carried at once into an uncontaminated atmosphere. If breathing has stopped, effective artificial respiration such as that obtained by the Nielsen arm lift - back pressure method, or the Eve rocking method should be started immediately and a physician should be called at once. If oxygen inhalation apparatus is available, oxygen should be administered, but only if one familiar with the operation of such apparatus is present to administer it. 100% oxygen should be administered and maintained, preferably at 4 cm of water pressure resistance against exhalation. The patient should be kept comfortable and warm.

6. BENZENE

Most comments previously made concerning toluene are also true for benzene except that benzene is a highly toxic chemical and completely different from toluene in that respect.

Description: Colorless liquid with aromatic odor.

Flammable liquid. Vapor forms explosive mixtures with air. Flammable limits, 1.3% and 7.1%. Flash point, 262° K. Ignition temperature, 835° K. Liquid is lighter than water (specific gravity, 0.9). Vapor is heavier than air (vapor-air density at 311° K is 1.4) and may travel considerable distance to a source of ignition and flash back. Not soluble in water.

Breathing of high concentrations of benzene may cause acute poisoning and death. Repeated inhalation of low concentrations often results in severe or fatal anemia. It is also a skin and eye irritant.

The use of benzene in open containers should be only undertaken in well ventilated or chemical hood areas. The use of

respiratory protective equipment is necessary and self-contained breathing apparatus is preferred. Benzene can be absorbed through the skin if in contact with the liquid, hence protective clothing is necessary.

Fire Fighting: Use dry chemical, foam, or carbon dioxide. Water may be ineffective, but water should be used to keep fire-ignited, use water spray to disperse the vapors and to protect men attempting to stop a leak. Water spray may be used to flush spills away from exposures.

Storage: Protect against physical damage. Outside or detached storage is preferable. Inside storage should be in a standard flammable liquids storage room or cabinet. Separate from oxidizing materials.

7. NAPHTHALENE

Description: White, crystalline volatile solid or flakes having moth ball odor.

Volatile solid which gives off flammable vapors when heated. Vapor forms explosive mixtures with air. Flammable limits, 0.9% and 5.9%. Flash point 174° F. Ignition temperature, 979° F.

Naphthalene in high concentrations can be toxic and in such cases self-contained breathing apparatus should be used. Naphthalene should be used in a chemical hood or well ventilated area. It is a skin, eye, and respiratory irritant.

Fire Fighting: Use water, carbon dioxide, dry chemical or foam. Foam or direct water spray on molten naphthalene may cause extensive foaming.

Storage: Protect against physical damage. Store in cool place, away from sources of heat and ignition. Separate from oxidizing materials.

8. CESIUM SALTS

Cesium has been utilized as a seed material in the form of cesium carbonate Cs_2CO_3 and cesium nitrate CsNO_3 in large MHD systems pollucite is a candidate seed material.

Cesium carbonate is a white or colorless deliquescent crystal; Cs_2CO_3 is capable of dissolving into cold water at the rate of 260.5 gms per 100 cc of water. In contact with water the resultant solution is extremely alkaline and can cause severe burns. Its deliquescent nature will cause it to absorb moisture from skin and tissue, again causing severe burns. Inhalation of the dust of Cs_2CO_3 can cause severe lung damage; therefore, Cs_2CO_3 should only be handled using protective clothing and full face dust masks or self-contained breathing apparatus.

Cesium nitrate is a colorless or white hexagonal or cubic crystal having a specific gravity of 3.685. Its solubility is 9.2 gm per 100 cc of water, far less than Cs_2CO_3 . Contact with the skin for short periods causes no adverse effects but is not recommended. CsNO_3 dust, too, is injurious to lung tissue.

Since 1961, the primary source of cesium chemicals has been the rare mineral pollucite, ideally $\text{Cs}_2\text{O} \cdot \text{Al}_2\text{O}_3 \cdot 4\text{SiO}_2$. Known reserves of this rare mineral are sufficient for current and any anticipated future cesium requirements. One of the world's richest sources of cesium is located at Bernic Lake, Manitoba. The deposits are estimated to contain 300,000 tons of pollucite averaging 20% cesium.

The cesium content of theoretically pure pollucite would be 45% Cs_2O ; but natural pollucite usually contains only about 6-32% Cs_2O due to the presence of other gangue minerals intimately associated with the pollucite, and also due to the fact that natural pollucite can contain varying amounts of Rb, K, or Na + H_2O in place of Cs in the pollucite crystal structure. Thus natural pollucite can be considered as an intermediate mineral in a continuous series between analcite, $\text{Na}_2\text{O} \cdot \text{Al}_2\text{O}_3 \cdot 4\text{SiO}_2 \cdot 2\text{H}_2\text{O}$, and theoretical pollucite, $\text{Cs}_2\text{O} \cdot \text{Al}_2\text{O}_3 \cdot 4\text{SiO}_2$.

Cesium is very similar in chemical behavior to potassium and rubidium except that cesium is oxidized more readily than any of the other alkali metals.

Cesium is the most reactive alkali metal in reactions with oxygen and the halogens, but it is the least reactive of the alkali metals with nitrogen, carbon, and hydrogen. Cesium hydroxide is the strongest alkali known. The hydroxide absorbs carbon dioxide readily and attacks glass relatively rapidly.

Cesium forms simple alkyl and aryl compounds which are similar to those of the other alkali metals. The simple alkyl and aryl compounds are colorless, solid, amorphous, nonvolatile, and insoluble (except by decomposition) in most solvents except diethylzinc. The reactivity of cesium alkyls with halides and nitriles is greater than that of the other alkali metal alkyls and, because of their exceptional reactivity, cesium alkyls should be effective in alkylations wherever other alkaline alkyls have failed. Cesium reacts readily with hydrocarbons in which the activity of a C-H link is increased by the attachment to its carbon atom of doubly linked or aromatic radicals. A brown, solid addition product is formed when cesium reacts with ethylene. [53]

Cesium forms neutral complex compounds with two or four moles of salicylaldehyde per mole of cesium, indicating a coordination number of four or six. However, cesium does not form such complexes readily, and the relatively high ionic mobility of the cesium ion in aqueous solutions indicates that any hydration water about the cesium ions is held very loosely if held at all.

Cesium salts are generally similar chemically to other alkali-metal salts. The differences between cesium and potassium compounds are generally intensifications of the differences between potassium and sodium compounds. The solubilities of alkali-metal salts of simple anions generally increase with the atomic weight of the alkali ion from lithium to sodium to potassium to rubidium to a maximum with cesium. In contrast, the solubility of the alkali-metal salts of complex anions generally decreases from lithium to a minimum with cesium. The salts of cesium and simple anions are usually hygroscopic as well as very soluble, but the sparingly soluble salts of cesium and complex anions are seldom hydrated and usually are not hygroscopic.

Cesium salts have been used as antishock reagents following the administration of arsenical drugs. Study of the physiological effects of cesium in comparison with potassium and rubidium on the function of various organs in small animals has shown that cesium has the greatest effect in causing disturbances of heart rhythm[54], although this effect has not been investigated in humans. As a result, all possible precautions should be taken against inhalation, ingestion, or absorption of cesium salts during handling.

Section VII
GENERAL OPERATING PRACTICES
in the KIVA-I MHD FACILITY

The following procedures have been adopted to assure safety of operation when preparing or handling fuels in the KIVA-I facility.

1. Prior to handling fuels the following steps should be taken:
 - A. Turn on red flashing lights
 - B. Post no smoking sign at doorway entering facility

NO SMOKING WHEN RED
LIGHTS ARE FLASHING

- C. Open large cell doors and turn on vent fans (2).
 - D. Locate large floor fans so as to force fuel vapors away from operator towards open door during mixing operation.
2. Liquid fuels must be transferred from base fuel supply to mixing bowl in fuel safety cans.
3. No more than 15 pounds of opened, powdered metal in MHD Cell No. 1 at a time.
4. All equipment used in the handling of powdered metals should be nonsparking and not build up static charges. Utensils must be copper, brass or aluminum. Do not use nylon or plastic because of static electrical charges.
5. The overhead exhaust fan must be on when working with powdered metals.
6. Care must be taken not to agitate the materials so as to introduce them into the air.

7. Persons handling the metals must wear dust masks and nonporous clothing. Shoes must be free of metal that may contact the floor.
8. No soldering irons, or other heat sources may be used in the MHD cell until all powdered metal fuels testing is complete and the room thoroughly cleaned.
9. No more than 20 gallons of prepared fuels are to be stored at the facility.
10. Emulsified fuels must be stored in closed containers. Liquid fuels are to be stored in safety cans.
11. During fuels testing, care must be taken not to empty fuel tank resulting in fuel vapors forced into the air. This can be avoided by weighing the amount of fuel placed into the tank and also weighing the fuel removed so the amount of fuel in the tank is known at all times.
12. After mixing the fuels ALL liquid fuels are to be placed back in base supply or in safety cans. Care_ fully sweep the working area using lightly oiled sawdust to insure no powdered fuel dust remains in cell area.

Section VIII

DISASSEMBLY AND INSPECTION OF THE KIVA-I 45° CONDUCTING WALL MHD GENERATOR CHANNEL

1. CHANNEL DISASSEMBLY AND INSPECTION

During the final four test series, HEF-15 and 15A, HEF-16, HEF-17, HEF-18 and 18A, and HEF-19, the power generated by this channel was radically lower than expected. After test HEF-15 the channel was inspected internally for signs of deterioration by use of a borescope. As noted previously, there was no indication of deterioration which could be seen nor was insulation deterioration noticeable when tested by use of a megger.

At the end of test HEF-19 the generator channel was removed from the test cell to repair the exhaust diffuser. After separating the diffuser and generator channel, it was decided to separate the inlet transition piece from the first electrode to determine the extent, if any, of seed penetration of the fiberfrax insulation. Figure L&\$ shows the fiberfrax insulation and inlet transition piece. Seed, soot and other contaminants can be seen to have penetrated the insulation to a depth of .5 to 1.0 cm. At the bottom of the figure (channel top) two deep arc tracks can be seen which not only penetrated the fiberfrax insulation but had also completely destroyed the plasma sprayed Al_2O_3 insulation under the arc tracks. Although not obvious from this figure, very little damage to the copper transition piece or matching electrode was in evidence. Blue powder deposits in the fiberfrax insulation and in the arc tracks are evidence of copper salts and hence chemical attack. The explanation for the arc penetration is that in all likelihood seed material penetrated the insulation until local arcing occurred as a result of seed salt conduction. Upon generation of an interelectrode arc the arc was propagated vertically upward along the interelectrode gap (through the insulation) under the influence of the magnetic field. Normally the interelectrode

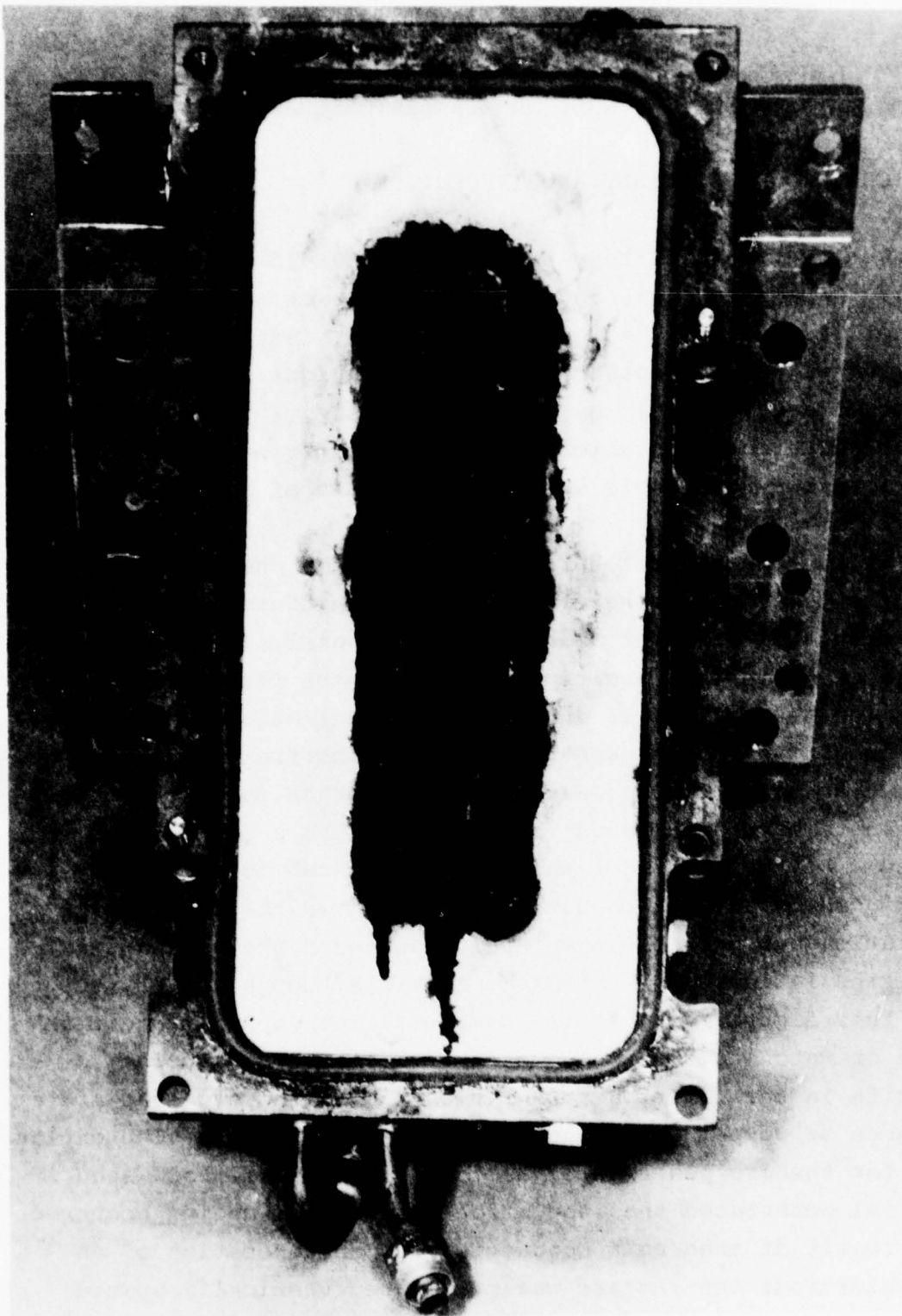


Figure 154. KIVA - I MHD Generator Inlet Transition Piece
with Fiberfrax Insulation

voltage here is less than 30 volts. Note that as would be expected there is no arc propagation at the cathode. Figure 155 shows the exhaust transition piece with sections of fiberfrax insulation still attached. Note here that there is very little evidence of seed penetration, except in local areas, which are likely the result of a poor seal and start-up transient pressures. At this location the static pressure is normally sub-atmospheric resulting in little or no overpressure to cause seed penetration of the insulation. The anode of this transition piece is nearly covered with arc tracks. On the bottom surface of the transition piece (bottom of the figure) the white deposit is a result of combustion of aluminum powder in the fuel forming Al_2O_3 . Some magnesia is also present. As in the previous Figure 154, the intense blue powder on the surface is a result of chemical attack of the copper.

Figures 156 and 157 show the effects of arc propagation on several electrodes. Figure 156 indicates very little seed or soot penetration of the insulation, but severe arcing to the point where the seal was burned through causing a gas leak. Surprisingly the copper was not deeply etched by the arcing or burned by the passage of high temperature gas. The same effects are seen in the matching electrode faces, Figure 157, which were plasma sprayed. Figures 158 and 159 are close-up photographs of the severe interelectrode arcing on the uncoated and plasma sprayed surface. The total destruction of both the fiberfrax and plasma spray is obvious. An interesting section of Figure 159 shows a very smooth electrode gas surface where molten Al_2O_3 has condensed on the cold copper surface. This type of surface was typical throughout the channel length and can also be seen in the inlet and exhaust transition sections.

The entire channel was disassembled and evidence of arcing was found on all electrodes severe enough to require removal of the plasma sprayed insulation. The plasma spray was removed by

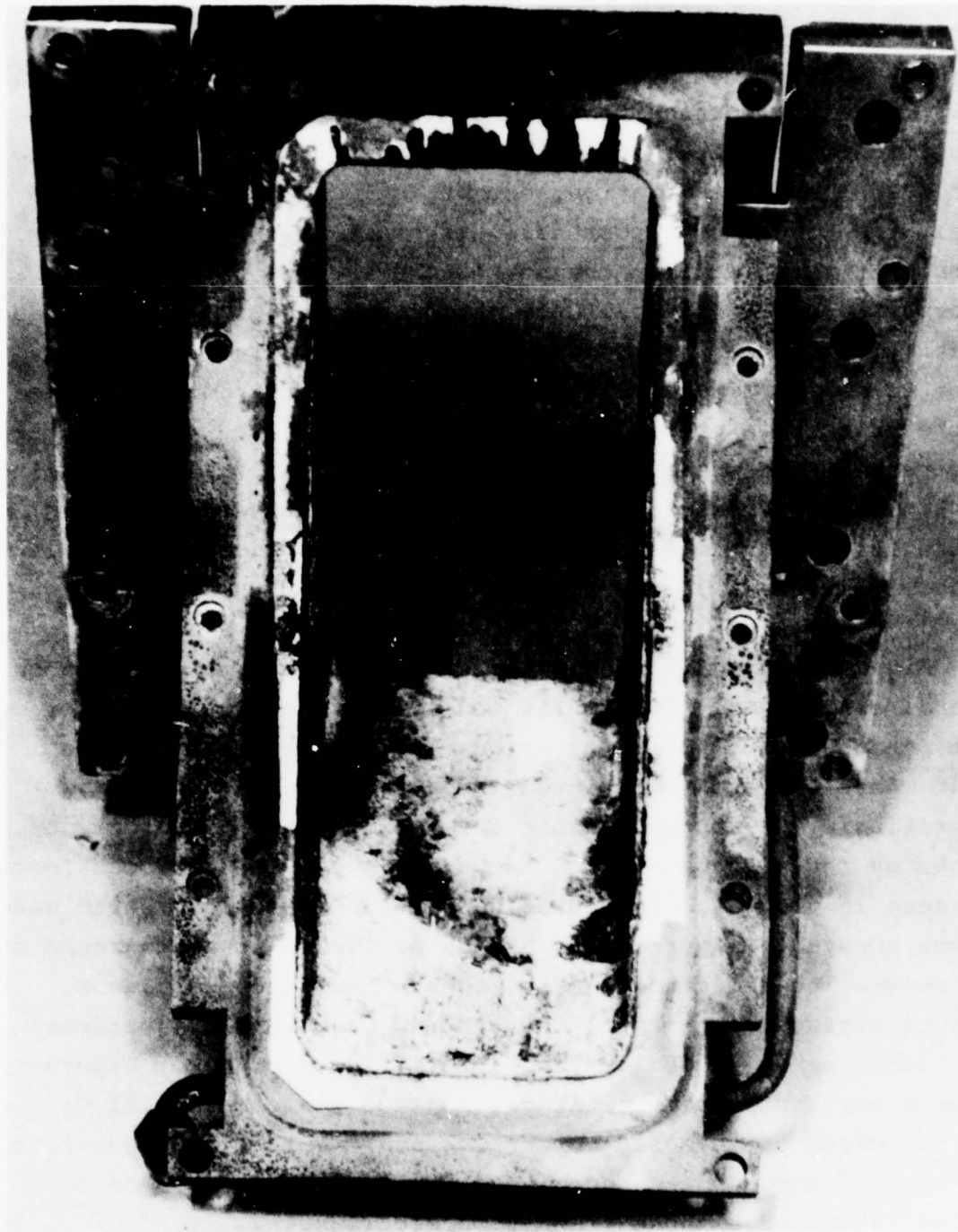


Figure 155. KIVA - I MHD Generator Exit Transition Piece

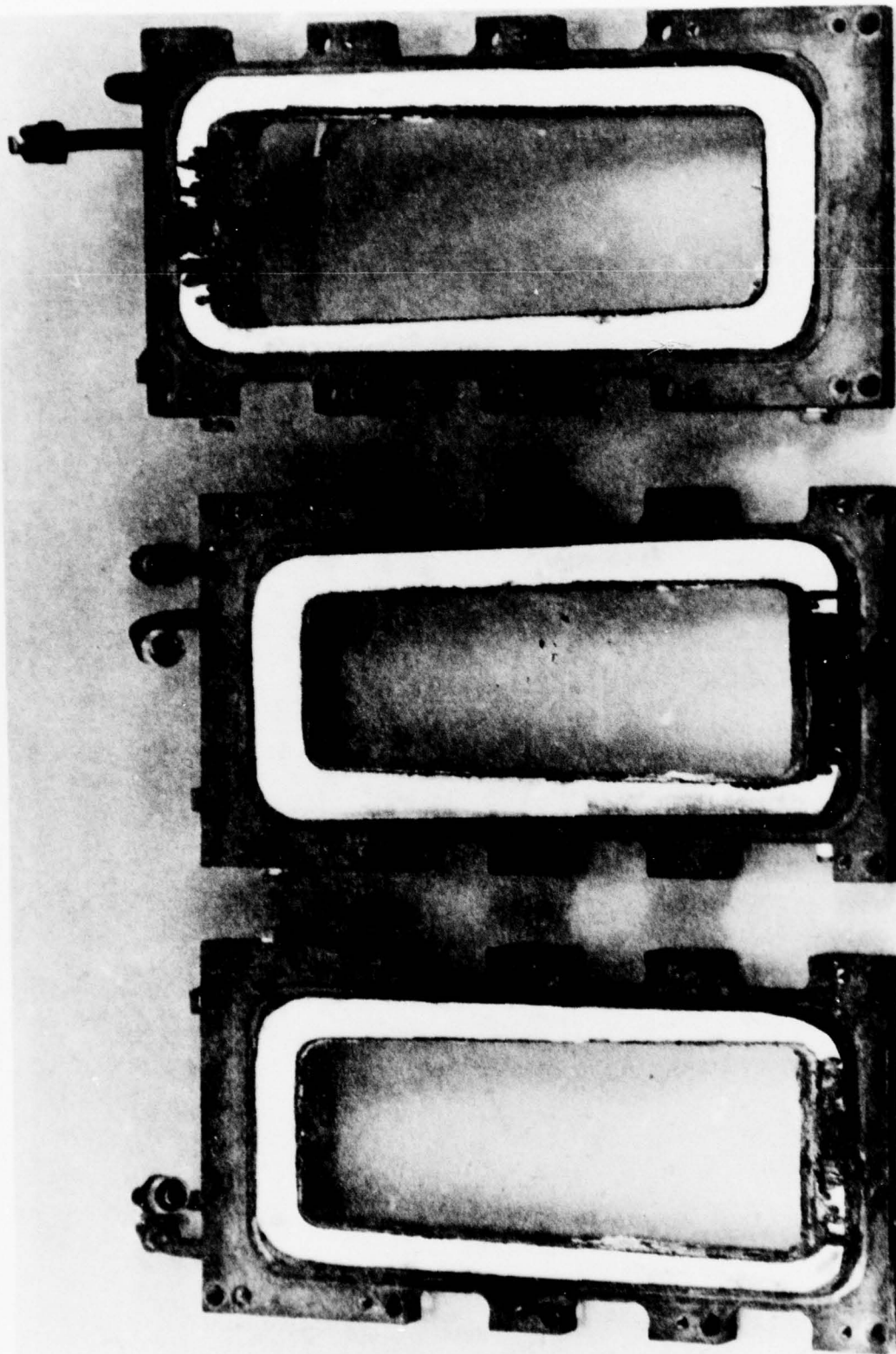


Figure 156. KIVA - I MHD Generator Electrodes with
Fiberfrax Insulation

Figure 157. KIVA - I MHD Generator Electrodes Showing Al_2O_3
Plasma Sprayed Side of Electrodes

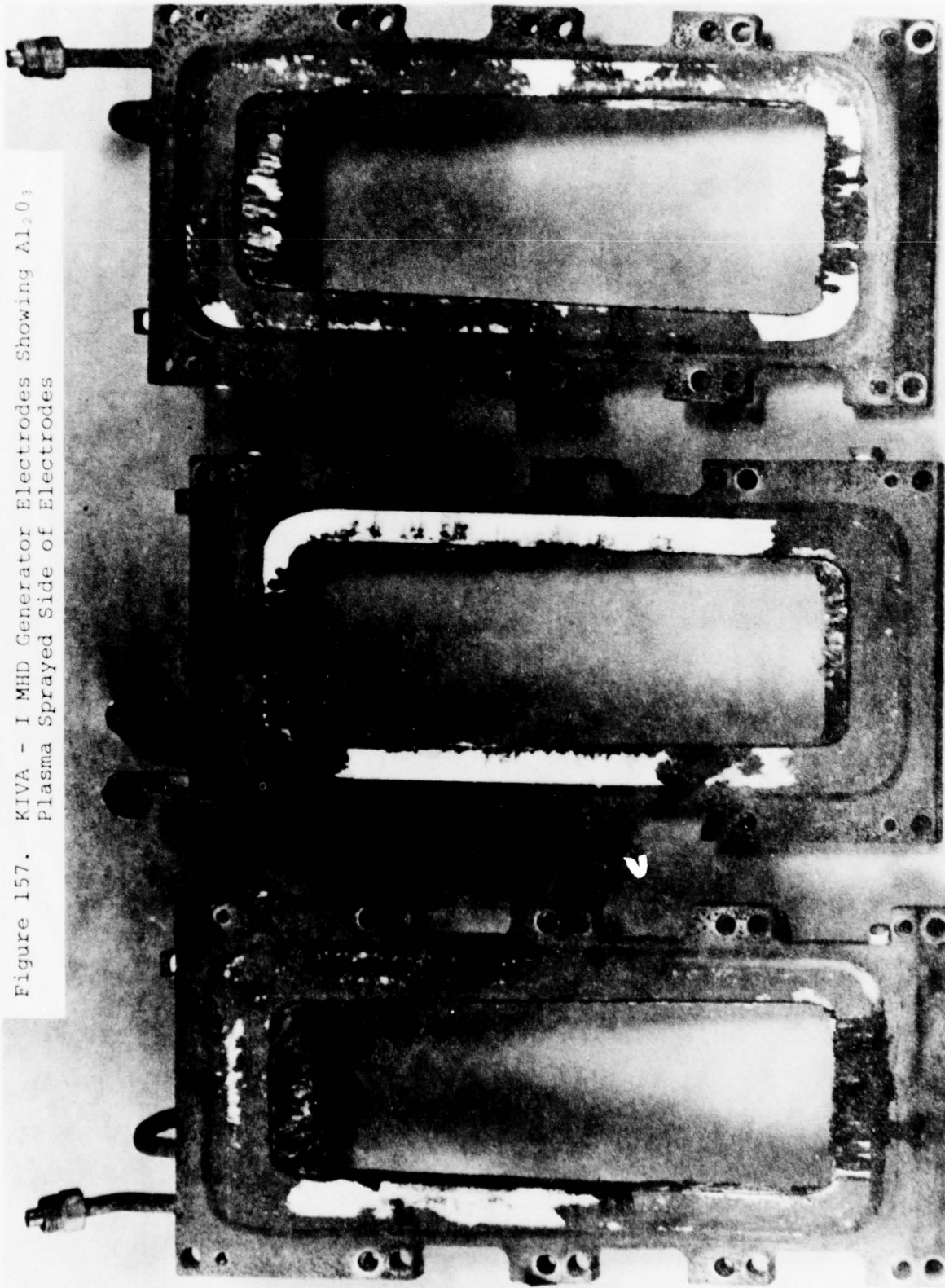


Figure 158. Arc Tracks in Al_2O_3 Plasma Sprayed Electrodes

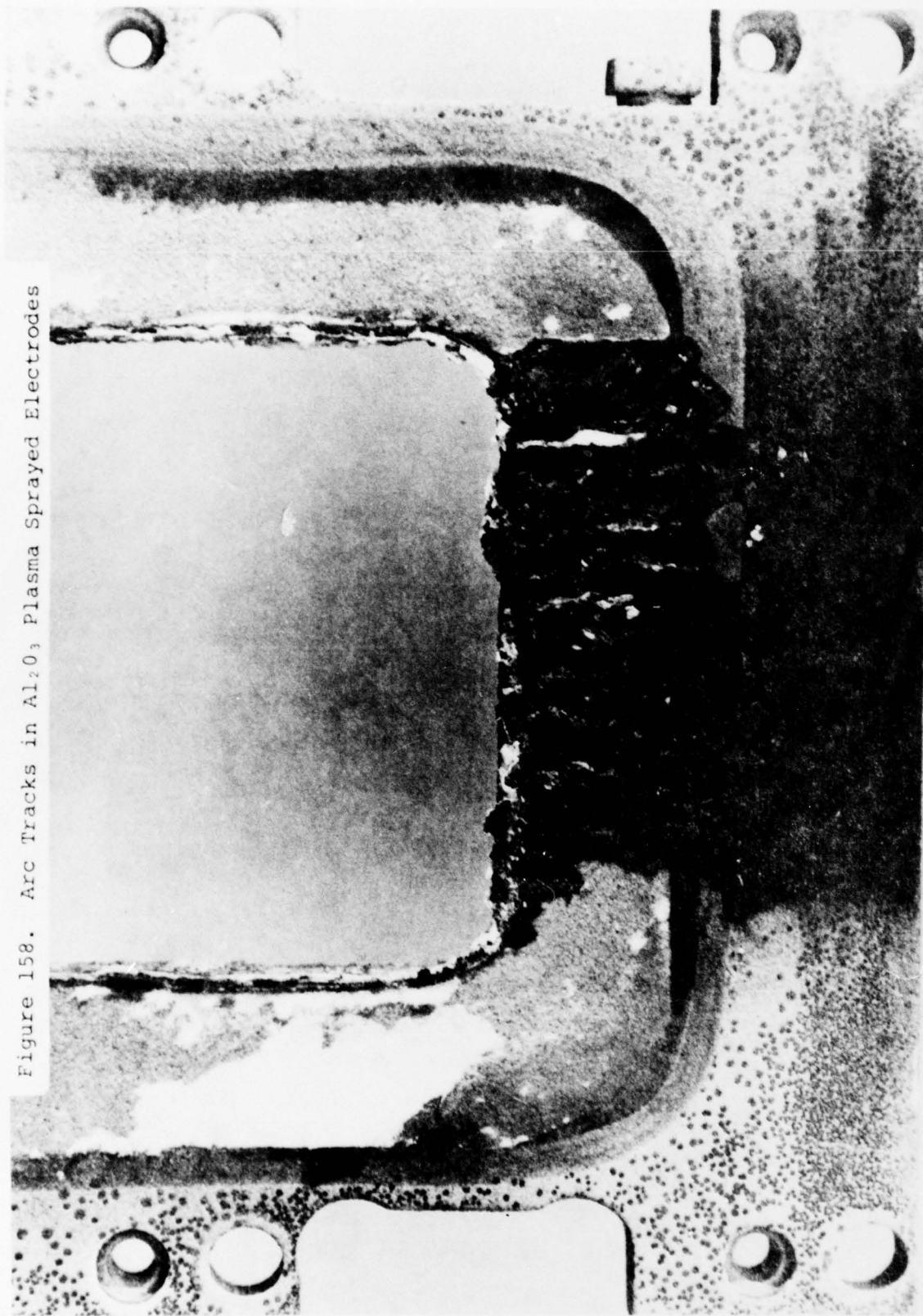
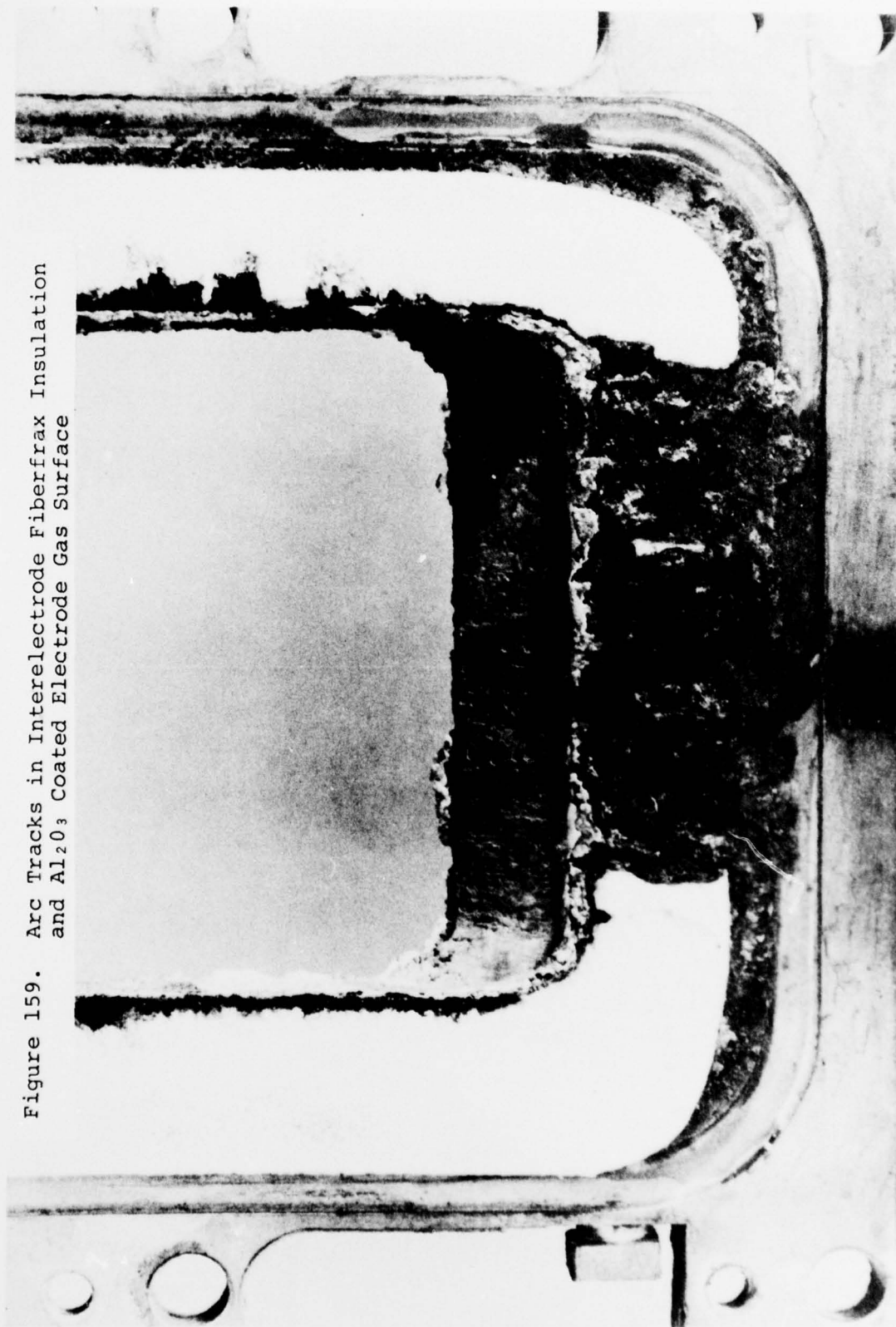


Figure 159. Arc Tracks in Interelectrode Fiberfrax Insulation and Al_2O_3 Coated Electrode Gas Surface



heating the electrodes to just under the copper transition temperature and quenching them to fracture the plasma spray. The electrodes were then soaked in a proprietary reagent to selectively attack the nickel metal spray surface used as an interface between the copper electrode and the Al_2O_3 plasma spray. When the nickel had been sufficiently dissolved, the plasma spray sloughed off of the electrodes.

Prior to reassembly, each electrode was pressure checked and several electrodes were found to be leaking at the coolant passage plugs. Figure 160 shows the result of removal of one of the coolant passage plugs. Also, several electrodes were found to have restricted coolant passages. Although there was no attack of the copper electrodes, there was extensive intergranular corrosion of several of the brass plugs.

Figure 161 shows the amount of intergranular attack on the brass plugs. All plugs were attacked to some degree, the minimum being shown by the top plug in Figure 161. Figure 162 shows a coolant passage port having minimal corrosion as contrasted to Figure 160. As a result, all plugs were removed and all coolant ports and passages were cleaned out using a long section of drill having the same diameter as the original gun drill.

2. DIFFUSER DISASSEMBLY AND INSPECTION

Figure 163 and 164 show the diffuser with one side wall removed and the sidewall respectively. Dark black stains show where the start-up transient pressure spike stretched the cross-bolts and broke the gas seal. Coolant seals were broken as evidenced by leakage during the tests but no other evidence was found. In both figures the light colored wall deposit shows the channel to be flowing full at the channel exit, but immediately downstream the flow separates from the top surface. The Al_2O_3

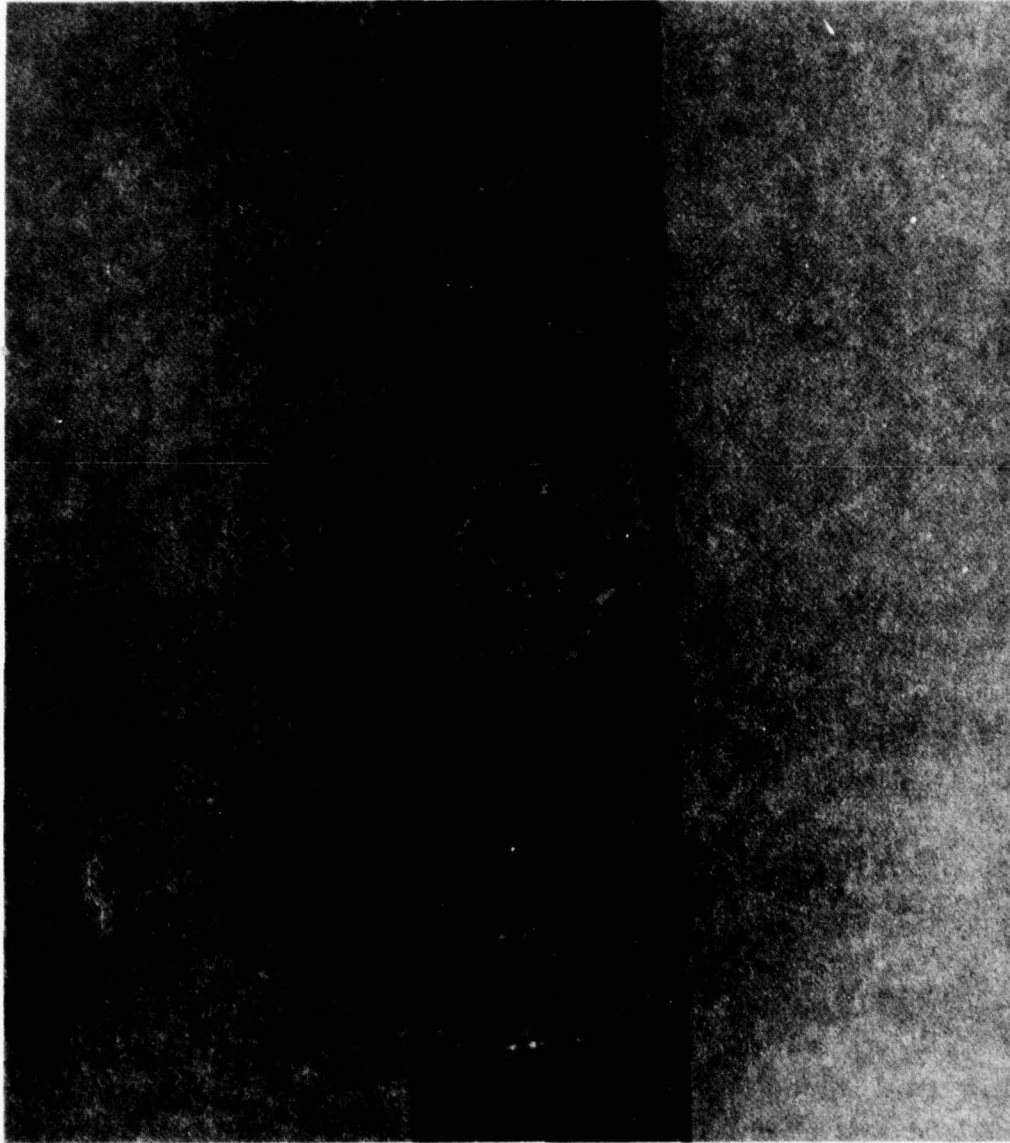


Figure 160. KIVA - I MHD Generator Electrode Coolant
Passage End Plug Removed



Figure 161. Coolant Passage End Plugs Showing Extent of Intergranular Corrosion

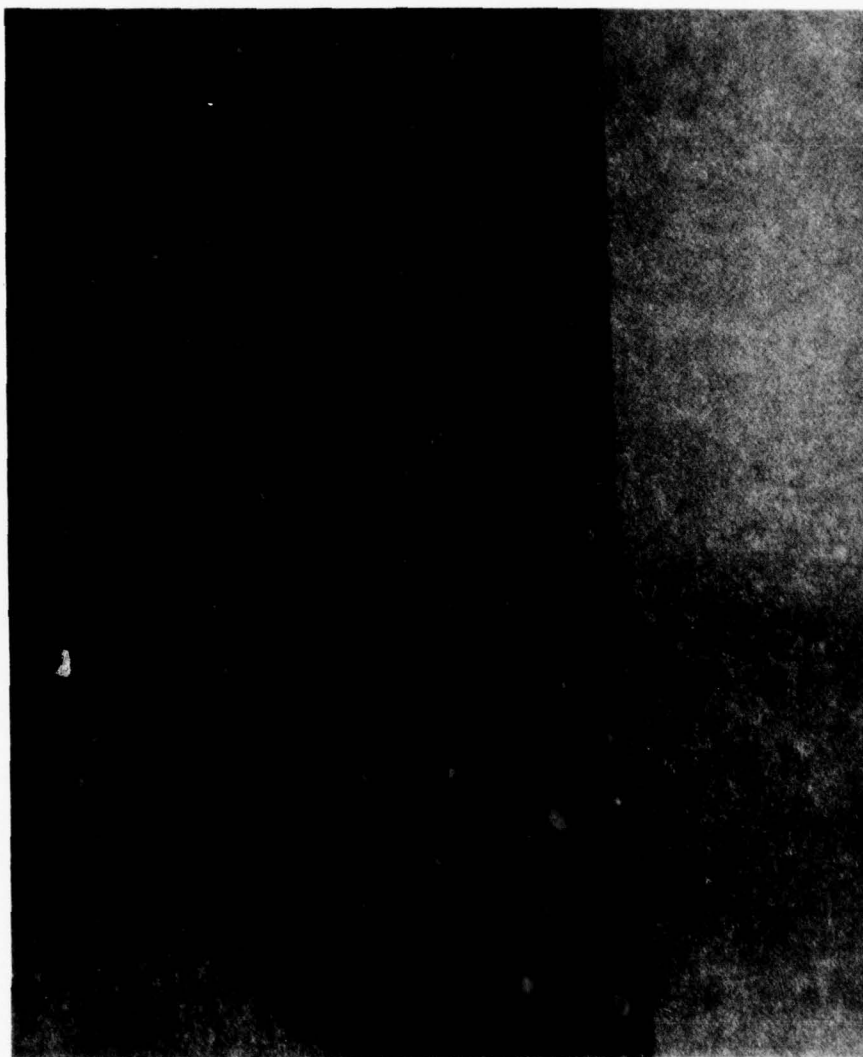


Figure 162. Electrode Coolant Port Having Minimal Corrosion

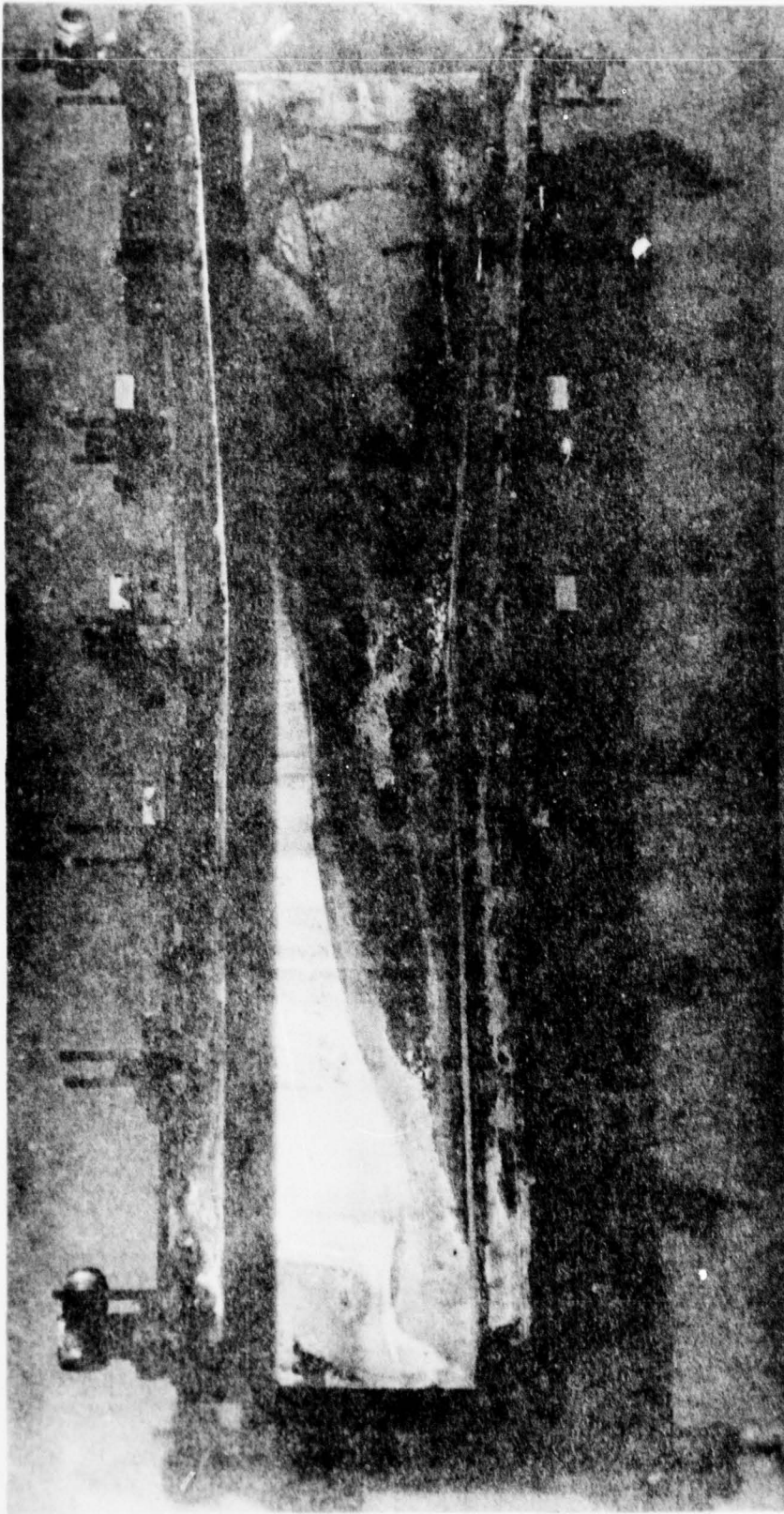


Figure 163. KIVA - I MHD Generator Diffuser with One
Sidewall Removed

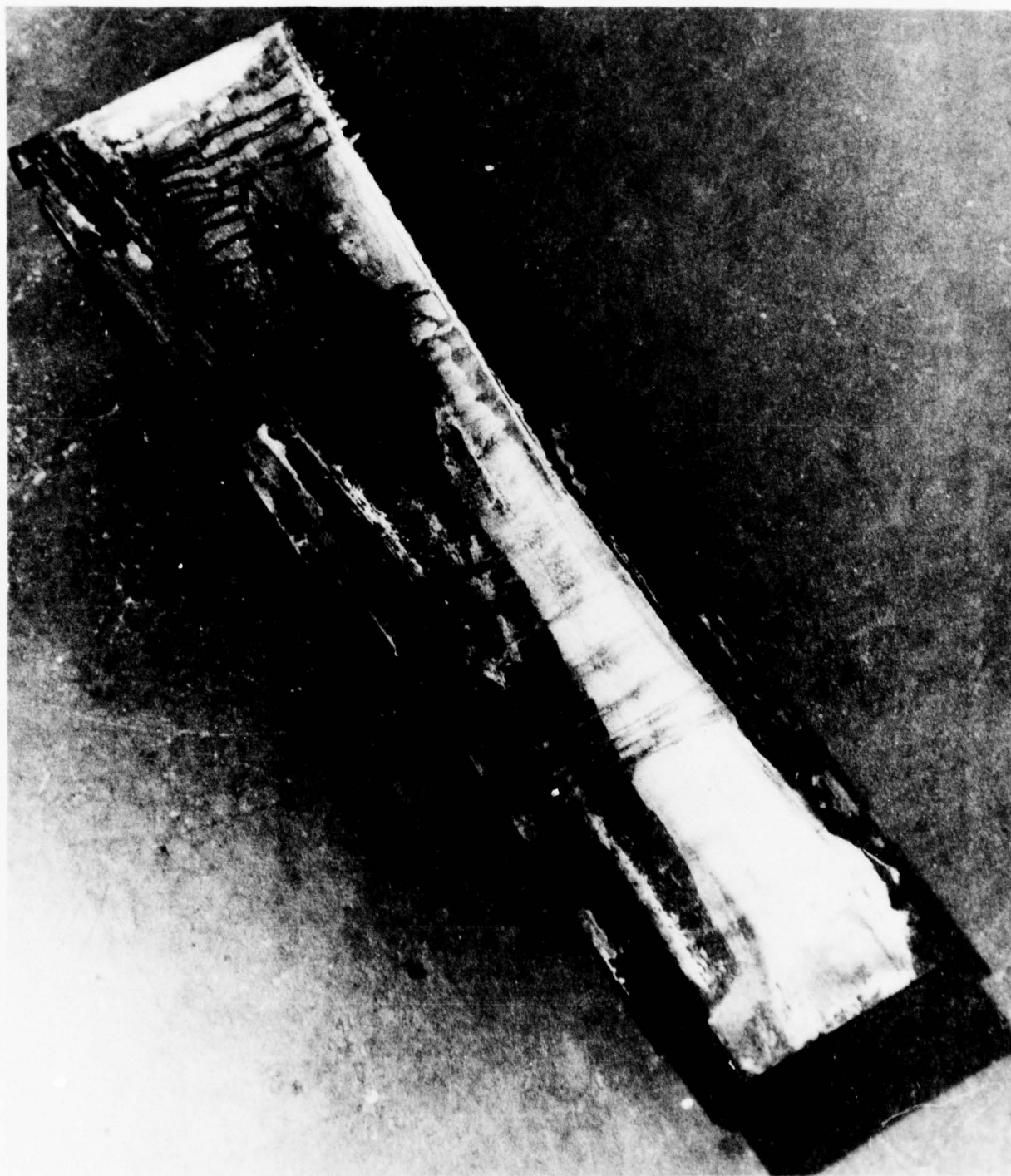


Figure 164. KIVA - I MHD Generator Diffuser Side Wall

deposit was very smooth and tenacious. Both chemical and light abrasives were used to remove the condensed Al_2O_3 adhering to the diffuser walls. After the diffuser had been completely disassembled and inspected, no damage other than the stretched cross bolts was found. The cross bolts were replaced during reassembly.

Section IX
REFURBISHMENT OF THE KIVA-I
HEAT SINK PEG WALL MHD CHANNEL

The heat sink peg wall MHD channel was operated using only JP-4 or toluene as fuel with granulated Cs_2CO_3 injected with the oxidizer stream as seed. The channel had been previously tested and determined to need refurbishment.

Figure 165 and 166 show the channel disassembled into top and right side, Figure 165 and bottom and left side, Figure 166. Both figures show extensive penetration of seed and soot at the inlet end with lesser penetration further on downstream. Light blue deposits indicate the presence of copper salts due to chemical attack. At the inlet end of the channel poor grout penetration and sealing between bottom electrodes, cathode, and the side wall can be seen in Figure 166. The same result, though less extensive, can be seen between the side wall and top electrodes, anode, in Figure 165. The slightly better insulating grout penetration and resulting better sealing are evidenced by less extensive seed and soot penetration.

Upon removal of the electrodes from the insulating support plate, extensive arc penetration of the anode was found similar to that in the diagonal conducting wall channel. Figures 167 and 168 show numerous arc pits which have penetrated the Al_2O_3 insulating grout. Figure 168 also shows the electrode/insulator construction where a fiberglass insulation board is used as an insulator over most of the interelectrode surface, but insulating grout fills the gas flow side contact area. Figure 169 shows the exhaust end electrode block, fiberglass insulating board and matching electrode. Extensive arc penetration through the insulating grout and into the fiberglass board is evident. The presence of a light blue powder deposit is evidence of chemical attack. Figure 170 shows two matching electrodes after cleaning. The evidence of seed penetration and chemical attack is still

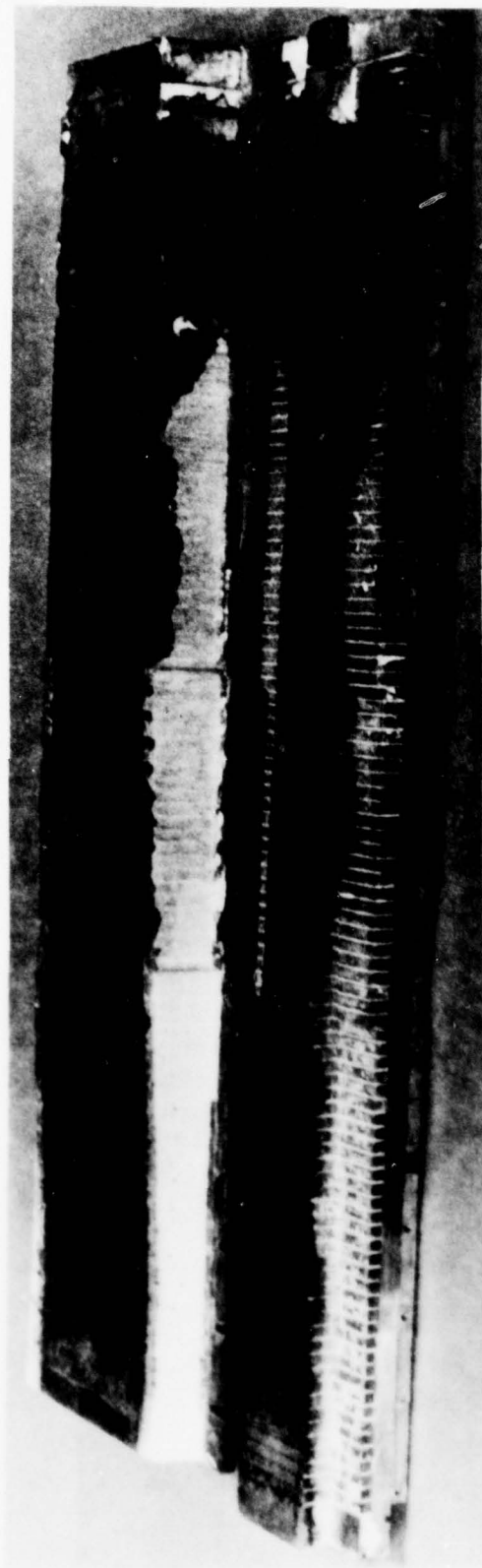


Figure 165. KIVA - I Pegwall Heat Sink MHD Channel
Top Electrode and Right Side

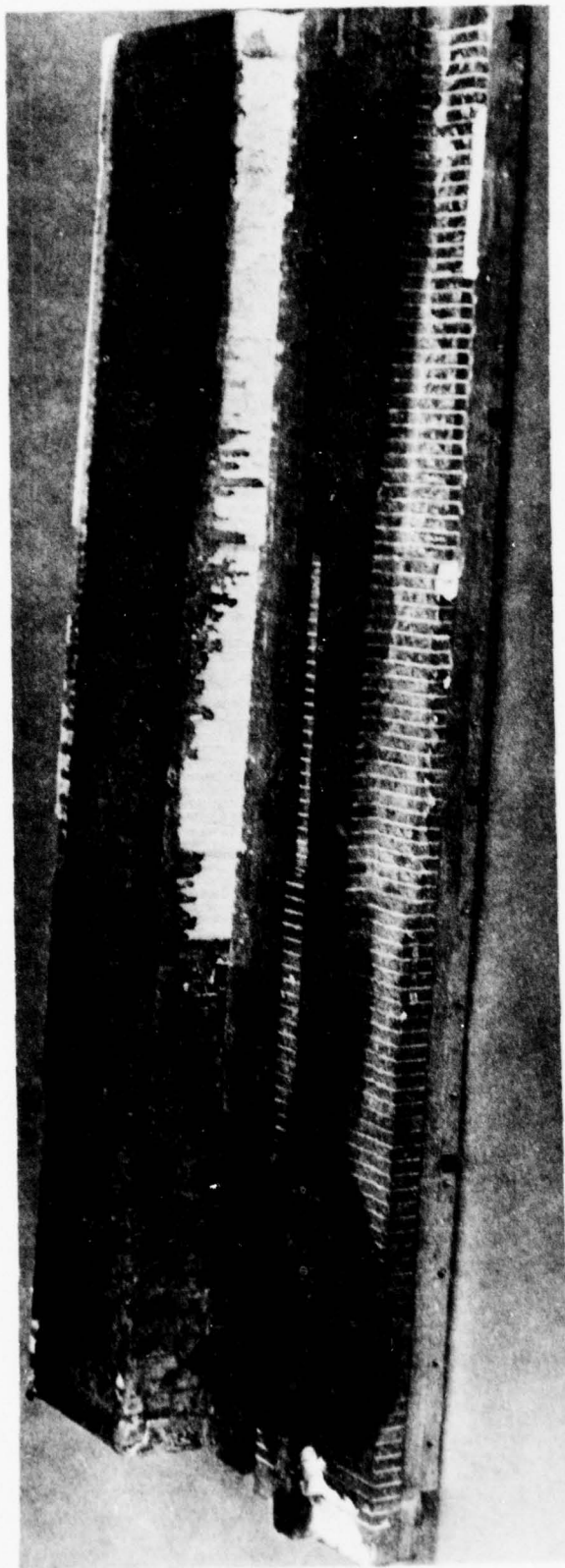


Figure 166. KIVA - I Pegwall Heat Sink MHD Channel
Bottom Electrode and Left Side



Figure 167. KIVA - I Heat Sink MHD Generator Electrode
with Arc Tracks in Al_2O_3 Grout



Figure 168. KIVA - I Heat Sink Generator Electrode Showing Al_2O_3 Grout and Fiberglass Insulator Construction with Arc Tracks in Grout

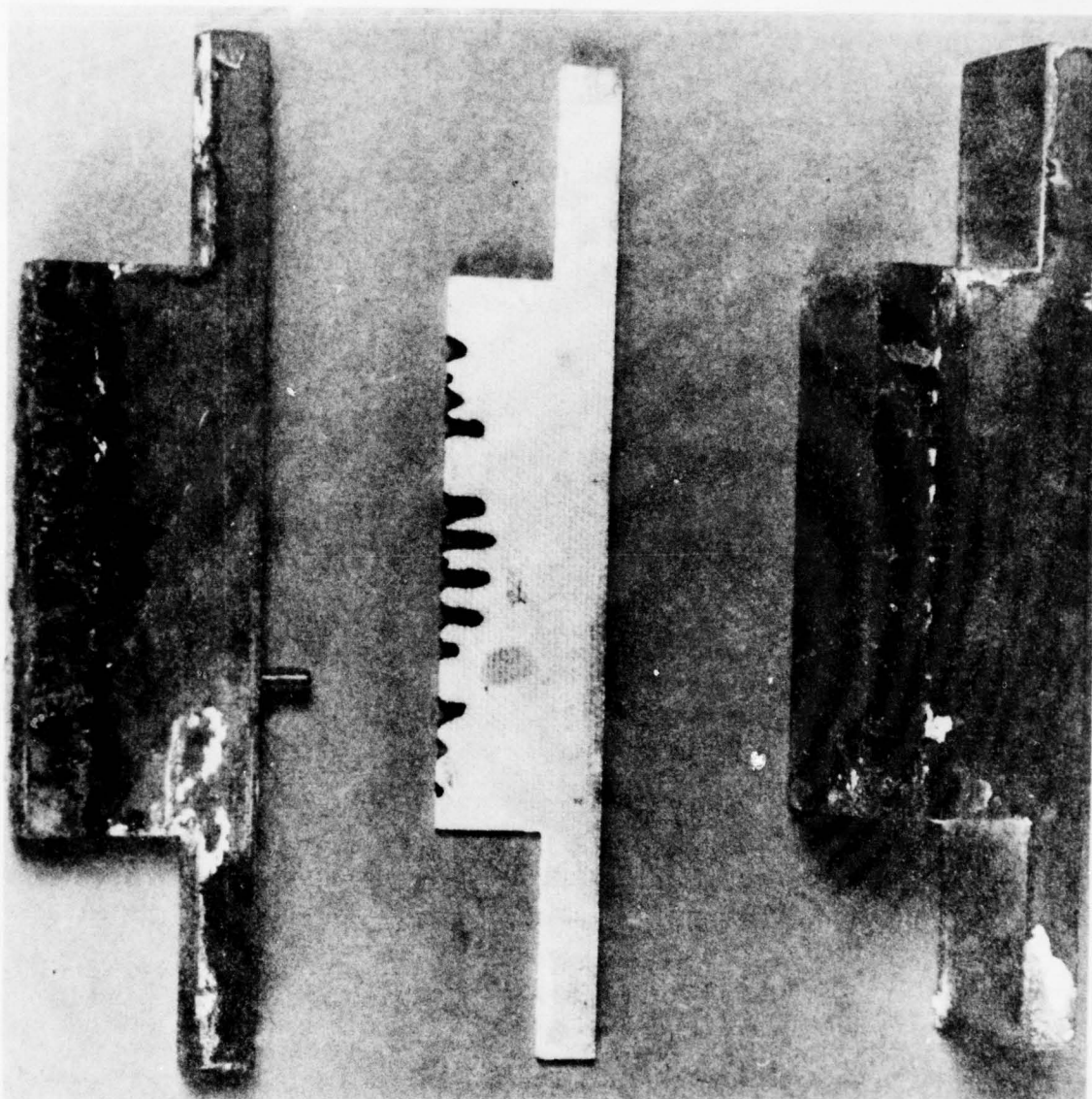


Figure 169. KIVA - I Heat Sink MHD Generator End Block, Insulator and Matching Electrode with Arc Tracks

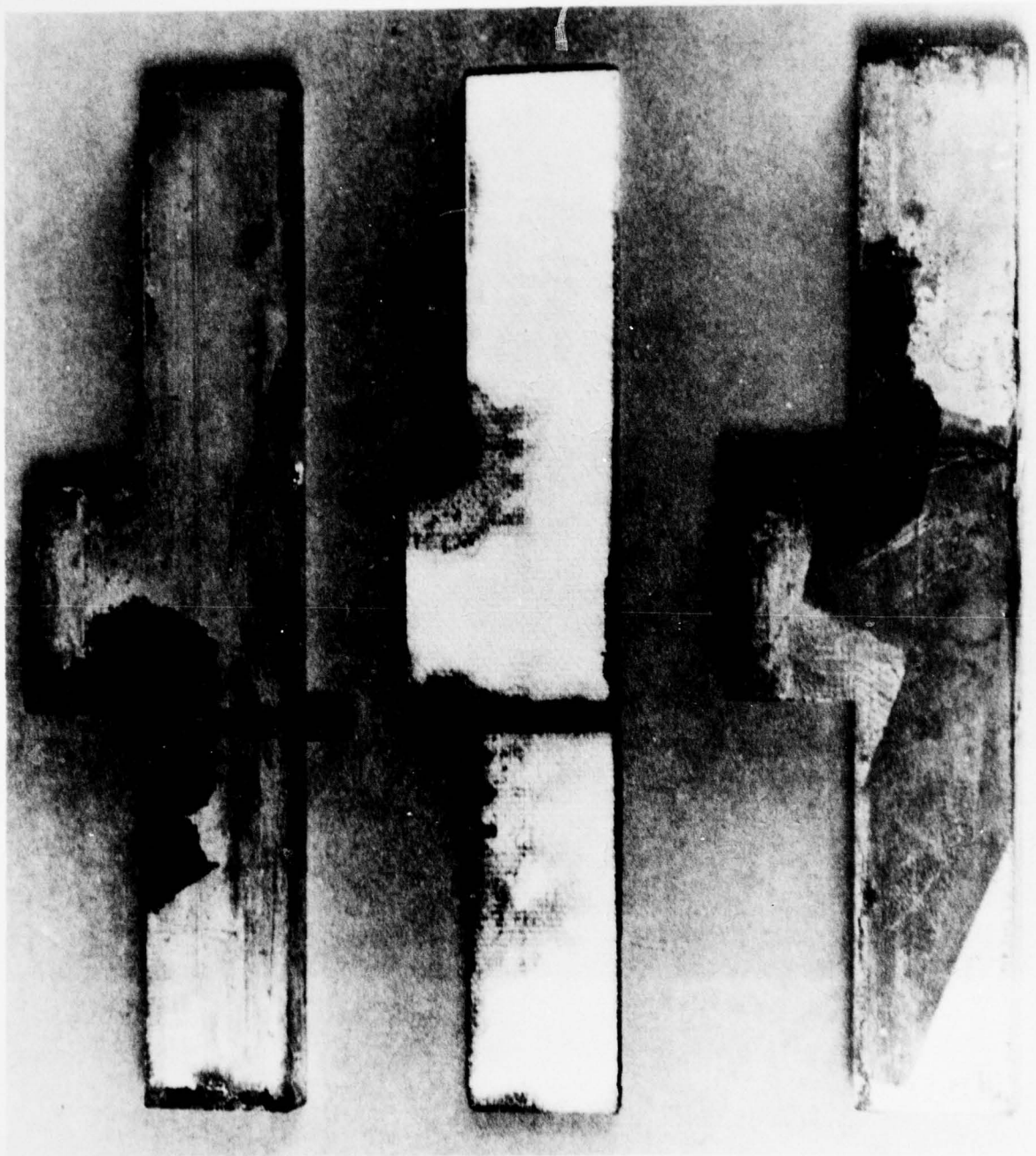


Figure 170. KIVA - I Heat Sink MHD Generator Matching
Electrodes and Inerelectrode Insulator

visible after the electrodes have been cleaned. In this photograph the arc tracks are still visible, but the lack of penetration can be better seen than on the other pictured electrodes. Of particular interest is the single arc track which did not originate at the electrode surface, but rather started at the junction point of the sidewall insulation and electrode. The single arc penetrated the entire depth of the electrode severing the fiberglass insulation board into two pieces.

The evidence here is probably clearer than in the case of the DCW channel with fiberfrax insulation that the arcing originates at a point where conduction can take place through a path provided by seed or other conductive salts. This is in opposition to, but not supplanting, the high interelectrode voltage arc mode of breakdown which occurs when the E_x field is high enough to create interelectrode voltages of 40 V or greater. In this channel and the 45° DCW the interelectrode voltage was seldom above 30 V which although in a "transistion" range should not be sufficient to cause high voltage arc breakdown. Naturally if the interelectrode voltage were kept to 20-25 V or below, there is little or no chance of high voltage arcing. Additionally, it should be obvious from both the 45° DCW experience and the peg wall channel that the electrode insulation must be dense enough to prevent penetration of the insulation by seed or other salts in aqueous solution or other form from creating conductive paths. The evidence is clear that neither fired Al_2O_3 grout or compressed fiberfrax is a satisfactory long-term interelectrode insulation.

The peg wall channel was disassembled for repair using the following stepwise procedure.

Peg Walls

- o Remove all peg contact and retaining screws and seals.
- o Place peg wall pegs and insulation mass intact on a plate, removing the insulating phenolic board that the side wall is assembled on.
- o Clean insulating phenolic walls.
- o Remove pegs one row at a time marking each peg to indicate orientation.
- o Using only one row at a time, scrape Al_2O_3 grout from pegs individually.
- o Chemically clean pegs and neutralize.
- o Assemble pegs on the phenolic board with new seals.
- o After completely cleaning all pegs, installing them, and installing electrode wall templates, place the peg wall on vibration table.
- o Pour a 100:1 water detergent solution over the pegs and rinse.
- o Mix the grout and while pegs are still wet from the detergent rinse pour over the pegs.
- o Start shake table vibration to remove bubbles from grout.

- o After grout has been settled, remove excess grout, cover pegs and grout with wet cloths for 48 hours. Do not allow cloths to dry.
- o After 48 hour curing period, allow the peg wall to air dry for several days.
- o Oven fire the grout.

Electrode Walls

- o Remove all retaining and contact screws and seals.
- o Place electrode/insulation mass on a separate plate.
- o Remove electrodes and fiberglass insulation segments.
- o Remove electrodes individually and scrape the Al_2O_3 grout from the electrodes individually.
- o Chemically clean and neutralize.
- o Reinstall electrodes and new fiberglass insulation segments.
- o Place peg wall templates on the electrode wall and place the electrode wall on the vibration table.
- o Mix grout and squeeze into interelectrode spaces while vibrating the electrode wall on the shake table.
- o Remove excess grout and cover with wet cloths for 48 hours.
- o After curing allow grout to dry.

Assemble peg walls and electrode walls with an excess of grout in the seams. Squeeze grout out of seams as the walls are assembled. When the walls are completely tightened, scrape excess grout from wall corners and stuff the channel with wet cloths for curing period. When the curing period is over, remove the wet cloths and allow the channel to air dry. The channel is now ready to be installed for use.

Section X

TEST DATA

The following test data is presented as recorded but converted to engineering units. Data recording sequence is from left to right. All parameters are in the sequence recorded except for \dot{W}_f , \dot{W}_o and O/F which are calculated quantities. Where power, P_p , is indicated this parameter is recorded from the power meter.

Run No. HEF-8A

O ₂ /Venturi														
P _c	P _f	P _{s2}	P _t	P _{s1}	T _t	E _p	I _p	P _p	Seed Tach	V _{L2}	V _{L1}	W _f W _o		O/F
Kg/Cm ²	Kg/Cm ²	Kg/Cm ²	Kg/Cm ²	Kg/Cm ²	*K	Volts	Amps	KW	RPM	Volts	Volts	Kg/Sec		-
8.692	24.502	27.273	34.741	34.924	291	401	41	19.6	63.5	504	80	.136	.412	3.03
8.116	24.474	17.216	34.981	34.924	292	1348	121.2	167.6	132.3	1440	176	.139	.413	2.97
8.017	24.558	16.513	35.037	35.149	292	1330	116.9	165.6	134	1496	166	.140	.413	2.96
8.158	24.628	16.400	35.051	35.107	291	1324	153.2	153.2	135	1470	171	.139	.414	2.98
8.144	24.544	16.386	35.051	35.177	291	1298	162	162.0	135	1488	175	.139	.415	2.98
8.411	25.697	16.400	35.079	35.599	290	516	29.8	29.8	134	654	73	.143	.420	2.94
8.088	24.643	16.414	35.318	35.192	291	397	17.4	17.4	135	560	85	.140	.415	2.96
8.031	24.530	16.400	35.079	35.206	291	400	10.6	10.6	135	370	82	.139	.415	2.99
8.088	24.530	16.386	35.051	35.163	291	270	12.3	12.3	135	311	73	.139	.415	2.99
8.172	24.558	16.358	35.079	35.192	291	315	7.3	7.3	45.7	242	51	.139	.415	2.99
8.116	24.558	16.400	35.051	35.121	290	221	2.3	2.3	5.92	0	0	.139	.415	2.99

Total seed - 0.213 Kg

Total seed time - 6 sec

Seed rate - 35.4 gm/sec

Run No. HEP-8B

Pc Kg/Cm ²	Pf Kg/Cm ²	Pg ₂ Kg/Cm ²	Pt Kg/Cm ²	Pg ₁ Kg/Cm ²	Tc °K	Ep Volts	Ip Amps	Pp KW	Seed Tach RPM	VL ₂ Volts	VL ₁ Volts	W _f Kg/Sec		O/F
												W _f	W _o	
5.865	24.614	31.338	35.149	34.784	287	236	24.8	9.0	40	355	87	.150	.413	2.75
8.256	24.586	17.610	34.910	34.784	287	1056	89.4	130	80	1466	202	.139	.413	2.97
8.144	24.586	16.541	34.981	34.826	286	1336	114.4	163	79	1304	203	.139	.414	2.98
8.284	24.586	16.527	34.966	34.882	286	1200	99.2	124	80	1508	209	.138	.415	3.01
8.186	24.586	16.471	34.966	34.896	287	1214	108.7	140	81	1492	192	.139	.415	2.98
8.313	24.614	16.428	34.938	34.840	286	1312	112.9	112	82	1408	204	.138	.414	3.00
8.242	24.586	16.485	34.966	34.910	286	1336	117.4	174	81	1330	205	.139	.415	2.99
8.242	24.586	16.442	35.009	34.882	289	1056	46.7	50	81	730	101	.139	.413	2.97
8.299	24.643	16.428	35.037	34.882	287	369	41.1	14	81	354	110	.139	.414	2.98
8.270	24.643	16.428	35.065	34.924	287	336	28.3	12	48	480	93	.139	.415	2.99
8.200	24.586	16.471	35.037	34.936	287	2.3	1.2	2.4	-	-	-	.139	.415	2.98

Total seed - 0.198 Kg

Total seed time - 9.4 sec

Seed rate - 21.1 gm/sec

Run No. HEP-8C

Pc	Pf	P _{S2}	P _t	P _{S1}	T _t	E _p	I _p	P _p	Seed Tach	V _{L2}	V _{L1}	\dot{W}_f		\dot{W}_o	O/F
Kg/Cm ²	Kg/Cm ²	Kg/Cm ²	Kg/Cm ²	Kg/Cm ²	*K	Volts	Amps	KW	RPM	Volts	Volts	Kg/Sec			-
8.031	25.318	30.282	35.037	34.559	287	328	31	15.4	29	506	101	.143	.410	2.87	
8.341	25.093	17.524	34.966	34.559	286	836	87	174	53	1470	187	.141	.414	2.93	
8.186	25.064	16.112	35.093	34.896	286	916	74		53	1238	204	.141	.415	2.94	
8.299	25.191	16.555	35.093	34.896	287	1218	98.2	117.2	54	1160	204	.141	.415	2.94	
8.327	25.219	16.541	35.149	34.910	287	1313	117.1	96.2	53	1060	196	.141	.415	2.94	
8.341	25.135	16.569	35.163	34.924	287	1300	117.7	70.3	54	1030	180	.141	.415	2.94	
8.327	25.107	16.513	35.135	34.952	287	1182	114.8	111.2	54	1438	169	.141	.415	2.95	
8.327	25.247	16.569	35.177	34.868	287	556	29	18.6	53	502	91	.141	.414	2.94	
8.242	25.107	16.541	35.177	34.952	287	379	29	20.8	54	443	77	.141	.415	2.95	
8.327	25.107	16.555	35.121	34.896	287	264	19	9.8	24	265	91	.141	.414	2.94	
8.397	25.233	16.513	35.149	34.952	286	1.9	1.2	2.5	2	-	-	.141	.416	2.95	

Total seed - 0.142 Kg

Total seed time - 8.9 sec

Seed rate - 15.9 gm/sec

Run No. - HEP-8D

DATA UNUSABLE

Run No. - HEP-9B

$V_{L2}-V_{L1}$ Volts	P_C Kg/Cm ²	P_f Kg/Cm ²	P_{t-O_2} Kg/Cm ²	$V_{L2}-V_{L1}$ Volts	O_2-T_t °K	R Ohms	$V_{L2}-V_{L1}$ Volts	Seed Tach RPM	$V_{L2}-V_{L1}$ Volts	\dot{W}_f Kg/Sec	\dot{W}_O Kg/Sec	O/F	P KW
0	0	27.456	40.565	0	287	6	0	0	204	-	.480	-	-
263	9.353	27.287	39.158	210	287	8	192	0	209	.140	.465	3.32	-
1410	8.861	27.329	39.158	1322	287	10	1340	61	1231	.142	.465	3.27	176
1029	8.960	27.287	39.102	1159	286	12	1143	63	1118	.142	.464	3.26	199
574	8.917	27.315	39.060	492	287	6	540	63	465	.142	.464	3.26	-
96	8.875	27.301	39.045	42	287	8	101	63	49	.142	.463	3.26	-

Short Circuit

Run NO. HEF-10

$V_{L2-V_{L1}}$ Volts	P_c Kg/Cm ²	P_f Kg/Cm ²	P_{t-O_2} Kg/Cm ²	$V_{L2-V_{L1}}$ Volts	T_{t-O_2} °K	$V_{L2-V_{L1}}$ Volts	Seed Tach RPM	$V_{L2-V_{L1}}$ Volts	W_f Kg/Sec	W_o Kg/Sec	O/F	P KW
0	0		38.525	0	287	573	0	568	-	.457	-	14.5
552	9.480	29.748	38.708	532	287	545	0	651	.14	.459	3.73	32.5
930	9.030	29.678	38.877	1214	287	1292	60	1307	.145	.461	3.18	140.7
1321	8.917	29.664	38.820	1265	287	1309	64	1343	.145	.461	3.18	171.5
1365	8.974	29.664	38.764	1264	287	1176	66	1183	.145	.460	3.17	155.5
1229	8.932	29.664	38.834	1346	287	1383	66	1289	.145	.461	3.18	172.0
1392	9.016	29.678	38.778	1286	287	1268	66	1320	.145	.460	3.17	173.3
1170	8.903	29.664	38.820	1391	287	1348	66	1246	.145	.461	3.18	166.1
1362	9.016	29.650	38.806	1158	287	1305	66	1361	.145	.460	3.17	168.1
1355	9.016	29.650	38.792	1291	287	1230	66	1248	.145	.460	3.17	164.1
1177	8.903	29.664	38.820	1236	287	1369	66	1360	.145	.461	3.18	165.2
1387	8.974	29.650	38.792	1254	287	1151	66	1153	.145	.460	3.17	152.8
1102	8.946	29.650	38.806	1326	287	1338	66	1121	.145	.461	3.18	149.3
860	8.847	29.664	38.834	498	287	460	66	427	.146	.460	3.15	31.5
513	8.791	29.636	38.806	458	287	452	66	568	.146	.461	3.16	24.8
-	8.777	29.622	38.778	580	287	362	66	366	.146	.460	3.15	19.0
468	8.777	29.650	38.792	466	287	410	0	261	.146	.460	3.15	16.1
267	8.749	29.664	38.877	337	287	233	0	245	.146	.461	3.16	7.3
303	8.777	29.664	38.764	0	287	0	0	0	.146	.460	3.15	0

Load Resistance 10n

Run No. HEF-10A

$V_{L2-V_{L1}}$ Volts	P_C Kg/Cm ²	P_f Kg/Cm ²	P_{t-O_2} Kg/Cm ²	$V_{L2-V_{L1}}$ Volts	T_{t-O_2} °K	$V_{L2-V_{L1}}$ Volts	Seed Tach RPM	$V_{L2-V_{L1}}$ Volts	W_f Kg/Sec	W_O Kg/Sec	O/F	P KW	R Ohms
0	8.172	30.381	38.398	176	286	460	0	572	.154	.456	2.96	-	10
600	9.007	30.241	38.328	593	285	619	0	559	.145	.456	3.14	-	10
649	9.058	30.241	38.680	802	285	1524	60	1595	.148	.460	3.11	162.8	10
1499	8.861	30.283	38.609	1575	286	1603	64	1544	.149	.459	3.08	172.8	10
1575	8.973	30.241	38.609	1576	285	1572	66	1638	.148	.460	3.11	180.6	10
1550	8.946	30.241	38.609	1577	285	1530	66	1505	.148	.460	3.11	169.6	10
1543	9.002	30.297	38.595	1422	286	1540							
1485	8.932	30.269	38.609	135	286	1369	66	1415	.148	.459	3.10	162.5	8
1373	8.917	30.283	38.581	1493	286	1404	66	1388	.149	.459	3.08	171.7	8
1470	8.932	30.283	38.553	1350	286	1320	66	1473	.149	.459	3.08	166.7	8
1402	8.932	30.269	38.581	1476	286	1432	66	1427	.149	.459	3.08	163.8	8
1344	8.917	30.269	38.581	1462	285	1415	66	1400	.149	.459	3.08	171.4	8
1443	8.903	30.283	38.539	1343	286	1091	66	710	.149	.458	3.07	164.5	8
790	8.777	30.297	38.581	546	286	493	66	478	.150	.458	3.05	109.6	8
458	8.763	30.283	38.581	716	286	574	66	449	.150	.458	3.05	-	8
516	8.777	30.297	38.595	357	286	562	66	393	.150	.459	3.06	-	8
389	8.791	30.283	38.553	450	286	316	22	446	.150	.459	3.06	-	8
387	8.791	30.283	38.567	394	286	287	0	477	.150	.458	3.05	-	8
516	8.805	30.269	38.595	0	286	0	0	0	.149	.459	3.08	-	8

Run No. HEP-108

$V_{L2-V_{L1}}$ Volts	P_c Kg/Cm ²	P_f Kg/Cm ²	P_{t-O_2} Kg/Cm ²	$V_{L2-V_{L1}}$ Volts	T_{t-O_2} °K	$V_{L2-V_{L1}}$ Volts	Seed Tach RPM	$V_{L2-V_{L1}}$ Volts	\dot{W}_f Kg/Sec	\dot{W}_O Kg/Sec	O/F	P KW	R Ohms
457	9.818	30.466	38.145	423	285	468	0	537	.145	.454	3.13	-	10
616	8.946	30.466	38.905	617	285	1241	60	1308	.149	.463	3.11	162.4	10
1248	8.805	30.353	38.891	1348	286	1164	61	1330	.150	.462	3.08	161.9	10
1200	8.777	30.353	38.778	1355	285	1291	65	1243	.150	.462	3.08	161.8	10
1282	8.875	30.381	38.736	1199	286	1301	66	1410	.150	.460	3.07	168.5	10
1382	8.889	30.381	38.806	1288	286	1196	66	1187	.150	.461	3.07	159.6	10
1268	8.917	30.353	38.778	1152	286	1298	66	1407	.149	.461	3.09	164.2	10
1329	8.946	30.353	38.820	1349	286	1308	66	1018	.149	.462	3.10	-	8
1085	8.988	30.339	38.806	1224	285	1163	66	1150	.149	.462	3.10	166.9	8
1221	8.974	30.353	38.764	1079	286	997	66	1185	.149	.461	3.09	156.9	8
1046	8.847	30.353	38.778	1224	285	1188	66	1220	.150	.462	3.08	171.0	8
1210	8.946	30.367	38.792	1083	285	1113	66	1054	.149	.462	3.10	155.4	8
1056	8.946	30.367	38.820	653	286	409	66	413	.149	.461	3.09	50.1	8
618	8.791	30.353	38.778	364	286	442	66	395	.150	.461	3.07	25.8	8
460	8.791	30.339	38.778	393	286	423	67	390	.150	.461	3.07	-	8
429	8.763	30.367	38.806	278	286	412	0	253	.150	.461	3.07	-	8
297	8.763	30.353	38.806	198	286	202	0	319	.150	.461	3.07	-	8
201	8.833	30.325	38.806	95	286	0	0	0	.150	.461	3.07	-	8

Run No. HEF-11

$V_{L2-V_{L1}}$ Volts	P_c Kg/Cm ²	P_f Kg/Cm ²	P_{t-O_2} Kg/Cm ²	$V_{L2-V_{L1}}$ Volts	T_{t-O_2} °K	$V_{L2-V_{L1}}$ Volts	Seed Tach RPM	$V_{L2-V_{L1}}$ Volts	W_f Kg/Sec	W_o Kg/Sec	O/F	P KW	R Ohms
1284	8.692	34.418	39.214	1289	282	1276	-	1201		.469	-	159.9	10
1262	8.833	34.404	39.158	1202	282	1179	-	1231		.468	-	148.5	10
1151	8.805	34.404	39.102	1204	282	1368	-	1270		.468	-	155.8	10
1218	8.889	34.376	39.116	1244	282	1201	-	1196		.468	-	147.6	10
1208	8.917	34.362	39.102	1199	281	1203	-	1231		.469	-	146.5	10
1205	8.889	34.390	39.060	1152	281	1232	-	1281		.468	-	148.3	10
1187	8.917	34.390	39.060	1143	282	1219	-	1156		.467	-	138.4	10
1083	8.932	34.390	39.088	1073	282	1019	-	1008		.468	-	134.8	8
1041	9.016	34.390	39.088	1041	281	1017	-	1026		.468	-	132.9	8
1048	9.002	34.404	39.088	995	281	1080	-	1056		.468	-	136.5	8
1037	8.974	34.390	38.989	1079	281	1070	-	1061		.467	-	140.9	8
1028	9.016	34.418	39.003	1054	282	1045	-	1040		.467	-	135.7	8
1081	9.030	34.362	38.975	1065	282	1077	-	1036		.467	-	141.7	8
1019	9.044	34.404	38.933	1056	282	1042	-	1014		.466	-	133.3	8
1020	9.030	34.390	38.961	992	281	1026	-	1012		.467	-	128.1	8
1033	9.002	34.376	38.919	682	281	0	-	0		.466	-	-	8

Run No. HEF-11A

$V_{L2-V_{L1}}$ Volts	P_C Kg/Cm ²	P_f Kg/Cm ²	P_{t-O_2} Kg/Cm ²	$V_{L2-V_{L1}}$ Volts	T_{t-O_2} Kg/Cm ²	$V_{L2-V_{L1}}$ Volts	Seed Tach RPM	$V_{L2-V_{L1}}$ Kg/Cm ²	W_f Kg/Sec	W_o Kg/Sec	O/F	P KW	R Ohms
1062	10.085	35.079	38.511	1285	280	1403	-	1415	.463	.463	-	119.1	14
1332	9.185	34.981	38.975	1413	280	1398	-	1425	.468	.468	-	137.0	14
1347	8.988	34.966	38.989	1404	280	1413	-	1399	.469	.469	-	138.2	14
1416	8.932	34.951	39.017	1381	281	1342	-	1382	.468	.468	-	136.1	14
1371	8.988	34.966	38.961	1338	280	1445	-	1387	.468	.468	-	137.1	14
1379	8.932	34.952	39.003	1413	280	1369	-	1418	.468	.468	-	138.9	14
1426	8.903	34.952	39.045	1425	280	1436	-	1393	.469	.469	-	144.0	14
1339	8.960	34.981	39.060	1372	280	1259	-	1292	.469	.469	-	141.6	12
1289	8.932	34.938	39.074	1295	280	1310	-	1320	.470	.470	-	145.9	12
1347	8.932	34.952	39.088	1314	280	1301	-	1331	.470	.470	-	124.8	12
1248	8.960	34.938	39.116	1218	280	1221	-	1209	.470	.470	-	127.3	12
1216	9.016	34.924	39.088	1269	280	1227	-	1233	.470	.470	-	134.9	12
1266	8.932	34.952	39.130	1292	280	1317	-	1214	.470	.470	-	124.2	12
1166	8.932	34.924	39.088	1198	280	1235	-	1284	.471	.471	-	132.8	12
1253	9.016	34.981	39.158	1268	280	1287	-	1243	.470	.470	-	141.1	12
1300	8.974	34.910	39.116	1281	280	1298	-	1326	.470	.470	-	141.8	12
1355	9.002	34.938	39.158	1284	281	1267	-	1313	.470	.470	-	136.8	12
1281	9.002	34.966	39.186	113	280	0	-	0	.470	.470	-	-	12
0	4.248	35.023	39.186	0	280	0	-	0	.470	.470	-	-	12

Run No. HEP-11B

V_{L2-VL1} Volts	P_C Kg/Cm ²	P_f Kg/Cm ²	P_{t-O_2} Kg/Cm ²	V_{L2-VL1} Volts	T_{t-O_2} °K	V_{L2-VL1} Volts	Seed Tach RPM	V_{L2-VL1} Volts	\dot{W}_f Kg/Sec	\dot{W}_O Kg/Sec	O/F	P KW	R Ohms
0	8.622	35.107	36.471	959	280	1112	-	1186		.439	-	132.0	10
1230	8.932	34.966	37.203	1280	280	1282	-	1252		.448	-	159.0	10
1238	8.749	34.981	37.217	1267	279	1221	-	1318		.448	-	159.1	10
1226	8.777	34.938	37.175	1251	280	1216	-	1246		.447	-	152.4	10
1262	8.735	34.924	37.161	1278	280	1232	-	1284		.447	-	159.7	10
1247	8.692	34.924	37.161	1214	279	1193	-	1197		.448	-	147.1	10
1202	8.763	34.938	37.175	1259	279	1223	-	1212		.448	-	149.8	10
1237	8.749	34.952	37.231	1217	279	1285	-	1228		.448	-	154.2	10
1273	8.805	34.938	37.428	121	280	1230	-				-		
1071	8.777	34.952	37.723	1070	280	1045	-	1018	.450	.450	-	142.3	8
1100	8.861	34.966	38.075	1015	280	1033	-	1082	.454	.454	-	137.5	8
1023	8.903	34.952	38.356	990	279	1025	-	1047	.458	.458	-	130.6	8
1030	8.875	34.938	38.539	1058	279	1064	-	1051	.462	.462	-	136.2	8
1027	8.974	34.966	38.609	1047	280	1024	-	1024	.464	.464	-	131.3	8
1051	8.903	34.938	38.778	1065	279	980	-	1001	.464	.464	-	133.8	8
1059	9.016	34.952	38.820	954	280	1050	-	1043	.467	.467	-	130.4	8
1045	8.960	34.966	38.863	1001	280	959	-	1022	.467	.467	-	130.9	8
981	8.917	34.966	38.863	546	280	0	-	987	.467	.467	-	-	8
							-	0			-		

Run No. HEF-11C

$V_{L2-V_{L1}}$ Volts	P_C Kg/Cm ²	P_f Kg/Cm ²	P_{t-O_2} Kg/Cm ²	$V_{L2-V_{L1}}$ Volts	T_t-C_{-} °K	$V_{L2-V_{L1}}$ Volts	Seed Tach RPM	$V_{L2-V_{L1}}$ Volts	\dot{W}_f Kg/Sec	\dot{W}_O Kg/Sec	O/F	P KW	R Ohms
1113	10.619	35.107	34.643	1045	281	1242	-	1349	.417		-	100.7	14
1386	9.114	35.037	35.628	1437	280	1477	-	1545	.429		-	152.5	14
1500	8.692	35.037	35.754	1562	280	1491	-	1481	.430		-	162.5	14
1442	8.538	35.051	35.782	1441	280	1520	-	1416	.431		-	151.1	14
1510	8.524	35.037	35.796	1521	281	1599	-	1515	.430		-	168.6	14
1468	8.538	35.037	36.050	1555	281	1494	-	1500	.433		-	161.6	14
1542	8.580	35.037	36.486	1536	280	1517	-	1491	.439		-	165.4	14
1485	8.560	35.023	36.879	1437	281	1490	-	1491	.443		-	155.6	14
1521	8.678	35.037	37.245	1507	280	1455	-	1509	.448		-	160.3	14
1436	8.763	35.065	37.555										
1323	8.777	35.009	37.766	1345	281	1306	-	1281	.451		-		12
1276	8.791	35.037	38.005	1326	281	1293	-	1346	.453		-	145.6	12
1308	8.805	35.037	38.187	1292	280	1254	-	1324	.457		-	137.9	12
1317	8.819	35.051	38.370	1289	280	1336	-	1332	.459		-	144.4	12
1263	8.847	35.037	38.469	1259	281	1319	-	1312	.460		-	141.2	12
1331	8.875	35.037	38.591	1335	281	1270	-	1343	.462		-	141.4	12
1271	8.917	35.037	38.680	1252	280	1288	-	1445	.463		-	136.3	12
1271	8.932	35.037	38.708	1229	280	1317	-	1209	.465		-	131.6	12
				1257	280	116	-	0	.465		-	133.2	12

Run No. HEP-12

$V_{L2}-V_{L1}$ Volts	P_c Kg/Cm ²	P_f Kg/Cm ²	P_{t-O_2} Kg/Cm ²	$V_{L2}-V_{L1}$ Volts	T_{t-O_2} °K	$V_{L2}-V_{L1}$ Volts	Seed Tach RPM	$V_{L2}-V_{L1}$ Volts	\dot{W}_f Kg/Sec	\dot{W}_o Kg/Sec	O/F	P KW	R Ohms
0	1.900	38.384	35.515	0	284	0	-	0	0	.425	-	-	10
0	1.218	38.342	36.232	0	285	0	65	0	0	.432	-	-	10
0	1.097	38.342	36.387	0	285	0	60	0	0	.434	-	-	10
0	1.018	38.356	36.429	0	285	0	64	1199	.189	.434	2.30	143.7	10
1202	8.059	38.300	36.415	1387	285	1383	66	1355	.189	.434	2.30	177.3	10
1326	8.917	38.061	36.373	1315	285	1307	66						
1242	8.988	37.920	36.401	1022	285	1126	66	1129	.182	.434	2.38		8
1091	9.002	37.850	36.331	1079	285	1183	66	1212	.181	.434	2.40	165.4	8
1154	9.213	38.836	36.387	959	285	1112	66	1099	.180	.433	2.41	154.8	8
1128	9.255	38.836	36.373	1257	285	1107	66	1104	.179	.434	2.42	157.9	8
1133	9.227	38.836	36.373	1154	285	1114	66	1145	.179	.434	2.42	168.0	8
1139	9.157	38.850	36.359	1153	285	1225	66	1136	.179	.434	2.42	160.8	8
1148	9.283	37.822	36.401	1126	285	1149	66	1168	.180	.434	2.41	171.5	8
1143	9.339	37.808	36.401	942	285	876	66	1178	.179	.434	2.41	165.3	8
633	9.339	38.836	36.443	675	285	707	66	765	.178	.434	2.44	163.3	8
761	9.368	38.836	36.387	622	285	444	66	509	.178	.435	2.44	-	8
528	9.509	38.836	36.429	458	285	595	0	436	.178	.434	2.44	-	8
387	9.621	37.808	36.401	381	286	487	0	389	.177	.435	2.46	-	8
542	9.818	37.808	36.387	284	285	0	0	636	.177	.434	2.45	-	8
								0	.175	.434	2.48	-	8

Run No. HEF-12A

$V_{L2-V_{L1}}$ Volts	P_c Kg/Cm ²	P_f Kg/Cm ²	P_{t-O_2} Kg/Cm ²	$V_{L2-V_{L1}}$ Volts	T_t-O_2 °K	$V_{L2-V_{L1}}$ Volts	Seed Tach RPM	$V_{L2-V_{L1}}$ Volts	W_f Kg/Sec	W_o Kg/Sec	O/F	P KW	R Ohms
0	.024	38.525	39.833	0	285	0	0	0	-	.466	-	-	14
0	1.079	38.497	37.723	0	286	0	0	0	-	.449	-	-	14
0	1.409	38.511	37.864	0	285	0	0	0	-	.451	-	-	14
0	1.201	38.441	38.131	0	285	0	61	1298	-	.456	-	120.3	14
1340	9.058	38.511	38.103	1497	285	1521	64	1361	.183	.454	2.48	146.1	14
1411	9.846	38.314	38.075	1406	285	1372	64	1453	.178	.454	2.55	142.1	14
1387	10.113	38.230	37.976	1300	284	1368	65	1492	.176	.453	2.57	137.3	14
1494	10.155	38.216	38.005	1324	285	1489	65	1201	.176	.453	2.57	-	12
1318	10.310	38.216	37.991	103	285	0	64	0	.175	.452	2.58	144.8	12
0	2.117	38.131	37.834	0	285	0	65	0	-	.452	-	-	12
0	3.533	38.061	37.976	0	285	0	65	0	-	.452	-	-	12

Run No. HEF-13

$V_{L2-V_{L1}}$ Volts	P_c Kg/Cm ²	P_f Kg/Cm ²	P_{t-O_2} Kg/Cm ²	$V_{L2-V_{L1}}$ Volts	T_{t-O_2} °K	$V_{L2-V_{L1}}$ Volts	Fuel Meter Kg/Sec	$V_{L2-V_{L1}}$ Volts	\dot{W}_f Kg/Sec	\dot{W}_o Kg/Sec	O/F (Calc.)	O/F Fuel Meter	R Ohms
0	0	38.384	29.397	0	266	1073	.082	1040	.174	-	-	-	10
1102	10.563	39.031	27.357	699	266	701	.140	565	.141	.495	3.51	3.54	10
572	10.324	39.003	27.568	1157	266	1215	.149	1250	.142	.499	3.51	3.35	10
1299	10.591	38.919	27.652	1227	266	1361	.151	1271	.141	.500	3.54	3.31	10
1220	10.507	38.919	27.681	1297	266	1325	.152	1287	.141	.500	3.55	3.29	10
1295	10.563	38.933	27.723	1295	266	1366	.151	1310	.141	.502	3.56	3.32	10
1371	10.549	38.947	27.681	1318	266	1304	.152						
1161	10.662	38.947	27.638	1179	266	1196	.152	1173	.141	.501	3.55	3.30	8
1168	10.591	38.905	27.737	1188	266	1215	.152	1144	.140	.500	3.57	3.29	8
1255	10.619	38.961	27.653	1185	266	1147	.153	1201	.141	.502	3.56	3.30	8
1231	10.563	38.905	27.273	1085	266	1185	.153	1253	.141	.500	3.55	3.27	8
1134	10.619	38.933	26.921	1066	266	1114	.154	1159	.141	.492	3.49	3.22	8
1111	10.633	38.905	26.527	977	266	1173	.153	1204	.141	.488	3.40	3.17	8
1127	10.240	38.947	26.105	1091	266	1014	.153	1086	.140	.481	3.44	3.14	8
1138	10.422	38.975	25.613	917	266	958	.153	1033	.142	.473	3.33	3.09	8
852	10.226	38.947	25.374	801	266	458	.154	808	.141	.465	3.30	3.04	8
472	10.029	38.989	24.924	447	266	0	.154	0	.142	.460	3.24	2.99	8
									.143	.453	3.19	2.94	8

Run No. HEF-13A

$V_{L2-V_{L1}}$ Volts	P_C Kg/Cm ²	P_f Kg/Cm ²	P_{t-O_2} Kg/Cm ²	$V_{L2-V_{L1}}$ Volts	T_{t-O_2} °K	$V_{L2-V_{L1}}$ Volts	Fuel Meter Kg/Sec	$V_{L2-V_{L1}}$ Volts	\dot{W}_f Kg/Sec	\dot{W}_O Kg/Sec	O/F (Calc.)	O/F (Fuel Meter)	R Ohms
0	0.24	37.611	28.370	0	264	0	0	0	-	-	-	-	14
0	0.23	37.611	28.370	0	264	0	0	0	-	-	-	-	14
0	0.44	36.922	28.131	0	264	0	.084	389	.167	-	-	-	14
486	9.508	36.809	25.993	1306	264	1156	.134	1043	.137	.474	3.46	3.54	14
1052	10.310	36.936	26.176	1348	264	1550	.143	1588	.135	.477	3.53	3.34	14
410	-	-	-	-	Arcing destroyed all instrumentation								

Run No. HEP-14

$V_{L2-V_{L1}}$ Volts	PC Kg/Cm ²	Pf Kg/Cm ²	PO ₂ Kg/Cm ²	$V_{L2-V_{L1}}$ Volts	TO ₂ °K	$V_{L2-V_{L1}}$ Volts	Seed Gm/Sec	Fuel Meter Kg/Sec	$V_{L2-V_{L1}}$ Volts	Wf Kg/Sec	WO ₂ Kg/Sec	O/P -	P KW	R Ohms
481	9.269	37.822	26.710	390	320	1161	44.1	.094	1141	.141	.463	3.28	62.89	10
1050	9.086	37.878	26.766	1087	293	894	44.1	.130	1095	.142	.464	3.27	111.7	10
1107	9.199	37.864	26.780	990	288	1117	44.1	.024	1142	.142	.464	3.27	118.6	10
1101	9.368	37.822	26.780	1267	295	1113	44.1	2.401	1056	.141	.464	3.29	128.6	10
1128	9.269	37.864	26.780	1159	300	1152	44.1	.141	1168	.141	.464	3.29	132.6	10
1263	9.199	37.878	26.809	1196	291	1082	44.1	.127	1053	.142	.465	3.27	131.9	10
1146	9.536	37.850	26.837	1197	291	1272	44.1	.463						
945	9.339	37.850	26.823	1051	289	1122	44.1	.029	984	.141	.465	3.30	132.1	8
1024	9.480	37.836	26.851	983	287	1054	44.1	.104	1039	.141	.466	3.30	137.3	8
1034	9.410	37.850	26.851	1003	286	1004	44.1	.116	1045	.141	.466	3.30	130.43	8
1026	9.368	37.850	26.668	1136	318	1093	44.1	2.411	994	.141	.462	3.28	141.1	8
903	9.269	37.836	26.260	990	290	1002	44.1	.167	936	.141	.456	3.23	114.7	8
889	9.269	37.864	25.810	739	290	465	44.1	.111	547	.141	.448	3.18	54.4	8
408	9.002	37.892	25.290	250	286	340	-	2.437	223	.142	.439	3.09		8
270	8.833	37.864	24.811	202	292	164	-	.518	194	.143	.431	3.01		8
232	9.382	38.117	24.456	143	289	135	-	.040	221	.142	.425	2.99		8
86	9.100	38.117	23.883	124	293	172	-	.109		.143	.416	2.91		8

Run No. HEP-14A

$V_{L2-V_{L1}}$ Volts	PC Kg/Cm ²	P_f Kg/Cm ²	PO ₂ Kg/Cm ²	$V_{L2-V_{L1}}$ Volts	TO ₂ °K	$V_{L2-V_{L1}}$ Volts	Seed Gm/Sec	Fuel Meter Kg/Sec	$V_{L2-V_{L1}}$ Volts	M_f Kg/Sec	WO ₂ Kg/Sec	O/F -	P KW	R Ohms
673	9.691	37.695	25.585	653	295	1477	44.1	.112	1375	.140	.446	3.19	145.3	14
1373	9.649	37.766	25.529	1354	290	1404	44.1	.125	1317	.140	.445	3.18	132.5	14
1355	9.410	37.709	25.515	1332	290	1398	44.1	.133	1406	.140	.445	3.18	134.6	14
1261	9.607	37.751	25.529	1277	292	1394	44.1	.128	1240	.140	.445	3.18	119.4	14
1389	9.804	37.695	25.557	1340	294	1323	44.1	.031	1300	.139	.445	3.20	127.9	14
1197	9.677	37.737	25.529	1272	289	1318	44.1	.106	1129	.140	.445	3.18	107.9	14
1342	9.494	37.723	25.529	1358	292	1189	44.1	.484	1377	.140	.445	3.18	123.8	14
1310	9.649	37.709	25.543	1375	281	1344	44.1	.196	1307	.140	.445	3.18	127.1	14
1307	9.775	37.681	25.529	1272	285	1086	44.1	.126						
1181	9.536	37.751	25.571	1280	279	1280	44.1	.223	1157	.139	.445	3.20		12
1150	9.818	37.695	25.557	1264	284	1286	44.1	.221	1165	.140	.446	3.19	127.3	12
1125	9.691	37.709	25.543	1183	287	1248	44.1	.191	1269	.139	.445	3.2	128.6	12
1379	9.761	37.709	25.543	1034	284	832	-	.034	1154	.140	.445	3.18	115.5	12
593	9.621	37.695	25.557	590	280	510	-	.109	574	.139	.445	3.20	121.4	12
448									581	.140	.445	3.18		12

Run No. HEP-15

$V_{L2-V_{L1}}$ Volts	PC Kg/Cm ²	Pf Kg/Cm ²	PO ₂ Kg/Cm ²	$V_{L2-V_{L1}}$ Volts	TO ₂ °K	$V_{L2-V_{L1}}$ Volts	Seed Gm/Sec	Fuel Meter Kg/Sec	$V_{L2-V_{L1}}$ Volts	W _F Kg/Sec	WO ₂ Kg/Sec	O/F -	P KW	R Ohms
4.04	1.016	35.881	24.882	430	303	380	-	.143	407		.424			10
298.6	6.737	35.824	24.811	484	301	442	-	.115	583	.196	.424	2.16	34.0	10
606.4	6.948	35.810	24.839	533	302	465	-	.119	2633	.195	.424	2.17	36.8	10
420.8	6.906	35.810	24.825	582	303	565	-	.129	516	.195	.423	2.17	33.9	10
676	7.061	35.768	24.825	622	302	588	-	.136	563	.194	.423	2.18	45.7	10
630.4	7.089	35.782	24.868	656	302	789	-	.135	672	.194	.424	2.19	62.2	10
661.2	7.398	35.810	24.839	617	302	611	-	.134	508	.193	.424	2.2	43.7	10
498.2	7.047	35.824	24.853	689	301	673	-	.134	625	.195	.425	2.18	47.5	10
620.8	7.230	35.782	24.853	634	301	683	-	.145	689	.194	.424	2.19	47.5	10
574.6	7.258	35.768	24.882	654	302	655	-	.143	677	.194	.425	2.19	45.8	10
862.2	7.511	35.895	24.910	792	302	765	-	.155	777	.193	.425	2.2	74.3	10
680.6	7.623	35.796	25.304	749	302	781	-	.159	776	.192	.431	2.24	61.0	10
619	7.581	35.796	25.838	668	302	668	-							
559.8	7.778	35.824	26.302	573	302	675	-	.156	714	.192	.440	2.29	63.7	8
671.4	7.863	35.810	26.795	628	299	596	-	.156	662	.192	.447	2.33	57.0	8
504.8	7.877	35.824	27.231	515	303	604	-	.152	565	.191	.458	2.40	56.3	8
515.6	8.003	35.810	27.653	585	302	529	-	.152	596	.191	.462	2.42	45.2	8
486	8.031	35.810	28.131	52.3	303	2.02	-	.153	545	.191	.470	2.46	47.8	8
2.95	2.355	36.486	28.581	3.19	303	3.40	-	.110	2.79	.190	.477	2.51		8
							-		3.63		.484			8

Run No. HEF-15A

$V_{L2-V_{L1}}$ Volts	PC Kg/Cm ²	Pf Kg/Cm ²	PO ₂ Kg/Cm ²	$V_{L2-V_{L1}}$ Volts	TO ₂ °K	$V_{L2-V_{L1}}$ Volts	Seed Gm/Sec	Fuel Meter Kg/Sec	$V_{L2-V_{L1}}$ Volts	W _F Kg/Sec	WO ₂ Kg/Sec	O/F -	P KW	R Ohms
4.1	.520	35.909	26.485	4.41	303	4.04	-		776		.450		43.0	14
408	7.947	35.824	25.599	1024	302	1272	-	.134	1187	.191	.436	2.283	115.6	14
1187	7.89	35.810	25.557	949	300	987	-	1.43	1103	.191	.437	2.288	100.6	14
1056	7.19	35.768	25.444	1039	302	1107	-	.158	1128	.191	.434	2.272	90.9	14
1129	7.989	35.740	25.515	1194	301	1068	-	.169	1129	.190	.436	2.295	101.8	14
1114	7.891	35.740	25.543	1118	301	1230	-	.167	1186	.191	.436	2.283	108.0	14
1177	7.947	35.782	25.557	1137	298									
825	7.820	35.782	25.557	898	302	1072	-	.160	914	.191	.438	2.293	95.8	12
918	7.891	35.782	25.852	1164	301	957	-	.155	943	.191	.435	2.277	76.3	12
948	8.017	35.740	26.232	1001	297	1038	-	.159	935	.191	.451	2.361	112.7	12
960	8.088	35.726	26.710	891	302	1173	-	.164	929	.190	.450	2.368	114.7	12
879	8.214	35.782	27.160	799	303	922	-	.163	894	.190	.454	2.389	76.8	12
904	8.299	35.782	27.638	853	302	842	-	.163	769	.190	.461	2.426	64.4	12
797	8.327	35.768	28.117	927	303	848	-	.159	874	.189	.469	2.481	68.1	12
793	8.453	35.768	28.595	719	299	801	-	.160	1015	.189	.477	2.524	85.9	12
693	8.510	35.712	29.073	681	302	743	-	.156	663	.189	.488	2.582	52.4	12
727	8.271	35.712	29.495	717	297	691	-	.155	773	.188	.493	2.622	49.8	12
586	8.777	35.768	29.945	619	302	624	-	.160	842	.187	.505	2.700	59.1	12
1.28	6.301	35.768	30.353	3.23	302	607	-	.157	43.6	.187	.507	2.711	31.9	12
3.82	2.477	35.796	30.775	3.95	300	3.64	-		2.78		.514			12
						4.03	-		4.07		.523			12

Run No. HEF-16

$V_{L2-V_{L1}}$ Volts	PC Kg/Cm ²	Pf Kg/Cm ²	PO ₂ Kg/Cm ²	$V_{L2-V_{L1}}$ Volts	TO ₂ °K	$V_{L2-V_{L1}}$ Volts	Seed Gm/Sec	Fuel Meter Kg/Sec	$V_{L2-V_{L1}}$ Volts	W _F Kg/Sec	WO ₂ Kg/Sec	O/F	P KW	R O ₂ ms
743	9.382	32.294	26.274	724	269	658	-	-	536	.13	.456	3.51	55.2	10
572	9.227	32.294	26.218	1008	269	1194	29.4	-	1110	.132	.455	3.45	142.6	10
1102	9.241	32.223	25.993	1150	269	1158	29.4	-	1078	.131	.451	3.44	134.1	10
1178	9.185	32.252	25.543	1032	269	1108	29.4	-	1214	.132	.444	3.36	147.4	10
1058	9.213	32.210	25.388	1146	269	1010	29.4	-	1124	.131	.444	3.39	131.3	10
1116	9.142	32.210	25.374	1058	269	1044	29.4	-	1124	.132	.441	3.34	126.3	10
1014	9.199	32.139	25.374	1182	269	1052	29.4	-	1060	.131	.441	3.37	139.7	10
1098	9.030	32.139	25.402	1012	269	1046	29.4	-	1004	.131	.441	3.37	120.6	10
966	9.114	32.139	25.416	1096	269	1124	29.4	-	1178	.131	.441	3.37	138.8	10
1036	9.213	32.167	25.458	1110	269	1134	29.4	-	1110	.131	.442	3.37	128.6	10
1124	9.114	32.210	25.430	1094	269	1060	29.4	-	1088	.132	.442	3.35	126.3	10
1078	9.185	32.182	25.852	1092	269	1130	29.4	-	1032	.131	.448	3.42	127.7	10
1148	9.269	32.196	26.190	1100	269	1050	29.4	-	1200	.131	.455	3.47	144.0	10
1018	9.325	32.167	26.598	1220	269	1210	29.4	-	1170	.130	.462	3.55	148.8	10
1224	9.424	32.182	27.020	1098	269	1096	29.4	-	1162	.130	.469	3.61	149.8	10
1178	9.564	32.182	27.427	1228	269	1228	29.4	-	1246	.128	.476	3.72	155.3	10
1246	9.494	32.182	27.835	1182	269	1116	29.4	-	1120	.129	.483	3.74	155.3	10
1206	9.775	32.167	28.285											
1104	9.705	32.182	28.707	1070	269	952	29.4	-	1042	.127	.491	3.87	143.1	8
1110	9.719	32.182	29.200	994	269	1010	29.4	-	994	.127	.499	3.93	152.3	8
936	10.029	32.182	29.565	970	269	946	29.4	-	874	.126	.507	4.02	154.0	8
1012	9.958	32.153	29.959	1008	269	1006	29.4	-	1012	.125	.513	4.10	128.0	8
970	10.240	32.069	30.339	948	269	930	29.4	-	868	.125	.520	4.16	128.0	8
				974	269	1042	29.4	-	896	.121	.527	4.36	135.7	8

Run No. HEF-17

$V_{L2-V_{L1}}$ Volts	PC Kg/Cm ²	Pf Kg/Cm ²	PO ₂ Kg/Cm ²	$V_{L2-V_{L1}}$ Volts	TO ₂ °K	$V_{L2-V_{L1}}$ Volts	Seed Gm/Sec	Fuel Meter Kg/Sec	$V_{L2-V_{L1}}$ Volts	W _F Kg/Sec	WO ₂ Kg/Sec	O/F -	P KW	R Ohms
650	9.663	32.013	26.823	446	275	506	-	-	506	.125	.461	3.69	42.3	10
534	9.353	31.999	26.752	664	275	1038	29.4	-	1124	.127	.460	3.62	126.3	10
1060	9.339	32.027	26.668	1218	275	1136	29.4	-	1130	.128	.458	3.58	148.3	10
1076	9.424	31.985	26.696	1194	275	1140	29.4	-	1116	.127	.459	3.61	142.6	10
1168	9.438	32.041	26.724	1234	275	1216	29.4	-	1196	.127	.459	3.61	152.3	10
1200	9.311	31.971	26.724	1120	275	1180	29.4	-	1240	.127	.459	3.61	153.8	10
1130	9.466	31.928	26.724	1182	275									
1050	9.494	31.942	26.724	964	275	1066	29.4	-	996	.126	.459	3.64	142.0	8
1018	9.339	31.928	26.696	992	275	1050	29.4	-	982	.125	.459	3.67	137.8	8
1040	9.368	31.957	26.752	944	275	1052	29.4	-	1032	.126	.459	3.64	138.3	8
1012	9.396	31.914	26.780	980	275	924	29.4	-	1078	.126	.460	3.65	145.3	8
966	9.480	31.928	26.766	1070	275	916	29.4	-	1068	.125	.460	3.68	142.6	8
966	9.424	31.900	26.752	1068	275	1014	29.4	-	1068	.125	.460	3.68	143.1	8
938	9.550	31.957	26.780	1016	275	1028	29.4	-	960	.125	.460	3.68	142.6	8
1000	9.508	31.914	26.766	1068	275	1072	29.4	-	924	.124	.460	3.71	143.6	8
1040	9.325	31.928	26.752	980	275	1012	29.4	-	992	.124	.460	3.71	142.6	8
956	9.522	31.928	26.724	1062	275	942	29.4	-	1046	.126	.460	3.65	136.8	8
1034	9.536	31.942	26.738	940	275	1036	29.4	-	998	.125	.459	3.67	141.0	8
1060	9.353	31.914	26.752	998	275	900	29.4	-	1004	.126	.460	3.65	133.6	8
938	9.424	31.942	26.766	1064	275	950	29.4	-	1080	.126	.460	3.65	145.8	8
910	9.536	31.957	26.766	1060	275	1010	29.4	-	1012	.126	.460	3.65	141.5	8
922	9.480	31.914	26.752	1044	275	1052	29.4	-	940	.125	.460	3.65	140.5	8
1012	9.550	31.942	26.710	1028	275	1052	29.4	-	932	.126	.460	3.65	138.3	8
1044	9.466	31.928	26.752	710	275	1048	29.4	-	982	.125	.459	3.67	137.3	8
486	9.368	31.957	26.738	438	275	470	-	-	412	.126	.460	3.65	136.2	8
432	9.297	31.957	26.738	336	275	354	-	-	286	.127	.460	3.62	29.5	8
380	9.325	31.928	26.766	200	275	300	-	-	270	.127	.460	3.62	23.3	8
						-1.5	-	-	4.1	.127	.460	3.62	18.1	8

Run No. HEF-13

$V_{L2-V_{L1}}$ Volts	PC Kg/Cm ²	P_f Kg/Cm ²	PO_2 Kg/Cm ²	$V_{L2-V_{L1}}$ Volts	TO_2 °K	$V_{L2-V_{L1}}$ Volts	Seed Gm/Sec	Fuel Meter Kg/Sec	$V_{L2-V_{L1}}$ Volts	W_f Kg/Sec	WO_2 Kg/Sec	O/F	P KW	R Ohms
918	8.341	31.436	24.263	938	298	848	-	-	798	.147	.401	2.73	88.0	10
806	8.256	31.380	24.305	820	294	1206	29.4	-	1148	.147	.404	2.75	145.4	10
1150	8.481	31.366	24.305	1104	292	1188	29.4	-	1132	.146	.404	2.77	141.1	10
1108	8.552	31.352	24.305	1148	288	1110	29.4	-	1138	.145	.408	2.81	131.8	10
1146	8.721	31.352	24.305	1174	290	1172	29.4	-	1170	.144	.407	2.83	137.8	10
1148	8.664	31.338	24.277	1140	284	1182	29.4	-	1120	.145	.411	2.83	139.7	10
1118	8.735	31.352	24.291	1130	287	1132	29.4	-	1154	.144	.408	2.83	133.2	10
1170	8.833	31.366	24.319	1194	282	1146	29.4	-	974	.144	.412	2.86	142.6	8
1052	8.791	31.338	24.263	1072	287	1064	29.4	-	988	.144	.408	2.83	143.6	8
1016	8.664	31.366	24.277	1026	287	994	29.4	-	1028	.144	.408	2.83	132.1	8
1054	8.735	31.366	24.291	1032	286	1036	29.4	-	1056	.143	.409	2.86	139.4	8
1022	8.889	31.366	24.305	1038	286	1044	29.4	-	1058	.143	.410	2.87	139.9	8
1056	8.960	31.380	24.305	1086	286	1086	29.4	-	1048	.143	.410	2.87	147.4	8
1040	8.861	31.324	24.347	1070	279	1076	29.4	-	1070	.143	.416	2.91	144.7	8
1120	8.889	31.366	24.333	1054	281	1048	29.4	-	1060	.143	.414	2.90	140.5	8
1026	8.846	31.352	24.333	1080	285	1056	29.4	-	1026	.143	.411	2.87	145.8	8
1022	9.002	31.352	24.361	1008	283	1094	29.4	-	1044	.143	.413	2.89	149.6	8
1030	8.805	31.366	24.333	1000	284	1090	29.4	-	886	.144	.411	2.85	148.5	8
950	8.889	31.324	24.319	1024	283	1044	29.4	-	1046	.143	.412	2.88	136.8	8
1084	8.960	31.366	24.347	1032	282	1080	29.4	-	1054	.143	.413	2.89	146.9	8
1062	9.128	31.352	24.333	1072	283	1072	29.4	-	1078	.142	.412	2.90	145.3	8
1056	9.030	31.378	24.347	1052	282	1120	29.4	-	1106	.142	.413	2.91	156.8	8
1090	8.974	31.324	24.333	1046	281	1060	29.4	-	798	.143	.414	2.90	148.5	8
770	8.903	31.380	24.333	738	281	672	-	-	692	.143	.414	2.90	74.1	8
616	8.819	31.366	24.347	600	280	506	-	-	596	.143	.414	2.90	47.4	8
554	8.875	31.380	24.347	510	281	542	-	-	472	.143	.414	2.90	38.4	8
614	8.861	31.366	24.347	460	281	464	-	-	4.0	.143	.414	2.90	47.1	8

Run No. HEP-18A

$V_{L2-V_{L1}}$ Volts	PC Kg/Cm ²	Pf Kg/Cm ²	PO ₂ Kg/Cm ²	$V_{L2-V_{L1}}$ Volts	TO ₂ °K	$V_{L2-V_{L1}}$ Volts	Seed Gm/Sec	Fuel Meter Kg/Sec	$V_{L2-V_{L1}}$ Volts	Wf Kg/Sec	WO ₂ Kg/Sec	O/F	P KW	R Ohms
0	0	31.450	25.852	0	290	1282	29.4	-	1304				121.5	14
1238	8.706	31.211	24.122	1176	287	958	29.4	-	876	.144	.406	2.82	109.5	14
920	8.566	31.113	24.094	978	284	1260	29.4	-	1290	.144	.407	2.83	118.9	14
1282	8.552	31.141	24.108	1246	282	1268	29.4	-	1198	.144	.409	2.84	117.4	14
1288	8.777	31.042	24.080	1278	281	1252	29.4	-	1238	.142	.409	2.88	118.5	14
1264	8.861	31.070	24.080	1308	281	1294	29.4	-	1192	.142	.409	2.88	122.2	14
1212	8.721	31.127	24.108	1182	279	1200	29.4	-	1274	.143	.411	2.87	115.9	14
1240	8.833	31.084	24.136	1196	277	1188	29.4	-	1190	.142	.412	2.90	109.8	14
1212	8.932	31.113	24.094	1220	279	1146	29.4	-	1158	.142	.411	2.89	106.6	14
1188	8.847	31.084	24.108	1188	278	1158	29.4	-						
									1112	.142	.412	2.90	103.0	12
1134	8.960	31.000	24.108	1066	274	1120	29.4	-	1198	.141	.415	2.94	119.6	12
1060	8.974	31.056	24.066	1200	279	1212	29.4	-	1120	.141	.411	2.91	122.4	12
1128	8.791	31.113	24.066	1160	278	1186	29.4	-	1150	.142	.411	2.89	117.2	12
1150	8.861	31.155	24.066	1182	274	1170	29.4	-	1138	.143	.414	2.90	116.4	12
1192	8.875	31.099	24.080	1148	274	1146	29.4	-	1210	.142	.414	2.92	122.0	12
1102	8.960	31.127	24.106	1144	277	1122	29.4	-	1132	.142	.413	2.91	109.1	12
1116	9.142	31.127	24.094	1166	276	3.5	-	-	3.9	.140	.413	2.95	113.3	12

Run No. HEP-19

$V_{L2-V_{L1}}$ Volts	PC Kg/Cm ²	Pf Kg/Cm ²	PO ₂ Kg/Cm ²	$V_{L2-V_{L1}}$ Volts	TO ₂ °K	$V_{L2-V_{L1}}$ Volts	Seed Gm/Sec	Fuel Meter Kg/Sec	$V_{L2-V_{L1}}$ Volts	W _F Kg/Sec	WO ₂ Kg/Sec	O/F	P KW	R Ohms
0	0	32.139	25.008	0	299	0	-	-	0	0	0		0	10
0	0	32.139	24.305	0	296	0	-	-	0	.33	.403	.122	0	10
0	0	32.083	24.235	0	296	0	-	-	0	.33	.402	.122	0	10
0	0	31.802	24.221	0	299	0	-	-	0	.32	.399	.125	0	10
0	0	31.563	24.192	0	300	994	29.4	-	858	.32	.398	.124	98.8	10
1032	8.130	31.394	24.235	980	299	1074	29.4	-	1040	.128	.399	3.12	115.3	10
1038	8.116	31.197	24.235	1013	296	1074	29.4	-	1032	.127	.402	3.17	115.3	10
1073	8.256	31.042	24.291	1016	295	998	29.4	-	1048	.122	.403	3.30	115.1	10
1036	8.327	30.873	24.340	1012	298	1006	29.4	-	998	.119	.402	3.38	107.3	10
990	8.510	30.705	24.291	1052	299	1066	29.4	-	998	.113	.400	3.54	113.6	10
1054	8.270	30.522	24.305	1010	299									
916	8.439	30.353	24.305	884	299	866	29.4	-	928	.115	.400	3.48	101.6	8
884	8.411	30.170	24.333	888	298	892	29.4	-	924	.110	.400	3.64	106.7	8
872	8.439	30.044	24.319	918	297	894	29.4	-	910	.108	.402	3.72	103.5	8
872	8.453	29.875	24.305	898	297	910	29.4	-	892	.105	.402	3.83	105.3	8
922	8.467	29.748	24.277	898	298	498	-	-	882	.103	.402	3.90	103.5	8
456	8.327	29.565	24.291	486	297	370	-	-	478	.101	.401	3.97	106.3	8
340	8.313	29.411	24.333	346	297	342	-	-	364	.101	.401	3.97	29.5	8
328	8.256	29.397	24.333	214	297	0	-	-	292	.099	.402	4.06	15.0	8
									0	.099	.402	4.06	13.1	8

Section XI
FUEL EMULSION MIXTURE FORMULATIONS

The following is a listing of successful emulsion formulations.

Water/Oil - JP-4

EM-120	1%	1%
JP-4	2%	4%
H ₂ O	97%	95%
Glycomul-O	0.5%	1%
JP-4	2 2%	3%
Water	97.5%	96%

Water/Coal

Glycomul-O	1%	1%
JP-4	2%	2%
Coal	30%	50%
Water	67%	47%
EM-120	1%	1%
JP-4	4%	4%
Coal	10%	20%
H ₂ O	85%	75%

Toluene/Emulsion

LMF 4229	1%
H ₂ O	4%
Toluene	95%

Toluene/Emulsion

LMF-4229	1%
H ₂ O	3%
Tolene	96%

Distilled H₂O - .638 @12.66 V
Tap H₂O - .88 @11.96 V
Power supply unloaded 175.0 ma @13.52 V

Tween 20	1%
H ₂ O	3.5%
Toluene	95.5%

Distilled H₂O - .273 @12.63 V
Tap H₂O - .431 @12.60 V
Power supply unloaded 175.0 ma @13.52 V

Tol/CsNO₃

LMF 4229	1%
H ₂ O	4%
CsNO ₃	10%
Toluene	85%

Toluene/Seed

Tween 20	1%	1%	1%
H ₂ O	4%	3%	2%
KNO ₃ - CsNO ₃	20%	20%	20%
Toluene	75%	76%	77%

Toluene/Seed

Tween 20	81%	}	1%
Span 20	19%		
H ₂ O			3%
KNO ₃ - CsNO ₃			15%
Toluene			81%

Toluene/AL

LMF - 4229	1 1/4%
H ₂ O	3 3/4%
Aluminum	30%
Toluene	65%

LMF - 4234	5%	5%	5%
Aluminum	10%	20%	30%
Toluene	85%	75%	65%

Tween 20	1%
H ₂ O	2-4%
Aluminum	30%
Toluene	65-67%

Toluene/Al/KNO₃ - CsNO₃

Tween 20	1%
H ₂ O	2%
KNO ₃ - CsNO ₃	15%
Al	30%
Toluene	50%

Toluene/Boron

LMF 4235	4%
H ₂ O	6%
Boron	30%
Toluene	60%

Toluene/Carbon

Tween 20	1%	2%
H ₂ O	3%	3%
Carbon	30%	30%
Toluene	66%	65%

Tween 40	1%	2%
H ₂ O	2%	2%
Carbon	30%	30%
Toluene	67%	66%

Toluene/Coal

Tween 20	2%	2%
H ₂ O	5%	2%
Coal	30%	30%
Toluene	63%	66%

Toluene/Coal Slag

Tween 20	81%	}	1%
Span 20	19%		
H ₂ O			3%
Coal Slag			8%
Toluene			88%

Up to 15% KNO₃ and CsNO₃ have been added to this form.

Toluene/Mg

LMF - 4234	5%
Mg	30%
Toluene	65%

Toluene/Napthalene

Tween 20	1%
H ₂ O	4%
Napthalene	34%
Toluene	61%

15% KNO₃ - CsNO₃ added after formation, remained stable

Toluene/Pollucite (Cs₂O·Al₂O₃·4SiO₂)

Tween 20	81%	}	1%
Span 20	19%		
H ₂ O			3%
Pollucite			25%
Toluene			71%

Benzene/KNO₃ - CsNO₃

Tween 20	1%
H ₂ O	4%
KNO ₃ - CsNO ₃	15%
Benzene	80%

Tween 20	81%	} 1%
Span 20	19%	
H ₂ O	4%	
KNO ₃ - CsNO ₃	15%	
Benzene	80%	

Tween 40	1%
H ₂ O	4%
KNO ₃ - CsNO ₃	15%
Benzene	80%

Tween 60	1%
H ₂ O	4%
KNO ₃ - CsNO ₃	15%
Benzene	80%

Tween 80	1%
H ₂ O	4%
KNO ₃ - CsNO ₃	15%
Benzene	80%

Benzene/Napthalene/KNO₃ - CsNO₃

Tween 20	1%
H ₂ O	4%
KNO ₃ - CsNO ₃	15%
	29%
Benzene	51%

Benzene/Napthalene Waterless Emulsion

Tween 20	1.1%
C ₃ H ₈ O ₂	4.4%
Napthalene (C ₁₀ H ₈)	33.3%
Benzene (C ₆ H ₆)	61.1%

Stable until Cs₂CO₃ was added

JP-4 Emulsion

Tween 20	1%
H ₂ O	4-3%
JP-4	Remainder

Distilled H₂O .190 @12.80 V

Tap H₂O .260 @12.93 V

Power supply unloaded 175 ma @13.52 V

JP-4

Tween 20	81%	} 1%
Span 20	19%	
H ₂ O		4%
JP-4		95%

JP-4

Tween 60	99% } 1%
Span 60	1% }
H ₂ O	4%
JP-4	95%

JP-4/KNO₃ - CsNO₃

Tween 20	81% } 1%
Span 20	19% }
H ₂ O	4%
KNO ₃ - CsNO ₃	15%
JP-4	80%

Tween 40	1%
H ₂ O	4%
KNO ₃ - CsNO ₃	15%
JP-4	80%

Tween 40	85% } 1%
Span 40	15% }
H ₂ O	4%
KNO ₃ - CsNO ₃	15%
JP-4	80%

JP-4/KNO₃ - CsNO₃ Emulsion

Tween 60	1%
H ₂ O	4%
KNO ₃ - CsNO ₃	15%
JP-4	80%

JP-4/KNO₃ - CsNO₃

Tween 80	99% } 1%
Span 80	1% }
H ₂ O	4%
KNO ₃ - CsNO ₃	15%
JP-4	80%

JP-4/Coal

EM-23D	2%
H ₂ O	6%
Coal	30%
JP-4	62%

Tween 20	0.5%	0.75%	1%
H ₂ O	5.0%	5.0 %	4%
Coal	20.0%	20.0 %	30%
JP-4	74.5%	74.25%	65%

Tween 20	68% } 1%
Span 20	42% }
H ₂ O	3-4%
Coal	30%
JP-4	65-66%

JP-4/SRC Coal

EM-23D	0.6%
H ₂ O	4.4%
SRC Coal	40 %
JP-4	55 %

JP-4/Coal/KNO₃ - CsNO₃

Tween 20	1%	1%
H ₂ O	4%	4%
KNO ₃ - CsNO ₃	15%	15%
Coal	30%	50%
JP-4	50%	30%

Tween 20	68%	} 1%
Span 20	42%	
H ₂ O		4%
Coal		30%
KNO ₃ - CsNO ₃		15%
JP-4		50%

JP-4/Coal Slag

Tween 80	92%	} 1%
Span 80	8%	
H ₂ O		3%
Coal Slag		10%
JP-4		86%

Up to 15% KNO₃ - CsNO₃ has been added to this formulation

JP-4 Waterless Emulsion

Tween 20	1%
C ₃ H ₈ O ₂	6%
JP-4	93%

JP-4 Waterless Emulsion

Tween 40 1%

C₃H₈O₂ 10%

JP-4 89%

Addition of 25% Cs₂CO₃ stable for only a few hours

JP-4/Mg/Waterless

Tween 20 .7%

C₃H₈O₂ 5.6%

Mg 30% %

JP-4 63.7%

JP-4/Na₂CO₃ - Cs₂CO₃

Brij 92 20% } 2.5

Brij 98 80% }

C₃H₈O₂ 4 %

H₂O 4 %

Na₂CO₃ - Cs₂CO₃ 15 %

JP-4 74.5%

No. 2 Fuel Oil/Coal

Tween 20 68% } 1%

Span 20 42% }

H₂O 4%

Coal 50%

Oil 45%

APPENDIX

Tyler Standard Screen Scale

<u>Mesh</u>	<u>μm scale</u>	<u>inch scale</u>
10	1650	.0650
20	830	.0327
35	420	.0165
48	300	.0118
65	220	.0087
100	150	.0059
150	110	.0043
200	74	.0029
325	44	.0017

Examples:	common gas molecules	0.0003 - 0.00045 μm
	pulverized coal (normal)	10 - 400 μm
	mist	40 - 500 μm
	fog	1 - 40 μm
	oil smoke	0.03 - 1 μm
	dust causing silicosis	<10 μm

REFERENCES

1. Powers, W. L., Dicks, J. B., Snyder, W. F. A Generalized Graphical Presentation of MHD Generator and Accelerator Performance Characteristics. 6th Proc. Symp. Engr. Aspects of MHD, Pittsburgh, Pennsylvania, 1965.
2. Rosa, Richard S. Magnetohydrodynamic Energy Conversion. McGraw-Hill Book Co.
3. Bitter, David and Brokaw, Richard. Estimate of Chemical Space Heating Rates in Gas-Phase Combustion with Application to Rocket Propellants. ARS Journal, February 1960.
4. Shanklin, R. V., III. Private Communication.
5. Salmi, Reino J., Wankainen, John P., and Hannum, Ned P. Effect of Thrust Per Element on Combustion Stability Characteristics of Hydrogen-oxygen Rocket Engines. NASA TN D-4851.
6. Priem, Richard J. and Heidman, Marcus F. Propellant Vaporization as a Design Criterion for Rocket-engine Combustion Chambers. NASA TR-R-67.
7. Kossoy, A. A., Ozerov, Ye. S., and Sirkunen, G. I. Burning of Low-Boiling Binder from Particle of a Two-Component Meta-containing Fuel. Leningrad, USAF Foreign Technology Division.
8. Heidman, M. F., and Auble, C. M. Injection Principles from Combustion Studies in a 200-pound Thrust Rocket Engine Using Liquid Oxygen and Heptane. NASA RM-E55C22.
9. Stein, Samuel. A High-Performance 250-pound Thrust Rocket Engine Utilizing Coaxial-flow Injection of JP-4. NASA TN-D-126.
10. Hersch, Margin. Effect of Interchanging Propellants on Rocket Combustor Performance with Coaxial Injection. NASA TN-D-2169.
11. Adelberg, M. Mean Drop Size Resulting from The Injection of a Liquid Jet into a High-Speed Gas Stream. AIAA Journal, Vol 6, No. 6, June 1968.
12. Brokaw, Richard S., Belles, Frank E., Clark, Bruce J. and Zeleznik, Frank J. Combustion. Conference on Selected Technology for the Petroleum Industry. NASA SP-5053.

13. Putnam, A. A., et al. Injection and Combustion of Liquid Fuels. Tech Report 56-344; Document AD 118142.
14. Gordon and McBride. Computer Program for Calculation of Complex Chemical Equilibrium Compositions, Rocket Performance, Incident and Reflected Shocks, and Chapman-Jouquet Detonations. NASA SP-273.
15. King, Merrill K. Combustion Studies of Fuel Rich Propellants. AFOSR-TR-76-1079. Atlantic Research Corp.
16. Peacock, A. T., et al. A Study of The Compatibility of a Four Engine Commercial Jet Transport Aircraft Fuel System with Gelled and Emulsified Fuels. Douglas Aircraft Co. Report Nos. AD 714030, NA-7011, DS-70-1.
17. Rachow, R. A. and Shaw, L. M. Crashworthiness of Safe Fuels. Dynamic Science, Phoenix, Arizona.
18. Weeks, Lloyd E. U.S. Patent 2,920,948. Monsanto Chemical Co. January 12, 1960.
19. Brained, Harold W. U.S. Patent 2,742,426. Standard Oil & Gas Co. April 17, 1956.
20. Greblich, Julius L. U.S. Patent 2,927,849. Ethyl Corp. March 8, 1960.
21. Skolnik, Sol and Mayolin, Emanuel D. U.S. Patent 3,197,348. U.S. Navy. July 27, 1965.
22. Lissant, Kenneth J. U.S. Patent 3,352,109. Petrolite Corp. November 14, 1967.
23. Lissant, Kenneth J. U.S. Patent 3,539,406. Petrolite Corp. November 10, 1970.
24. Lissant, Kenneth J. U.S. Patent 3,613,372. Petrolite Corp. October 19, 1971.
25. Lissant, Kenneth J. U.S. Patent 3,617,095. Petrolite Corp. November 2, 1971.
26. Roberts, R. A. and Van Keuren, W. C. Evaluation of EF-104 Emulsified Fuel in a Pratt & Whitney Aircraft JT-12 Engine. Pratt & Whitney Aircraft Pub.
27. Koblish, T. R., et al. Emulsified Fuels Combustion Study. USAAV Labs Tech Report 69-4, AD 682325. Pratt & Whitney Aircraft, February 1969.

28. Nixon, James, et al. Investigation and Analysis of Aircraft Fuel Emulsions. USAAV Labs Tech Report 67-62, AD 827051. Esso Research & Engineering Co.
29. Beardell, A. J., et al. Rheological Evaluation of Emulsified JP-4 Fuel. USAAV Labs Tech Report 68-27. Thiokol Chemical Corp.
30. Harvey, Thomas and Monarch, John. Environmental Testing of a Gas Turbine Engine Utilizing EF4-10 Emulsified JP-4 Fuel. USAAV Labs Tech Report 68-55. Continental Aviation & Engineering Corp.
31. Erikson, Albert and Beth, Larry D. Emulsified Fuel Vulnerability Study. U.S. Army Aviation Material Labs, Fort Eustis, Virginia. AD 879704.
32. McCutcheon's Detergents & Emulsifiers. North American Edition. 1975 Annual, McCutcheon's Publications.
33. The Atlas HLB System. Atlas Chemical Industries, Inc. 4th printing from Chemmuniqué.
34. Lissant, K. J. Structure of High-Internal-Phase-Ratio Emulsions. Journal of Colloid and Interface Science, Vol 47, No. 2, May 1974.
35. Lissant, K. J. The Geometry of High-Internal-Phase-Ratio Emulsion. Journal of Colloid and Interface Science, Vol 22, No 5, 462-468, November 1966.
36. Lissant, K. J. Geometry of Emulsions. Journal of Society of Cosmetic Chemists, 21, 141-154 (March, 1970).
37. Lissant, K. J. A Unified Method of Delineating Polymeric Species. Journal of Chemical Documentation, 3, 103 (1963).
38. Lissant, K. J. and Mayhan, Kenneth C. A Study of Medium and High Internal Phase Ratio Water/Polymer Emulsions. Journal of Colloid and Interface Science, Vol 42, No. 1, January 1973.
39. Fochtman, E. G., Bitten, J. F., and Katz, Signey. Preparation of a Magnesium-JP-4 Slurry Fuel. I & EC Product Research & Development, Vol 2, September 1963.

40. Darlington, C. R., Gilburth, R. E. and Ballard, R. S. Design Characteristics and Performance of a Combustor for Use as an Ionized Gas Source in MHD Power Generation Studies. AEDC-TR-69-167.
41. Hidy, G. M. and Brock, J. R. The Dynamics of Aero-colloidal Systems. Pergammon Press.
42. Shapiro, Ascher H. The Dynamics and Thermodynamics of Compressible Fluid Flow. The Ronald Press Co.
43. Baumeister and Marks. Standard Handbook for Mechanical Engineers. McGraw-Hill, 8th ed.
44. CRC Handbook of Chemistry and Physics. 53rd ed.
45. Van Wylen, Gordon J. Thermodynamics. John Wiley & Sons, Inc.
46. Lissant, K. J. U.S. Patent 3,523,826. Petrolite Corp. August 11, 1970.
47. Perry, R. H. and Chilton, C. H. Chemical Engineer's Handbook. McGraw Hill, 5th ed., 1973.
48. Sonju, O. K., Teno, J., Lothrop, J. W., and Petty, S. W. Experimental Research on a 400KW High Power Density MHD Generator. AFAPL-TR-71-5.
49. Stratford, B. S. The Calculation of The Discharge Coefficient of Profiled Choked Nozzles and the Optimum Profile for Absolute Air Flow Measurement. Journal of the Royal Aeronautical Society, Vol 68, April 1964.
50. Fluid Meters -- Their Theory and Application. The ASME, 6th ed., 1971.
51. Fire Protection Guide on Hazardous Materials. NFPA, 6th ed.
52. Hartmann, J., Nagy, John and Brown, H. R. Inflammability and Explosibility of Meta Powders. Report of Investigations. U.S. Department of the Interior; U.S. Bureau of Mines.
53. Kirk-Ohmer. Encyclopedia of Chemical Technology. 2nd ed., Vol 4.
54. Hazard, R., Boissier, J. R., Hazard, J. and Mouilleé. Compt. Rend. 243, 452-454 (1956); Chem. Abstr. 50, 17208 N(1956).